# Density and Compressibility of FeO-bearing Silicate Melt: Relevance to Magma Behavior in the Earth

by

Xuan Guo

A dissertation submitted in partial fulfillment
of the requirements for the degree of
Doctor of Philosophy
(Geology)
in The University of Michigan
2013

Doctoral committee:

Professor Rebecca Ann Lange, Chair
Research Professor Jeffrey C. Alt
Professor John Kieffer
Associate Professor Jie (Jackie) Li
Professor Youxue Zhang

*To*
*Xiao and Zixin & Ziqi*

# ACKNOWLEDGMENTS

I would like to express my sincere gratitude to my advisor, Dr. Rebecca Lange, for her valuable guidance and financial support throughout my PhD study at the University of Michigan. She introduced me to the field of experimental petrology with great enthusiasm. I have been benefited from her passion on scientific research, critical thinking, broad knowledge, and scrutiny in writing scientific papers. I especially appreciate her understanding and support during my pregnancy. I would like to thank the other four members on my dissertation committee: Drs. Youxue Zhang, Jie Li, Jeffrey Alt and John Kieffer for their constructive comments on my manuscripts of this thesis. Particular thanks for Dr. Youxue Zhang, who allowed me to use his lab facilities. I am also grateful to Dr. Samuel Mukasa who was one of my committee members when he was at University of Michigan. He helped me learn isotope geology, as well as giving me a lot of advice on my study and research.

In addition, I would like to thank all the people who have contributed to this dissertation in various ways. In particular, Yuhui Ai taught me how to make sound speed measurements which is essential in my study. Mary Catherine O'Leary helped me a lot in lab work, course study, daily life, as well as improving my English skills. Laura Waters, Stephen Crabtree, Christopher Stefano, and Carl Henderson showed me how to prepare my glass samples and assisted to do the electron microprobe analysis. Zhenjiu Xu provided a lot of information on lab supplies. When I need XRD information for my

study, Jiaming Zhang and Fuxiang Zhang shared their knowledge, experience and resources with me. When I was having a very difficult time with lab equipment problems, Qiong Liu shared her precious experience with me by email contact.

Many thanks are due to my fellow graduate students for their friendship and support, including Huawei Ni, Wenjun Yong, Yang Chen, Hejiu Hui, Ni Sun, Tie Sun, Jing Zhou, Yang Zhang, Qiaona Hu, Jiachao Liu, Zeyu Li and Ran Feng. Moreover, I really enjoyed the time with my good friends Yajun Liu and Zhenguang Huang. They provided a lot of help and support during my living in Ann Arbor.

Last but no the least, I would like to give my great appreciation to my husband Xiao Qin, who accompanies me through my Ph.D studies. My thesis could not have been finished without his fully support and encouragement. My twin boys, Zixin and Ziqi, made the last year special and impressive. Many thanks to my mother and my parents-in-law, they helped a lot in taking care of my babies. With the love and support from so many people, this work was accomplished.

## TABLE OF CONTENTS

## LIST OF TABLES

**TABLES**

## LIST OF FIGURES

**FIGURES**

# CHAPTER I

## Introduction

Melting is an important process for early Earth history and the modern Earth. Whenever melting occurs, the changes to our planet are significant and irreversible. During early Earth history, deep and extensive melting formed a global magma ocean. Subsequent crystal-melt segregation, often driven by density differences between crystallizing phases and the magma ocean as a function of depth (e.g., Nisbet and Walker, 1982; Ohtani, 1984; Herzberg, 1984; Agee and Waker, 1988; Li and Agee, 1996; Walter et al., 2000; Wood et al., 2006) were important processes in the formation of the Earth's crust, mantle and the core. For the modern Earth, partial melting continues to play a key role in the generation of oceanic crust at mid-ocean spreading ridges and the formation of continental crust at subduction zones, both from a thermodynamic perspective, in controlling the pressure dependence of mantle melting, and from a dynamic perspective, in controlling the buoyancy drive for melt migration. Therefore, the determination of how melt density varies with composition, temperature and pressure is one of the essential problems in the geological sciences.

An equation of state (P-V-T model) for multi-component silicate melts is needed in order to extend thermodynamic models of crystal-melt equilibrium to elevated pressures within the deep Earth. To date, there is only successful thermodynamic model,

called pMETLS (Ghiorso et al., 2002), breaks down at pressures higher than 3 GPa (~100 km depth). That is most likely due to the lack of high-quality liquid density data at high pressure. Therefore, in order to build a versatile thermodynamic model effective in the deep Earth, more accurate density and compressibility data are needed. In various equations of state (e.g., the 3$^{rd}$-order Birth-Murnaghan and Vinet equations of state), three critical parameters are needed for silicate melts: (1) molar volume (density) at one bar, $V_{T,0}$, (2) the isothermal bulk modulus (or compressibility) at one bar, $K_{T,0}$, and (3) the pressure-dependence of the bulk modulus ($K_0' = dK_{T,0}/dP$). In this PhD thesis, new experimental data are provided for the first two parameters, which are needed before high-pressure density measurements can be used to constrain accurate values of $K_0'$ in calibrated equations of state. By combing the 1-bar density and compressibility data with density data at high pressure, which can be measured by sink/float and shockwave methods, the relation of $K_0'$ with melt composition can be established.

To date, there have been many measurements of melt density at one bar in the system $Na_2O$-$K_2O$-CaO-MgO-$Fe_2O_3$-$Al_2O_3$-$TiO_2$-$SiO_2$ system (e.g. Bockris, 1956; Stein et al., 1986; Courtial and Dingwell, 1999; Dingwell, 1992; Lange and Carmichael, 1987; Lange, 1996, 1997; Liu and Lange, 2001, 2006). Nearly all of these measurements have been made in air and for the major element oxide components in magmatic liquids (i.e., $SiO_2$-$Al_2O_3$-MgO-CaO-$Na_2O$-$K_2O$) the partial molar volumes are all independent of composition, at least for liquids that are not peraluminous and where $X_i \leq 0.5$ for all oxide components except $SiO_2$ (Lange, 1997). This means that a simple linear model for molar volume can be used to describe the density of most magmatic liquids as a function of composition and temperature:

However, in the most commonly used model equation to describe the density of magmatic liquids (Lange and Carmichael, 1987), one important component that is poorly constrained is FeO (ferrous iron). Ferrous iron is an important component in magmatic melts both because it is abundant (ranging between 10 and 20 wt% in terrestrial and lunar basalts) and because it forms a redox couple with ferric iron, and their ratio is a sensitive indicator of magma oxidation state. Precise volumetric information on both the FeO and $Fe_2O_3$ components is necessary to calculate the oxygen fugacity of magmatic liquids as a function of depth in the mantle (Mo et al., 1982; Kress and Carmichael, 1991).

Currently, only three sets of double-bob density measurements have been made on iron-bearing liquids under reducing conditions and these are restricted to liquids along the FeO-$SiO_2$ binary (Shirashi et al., 1978; Mo et al., 1982; Thomas et al., 2012). In all cases, the derived partial molar volume of FeO at 1673 K ranges from 13.8 to 16.0 $cm^3$/mol, which is ~15-33% larger than that for crystalline FeO (wüstite; 6-coordinated $Fe^{2+}$) at room temperature (12.06 $cm^3$/mol; Smyth and McCormick, 1995). In contrast, Lange (1997) reports a partial molar volume of MgO in multicomponent silicate liquids at 1723 K of 11.86 (± 0.07) $cm^3$/mol, which is similar to that derived for crystalline MgO (periclase; 6-coordinated $Mg^{2+}$) at room temperature (11.24 $cm^3$/mol; Smyth and McCormick, 1995). The relatively large $\overline{V}_{FeO}$ in the FeO-$SiO_2$ liquids is consistent with the high-temperature X-ray absorption spectroscopic results from Jackson et al. (1993), which indicate an average $Fe^{2+}$ coordination closer to four than six in fayalite liquid. However, additional spectroscopic evidence shows that $Fe^{2+}$ can occur in four-, five- and six-fold coordination in a wide variety of multi-component silicate glasses and liquids at one bar, with an average coordination number that varies with composition (e.g., Jackson

et al., 1991, 1993, 2005; Dunlap, 1998; Rossano et al., 1999, 2000; Farges et al., 2004; Wilke et al., 2004, 2007). Because the density and compressibility of a silicate melt are largely determined from the geometrical packing and coordination of its network-forming ions, the capacity of $Fe^{2+}$ to shift coordination affects the volumetric properties of iron-bearing liquids, it is currently unknown how variations in the composition of magmatic melts will affect the partial molar volume, thermal expansivity and compressibility of the FeO component.

In this study a systematic investigation of both melt density and compressibility as functions of melt composition is performed on Fe-bearing liquids under reducing conditions. Although previous measurements of sound speeds (to derive melt compressibility) have been performed on several $Fe^{2+}$-bearing silicate liquids (Rivers and Carmichael, 1987), conversion of these data to adiabatic compressibility requires accurate information on liquid density ($\beta_S = 1/\rho c^2$), which as described above, has not been available for $Fe^{2+}$-bearing liquids.

This study is a systematic investigation of the high temperature density and compressibility of $Fe^{2+}$-bearing silicate melts at one bar. The goal is to establish how the partial molar volume, thermal expansivity, and compressibility of the FeO component vary with melt composition at one bar (reflecting composition-induced changes in $Fe^{2+}$ coordination). The experimental liquids include CaO-FeO-$SiO_2$ liquids (Chapter II), ternary model basalts ($CaAl_2Si_2O_6$-$CaMgSi_2O_6$-$CaFeSi_2O_6$ system, Chapter III), $Na_2O$-FeO-$SiO_2$ liquids (Chapter IV), and alkali-bearing model basalts ($K_2O$-$Na_2O$-CaO-MgO-FeO-$Al_2O_3$-$SiO_2$ system) (Chapter V).

In Chapter II double-bob density measurements using molybdenum bobs in a reducing atmosphere are presented for five CaO-FeO-$SiO_2$ (CFS) liquids, including $CaFeSi_2O_6$ (hedenbergite) liquid. In addition, relaxed sound speeds were measured with an acoustic interferometer at centered frequencies of 4.5 and 5.5 MHz between 1300 and 1600°C. When each experimental liquid is fitted individually, the partial molar volume and isothermal compressibility of the FeO component ($\overline{V}_{FeO}$ and $\overline{\beta}_{T,FeO}$, respectively) increase systematically with CaO concentration, consistent with a composition-induced decrease in the average $Fe^{2+}$ coordination number. When the components of the CFS liquids are recast in terms of $CaFeO_2$-FeO-$SiO_2$, an ideal mixing model for both volume and compressibility recovers both the volume and compressibility data within experimental error. At 1723 K, the fitted $\overline{V}_{FeO}$ and $\overline{\beta}_{T,FeO}$ values are 12.1 ± 0.2 $cm^3$/mol and 3.5 ± 0.3 x $10^{-2}$ $GPa^{-1}$, respectively, which are postulated to reflect $Fe^{2+}$ in 6-fold coordination given the similarity of $\overline{V}_{FeO}$ in the melt to that for crystalline FeO (wüstite). In contrast, the derived values of $\overline{V}_{FeO}$ and $\overline{\beta}_{T,FeO}$ in the $CaFeO_2$ component are 17.1 ± 0.2 $cm^3$/mol and 7.1 ± 0.2 x $10^{-2}$ $GPa^{-1}$, respectively, which are postulated to reflect $Fe^{2+}$ in 4-fold coordination given that crystalline $CaFeO_2$ contains 4-coordinated $Fe^{2+}$. These two end-member values for $\overline{V}_{FeO}$ at 1723 K are used to develop a linear equation to calculate $Fe^{2+}$ coordination as a function of $\overline{V}_{FeO}$, which leads to average $Fe^{2+}$ coordination numbers in the CFS liquids that range from 5.2 to 4.6, including a value of 4.7 for hedenbergite ($CaFe_2Si_2O_6$) liquid. This manuscript is to be submitted to *Geochimica et Cosmochimica Acta.*

Because the CaO-FeO-SiO2 liquids in Chapter II have compositions far simpler than those of magmatic liquids, Chapter III expands the compositional range to liquids that additionally contain MgO and $Al_2O_3$, by focusing on three model basalt compositions in the ternary anorthite-diopside-hedenbergite ($CaAl_2Si_2O_8$-$CaMgSi_2O_6$-$CaFeSi_2O_6$) system. The densities of the three model basalts at high temperature were measured by the double-bob Archimedean method at high temperatures with molybdenum bobs. In addition, low-temperature liquid density data were obtained at their respective limiting fictive temperatures ($T_f$'), providing density data over a wide temperature interval spanning >900 degrees. Finally, relaxed sound speed measurements were performed from 1653 to 1876K at 1 bar with a frequency sweep acoustic interferometer. An ideal mixing model leads to a partial molar volume (at 1723 K), thermal expansivity and compressibility for FeO of 12.82 (±0.16) $cm^3$/mol, 3.69 (±0.58) $10^{-3}cm^3$/mol-K, and 4.75 (±0.20) $10^{-2}$ $GPa^{-1}$, respectively. Using the equation derived in Chapter II, the fitted value for $\overline{V}_{FeO}$ of 12.82 leads to an estimated $Fe^{2+}$ coordination number of 5.7, indicating that in alkali-free model basalts there is an abundance of 6-coordianted $Fe^{2+}$. These results have implications for the pressure dependence of the Fe-Mg exchange reaction between basaltic liquids and ferromagnesian minerals, such as olivine and orthopyroxene. Comparison to observed changes in ${}^{Fe\text{-}Mg}K_D$ (orthopyroxene-liquid) with pressure from partial melting experiments of peridotite from the literature (Walter, 1998), where the melts contain small amounts of alkalis, provide evidence that average $Fe^{2+}$ coordination numbers in high-pressure melts are closer to 5 than 6. Therefore, additional density and sound speed measurements are needed on $Fe^{2+}$-bearing liquids that also contain $Na_2O$ and $K_2O$. This manuscript is to be submitted *Earth and*

*Planetary Science Letters*.

Chapters II and III did not study any sample with alkalis, whereas spectroscopic studies indicate that alkalis have the effect of lowering the coordination number of $Fe^{2+}$ to values near 5. Therefore, chapter IV is a study of the density and compressibility of four $Na_2O$-FeO-$SiO_2$ liquids. The experimental methods are the same as in Chapter II and III. An ideal mixing model using the oxide components ($Na_2O$-FeO-$SiO_2$) for molar volume and isothermal compressibility cannot recover the experimental results within error. However, when each experimental liquid is fitted individually, the partial molar volume of the FeO component ($\overline{V}_{FeO}$) increases systematically with $Na_2O$ concentration, consistent with a composition-induced decrease in the average $Fe^{2+}$ coordination number from 5.2 to 4.5. In contrast, fitted values of isothermal compressibility ($\overline{\beta}_{T,FeO}$) are anomalously high, 10.1 to 14.9 $10^{-2}$ $GPa^{-1}$, and decrease systematically with $Na_2O$ concentration (opposite the behavior seen for CaO-FeO-$SiO_2$ liquids). By applying the coordination model from early study, the calculated average coordination number range from 4.5 to 5.2. The high values of $\overline{\beta}_{T,FeO}$ in sodic liquids are similar to those observed for $\overline{\beta}_{T,TiO_2}$ in sodic liquids, and it is proposed they are related to $Fe^{2+}$ and $Ti^{4+}$ in square-pyramidal coordination sites at the interface of alkali-rich and silica-rich domains in the melt, which promotes topological mechanisms of compression. This manuscript is to be submitted to *American Mineralogist*.

Chapter V is a study of the density and compressibility of three alkali-bearing model basalts in the $K_2O$-$Na_2O$-CaO-MgO-FeO-$Al_2O_3$-$SiO_2$ system under reducing conditions. The densities of the three alkali-bearing basalts at high temperature were measured by the double-bob Archimedean method. Low-temperature liquid densities

were also obtained at $T_f$', providing density data over a wide temperature interval of ~800-900 degrees. By fitting the molar volume data into a linear model, the derived partial molar volume (±1σ) of FeO is 14.76 (± 0.15) $cm^3$/mol, with a thermal expansivity of 1.03 (± 0.61) $\times 10^{-3} cm^3$/mol-K, consistent with an average $Fe^{2+}$ coordination number close to 5. In addition, relaxed sound speed measurements were performed on the three alkali model basalts from 1637 to 1869 K at 1 bar with the frequency sweep acoustic interferometer. The sound speeds of another four $Na_2O/K_2O$-bearing silicate liquids were measured as well to further constrain the compressibility of alkali-bearing silicate liquids. Because the alkali-bearing basalt liquids contain both alkalis and alkaline-earth components, and because results from the literature show that the compressibility of the $Al_2O_3$ component differs in alkali vs. alkaline-earth silicate melts (Kress et al., 1988; Ai and Lange, 2008), an ideal mixing model equations for melt compressibility was calibrated on liquids from this study and the literature with components recast as $KAlO_2$-$K_2O$-$NaAlO_2$-$Na_2O$-CaO-MgO-FeO-$Al_2O_3$-$SiO_2$. The results lead to a partial molar compressibility of FeO of 5.22 (±0.47) ($\times 10^{-2}$ $GPa^{-1}$), which does not display an anomalously large value as seen in the simple $Na_2O$-FeO-$SiO_2$ liquids. This may be due to the interaction of $Al^{3+}$ with $Na^+$ and $K^+$ in the model basalt liquids, in contrast to the Al-free NFAS liquids. In this paper, simple equations to calculate appropriate values of $\overline{V}_{FeO}$, $\partial\overline{V}_{FeO}/\partial T$ and $\overline{\beta}_{T,FeO}$ to apply to naturally occurring basalt liquids are provided. This manuscript is to be submitted to to *Contributions to Mineralogy and Petrology*.

## Reference


Agee C.B. and Waker D., 1988. Mass balance and phase density constraints on early differentiation of chonodritic mantle. Earth and Planetary Science Letters. 90, 144-156.

Ai Y. and Lange R. A., 2008. New acoustic velocity measurements on CaO-MgO-$Al_2O_3$-$SiO_2$ liquids: Reevaluation of the volume and compressibility of $CaMgSi_2O_6$-$CaAl_2Si_2O_8$ liquids to 25 GPa. Journal of Geophysical Research **113**, B04203, doi:10.1029/2007JB005010.

Bockris J. O'M., Tomlinson J.W., White J.L., 1956. The structure of the liquid silicates: partial molar volumes and expansivities. Trans Faraday Soc. 52, 299-310.

Courtial P. and Dingwell D.B., 1999. Densities of melts in the CaO-MgO-$Al_2O_3$-$SiO_2$ system. American Mineralogist. 84 (4), 465-476.

Dingwell D.B, 1992. Density of some titanium-bearing liquids and the compositional dependence of the partial molar volume of TiO2. Geochim. Cosmochim. Acta. 56, 3403–3407.

Dunlap, R.A., Edelman, D.A. and Mackay, G.R., 1998. A Mossbauer effect investigation of correlated hyperfine parameters in natural glasses (tektites). J. Non-Crystal. Solids. 223, 141-146.

Farges F., Lefrere Y., Rossano S., Berthereau A., Calas G. and Brown G. E. Jr., 2004. The effect of redox state on the local structural environment of iron in silicate glasses: A molecular dynamics, combined XAFS spectroscopy, and bond valence study. Journal of Non-Crystalline Solids 344, 176-188

Ghiorso M.S., Hirschmann M.M., Reiners P.W., Kress V.C., 2002. The pMELTS: A revision of MELTS for improved calculation of phase relations and major element partitioning related to partial melting of the mantle to 3 GPa, Geochemistry Geophysics Geosystems. 3(5), 10.1029/2001GC000217

Herzberg C.T., 1984. Chemical stratification in the silicate Earth. Earth and Planetary Science Letters. 67, 249-260.

Jackson, W.E., 1991. Spectroscopic studies of ferrous iron in silicate liquids, glasses and crystals. Ph.D. dissertation, Department of Geology, Standford University. 162pp.

Jackson, W.E., Waychunas, G.A., Brown, G.E., Leon, J.M., Conradson, S. and Combes, J.-M., 1993. High-temperature XAS study of Fe2SiO4 liquid: Reduced coordination of ferrous iron. Science 262, 229–232.Science, 262,229.

Jackson, W.E., Farges, F., Yeager, M., Mabrouk, P.A., Rossano, S., Waychunas, G.A., Solomon, E.I. and Brown $J_R$, G.E., 2005. Multi-spectroscopic study of Fe(II) in silicate glasses: Implications for the coordination environment of Fe(II) in silicate melts. Geochimica et Cosmochimica Acta, 69(17), 4315-4332.

Kress, V.C., Williams Q. and Carmichael I.S.E., 1988. Ultrasonic investigation of melts in the system $Na_2O$-$Al_2O_3$-$SiO_2$. Geochimica et Cosmochimica Acta, 52, 283-293.

Kress V. C. and Carmichael I. S. E., 1991. The compressibility of silicate liquids containing $Fe_2O_3$ and the effect of composition, temperature, oxygen fugacity and pressure on their redox states. Contributions to Mineralogy and Petrology **108**, 82-92.

Lange, R.A., Carmichael, I.S.E., 1987. Densities of $Na_2O$-$K_2O$-CaO-MgO-FeO-$Fe_2O_3$-$Al_2O_3$-$TiO_2$-$SiO_2$ liquids: New measurements and derived partial molar properties. Geochimica et Cosmochimica Acta, 51, 2931-2946

Lange, R.A., 1996. Temperature independent thermal expansivities of sodium aluminosilicate melts between 713 and 1835 K. Geochimica et Cosmochimica Acta, 60, 4989–4996.

Lange, R.A., 1997. A revised model for the density and thermal expansivity of $K_2O$-$Na_2O$-CaO-MgO-$Al_2O_3$-$SiO_2$ liquids from 700 to 1900 K: Extension to crustal magmatic temperatures. Contributions to Mineralogy and Petrology, 130, 1–11.

Li J. and Agee C.B, 1996. Geochemistry of mantle-core differentiation at high pressure. Nature. 381, 686-689

Liu, Q., Lange, R.A., 2001. The partial molar volume and thermal expansivity of $TiO_2$ in alkali silicate melts: Systematic variation with Ti coordination. Geochimica et Cosmochimica Acta, 65(14), 2379-2393

Liu, Q. and Lange, R.A., 2006. The partial molar volume of $Fe_2O_3$ in alkali silicate melts: Evidence for an average $Fe^{3+}$ coordination number near five. American Mineralogist, 91, 385-393.

Mo, X., Carmichael, I.S.E., Rivers, M. and Stebbins, J.F., 1982. The partial molar volume of $Fe_2O_3$ in multicomponent silicate liquids and the pressure-dependence of oxygen fugacity in magma. Mineralogical Magzine. 45, 237-245.

Nisbet E.G. and Walker D., 1982. Komatiites and the structure of the Archean mantle. Earth and Planetary Science Letters. 60, 105-113.

Ohtani E., 1984. Generation of komatiite magma and gravitational differentiation in the deep upper mantl. Earth and Planetary Science Letters. 67, 261-272

Rivers, M.L., Carmichael, I.S.E., 1987. Ultrasonic studies of silicate melts. J. Geophys. Res. Solid Earth Planets 92, 9247–9270.

Rossano, S., Balan, E., Morin, G., Bauer, J.-P., Brouder, C. and Calas, G., 1999. $^{57}Fe$ Mossbauer spectroscopy of tektite. Phys. Chem. Mineral. 26, 530-538.

Rossano, S., Ramos, A.Y. and Delaye, J.-M., 2000. Environment of ferrous iron in $CaFeSi_2O_6$ glass: contributions of EXAFS and molecular dynamics. Journal of Non-Crystalline Solids, 273, 48-52.

Smyth J. R. and McCormick T. C., 1995. Crystallographic data for minerals. In T. Ahrens, Ed., Mineral Physics and Crystallography, p.1-17. AGU Reference shelf 2, Washington, D.C.

Stein D. J., Stebbins J. F., and Carmichael I. S. E., 1986. Density of molten sodium aluminosilicates. J. Am. Ceram. Soc., 69, 396–399.

Walter M.J., Newsom H.E., Ertel W., Holzheid A., 2000. Siderophile elements in the Earth and Moon:metal/silicate partitioning and implications for core formation, in: R.M. Canup, K. Righter, (Eds),Origin of the Earth and Moon, The University of Arizona Press, 2000, pp. 265-289.

Wilke, M., Parzsch, G.M., Bernhardt, R. and Lattard, D., 2004; Determination of the iron oxidation state in basaltic glasses using XANES at the K-edge Chemical Geology. 213, 71-87

Wilke M., Farges F., Partzsch G. M., Schmidt C., Behrens H., 2007. Speciation of Fe in silicate glasses and melts by in-situ XANES spectroscopy. American Mineralogist. 92, 44-56

Wood B.J., Walter M.J., Wade J., 2006. Accretion of the Earth and segregation of its core, Nature. 441, 825-833.

# CHAPTER II

## The Density and Compressibility of CaO-FeO-$SiO_2$ Liquids: Evidence for Four-coordinated $Fe^{2+}$ in the $CaFeO_2$ Component


## Abstract

Double-bob density measurements using molybdenum bobs in a reducing atmosphere were made on five CaO-FeO-$SiO_2$ (CFS) liquids, including $CaFeSi_2O_6$ (hedenbergite) liquid. In addition, relaxed sound speeds were measured with an acoustic interferometer at centered frequencies of 4.5 and 5.5 MHz between 1571 and 1885 K. An ideal mixing model using the oxide components (CaO-FeO-$SiO_2$) for molar volume and isothermal compressibility cannot recover the experimental results within error. When each experimental liquid is fitted individually, the partial molar volume and isothermal compressibility of the FeO component ($\overline{V}_{FeO}$ and $\overline{\beta}_{T,FeO}$, respectively) increase systematically with CaO concentration, consistent with a composition-induced decrease in the average $Fe^{2+}$ coordination number. When the CFS liquids are recast in terms of the $CaFeO_2$-FeO-$SiO_2$ components, an ideal mixing model for both volume and compressibility recovers the data within experimental error. At 1723 K, the fitted $\overline{V}_{FeO}$ and $\overline{\beta}_{T,FeO}$ values are 12.1±0.2 $cm^3$/mol and (3.5±0.3) x $10^{-2}$ $GPa^{-1}$, respectively, which

are postulated to reflect $Fe^{2+}$ in 6-fold coordination given the similarity of $\overline{V}_{FeO}$ in the melt to that for crystalline FeO (wüstite). In contrast, the derived values of $\overline{V}_{FeO}$ and $\overline{\beta}_{T,FeO}$ from the $CaFeO_2$ component are 17.1 ± 0.2 $cm^3$/mol and (7.1 ± 0.2) x $10^{-2}$ $GPa^{-1}$, respectively, which are postulated to reflect $Fe^{2+}$ in 4-fold coordination given that crystalline $CaFeO_2$ contains 4-coordinated $Fe^{2+}$. These two end-member values for $\overline{V}_{FeO}$ at 1723K are used to develop a linear equation to calculate $Fe^{2+}$ coordination as a function of $\overline{V}_{FeO}$, which leads to average $Fe^{2+}$ coordination numbers in the CFS liquids that range from 5.2 to 4.6, including a value of 4.7 for hedenbergite ($CaFe_2Si_2O_6$) liquid.

## Introduction

Iron is a major element in magmatic liquids that occurs in two valence states, $Fe^{2+}$ and $Fe^{3+}$. Prior to the 1980s, it was often assumed that $Fe^{2+}$ and $Fe^{3+}$ were each largely restricted to octahedral and tetrahedral coordination, respectively, in silicate melts, following their coordination environments in commonly occurring minerals. Over the last three decades, however, numerous spectroscopic studies (e.g., de Grave, 1980; Fenstermacher, 1980; Calas and Petiau, 1983; Wang and Chen, 1987; Hannoyer et al., 1992; Bychkov et al., 1993; Alberto et al., 1996; Dunlap et al., 1998; Rossano et al., 1999), as well as K-edge extended x-ray absorption fine structure (EXAFS) and K-edge X-ray absorption near edge structure (XANES) studies (e.g., Waychunas et al., 1988, 1989; Jackson et al., 1991, 1993, 2005; Rossano et al., 2000; Farges et al., 2004;Wilke et al., 2004, 2007) have shown that the coordination of $Fe^{2+}$ and $Fe^{3+}$ in liquids and glasses is far more variable than that typically seen in minerals, and both $Fe^{2+}$ and $Fe^{3+}$ can occur

in multiple populations of four-, five- and six-fold coordination in various silicate glasses and melts at one bar, with average coordination numbers often near five.

Because the density and compressibility of a silicate melt are largely determined from the geometrical packing and coordination of its network-forming ions, the capacity of $Fe^{2+}$ and $Fe^{3+}$to shift coordination affects the volumetric properties of iron-bearing liquids. Density measurements performed in air at one bar, using the double-bob Archimedean method, have documented that the partial molar volume of $Fe_2O_3$ in silicate melts is strongly dependent on the average $Fe^{3+}$ coordination number (e.g., Dingwell et al., 1988; Liu and Lange, 2006). Similarly, the partial molar volume of the $TiO_2$ component has also been shown to vary systematically with $Ti^{4+}$ coordination change (Lange and Carmichael, 1987; Dingwell, 1992; Liu et al., 2001). In contrast, on the basis of numerous density measurements performed in air on multicomponent silicate liquids (e.g., Bockris, 1956; Stein et al., 1986; Lange and Carmichael, 1987; Lange, 1996, 1997), the other major element oxide components in magmatic liquids (i.e., $SiO_2$-$Al_2O_3$-MgO-CaO-$Na_2O$-$K_2O$) display no evidence that their partial molar volumes vary with composition, at least for liquids that are not peraluminous and where $X_i \leq 0.5$ for all oxide components except $SiO_2$ (Lange, 1997).

To date, $Fe_2O_3$ and $TiO_2$ are the only two major-element components that have been documented to deviate from an ideal mixing model to describe the molar volume of magmatic liquids. However, given the abundant multi-spectroscopic evidence that $Fe^{2+}$ occupies both a network-former and network-modifier role in several silicate liquid compositions (e.g., Jackson et al., 2005and references therein), the FeO component may

also have a partial molar volume that varies systematically with $Fe^{2+}$ coordination and thus composition.

Currently, published double-bob density measurements on iron-bearing liquids under reducing conditions are all restricted to liquids along the FeO-$SiO_2$ binary (60-88 mol% FeO). Shiraishi et al. (1978) and Mo et al. (1982) used iron bobs and crucibles in an Ar atmosphere, whereas Thomas et al. (2012) used molybdenum bobs and crucible in a stream of 1%CO-99%Ar. In all cases, the derived partial molar volume of FeO at 1673 K ranges from 13.8 to 16.0$cm^3$/mol, which is ~15-33% larger than that for crystalline FeO (wüstite; 6-coordinated $Fe^{2+}$) at room temperature (12.06 $cm^3$/mol; Smyth and McCormick, 1995). In contrast, Lange (1997) reports a partial molar volume of MgO in multicomponent silicate liquids at 1723 K of 11.86 (± 0.07) $cm^3$/mol, which is similar to that derived for crystalline MgO (periclase; 6-coordinated $Mg^{2+}$) at room temperature (11.24 $cm^3$/mol; Smyth and McCormick, 1995). The relatively large $\overline{V}_{FeO}$ in the FeO-$SiO_2$liquids is consistent with the high-temperature X-ray absorption spectroscopic results from Jackson et al. (1993), which indicate an average $Fe^{2+}$ coordination closer to four than six in fayalite liquid.

In this study, the density and compressibility of four CaO-FeO-$SiO_2$ liquids were measured to test whether the partial molar volume and compressibility of the FeO component vary as a systematic function of composition. In addition, the density and compressibility of hedenbergite ($CaFeSi_2O_6$) liquid was measured, as there is EXAFS data indicating an average $Fe^{2+}$ coordination of ~4.3 in the glass (Rossano et al., 2000).

# Experimental Methods

## Sample synthesis and composition

Each of the five CaO-FeO-$SiO_2$ (CFS) samples was synthesized in large quantities (200 g) by mixing appropriate proportions of reagent grade $CaCO_3$, $Fe_2O_3$ and $SiO_2$. Their compositions were chosen to test the effect of varying Ca/Si ratios on the partial molar volume and compressibility of FeO. Each powder was slowly dried, de-carbonated, and then fused in air at 1723 to 1923 K. The samples were then quenched, ground into powder and then re-fused. This procedure was repeated three times in total to ensure homogeneity. Two 200-g batches of hedenbergite were synthesized because most of the first batch was lost during the density measurements (discussed below). The second sample is the one used for the successful density and sound speed measurements.

Of the five CFS compositions, only the hedenbergite liquid quenched to a glass in air. The compositions of the hedenbergite glass samples were analyzed with a Cameca SX-100 electron microprobe at the University of Michigan (Table 2.1a). The analyses show that the synthesized samples are close to the ideal composition. Attempts to analyze the four iron-rich CFS samples by ICP-MS and XRF at Activation Laboratories (Ontario) led to low totals (less than 90%) and inaccurate analyses, presumably because available standards were not suitable for samples with 40 mol% FeO. Therefore, given the close match between the analyzed hedenbergite glass and its ideal (nominal) composition, the nominal compositions were used for the four CFS samples that did not quench to a glass. All compositions are listed in Table 2.1b and plotted in a ternary diagram (Fig. 2.1a). For each composition, the gram formula weight (g.f.w.=$X_iM_i$) is

tabulated in Table 2.1b as well, where $X_i$, $M_i$ are the mole fraction and molecular weight of each oxide component respectively.

**High-temperature measurements of liquid density**

High-temperature density measurements were made on the five CFS liquids using the double-bob Archimedean method, described in detail in Lange and Carmicheal (1987) and Liu and Lange (2001) for double-bob density measurements in air. In this study, density measurements were made in a stream of 1%CO-99%Ar gas, following similar procedures as those employed by Liu and Lange (2003) in their density measurements on carbonate liquids in a stream of $CO_2$ gas. To prevent iron loss from the sample to platinum under these reducing conditions, the crucibles and bobs were synthesized from molybdenum metal, which undergoes limited solid solution with metallic iron compared to platinum. Rivers and Carmichael (1987) analyzed several iron-bearing samples before and after being held in molybdenum crucibles under a stream of 1%CO-99%Ar gas for >24 hours at temperatures >1673 K and detected minimal iron loss.

For each experiment, ~75 g of sample powder was loaded into a Mo crucible (8.0 cm long x 4.0 cm O.D.), which was placed in a Deltech vertical tube furnace in a stream of 1%CO-99%Ar gas. The 75 g of sample was divided into four batches and added step-wise. After each batch was added to the molybdenum crucible, the sample was heated to 1673 K and held in a stream of 1%CO-99%Ar gas for an hour, which converted most of the ferric iron to ferrous iron. This was repeated four times until all 75 g of reduced sample were in the Mo crucible. A similar procedure was followed for fayalite liquid prior to density measurements in Thomas et al. (2012), and Mössbauer spectroscopy confirmed that $Fe^{3+}$ concentrations are low (< 5% of the total iron), consistent with

saturation of the experimental melts with molybdenum metal and oxygen fugacity conditions below the Mo-$MoO_2$ buffer (Chase, 1998). Because the activity of $MoO_2$ in the melt is less than one, and because the melts are not saturated with metallic iron, the oxygen fugacity of the experimental liquids at each temperature of measurement is constrained to be between the Mo-$MoO_2$ and Fe-FeO buffers (~4.3 log units below the Ni-NiO buffer). At this redox condition, the model of Kress and Carmichael (1989), calibrated on CaO-FeO-$SiO_2$ liquids, predicts 5 ± 1% of the total iron as $Fe^{3+}$.

The following procedure is followed to make a liquid density measurement. An electronic balance with a precision of ± 0.0001 g is mounted on an aluminum platform above the furnace to measure the weights of the molybdenum bobs before and after immersion into the sample liquids. A molybdenum bob is suspended from the balance into the vertical tube furnace, just above the sample liquid, and its mass is measured. The furnace and crucible are then raised (using a hydraulic jack) until the lower tip of the bob makes contact with the surface of the liquid. The contact causes a deflection on the balance and the point at which this occurs on the micrometer gauge is noted. Then the crucible and liquid are raised a measured distance (e.g., 2.0 cm) to submerge the Mo bob and its mass is measured on the balance. The difference in the mass of the Mo bob before and after submersion gives the buoyancy, *B(T)*, at the temperature of measurement. This procedure is repeated for different bobs, with each bob only used once at each temperature (and removed and cleaned between measurements). By using two molybdenum bobs of different mass (~19.5 and ~6.5 g), but with identical stem diameter (1 mm), the effect of surface tension on the stem is eliminated. The density of the liquid is calculated from the following equation:

$$\rho(T) = \frac{B_L(T) - B_S(T)}{V_L(T) - V_S(T)} \quad (1)$$

where $B_L(T)$ and $B_S(T)$ are the buoyancy of the large and small bobs, respectively, and $V_L(T)$ and $V_S(T)$ are the immersed volume of the large and small bob, respectively. To calculate the immersed volume of the Mo bobs as a function of temperature, it is necessary to know the density (10.22 g/cm$^3$ at 298 K) and thermal expansion (Gray, 1972) of molybdenum metal. Two bobs (one large and one small) allow a single density measurement to be made, whereas four bobs (two large and two small) allow four density determinations.

The accuracy of the Mo double-bob method was evaluated by measuring the density of NaCl liquid at 1206 and 1173K (Table 2.2, Fig. 2.2). Our results are consistent with previous density measurements on NaCl liquid using the Pt double-bob method (Stein et al., 1986; Lange and Carmichael, 1987; Liu and Lange, 2001).

Density measurements on the four iron-rich CFS liquids could only be made over a limited high-temperature interval for each liquid, because at lower temperatures the bobs seemed to resist immersion and they tended to slide sideways and stick to the crucible wall. Our hypothesis is that this problem was caused by high melt viscosity and high melt surface tension. In contrast, the problem with hedenbergite liquid was different; this fluid liquid strongly wetted the crucible wall (indicating a low liquid surface tension) and had a tendency to "crawl" out of the crucible, which prevented measurements from being made at temperatures > 1573 K.

**Surface tension measurements**

The double-bob Archimedean method not only allows density to be measured, but also permits the surface tension of the liquid samples on the metallic bob stem to be derived. During immersion of each bob in the melt, the force of the liquid surface tension on the stem "pulls" on the bob; this causes the mass of the bob, while it is immersed in the liquid, to appear larger than its true value, which in turn makes the buoyancy measurement smaller than its true value. As a consequence, if a single bob is used to measure melt density, the effect of surface tension must be added to the buoyancy measurement in order to calculate density:

$$\rho(T) = \frac{B(T) + S(T)}{V(T)} \tag{2}$$

where $B(T)$ is the buoyancy of the single bob, $S(T)$ is the effect of surface tension on the buoyancy measurement, and $V(T)$ is the immersed volume of the single bob. Equation (2) can be rearranged to allow $S(T)$ to be calculated for each bob that was used to measure the densities of the CFS liquids by the double-bob method:

$$S(T) = \rho^{liq}(T) V^{bob}(T) - B(T) \tag{3}$$

The surface tension, $\gamma$ (N/m), can be calculated from *S(T)* with the following equation (Janz and Lorenz, 1960):

$$\gamma(T) = \frac{S(T)}{\pi d} g \tag{4}$$

where *g* is the gravitational acceleration, and *d* is the diameter of the stem.

**Sound speed measurements**

Sound speeds were measured in each sample liquid at one bar with a frequency sweep ultrasonic interferometer, developed and designed by Ai and Lange (2004a, b). The instrument includes an upper and lower molybdenum rod in the interferometric circuit, and all experiments were run in a reducing environment in a stream of 1%CO-99%Ar gas. The lower buffer rod serves as the crucible for the melt samples. Approximately 4-5 g of each sample was placed in the crucible to ensure a melt thickness > 3mm.

For each temperature of measurement, a wide-band acoustic pulse, which spans 1-2MHz,travels down the molybdenum upper buffer rod (1.91 cm diameter and 40 cm long) to the rod-melt interface, at which point part is propagated into the liquid and part is reflected back up the upper rod. The acoustic pulse that is transmitted through the liquid reflects off the polished base of the crucible and two mirror reflections are returned up the buffer rod. The shape of the mirror reflections relative to the shape of the original transmitted signal allows an immediate assessment of whether the measurement was relaxed. If the mirror reflection viewed on the oscilloscope show distortion, the measurement is not relaxed.

The returned mirror reflections are delivered to the data acquisition system for signal processing, where a Fourier transform is performed, which allows the returned signal to be evaluated as a periodic function of frequency, $\Delta f$, from which the sound speed is measured from the relation: $\Delta f = c/2S$, where $S$ is melt thickness. For each temperature and centered frequency, measurements are made at two or three different rod positions to get accurate measurement of relative thickness ($\Delta S = S_1 - S_2$) by a micrometer

(resolution 0.001mm), which is mounted on the upper buffer rod. Because sound speed is independent of melt thickness, the relation can be expressed as:

$$c = \left| \frac{2\Delta S}{\Delta f_2^{-1} - \Delta f_1^{-1}} \right| . \quad (5)$$

# Results

## High-temperature liquid density and molar volumes

The high-temperature density data for the five CaO-FeO-$SiO_2$ liquids are listed in Table 2.3 and plotted in Figure 2.3. The standard deviations on replicated density measurements at the same temperature on the same liquid range from 0.19 to 0.74%. These density data were converted to molar volume by using the following equation

$$V(T) = g.f.w./\rho(T) \quad (6)$$

where g.f.w. is the gram formula weight (Table 2.1a) and $\rho(T)$ is the liquid density. Note that in Tables 2.1 and 2.3 all iron is treated as $Fe^{2+}$, whereas the effect of treating 4% of the total iron as $Fe^{3+}$ is discussed below.

## Modeling molar volumes

The liquid volume data for the five CaO-FeO-$SiO_2$ liquids in Table 2.3 were combined with density data from the literature on $K_2O$-$Na_2O$-CaO-MgO-$Al_2O_3$-$SiO_2$ liquids (Bockris et al., 1956; Stein et al., 1986; Lange and Carmichael, 1987; Lange, 1996, 1997) to calibrate the following linear volume equation:

$$V^{liq}(X,T) = \sum X_i \left[ \overline{V}_{i,T_{ref}} + \frac{\partial \overline{V}_i}{\partial T}(T - T_{ref}) \right] \quad (7)$$

where $X_i$ is the mole fraction of each oxide component, $\overline{V}_{i,T_{ref}}$ is the partial molar volume of each oxide component at a reference temperature ($T_{ref}$ = 1723 K), and $\partial \overline{V}_i / \partial T$ is the

partial molar thermal expansivity of each oxide component. The results of this regression led to a poor fit to the data (Fig. 4a), outside experimental error, in contrast to a regression of the same data set minus the CaO-FeO-$SiO_2$ liquids (Lange, 1997). Note that because of the limited temperature interval over which density measurements could be made on the CFS liquids, the fitted value for $\partial\overline{V}_{FeO}/\partial T$ could not be resolved and was not included in any regression.

To test whether the poor fit to Eqn. 7 reflects a systematic variation in $\overline{V}_{FeO}$ with melt composition, the molar volumes of each individual liquid were added singly to the FeO-free data set in a series of regressions of Eqn. 7. The results are presented in Table 2.4a and Fig. 2.4b, and the fitted $\overline{V}_{FeO}$ values at 1723 K for each sample display a strong linear correlation with $X_{CaO}$ (Fig. 2.5). Extrapolation to melt compositions with 0 and 40 mol% CaO, respectively, leads to estimated $\overline{V}_{FeO}$ values of ~12 and ~17 $cm^3$/mol, respectively. The former is similar to that for crystalline FeO (wüstite; 6-fold $Fe^{2+}$) and corresponds to a liquid composition of 40%FeO-60%$SiO_2$. In contrast the much larger $\overline{V}_{FeO}$ of ~17 $cm^3$/mol corresponds to a composition that is 66.7%$CaFeO_2$-33.3% $SiO_2$. Since $Fe^{2+}$ is in 4-fold coordination in crystalline $CaFeO_2$ (Tassel et al., 2009), it is possible that the larger value of ~17 $cm^3$/mol may represent $\overline{V}_{FeO}$ with $Fe^{2+}$ in 4-fold coordination.

To test this hypothesis, the four iron-rich CFS liquids were recast in terms of the $CaFeO_2$-FeO-$SiO_2$ components, where all available CaO was assigned to FeO to make the $CaFeO_2$ component (Table 2.1c, Fig. 2.1b). The gram formula weight of these four liquids was recalculated (Table 2.1c), along with their molar volumes (Table 2.3) and these liquids were combined with those in the literature to test whether an ideal mixing

model works with these revised components. A regression that includes all four $CaFeO_2$-FeO-$SiO_2$ liquids (excluding hedenbergite), along with those from the literature for $K_2O$-$Na_2O$-CaO-MgO-$Al_2O_3$-$SiO_2$ liquids, recovers all measurements within experimental error (Fig. 2.4c). The results are presented in Table 2.4b and lead to a fitted $\overline{V}_{FeO}$ value of 12.11 (± 0.16) $cm^3$/mol and a fitted $\overline{V}_{CaFeO_2}$ value of 33.82 (± .13) $cm^3$/mol. When the fitted value for $\overline{V}_{CaO}$ in Table 2.4b is subtracted from that for $\overline{V}_{CaFeO_2}$, the derived value for $\overline{V}_{FeO}$ in the $CaFeO_2$ component is 17.10 (± 0.21) $cm^3$/mol. Note that the effect of treating 4% of the total iron as $Fe^{3+}$, and assuming that the partial molar volume of the $Fe_2O_3$ component is 41.5 $cm^3$/mol (Liu and Lange, 2006), leads to a fitted value for $\overline{V}_{FeO}$ of 11.9 vs. 12.1 $cm^3$/mol. Because this difference is relatively small, all iron is treated as $Fe^{2+}$ for simplicity.

Hedenbergite liquid was not included in the regression because it has equal abundance of CaO and FeO and after assigning all CaO to FeO to form the $CaFeO_2$ component there is no remaining FeO component. This necessarily leads to a $\overline{V}_{FeO}$ value of ~17 $cm^3$/mol in hedenbergite liquid, which is different from the value of ~15.5 $cm^3$/mol derived from the fit to individual liquids (Table 2.4a). Therefore, the simple rule of assigning all CaO to FeO to form the $CaFeO_2$ component is not always appropriate, and it appears that the FeO component in hedenbergite liquid is split between the $^{[6]}FeO$ and $Ca^{[4]}FeO_2$ components, which is discussed more fully in the discussion section.

**High-temperature surface tension data**

The surface tension of the CaO-FeO-$SiO_2$ liquids on molybdenum metal was derived from the density measurements, using Eqns (3) and (4). The values are listed in Table 2.3 and plotted in Fig. 2.6 as a function of temperature. The four iron-rich CFS liquids have surface tension values that range between 0.3-0.6 N/m, three times larger the range of those derived for carbonate liquids on platinum metal (0.1-0.2 N/m; Liu and Lange, 2003), and they show a negative temperature dependence. In contrast, the surface tension of hedenbergite liquid on molybdenum metal is remarkably low, with values that average to ~0 N/m (Table 2.3; Fig. 2.6), which explains why this liquid composition strongly wetted the molybdenum metal and "crawled" out of the crucible over time.

For the four iron-rich CFS liquids, the surface tension values are sufficiently large that if the single-bob method had been applied to measure density, the results would have been underestimated by 2-3% if the large bobs (~19.5 g) had been used and by 6-9% if the small bobs (~6.5 g) had been used. This result underscores the necessity of the double-bob method to obtain accurate measurements of melt density by eliminating the effect of surface tension.

**High-temperature sound speeds**

Thirty-four sound speed measurements are reported in Table 2.5 for the five CFS liquids at centered frequencies of 4.5 and 5.5 MHz. Only relaxed data are presented, where the mirror reflections showed no distortion and there is no frequency dependence to the sound speed. Measurements were made at three or four temperatures for each liquid and spanned intervals of 136 to 308 degrees. Because the sound speed measurements were performed more quickly (< 4 hours) than the double-bob density measurements (>2 days), the problem with hedenbergite liquid crawling out of the

crucible was minimal and measurements could be made to ≤ 1879 K. Experimental errors are typically ≤ 30 m/s on the basis of reproducibility, when a sample is re-loaded and measured weeks apart. A plot of the sound speed measurements as a function of temperature is presented for the five liquids in Figure 2.7. For each sample, sound speed decreases with temperature.

**Modeling sound speeds**

Although sound speed is not an extensive thermodynamic property, it can be empirically modeled as a linear function of composition and temperature:

$$c^{liq}(X,T) = \sum X_i \left( c_{i,1723K} + \frac{\partial c_i}{\partial T}(T - 1723K) \right) \quad (8)$$

where $X_i$ is the mole fraction of each oxide component, $c_i$ is the "partial molar" sound speed of each oxide component, and $\partial c_i / \partial T$ is the temperature dependence of the sound speed. The sound speed data obtained for the five CaO-FeO-$SiO_2$ liquids in this study were combined with sound speed data in the literature for CaO-MgO-$Al_2O_3$-$SiO_2$ liquids (Rivers and Carmichael, 1987; Secco et al., 1991; Webb and Courtial, 1996; Ai and Lange, 2008) in a regression of Eqn. 8. The results lead to large residuals, outside experimental error, in contrast to a regression of the same data set minus the CaO-FeO-$SiO_2$ liquids (Ai and Lange, 2008). To test whether this reflects a systematic variation in $c_{FeO}$ with composition, the sound speeds of each individual liquid were added singly to the FeO-free data set in a series of regressions of Eqn. 8. The results are presented in Table 2.6a and the fitted $c_{FeO}$ values at 1723 K for each sample display a systematic variation with $X_{CaO}$, similar to that seen for $\overline{V}_{FeO}$ (Fig. 2.5). This behavior suggests that

recasting the components in terms of $CaFeO_2$-FeO-$SiO_2$ may permit a more successful fit of the linear model in Eqn. 8.

Following what was done for molar volume, a regression of Eqn. 8 that includes the sound speeds of all four $CaFeO_2$-FeO-$SiO_2$ liquids (excluding hedenbergite), along with those from the literature for CaO-MgO-$Al_2O_3$-$SiO_2$, recovers the sound speed measurements within experimental error. The results are presented in Table 2.6b and lead to a fitted $c_{FeO}$ value of 2535(± 48) m/s and a fitted $c_{CaFeO_2}$ value of 3093 (± 34) m/s. Note that subtracting the fitted $c_{CaO}$ value from the $c_{CaFeO_2}$ value leads to a derived value for $c_{FeO}$ in the $CaFeO_2$ component that is negative (-1124 m/s). Because there is no theoretical reason for the sound speeds to either add linearly in composition or vary linearly in temperature, it is preferable to model the isothermal compressibility ($\beta_T$) of these CFS liquids.

**Modeling isothermal compressibility ($\beta_T$)**

The sound speed and density data compiled in Table 2.5 were used to calculate the adiabatic compressibility from the relation, $\beta_S = 1/\rho c^2$. The adiabatic compressibility is converted to isothermal compressibility from the relation:

$$\beta_T = \beta_S + \frac{TV_T\alpha^2}{Cp} \qquad (9)$$

where $T$ is temperature (K), $V_T$ is the molar volume at temperature T, $\alpha$ is the coefficient of thermal expansion and $Cp$ is the molar heat capacity. The $V_T$ and $\alpha$ terms were calculated from the results of this study (Table 2.4b). For the calculation of $\alpha = (1/V)(\partial V/\partial T)$, $\partial \overline{V}_i/\partial T$ for the FeO component was approximated from the average

of the fitted $\partial \overline{V}_i / \partial T$ terms for MgO and CaO in Table 2.4b (~ .0035 $cm^3$/mol-K). The *Cp* term was calculated from the model of Lange and Navrotsky (1992) for multicomponent silicate liquids. The difference between $\beta_S$ and $\beta_T$ ranges from 0.7 to 2.7% of the value for $\beta_S$ in the CFS liquids. The propagated maximum uncertainty in the $\beta_T$ value is ~3.2%.

Rivers and Carmichael (1987) showed that for an ideal solution, $\beta_T$ varies as a linear function of the *volume fraction* of each oxide component:

$$\beta_T(X) = \sum X_i \frac{\overline{V}_{i,T}}{V_T} \overline{\beta}_{i,T} \tag{10}$$

where $X_i$ is the mole fraction of each component i, $V_{i,T}$ is the partial molar volume of each oxide component at temperature T, $V_T$ is the molar volume of the liquid at temperature T and $\overline{\beta}_{i,T}$ is the partial molar compressibility of each oxide component at temperature T. The model equation can be expanded to include a linear dependence on temperature:

$$\beta_T(X,T) = \sum X_i \frac{\overline{V}_{i,T}}{V_T} \left( \overline{\beta}_{i,1723} + \frac{\partial \overline{\beta}_i}{\partial T} (T - 1723K) \right) \tag{11}$$

The data from both this study (Table 2.5) and from the literature (Rivers and Carmichael, 1987; Secco et al., 1991; Webb and Courtial, 1996; Ai and Lange, 2008) were used in a regression of Eqn. 11. Once again, the results of this regression lead to a poor fit to the data, with residuals that exceed experimental error (Fig. 2.8a), compared to a regression of the same data set that excludes the CFS liquids (Ai and Lange, 2008). When the CFS liquids are added singly in a series of regressions to Eqn. 11, the fitted values for $\overline{\beta}_{FeO}$ at 1723 K vary systematically with $X_{CaO}$ (Fig. 2.9), following the same pattern as that

displayed for $\overline{V}_{FeO}$ in Fig. 2.5. The results from these individual regressions are tabulated in Table 2.7a and the residuals are shown in Fig. 2.8b.

The linear behavior in Figure 2.9 suggests that recasting the components in terms of $CaFeO_2$-FeO-$SiO_2$ may permit a more successful fit of the ideal model in Eqn. 11 (Fig. 2.8c). The results of that regression are presented in Table 2.7b and Figure 2.8c at 1723 K, and lead to a fitted $\overline{\beta}_{FeO}$ value of 3.46 (± 0.30) x $10^{-2}$ $GPa^{-1}$ and a fitted $\overline{\beta}_{CaFeO_2}$ value of 2.84 (± .08) x $10^{-2}$ $GPa^{-1}$. When the fitted value for $\overline{\beta}_{CaO}$ is subtracted from that for $\overline{\beta}_{CaFeO_2}$, using Eqn. 11 on the basis of volume fractions, the derived value for $\overline{\beta}_{FeO}$ in the $CaFeO_2$ component is 7.05 (± 0.35) x $10^{-2}$ $GPa^{-1}$, which is similar that for $SiO_2$ (7.13 ± 0.05 x $10^{-2}$ $GPa^{-1}$).

**Modeling** $(\partial V/\partial P)_T$

A final regression equation is presented for $(\partial V/\partial P)_T$, the derivative of volume with pressure at constant T, which is defined as $(\partial V/\partial P)_T = -V_T\beta_T$. It can be calculated for each experimental liquid from the density (molar volume) and isothermal compressibility values tabulated in Table 2.5. For an ideal solution, $(\partial V/\partial P)_T$ varies as a linear function of composition:

$$\left(\frac{\partial V}{\partial P}\right)_T = \sum X_i \left(\frac{\partial \overline{V}_i}{\partial P}\right)_T \qquad (12)$$

Following Rivers and Carmichael (1987) and Kress and Carmichael (1991), the model can be expanded to include a linear dependence on temperature:

$$\left(\frac{\partial V}{\partial P}\right)_T = \sum X_i \left(\frac{\partial \overline{V}_{i,1723}}{\partial P} + \frac{\partial^2 \overline{V}_i}{\partial P \partial T}(T - 1723K)\right) \qquad (13)$$

Again, the data from this study (Table 2.5), using the components CaO-FeO-$SiO_2$, were combined with those from the literature (Rivers and Carmichael, 1987; Secco et al., 1991; Webb and Courtial, 1996; Ai and Lange, 2008) in a regression of Eqn. 13. The results lead to a poor fit to the data, with residuals in excess of experimental errors. To examine how $\partial\overline{V}_{FeO}/\partial P$ varies between the individual samples, each CFS liquid was added singly to the FeO-free data set in a series of regressions of Eqn. 13. The results are presented in Table 2.8a and show that fitted values for $\partial\overline{V}_{FeO}/\partial P$ vary systematically with $X_{CaO}$, as seen for $\overline{V}_{FeO}$, $c_{FeO}$ and $\overline{\beta}_{FeO}$. Therefore, the components of the CFS liquids were recast as $CaFeO_2$-FeO-$SiO_2$ and another regression of Eqn. 13 was performed (excluding only hedenbergite liquid). The results of that regression are presented in Table 2.8b and, at 1723 K, lead to a fitted $\partial\overline{V}_{FeO}/\partial P$ value of -0.263 (± 0.015) x $10^{-4}$ $cm^3bar^{-1}$ and a fitted $\partial\overline{V}_{CaFeO_2}/\partial P$ value of -0.954 (± 0.001) x $10^{-4}$ $cm^3$ $bar^{-1}$. When the fitted value for $\partial\overline{V}_{CaO}/\partial P$ is subtracted from that for $\partial\overline{V}_{CaFeO_2}/\partial P$, the derived value for $\partial\overline{V}_{FeO}/\partial P$ in the $CaFeO_2$ component is -1.201 (± 0.0015).

## Discussion

### A linear correlation between $\overline{V}_{FeO}$ and $Fe^{2+}$ coordination?

The success of the ideal mixing model for volume when the components are recast as $CaFeO_2$-FeO-$SiO_2$ raises the question of whether the fitted liquid values for $\overline{V}_{FeO}$ and $\overline{V}_{CaFeO_2}$ represent $Fe^{2+}$ in different coordination environments. The value for $\overline{V}_{FeO}$ of 12.11 $cm^3$/mole (Table 2.4b) is notably similar to the volume of crystalline FeO

(wüstite) at 298 K (12.06 $cm^3$/mol; Table 2.9), where $Fe^{2+}$ is 6-fold coordinated. A similarity is also seen when fitted liquid values for $\overline{V}_{MgO}$ and $\overline{V}_{CaO}$(11.86 and 16.72 $cm^3$/mol, respectively; Table 2.4b) are compared to those for periclase and lime (11.24 and 16.76 $cm^3$/mol, respectively, Table 2.9), where $Mg^{2+}$ and $Ca^{2+}$are each 6-fold coordinated.

A comparison can also be made between the fitted liquid value for $\overline{V}_{CaFeO_2}$ (33.82 $cm^3$/mol; Table 2.4b) and its crystalline equivalent (30.64 $cm^3$/mol; Tassel et al., 2009), where the liquid volume is ~10% larger. This 10% contrast between liquid and crystalline volume is also seen between $\overline{V}_{CaSiO_3}$ (calculated from Table 2.4b) and wollastonite, where there is no change in the coordination of $Ca^{2+}$ or $Si^{4+}$ between crystal and liquid (Waseda and Toguri, 1990). Crystalline $CaFeO_2$, which contains $Fe^{2+}$ in a distorted square-planar (approaching tetrahedral) 4-fold coordination, is a new material that has been characterized through neutron diffraction, synchrotron X-ray diffraction, Mössbauer spectroscopy, XAS experiments and first-principle DFT (density functional theory) calculations (Tassel et al., 2009). The derived $\overline{V}_{FeO}$ value of 17.1 $cm^3$/mol from the liquid $CaFeO_2$ component is ~42% larger than the volume of crystalline FeO (wüstite). This contrast in volume is of the same magnitude as that between liquid $\overline{V}_{Al_2O_3}$ (37.42 $cm^3$/mol; Table 2.4b), where $Al^{3+}$ is in tetrahedral coordination, and crystalline $Al_2O_3$ (corundum; 25.58 $cm^3$/mol; Table 2.9), where $Al^{3+}$ is in octahedral coordination.

Collectively, these comparisons between liquid and crystalline volumes support the postulate that the liquid $\overline{V}_{FeO}$ value of 12.1 $cm^3$/mol is representative of six-

coordinated $Fe^{2+}$, whereas the derived liquid $\overline{V}_{FeO}$ value of 17.1 $cm^3$/mol (in the $CaFeO_2$ component) is representative of four-coordinated $Fe^{2+}$. These two end-member $\overline{V}_{FeO}$ values can be used to develop a simple equation to calculate the coordination number of $Fe^{2+}$, if a linear relationship is assumed:

$$CN = 10.85 - 0.401(\overline{V}_{FeO,1723K}). \quad (14)$$

Equation 14 leads to average $Fe^{2+}$ coordination numbers for the five CFS liquids that range from 5.2 to 4.6 (Table 2.4a).This includes a $Fe^{2+}$ coordination number of 4.7 in hedenbergite liquid, which is similar to the value of 4.3 derived from an EXAFS study on hedenbergite glass (Rossano et al., 2000). The range of calculated $Fe^{2+}$ coordination numbers in the CFS liquids (5.2-4.6) is consistent with a recent multi-spectroscopic study (Mössbauer, XANES, EXAFS, infrared, and magnetic circular dichroism) on several $Fe^{2+}$-bearing multicomponent silicate glasses, spanning a wide range of composition, where it was found that $Fe^{2+}$ predominantly occupies 5- and 4-coordinated sites, with small amounts of 6-coordinated sites possible (Jackson et al., 2005). For the CFS liquids, it is unclear whether the average $Fe^{2+}$ coordination number reflects mixing of 4- and 6-coordinated sites (mixing of $CaFeO_2$ and FeO components), without any 5-coordinated sites, or all three populations. The spectroscopic evidence appears to support the occurrence of all three $Fe^{2+}$ coordination sites.

**A decrease in $Fe^{2+}$ coordination with decreasing polymerization**

The evidence cited above supports the conclusion that the trend of increasing $\overline{V}_{FeO}$ with increasing CaO content (Fig. 2.5) reflects a composition-induced decrease in $Fe^{2+}$ coordination. This is similar to the pattern seen for fitted values of $\overline{V}_{TiO_2}$ in various

$Na_2O$- and $K_2O$-bearing silicate liquids, where average $Ti^{4+}$coordination decreases (end-members are 6- and 4-fold) as $Na_2O$ and $K_2O$ concentrations increase (Liu and Lange, 2001). To explain this pattern, Liu et al. (2007) suggested that $Ti^{4+}$ coordination in alkali silicate melts might be controlled by the relative abundances of $Q^3$ (tetrahedra with three bridging oxygens) and $Q^4$(tetrahedral with four bridging oxygens) species. This model is adapted from the mechanism first proposed by Xue et al. (1991) where $^{[5]}$Si is formed from $^{[4]}$Si by consumption of non-bridging oxygens (NBOs) in partially polymerized melts, and predicts that $^{[5]}$Si species are maximized (at pressure) when $Q^3$ and $Q^4$ species are equally abundant. To examine whether this model may have applicability to the CFS liquids, the calculated $Fe^{2+}$ coordination is plotted in Fig. 2.10 as a function of molar Ca/(Si+Fe), which is a proxy for NBO/T, if Fe is considered a network former (T). This is a reasonable assumption for average $Fe^{2+}$ coordination numbers between four and five, the case for most of the CFS liquids. Nonetheless, from the results in Fig. 2.10, it does not appear that five-coordinated $Fe^{2+}$ is maximized when $Q^3$ and $Q^4$ species are equally abundant; instead the average coordination number steadily increases with depolymerization. Another possibility is that increasing Ca/Si increases the basicity of the melt (e.g., Duffy, 1989, 1996), which changes the bond valence variation around the oxygen anions and may, in turn, influence the optimal cation coordination number for $Fe^{2+}$. Regardless of the mechanism, the results from this study provide another example where depolymerization promotes lower average coordination numbers for cations occupying multiple coordination sites.

**Systematic variation in $\overline{\beta}_{T,FeO}$ with $\overline{V}_{FeO}$ (and $Fe^{2+}$ coordination)**

One of the most intriguing results of this study is the strong linear and positive correlation between individually fitted $\overline{\beta}_{T,FeO}$ values (Table 2.7a) and individually fitted $\overline{V}_{FeO}$ values (Table 2.4a) for the five CFS liquids, which is illustrated in Fig. 2.11. This is not a direct result of the relationship between density and compressibility, given in Eqn. 9, because the *opposite* behavior is seen in the $Na_2O$-$TiO_2$-$SiO_2$ system, where $\overline{\beta}_{T,TiO_2}$ and $\overline{V}_{TiO_2}$ are inversely correlated (Liu et al., 2007). The positive linear correlation in Fig. 2.11 provides evidence that the fitted liquid value for $\overline{\beta}_{T,FeO}$ ($3.5 \times 10^{-2}$ $GPa^{-1}$) represents $Fe^{2+}$ in 6-fold coordination, whereas the derived value of $\overline{\beta}_{T,FeO}$ in the $CaFeO_2$ component ($7.1 \times 10^{-2}$ $GPa^{-1}$) represents $Fe^{2+}$ in 4-fold coordination. The latter value is remarkably similar to the fitted values for both $\overline{\beta}_{T,SiO_2}$ ($7.1 \times 10^{-2}$ $GPa^{-1}$; Table 2.6b) and $\overline{\beta}_{T,TiO_2}$ ($6.6 \times 10^{-2}$ $GPa^{-1}$; Liu et al., 2007), where $Si^{4+}$ and $Ti^{4+}$ are both in 4-fold coordination.

Although the fitted $\overline{\beta}_{T,FeO}$ value for 6-coordinated $Fe^{2+}$ ($3.5 \times 10^{-2}$ $GPa^{-1}$) is smaller than that for 4-coordinated $Fe^{2+}$, it is significantly larger than that for $\overline{\beta}_{T,MgO}$ ($0.5 \times 10^{-2}$ $GPa^{-1}$). This result suggests that for silicate melts that contain 6-fold $Fe^{2+}$, although $\overline{V}_{FeO}$ has a similar value to $\overline{V}_{MgO}$ at one bar, it becomes smaller than $\overline{V}_{MgO}$ with increasing pressure. Conversely, for melts that contain 4- and 5-coordinated $Fe^{2+}$, $\overline{V}_{FeO}$ is larger than $\overline{V}_{MgO}$ at 1 bar, and despite higher compressibility values, $\overline{V}_{FeO}$ remains larger than $\overline{V}_{MgO}$ to depths $\leq$ 5GPa (irrespective of $K_0$' values employed in a 3rd-order Birch-Murnaghan equation of state). These results have implications for the pressure dependence of various Fe-Mg exchange reactions between minerals and magmatic melts.

The results of most partial melting experiments of lherzolite (e.g., Walter, 1998; Gudfinnsson and Presnall, 2000) show that $^{Fe\text{-}Mg}K_D$ mineral-liquid values show a slight increase with pressure, which suggests that the average $Fe^{2+}$ coordination in mantle-derived basalts may be closer to 5-fold than 6-fold. Density and sound speed measurements on basaltic liquids are needed to directly test what are the appropriate volumetric properties of the FeO component to apply.

## Acknowledgements

This research was supported by the National Science Foundation through award EAR-0855774.

Table 2.1a
Composition of Hedenbergite (wt%)

| Sample | $SiO_2$ | CaO | $Fe_2O_3$ | total |
|---|---|---|---|---|
| Hd-1 | 46.16 | 22.60 | 31.20 | 99.96 |
| Hd-2 | 45.68 | 22.40 | 31.93 | 100.01 |

Table 2.1b
Composition of samples (mol%)

| Sample | $SiO_2$ | CaO | FeO | g.f.w |
|---|---|---|---|---|
| CFS-1 | 44.00 | 16.00 | 40.00 | 64.15 |
| CFS-2 | 40.00 | 20.00 | 40.00 | 63.99 |
| CFS-3 | 36.00 | 24.00 | 40.00 | 63.83 |
| CFS-4 | 32.00 | 28.00 | 40.00 | 63.67 |
| Hd-1 | 49.19 | 25.80 | 25.02 | 61.99 |
| Hd-2 | 48.75 | 25.61 | 25.64 | 62.07 |

Table 2.1c
Re-normalized composition of samples (mol%)

| Sample | $SiO_2$ | FeO | $CaFeO_2$ | g.f.w |
|---|---|---|---|---|
| CFS-1 | 52.38 | 28.57 | 19.05 | 76.37 |
| CFS-2 | 50.00 | 25.00 | 25.00 | 79.98 |
| CFS-3 | 47.37 | 21.05 | 31.58 | 83.98 |
| CFS-4 | 44.44 | 16.67 | 38.89 | 88.43 |

Table 2.2
Density of molten NaCl using Mo crucibles and bobs

| Temperature (K) | density($g/cm^3$) |
|---|---|
| 1206 | 1.482 |
| 1206 | 1.481 |
| 1206 | 1.488 |
| 1206 | 1.487 |
| 1173 | 1.513 |

Table 2.3
Density, surface tension and volume of CFS liquids at high temperature

| Sample | T (K) | Density ($g/cm^3$) | $\gamma$(T) N/m | g.f.w.[1] | Vmeas[1] ($cm^3$/g.f.w) | g.f.w.[2] | Vmeas[2] ($cm^3$/g.f.w) |
|---|---|---|---|---|---|---|---|
| CFS-1 | 1722 | 3.198 | 0.37 | 64.15 | 20.06 | 76.37 | 23.88 |
| CFS-1 | 1722 | 3.195 | 0.35 | 64.15 | 20.08 | 76.37 | 23.90 |
| CFS-1 | 1722 | 3.175 | 0.32 | 64.15 | 20.20 | 76.37 | 24.05 |
| CFS-1 | 1722 | 3.173 | 0.31 | 64.15 | 20.22 | 76.37 | 24.07 |
| CFS-1 | 1813 | 3.181 | 0.30 | 64.15 | 20.17 | 76.37 | 24.01 |
| CFS-1 | 1813 | 3.193 | 0.37 | 64.15 | 20.09 | 76.37 | 23.92 |
| CFS-1 | 1813 | 3.176 | 0.29 | 64.15 | 20.20 | 76.37 | 24.04 |
| CFS-1 | 1813 | 3.187 | 0.36 | 64.15 | 20.13 | 76.37 | 23.96 |
| CFS-2 | 1721 | 3.193 | 0.29 | 63.99 | 20.04 | 79.98 | 25.05 |
| CFS-2 | 1721 | 3.185 | 0.28 | 63.99 | 20.09 | 79.98 | 25.11 |
| CFS-2 | 1594 | 3.229 | 0.40 | 63.99 | 19.82 | 79.98 | 24.77 |
| CFS-2 | 1594 | 3.247 | 0.50 | 63.99 | 19.71 | 79.98 | 24.63 |
| CFS-2 | 1594 | 3.207 | 0.35 | 63.99 | 19.95 | 79.98 | 24.94 |
| CFS-2 | 1594 | 3.224 | 0.46 | 63.99 | 19.85 | 79.98 | 24.81 |
| CFS-3 | 1727 | 3.238 | 0.27 | 63.83 | 19.71 | 83.98 | 25.94 |
| CFS-3 | 1727 | 3.210 | 0.21 | 63.83 | 19.88 | 83.98 | 26.16 |
| CFS-3 | 1727 | 3.269 | 0.45 | 63.83 | 19.52 | 83.98 | 25.69 |
| CFS-3 | 1727 | 3.240 | 0.39 | 63.83 | 19.70 | 83.98 | 25.92 |
| CFS-4 | 1721 | 3.272 | 0.53 | 63.67 | 19.46 | 88.43 | 27.02 |
| CFS-4 | 1721 | 3.254 | 0.49 | 63.67 | 19.57 | 88.43 | 27.17 |
| CFS-4 | 1721 | 3.277 | 0.55 | 63.67 | 19.43 | 88.43 | 26.98 |
| CFS-4 | 1721 | 3.259 | 0.52 | 63.67 | 19.54 | 88.43 | 27.13 |
| CFS-4 | 1813 | 3.237 | 0.38 | 63.67 | 19.67 | 88.43 | 27.32 |
| CFS-4 | 1813 | 3.248 | 0.44 | 63.67 | 19.60 | 88.43 | 27.22 |
| Hd | 1573 | 2.922 | -0.05 | 62.08 | 21.25 | - | - |
| Hd | 1573 | 2.938 | 0.05 | 62.08 | 21.13 | - | - |

g.f.w.[1] is from Table 1b, Vmeas[1] is calculated using g.f.w.[1]
g.f.w.[2] is for the adjusted components with $CaFeO_2$ from Table 1c, Vmeas[2] is calculated using g.f.w.[2]

Table 2.4a
Individually fitted partial molar volume of FeO in CFS liquids and other components at 1723K[a]

| Oxide component | $\overline{V_i}(1723K) \pm 1\sigma$ ($cm^3$/mol) | $\partial\overline{V_i}/\partial T \pm 1\sigma$ ($10^{-3}cm^3$/mol-K) | [b]coordination number of $Fe^{2+}$ |
|---|---|---|---|
| $SiO_2$ | 26.86 ± 0.03 | - | - |
| $Al_2O_3$ | 37.42 ± 0.09 | - | - |
| MgO | 11.86 ± 0.07 | 3.27 ± 0.17 | - |
| CaO | 16.72 ± 0.05 | 3.75 ± 0.12 | - |
| $Na_2O$ | 29.26 ± 0.07 | 7.68 ± 0.10 | - |
| $K_2O$ | 46.67 ± 0.10 | 12.08 ± 0.20 | - |
| FeO(CFS-1) | 14.06 ± 0.07 | - | 5.2 |
| FeO(CFS-2) | 14.72 ± 0.08 | - | 5.0 |
| FeO(CFS-3) | 15.05 ± 0.10 | - | 4.8 |
| FeO(CFS-4) | 15.59 ± 0.08 | - | 4.6 |
| FeO(Hd-2) | 15.47 ± 0.20 | - | 4.7 |

[a]Total of observations varies from 137 to 143; $R^2$ = 0.9999, and the average error varies from 0.21 to 0.22%.
[b]Calculated from Equation (14) in text

Table 2.4b
Linear regression of partial molar volume of each oxide for experimental liquids with new component $CaFeO_2$

| Oxide component | $\overline{V_i}(1723K) \pm 1\sigma$ ($cm^3$/mol) | $\partial\overline{V_i}/\partial T \pm 1\sigma$ ($10^{-3}cm^3$/mol-K) |
|---|---|---|
| $SiO_2$ | 26.86 ± 0.04 | - |
| $Al_2O_3$ | 37.42 ± 0.10 | - |
| MgO | 11.86 ± 0.08 | 3.27 ± 0.19 |
| CaO | 16.72 ± 0.06 | 3.74 ± 0.13 |
| $Na_2O$ | 29.26 ± 0.07 | 7.68 ± 0.11 |
| $K_2O$ | 46.67 ± 0.11 | 12.08 ± 0.22 |
| FeO | 12.11 ± 0.16 | - |
| $CaFeO_2$ | 33.82 ± 0.13 | 3.59 ± 0.91 |

[a]Total of 159 observations, $R^2$=0.9999, the average error is 0.24%

Table 2.5
Sound speed and compressibility data for CFS liquids

| Sample | $f$ (MHz) | T (K) | $c$ (m/s) | ρ* ($cm^3$/mol) | $\beta_s$ ($10^{-2}$ $GPa^{-1}$) | $\beta_T$ ($10^{-2}$ $GPa^{-1}$) | d$V$/d$P$ ($10^{-4}$$cm^3$/bar) |
|---|---|---|---|---|---|---|---|
| CFS-1 | 4.5 | 1879 | 2388 | 3.151 | 5.565 | 5.789 | -1.403 |
| CFS-1 | 5.5 | 1879 | 2388 | 3.151 | 5.565 | 5.789 | -1.403 |
| CFS-1 | 4.5 | 1813 | 2401 | 3.166 | 5.480 | 5.697 | -1.374 |
| CFS-1 | 5.5 | 1813 | 2406 | 3.166 | 5.457 | 5.674 | -1.369 |
| CFS-1 | 4.5 | 1744 | 2440 | 3.181 | 5.280 | 5.491 | -1.318 |
| CFS-1 | 5.5 | 1744 | 2453 | 3.181 | 5.224 | 5.435 | -1.305 |
| CFS-1 | 4.5 | 1656 | 2522 | 3.201 | 4.912 | 5.113 | -1.220 |
| CFS-1 | 5.5 | 1656 | 2457 | 3.201 | 5.175 | 5.376 | -1.283 |
| CFS-2 | 4.5 | 1749 | 2510 | 3.205 | 4.953 | 5.166 | -1.289 |
| CFS-2 | 5.5 | 1749 | 2499 | 3.205 | 4.997 | 5.210 | -1.300 |
| CFS-2 | 4.5 | 1818 | 2456 | 3.189 | 5.199 | 5.419 | -1.359 |
| CFS-2 | 5.5 | 1818 | 2463 | 3.189 | 5.169 | 5.390 | -1.352 |
| CFS-2 | 4.5 | 1885 | 2448 | 3.174 | 5.257 | 5.485 | -1.382 |
| CFS-2 | 4.5 | 1885 | 2438 | 3.174 | 5.301 | 5.528 | -1.393 |
| CFS-3 | 4.5 | 1867 | 2459 | 3.203 | 5.164 | 5.392 | -1.414 |
| CFS-3 | 5.5 | 1867 | 2460 | 3.203 | 5.160 | 5.388 | -1.413 |
| CFS-3 | 4.5 | 1730 | 2548 | 3.234 | 4.762 | 4.976 | -1.292 |
| CFS-3 | 5.5 | 1730 | 2533 | 3.234 | 4.819 | 5.033 | -1.307 |
| CFS-3 | 4.5 | 1578 | 2646 | 3.270 | 4.368 | 4.565 | -1.172 |
| CFS-3 | 5.5 | 1578 | 2627 | 3.270 | 4.431 | 4.628 | -1.189 |
| CFS-4 | 4.5 | 1851 | 2534 | 3.232 | 4.819 | 5.049 | -1.381 |
| CFS-4 | 5.5 | 1851 | 2544 | 3.232 | 4.781 | 5.011 | -1.371 |
| CFS-4 | 4.5 | 1726 | 2574 | 3.261 | 4.628 | 4.844 | -1.313 |
| CFS-4 | 5.5 | 1726 | 2577 | 3.261 | 4.617 | 4.833 | -1.311 |
| CFS-4 | 4.5 | 1630 | 2625 | 3.284 | 4.419 | 4.624 | -1.245 |
| CFS-4 | 5.5 | 1630 | 2618 | 3.284 | 4.442 | 4.648 | -1.251 |
| Hd | 4.5 | 1571 | 2637 | 2.937 | 4.896 | 4.839 | -1.284 |
| Hd | 5.5 | 1571 | 2651 | 2.937 | 4.845 | 4.839 | -1.271 |
| Hd | 4.5 | 1677 | 2584 | 2.919 | 5.131 | 4.839 | -1.354 |
| Hd | 5.5 | 1677 | 2617 | 2.919 | 5.002 | 4.839 | -1.321 |
| Hd | 4.5 | 1778 | 2579 | 2.902 | 5.181 | 4.839 | -1.377 |
| Hd | 5.5 | 1778 | 2603 | 2.902 | 5.086 | 4.839 | -1.352 |
| Hd | 4.5 | 1879 | 2555 | 2.885 | 5.309 | 4.839 | -1.420 |
| Hd | 5.5 | 1879 | 2575 | 2.885 | 5.227 | 4.839 | -1.399 |

*The value of ρ is calculated from Table 4b in Equation (7), using $\partial \overline{V}_{FeO}/\partial T = 0.0035\times10^{-2}\ GPa^{-1}K^{-1}$

Table 2.6a
Individual regression results for $c_i$ at 1723K by Equation (8) using data from this study and literature[a]

| Oxide | $c_i \pm 1\sigma$(m/s) | $\partial c_i/\partial T \pm 1\sigma$(ms$^{-1}$ K$^{-1}$) |
|---|---|---|
| $SiO_2$ | 2176 ± 17 | - |
| $Al_2O_3$ | 2650 ± 20 | - |
| MgO | 3603 ± 24 | - |
| CaO | 4219 ± 21 | -0.538 ± 0.079 |
| FeO(CFS-1) | 2010 ± 24 | - |
| FeO(CFS-2) | 1912 ± 24 | - |
| FeO(CFS-3) | 1877 ± 23 | - |
| FeO(CFS-4) | 1757 ± 23 | - |
| FeO(Hd) | 1794 ± 34 | - |

[a]Total of observations varies from 157 to 159; $R^2 = 0.9999$, the average error varies from 0.58 to 0.64%.

Table 2.6b
Regression results for $c_i$ at 1723K by Equation (8) using data from this study with $CaFeO_2$ component and from literature[a]

| Oxide | $c_i \pm 1\sigma$ (m/s) | $\partial c_i/\partial T \pm 1\sigma$ (ms$^{-1}$ K$^{-1}$) |
|---|---|---|
| $SiO_2$ | 2177 ± 16 | - |
| $Al_2O_3$ | 2649 ± 20 | - |
| MgO | 3601 ± 24 | - |
| CaO | 4217 ± 21 | -0.51 ± 0.08 |
| FeO | 2535 ± 48 | - |
| $CaFeO_2$ | 3093 ± 34 | -1.56 ± 0.15 |

[a]Total of 177 observations; $R^2 = 0.9999$, and average error is 0.59%.

Table 2.7a
Individual regression results for $\beta_i$ at 1723K by Equation (11) using data from this study and literature[a]

| Oxide | $\overline{\beta_i} \pm 1\sigma$ ($10^{-2}$ GPa$^{-1}$) | $\partial\overline{\beta_i}/\partial T \pm 1\sigma$ ($10^{-2}$ GPa$^{-1}$K$^{-1}$) |
|---|---|---|
| $SiO_2$ | 7.136 ± 0.042 | - |
| $Al_2O_3$ | 4.480 ± 0.036 | - |
| MgO | 0.491 ± 0.134 | - |
| CaO | -1.471 ± 0.083 | 0.0065 ± 0.0004 |
| FeO(CFS-1) | 4.725 ± 0.109 | - |
| FeO(CFS-2) | 5.187 ± 0.098 | - |
| FeO(CFS-3) | 5.418 ± 0.101 | - |
| FeO(CFS-4) | 6.022 ± 0.083 | - |
| FeO(Hd) | 5.848 ± 0.139 | - |

[a]Total of observations varies from 157 to 159; $R^2$ = 0.9999, the average error varies from 1.03 to 1.14%.

Table 2.7b
Regression results for $\beta_i$ at 1723K by Equation (11) using data from this study and literature[a]

| Oxide | $\overline{\beta_i} \pm 1\sigma$ ($10^{-2}$ GPa$^{-1}$) | $\partial\overline{\beta_i}/\partial T \pm 1\sigma$ ($10^{-2}$ GPa$^{-1}$K$^{-1}$) |
|---|---|---|
| $SiO_2$ | 7.131 ± 0.046 | - |
| $Al_2O_3$ | 4.483 ± 0.039 | - |
| MgO | 0.506 ± 0.146 | - |
| CaO | -1.463 ± 0.089 | 0.0064 ± 0.0004 |
| FeO | 3.462 ± 0.303 | - |
| $CaFeO_2$ | 2.837 ± 0.081 | 0.0060 ± 0.0004 |

[a] With $CaFeO_2$ component, using $\partial\overline{V}_{FeO}/\partial T = 0.0035\times10^{-2}$ GPa$^{-1}$K$^{-1}$
Total of 177 observations; $R^2$ = 0.9998, and average error is 1.09%.

Table 2.8a

Individually fit results for $\partial\overline{V_i}/\partial P$ at 1723K by Equation (13) using data from this study and literature[a]

| Oxide | $\partial\overline{V_i}/\partial P \pm 1\sigma$ ($10^{-4}$cm$^3$ bar$^{-1}$) | $\partial^2\overline{V_i}/\partial P\partial T \pm 1\sigma$ ($10^{-4}$ cm$^3$ bar$^{-1}$K$^{-1}$) |
|---|---|---|
| $SiO_2$ | -1.917 ± 0.011 | - |
| $Al_2O_3$ | -1.681 ± 0.013 | - |
| MgO | -0.060 ± 0.017 | - |
| CaO | 0.247 ± 0.015 | -0.0010 ± 0.0001 |
| FeO(CFS-1) | -0.666 ± 0.017 | - |
| FeO(CFS-2) | -0.765 ± 0.017 | - |
| FeO(CFS-3) | -0.819 ± 0.017 | - |
| FeO(CFS-4) | -0.941 ± 0.016 | - |
| FeO(Hd) | -0.909 ± 0.023 | - |

[a]Total of observations varies from 157 to 159; $R^2$ = 0.9999, the average error varies from 1.02 to 1.13%.

Table 2.8b

Regression results for $\partial\overline{V_i}/\partial P$ at 1723K by Equation (13) using data from this study and literature[a]

| Oxide | $\partial\overline{V_i}/\partial P \pm 1\sigma$ ($10^{-4}$cm$^3$ bar$^{-1}$) | $\partial^2\overline{V_i}/\partial P\partial T \pm 1\sigma$ ($10^{-4}$ cm$^3$ bar$^{-1}$K$^{-1}$) |
|---|---|---|
| $SiO_2$ | -1.917 ± 0.012 | - |
| $Al_2O_3$ | -1.682 ± 0.015 | - |
| MgO | -0.060 ± 0.018 | - |
| CaO | 0.247 ± 0.016 | -0.0010 ± 0.0001 |
| FeO | -0.419 ± 0.037 | - |
| $CaFeO_2$ | -0.962 ± 0.026 | -0.0022 ± 0.0001 |

[a] With $CaFeO_2$ component, using $\partial\overline{V}_{FeO}/\partial T$ =0.0035×$10^{-2}$ GPa$^{-1}$K$^{-1}$
Total of 177 observations; $R^2$ = 0.9998, and average error is 1.10%.

Table 2.9
Comparison of crystalline and liquid volumes for components

| Oxide | crystal | crystal (298 K)[a] | liquid (1723 K)[b] | ratio |
|---|---|---|---|---|
| $SiO_2$ | tridymite | 26.478 | 26.86 | 1.01 |
| $SiO_2$ | quartz | 22.688 | 26.86 | 1.18 |
| $Al_2O_3$ | corundum | 25.577 | 37.42 | 1.46 |
| MgO | periclase | 11.244 | 11.86 | 1.05 |
| CaO | lime | 16.762 | 16.72 | 1.00 |
| FeO | wustite | 12.062 | 12.11($^{[6]}Fe^{2+}$) | 1.00 |
| FeO | wustite | 12.062 | 17.10($^{[4]}Fe^{2+}$) | 1.42 |
| $CaSiO_3$ | wollastonite | 39.553 | 43.58 | 1.10 |
| $CaFeO_2$ | new material | 30.641 | 33.83 | 1.10 |

[a] Data from Smyth and McCormick, 1995
[b] Calculated from Table 4b

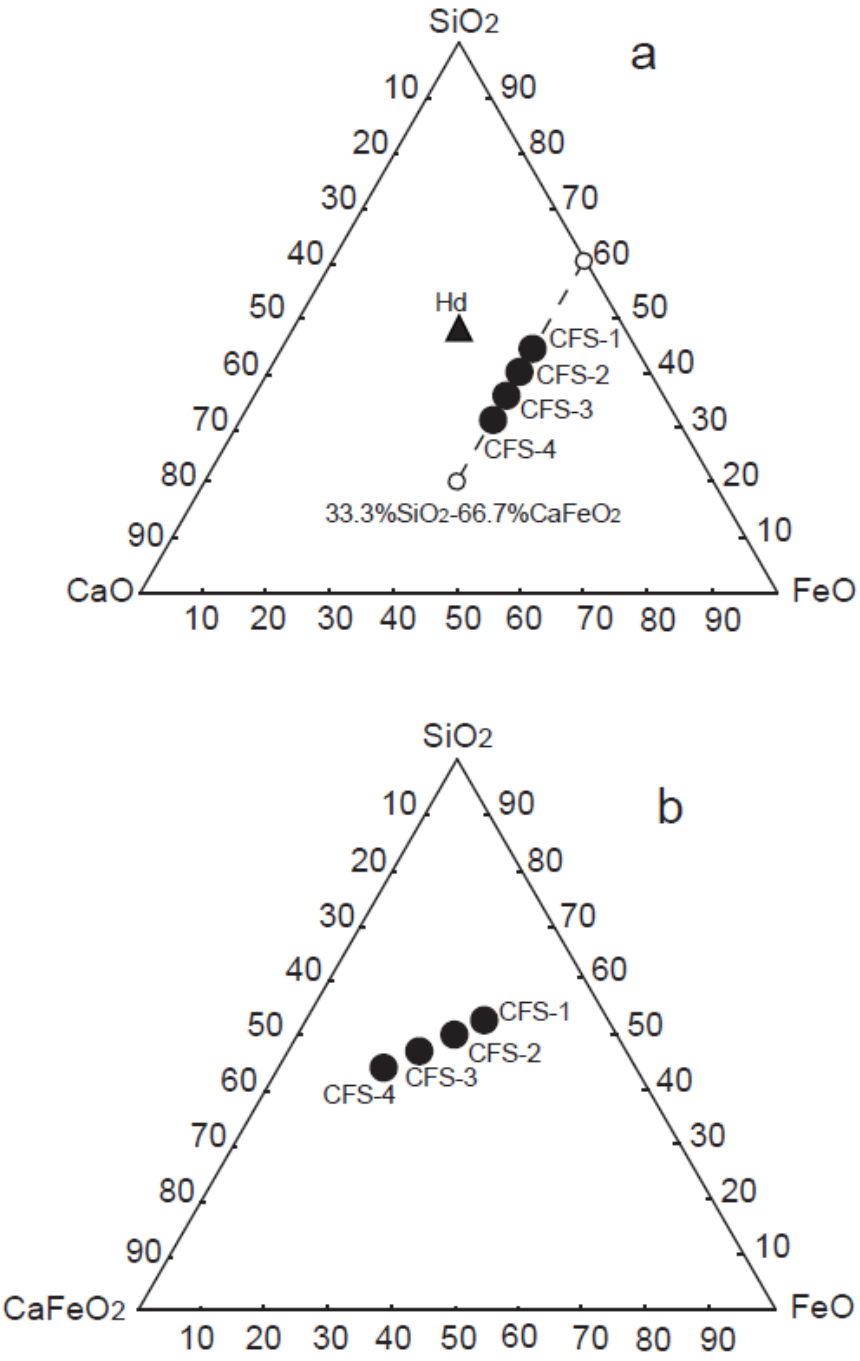


Figure 2.1 (a) Composition of the CFS liquids and hedenbergite liquid in $SiO_2$-CaO-FeO ternary diagram (mol%); (b) composition of the CFS liquids in $SiO_2$-$CaFeO_2$-FeO ternary diagram (mol%). The hedenbergite liquid is not showed in the diagram because its composition can not be projected based on its distribution of FeO in [6]FeO(1/3) and $CaFeO_2$(2/3).

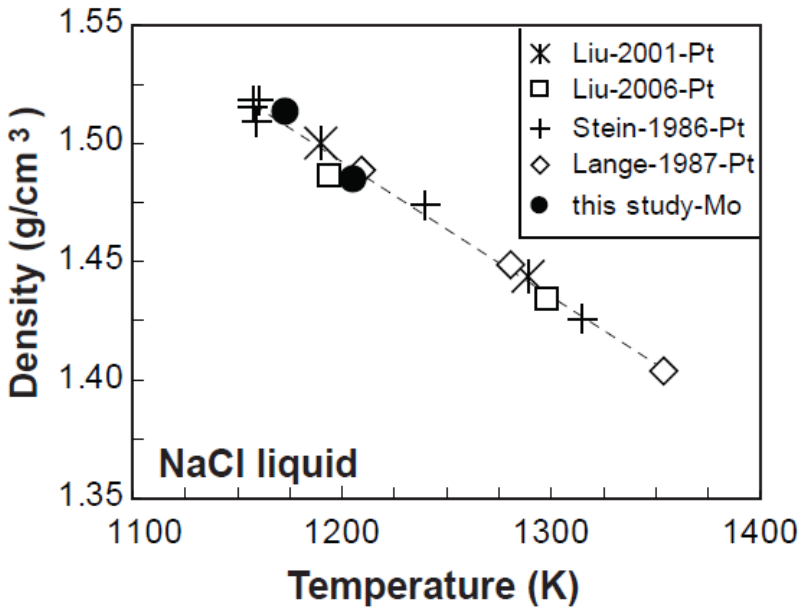


Figure 2.2 The density of molten NaCl vs. temperature. The data from this study are shown in solid dots. The dashed line ($\rho = 2.170\text{-}5.651\times10^{-4}$ T(K)) is from early studies including Lange and Carmichael (1987), Stein et al. (1986), Liu and Lange (2001) and Liu and Lange (2006), as well as this study. All the early studies used platinum in the measurement. This study used molybdenum bobs and crucibles to measure the density.

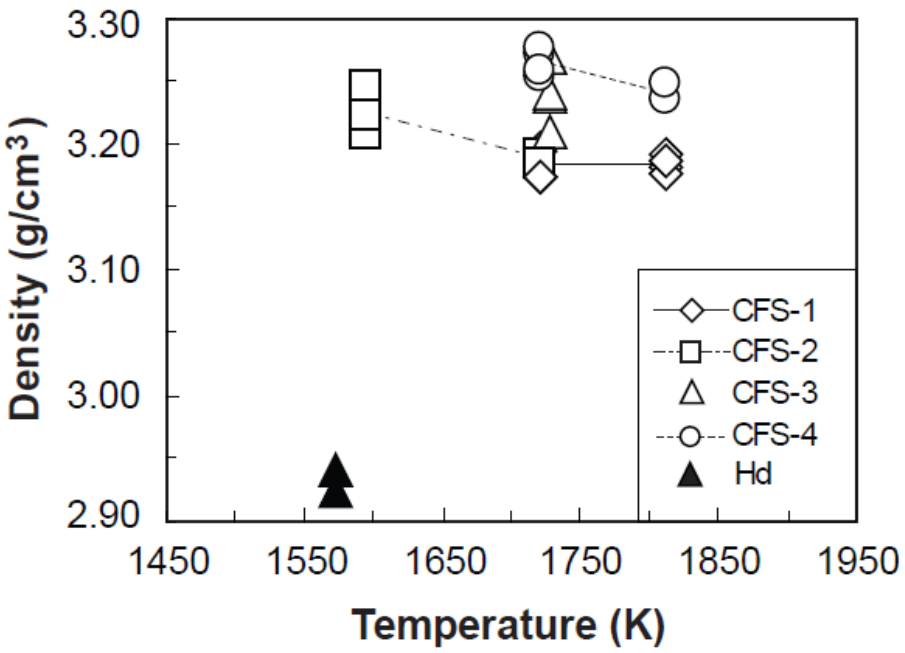


Figure 2.3 Plot of liquid density vs. Temperature. The open diamonds are for CFS-1 liquid; the open squares are for CFS-2; the open triangle is for CFS-3 liquid; the open dots are for CFS-4 liquid; the solid triangle is for hedenbergite liquid.

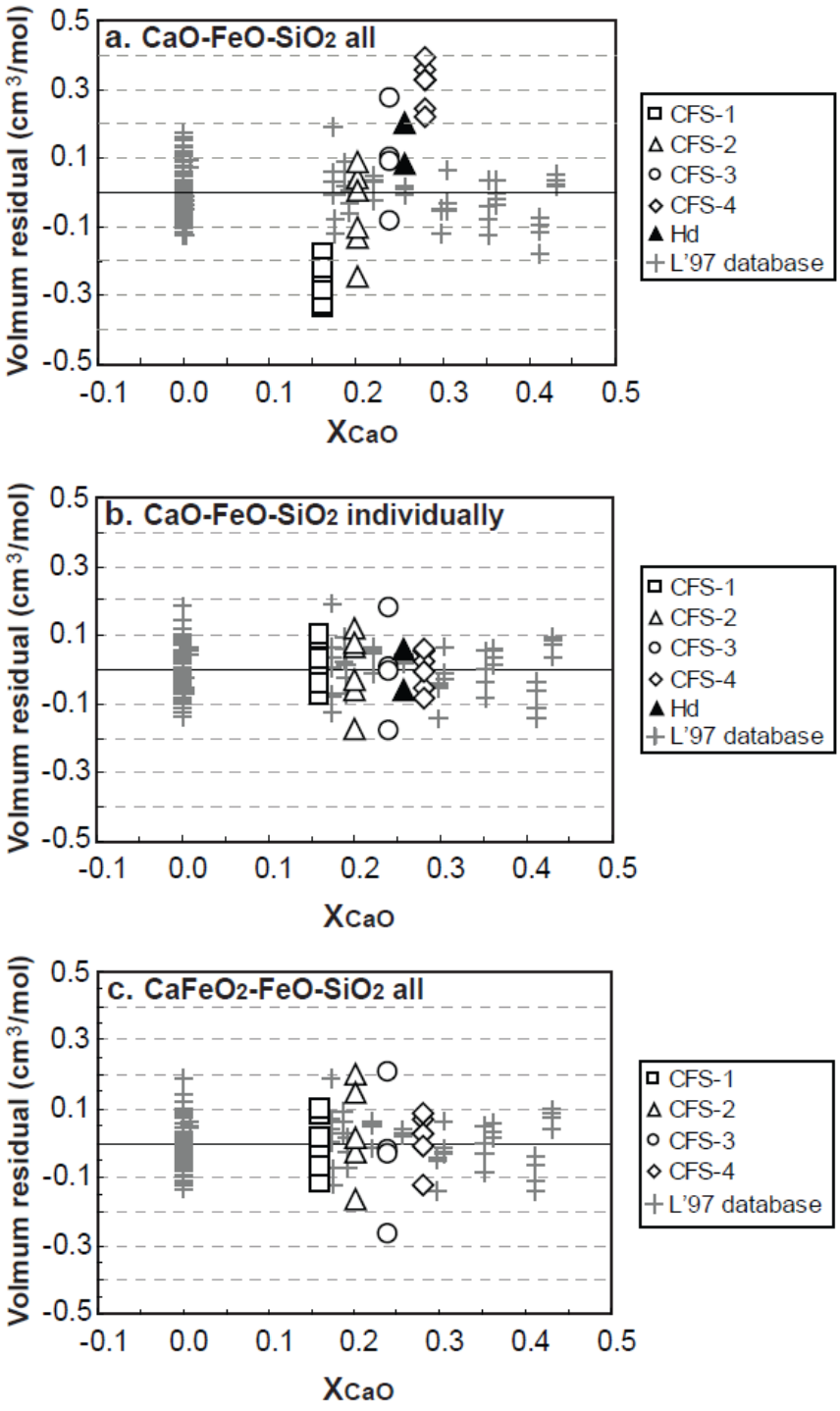


Figure 2.4 (a) Plot of volume residuals vs. $X_{CaO}$ for overall fit. The open squares are for CFS-1, the open triangles are for CFS-2, the open dots are for CFS-3, the open diamonds are for CFS-4, the solid triangles are for hedenbergite liquid. The database is shown as cross symbols. (b) Plot of volume residuals vs. $X_{CaO}$ for individually fit. Symbols are the same as in (a). (c) Plot of volume residuals vs. $X_{CaO}$ for fit with $CaFeO_2$ component. Symbols are the same as in (a).

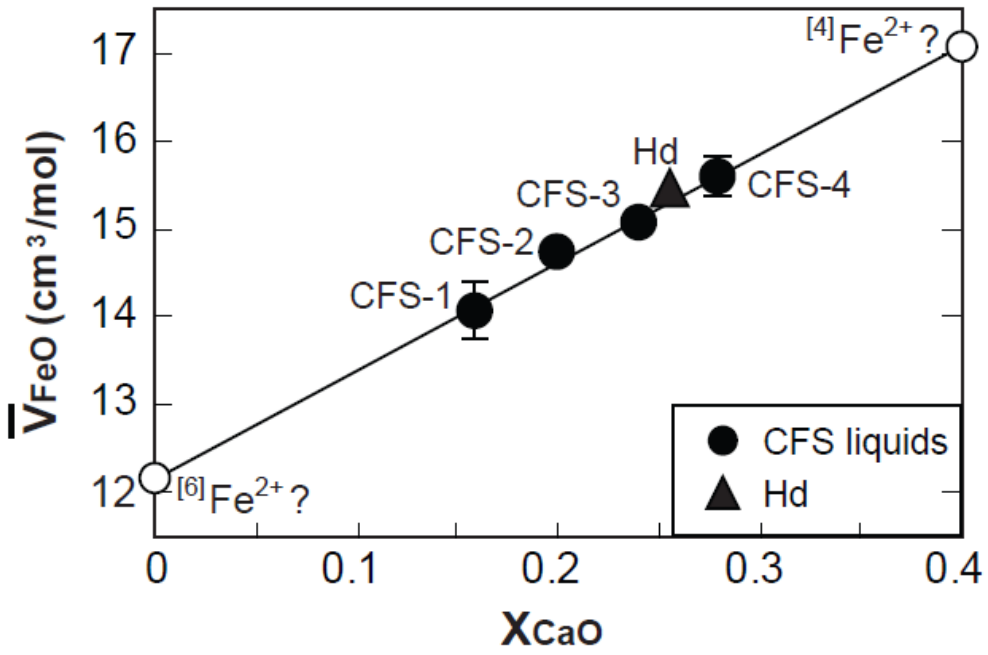


Figure 2.5 Plot of $\overline{V}_{FeO}$ vs. $X_{CaO}$. The solid dots are for CFS liquids, the solid triangle is for hedenbergite liquid (Hd). The error bars are for 2σ. The error bars are smaller than the symbols for CFS-2, CFS-3 and Hd. The solid line is a linear fit for the four CFS sample. The fitted equation is y=12.30x+12.15, $R^2$=0.9852. The open dots are extrapolation from the linear line to $X_{CaO}$=0 and 40mol%.

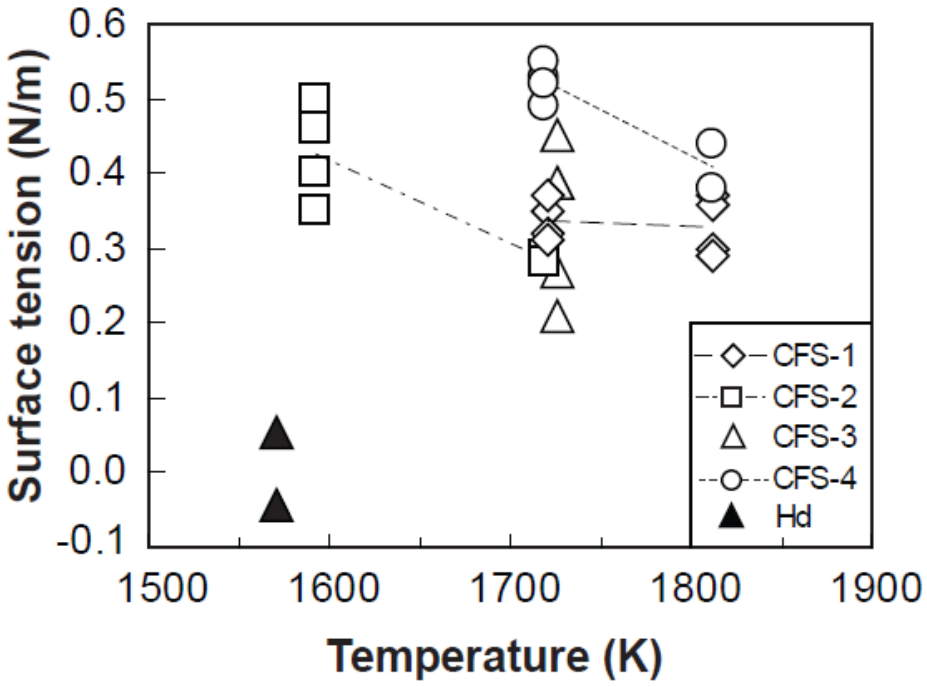


Figure 2.6 Plot of surface tension vs. Temperature for CFS liquids. The open diamonds are for CFS-1 liquid; the open squares are for CFS-2; the open triangle is for CFS-3 liquid; the open dots are for CFS-4 liquid; the solid triangle is for hedenbergite liquid.

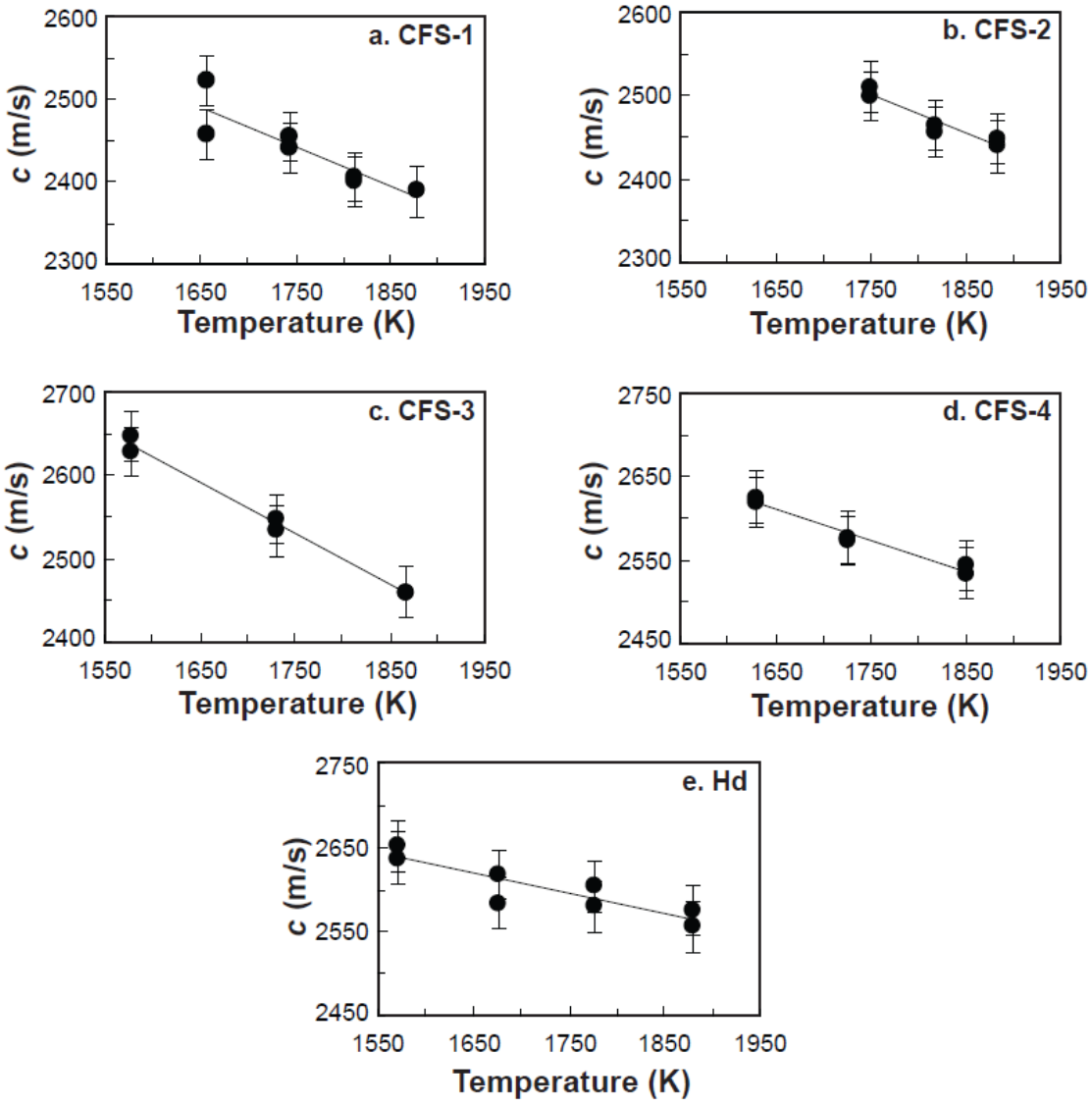


Figure 2.7 Plots of sound speed vs. Temperature for CFS liquids and hedenbergite liquid. The solid line is the linear fit to the data. The errors in sound speed are ±30m/s.

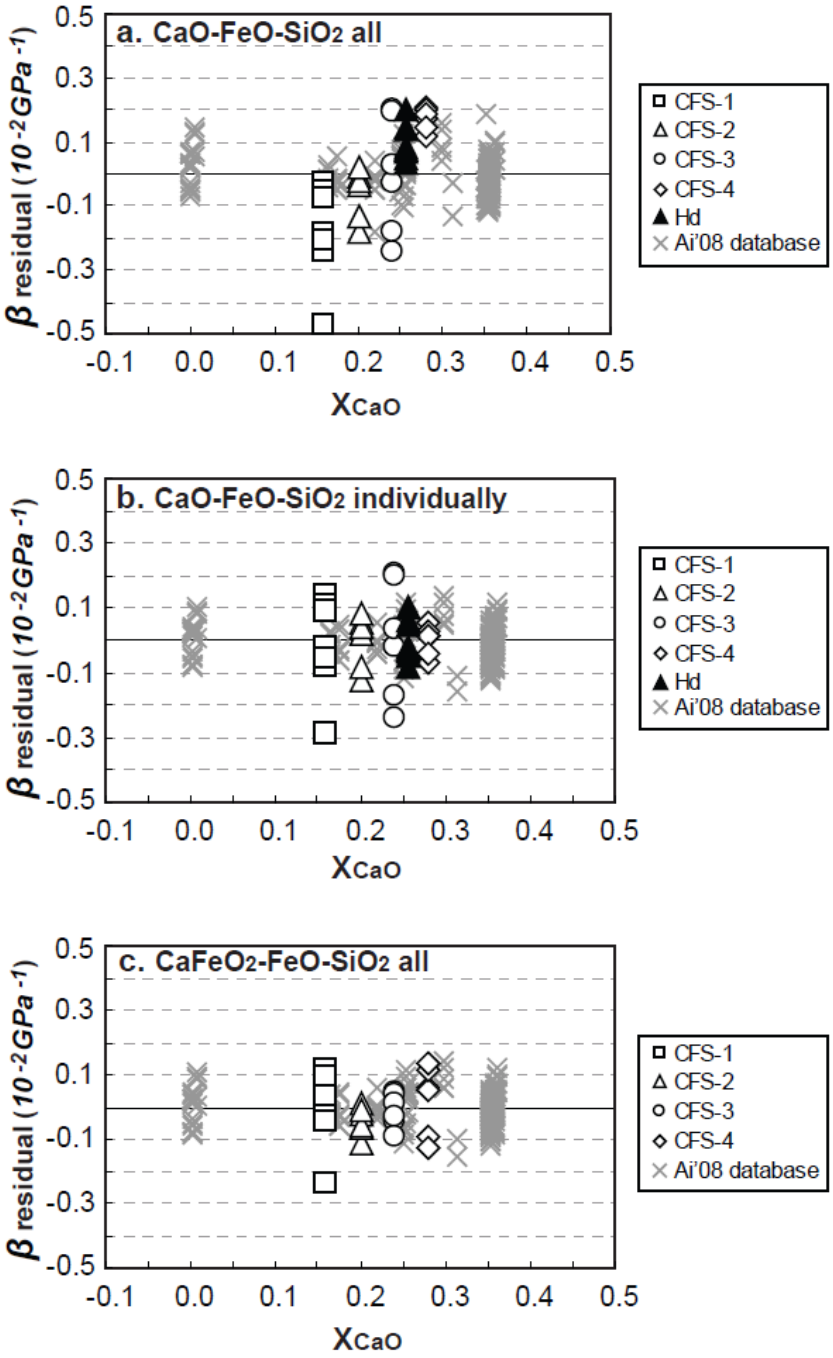


Figure 2.8 (a) Plot of compressibility residuals vs. $X_{CaO}$ for overall fit. The open squares are for CFS-1, the open triangles are for CFS-2, the open dots are for CFS-3, the open diamonds are for CFS-4, the solid triangles are for hedenbergite liquid. The database is shown as cross symbols. (b) Plot of compressibility residuals vs. $X_{CaO}$ for individually fit. Symbols are the same as in (a). (c) Plot of compressibility residuals vs. $X_{CaO}$ for fit with $CaFeO_2$ component. Symbols are the same as in (a).

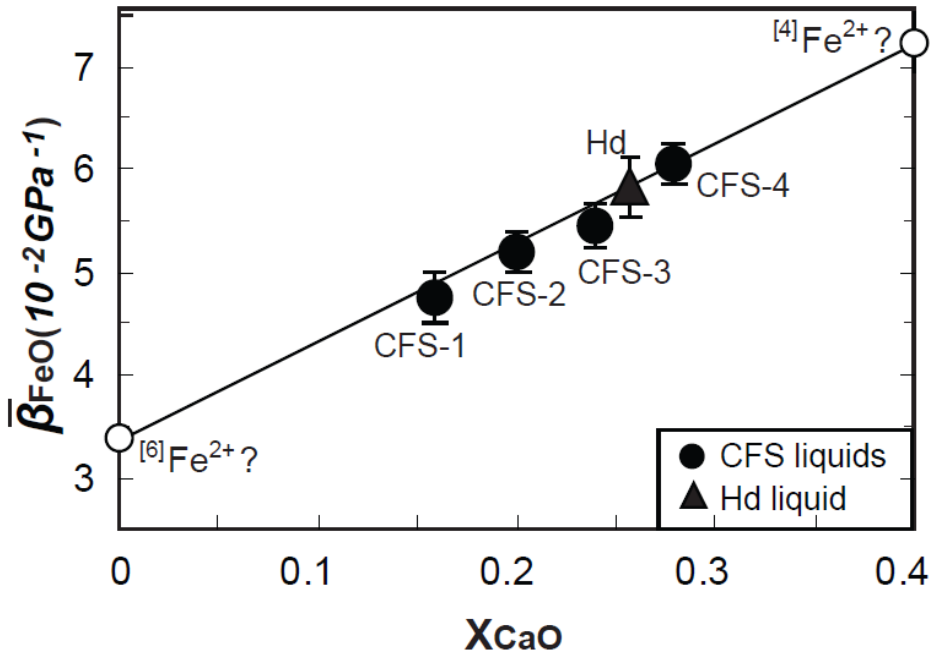


Figure 2.9 Plot of $\overline{\beta}_{FeO}$ vs. $X_{CaO}$. The solid dots are for CFS liquids, the solid square is for hedenbergite liquid. The solid line is a linear fit for the CFS sample. The error bars are 2σ. The fitted equation is y=10.31x+3.07 with $R^2$=0.9735. The open dots are extrapolation from the linear line to $X_{CaO}$=0 and 40mol%.

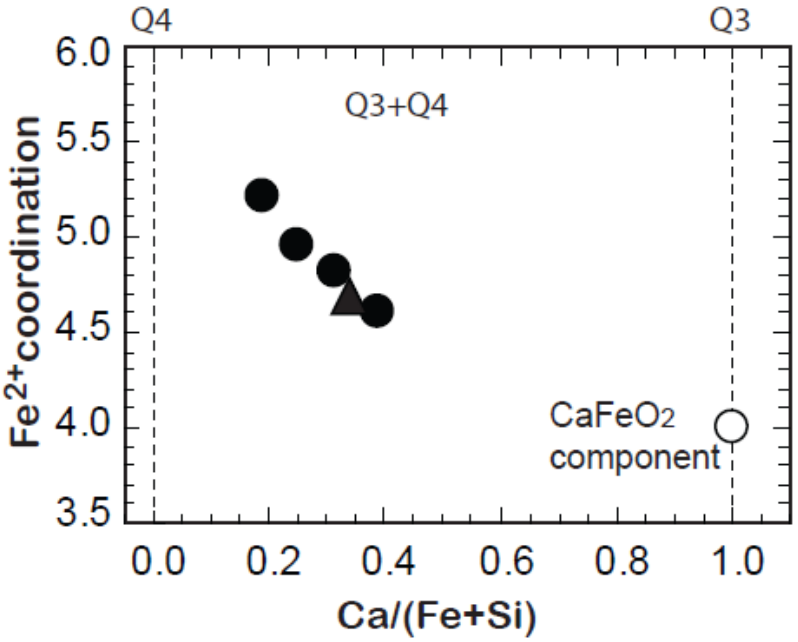


Figure 2.10 Plot of calculated $Fe^{2+}$ coordination number as a function of molar Ca/(Si+Fe). The solid dots are for CFS samples, the solid triangle is for hedenbergite liquid, the open dot is for FeO in $CaFeO_2$ component

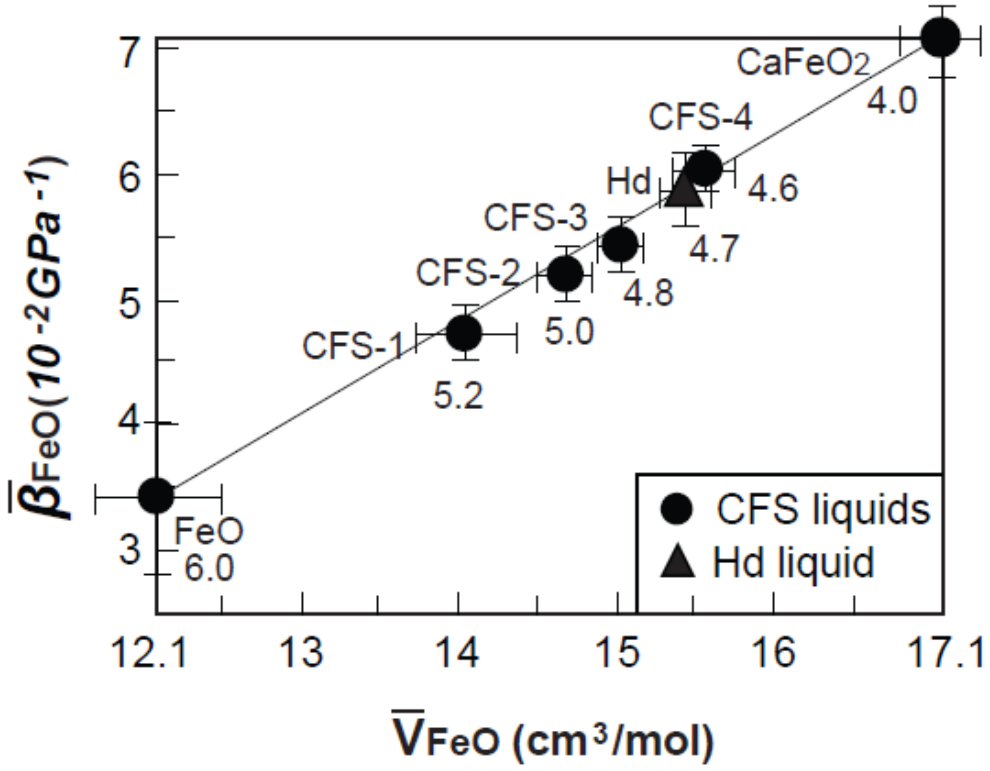


Figure 2.11 Plot of $\overline{\beta}_{FeO}$ vs. $\overline{V}_{FeO}$. The solid line is a linear fit for all the dots. The fitted equation is y=0.7781x-6.2212 with $R^2$=0.9974. The error bars are for 2σ. The average coordination number of $Fe^{2+}$ in each liquid is also shown.

# Reference


Ai Y. and Lange R. A. (2004a) An ultrasonic frequency sweep interferometer for liquids at high temperature: 1. Acoustic model. J.Geophys. Res. **109**, B12203, doi:10.1029/2003JB002842.

Ai Y. and Lange R. A. (2004b) An ultrasonic frequency sweep interferometer for liquids at high temperature: 2. Mechanical assembly, signal processing, and application. J. Geophys. Res. **109**, B12204, doi:10.1029/2004JB003062

Ai Y. and Lange R. A. (2008) New acoustic velocity measurements on CaO-MgO-$Al_2O_3$-$SiO_2$ liquids: Reevaluation of the volume and compressibility of $CaMgSi_2O_6$-$CaAl_2Si_2O_8$ liquids to 25 GPa. Journal of Geophysical Research **113**, B04203, doi:10.1029/2007JB005010.

Alberto H. V., Pinto da Cunha J. L., Mysen B. O., Gil J. M. and Ayres de Campos N. (1996) Analysis of Mossbauer spectra of silicate glasses using a two-dimensional Gaussian distribution of hyperfine parameters. J. Non-Crystal. Solids **194**, 48-57.

Bychkov A. M., Borisov A. A., Khramov D. A., and Urusov V. S. (1993) Change in the immediate environment of Fe atoms during the melting of minerals. Geochemistry International **30**, 1-25.

Bockris J. O'M., Tomlinson J. W. and White J. L. (1956) The structure of the liquid silicates: partial molar volumes and expansivities. Trans Faraday Soc. **52**, 299-310.

Calas G. and Petiau J. (1983) Coordination of iron in oxide glasses through high-resolution K-edge spectra-information from the pre-edge. Solid State Communications **48**, 625-629

Chase M. W. (1998) MIST-JANAF thermochemical tables, fourth edition. Journal of Physical Chemistry Reference Data, Monograph Springer: Heidelberg 9.

de Grave E., Chambaere D., van Iseghem P. and Batist R. (1980) Mossbauer spectroscopic study of some complex $M_2O$-MO-$M_2O_3$-$SiO_2$ glasses. Journal de Physique. Colloque (Paris) **41**, 269-270

Dingwell D. B., Brearley M. and Dickinson J. E. (1988) Melt densities in the $Na_2O$-FeO-$Fe_2O_3$-$SiO_2$ system and the partial molar volume of tetrahedrally-coordinated ferric iron in silicate melts. Geochimica et Cosmochimica Acta. **52**, 2467-2475

Duffy J. A. (1989) A common optical basicity scale for oxide and fluoride glasses. J. Non-Cryst. Solids **109**, 35-39

Duffy J. A. (1996) Redox equilibria in glass. J. Non-Cryst. Solids **196**, 45-50.

Dunlap R. A., Edelman D. A. and Mackay G. R. (1998) A Mossbauer effect investigation of correlated hyperfine parameters in natural glasses (tektites). J. Non-Crystal. Solids **223**, 141-146.

Farges F., Lefrere Y., Rossano S., Berthereau A., Calas G. and Brown G. E. Jr. (2004) The effect of redox state on the local structural environment of iron in silicate glasses: A molecular dynamics, combined XAFS spectroscopy, and bond valence study. Journal of Non-Crystalline Solids **344**, 176-188

Fenstermacher J. E. (1980) Optical-absorption due to tetrahedral and octahedral ferric iron in silicate-glasses. Journal of Non-Crystalline Solids **38**, 239-244

Gray D. E. (1972) American Institute of Physics Handbook, 3rd ed. 4-127.

Gudfinnsson G. H., Presnall D. C. (2000) Melting behavior of model lherzolite in the system CaO-MgO-$Al_2O_3$-$SiO_2$-FeO at 0.7 to 2.8 GPa. Journal of Petrology **41**, 1241-1269.

Hannoyer B., Lenglet M., Durr J. and Cortes R. (1992) Spectroscopic evidence of octahedral iron(III) in soda-lime silicate-glasses. Journal of Non-Crystalline Solids **151**, 209-216.

Jackson W. E. (1991) Spectroscopic studies of ferrous iron in silicate liquids, glasses and crystals. Ph.D. dissertation, Department of Geology, Standford University. 162pp.

Jackson W. E., Waychunas G. A., Brown G. E., Leon J. M., Conradson S. and Combes J. M. (1993) High-temperature XAS study of Fe2SiO4 liquid: Reduced coordination of ferrous iron. Science **262**, 229–232.

Jackson W. E., Farges F., Yeager M., Mabrouk P. A., Rossano S., Waychunas G. A., Solomon E. I. and Brown G. E. Jr (2005) Multi-spectroscopic study of Fe(II) in silicate glasses: Implications for the coordination environment of Fe(II) in silicate melts. Geochimica et Cosmochimica Acta **69**, 4315-4332.

Janz G. J. and Lorenz M. R. (1960) Precise measurement of density and surface tension at temperatures up to 1000$^{o}$C in one apparatus. The review of scientific instruments **31**, 18-22

Kress V. C. and Carmichael I. S. E. (1991) The compressibility of silicate liquids containing $Fe_2O_3$ and the effect of composition, temperature, oxygen fugacity and pressure on their redox states. Contributions to Mineralogy and Petrology **108**, 82-92.

Lange R. A. and Carmichael I. S. E. (1987) Densities of $Na_2O$-$K_2O$-CaO-MgO-FeO-Fe-$_2O_3$-$Al_2O_3$-$TiO_2$-$SiO_2$ liquids: New measurements and derived partial molar properties. Geochimica et Cosmochimica Acta **51**, 2931-2946.

Lange R. A. (1996) Temperature independent thermal expansivities of sodium aluminosilicate melts between 713 and 1835 K. Geochimica et Cosmochimica Acta **60**, 4989–4996.

Lange R. A., (1997). A revised model for the density and thermal expansivity of $K_2O$-$Na_2O$-CaO-MgO-$Al_2O_3$-$SiO_2$ liquids from 700 to 1900 K: Extension to crustal magmatic temperatures. Contributions to Mineralogy and Petrology **130**, 1–11.

Lange R. A. and Navtrotsky A. (1992) Heat capacities of $Fe_2O_3$-bearing silicate liquids. Contrib. Mineral Petrol **110**, 311-320.

Liu Q. and Lange R. A. (2001) The partial molar volume and thermal expansivity of $TiO_2$ in alkali silicate melts: Systematic variation with Ti coordination. Geochimica et Cosmochimica Acta **65**, 2379-2393.

Liu Q., and Lange R. A. (2003) New density measurements on carbonate liquids and the partial molar volume of the $CaCO_3$ component. Contributions to Mineralogy and Petrology **146**, 370-381.

Liu Q. and Lange R. A. (2006) The partial molar volume of $Fe_2O_3$ in alkali silicate melts: Evidence for an average Fe3+ coordination number near five. American Mineralogist **91**, 385-393.

Liu Q., Lange R. A. and Ai Y. (2007) Acoustic velocity measurements on $Na_2O$-$TiO_2$-$SiO_2$ liquids: Evidence for a highly compressible $TiO_2$ component related to five-coordinated Ti. Geochimica et Cosmochimica Acta **71**, 4314-4326.

Mo X., Carmichael I. S. E., Rivers M. and Stebbins J. F. (19820 The partial molar volume of $Fe_2O_3$ in multicomponent silicate liquids and the pressure-dependence of oxygen fugacity in magma. Mineralogical Magzine **45**, 237-245.

Rivers M. L. and Carmichael I. S. E. (1987) Ultrasonic studies of silicate melts. J. Geophys. Res. Solid Earth Planets **92**, 9247–9270.

Rossano S., Balan E., Morin G., Bauer J. P., Brouder C. and Calas G. (1999) $^{57}$Fe Mossbauer spectroscopy of tektite. Phys. Chem. Mineral **26**, 530-538.

Rossano S., Ramos A.Y. and Delaye J. M. (2000) Environment of ferrous iron in $CaFeSi_2O_6$ glass: contributions of EXAFS and molecular dynamics. Journal of Non-Crystalline Solids **273**, 48-52.

Secco R. A., Manghnani M. H., and Liu T. C. (1991) The bulk modulusattenuation-viscosity systematics of diopside-anorthite melts, Geophys. Res. Lett **18**, 93– 96.

Smyth J. R. and McCormick T. C. (1995) Crystallographic data for minerals. In T. Ahrens, Ed., Mineral Physics and Crystallography, p.1-17. AGU Reference shelf 2, Washington, D.C.

Shiraishi Y., Ikeda K., Tamura A., Saito T. (1978) On the viscosity and density of the molten FeO-$SiO_2$ system. Transactions of the Japan Institue of Metals **19**, 264-274.

Stein D. J., Stebbins J. F., and Carmichael I. S. E. (1986) Density of molten sodium aluminosilicates. J. Am. Ceram. Soc. **69**, 396–399.

Tassel C., Pruneda J. M., Hayashi N., Watanabe T., Kitada A., Tsujimoto Y., Kageyama H., Yoshimura K., Takano M., Nishi M., Ohayama K., Mizumaki M., Kawamura N., Iniguez J. and Canadell E. (2009) $CaFeO_2$: A new type of layered structure with iron in a distorted square planar coordination. Journal of the American chemical society **131**: 221-229.

Thomas C. W., Liu Q., Agee C. B., Asimow P. D., Lange R. A. (2012) Multi-technique equation of state for $Fe_2SiO_4$ melt and the density of Fe-bearing silicate melts from 0 to 161 GPa. Journal of Geophysical Research-Solid Earth **117**, B10206, doi: 10.1029/2012JB009403.

Walter M. J. (1998) Melting of garnet peridotite and the origin of komatitite and depleted lishosphere. J. Petrol. **39**, 29-60.

Wang C. M. and Chen H. (1987) Mixed coordination of $Fe^{3+}$ and its dependence on the iron content in sodium disilicate glasses. Physics and Chemistry of Glasses **28**, 39-47.

Waseda Y. and Toguri J. M. (1990) Structure of silicate melts determined by X-ray diffraction. In: Dynamic Processes of Material Transport and Transformation in the Earth's Interior, F Marumo (ed), p. 37-51. Terra Scientific, Tokyo.

Waychunas G. A., Brown G. E. Jr., Ponader C. W. and Jackson W. E. (1988) Evidence from X-ray absorption for network-former $Fe^{2+}$ in molten alkali silicates. Nature **332**, 251-253.

Waychunas G. A., Brown G. E. Jr., Jackson W. E. and Ponader C. W. (1989) In-situ high temperature x-ray absorption study of iron in alkali silicate melts and glasses. Physica B **21**, 144-146.

Webb S., and Courtial P. (1996) Compressibility of melts in the $CaOAl_2O_3$-$SiO_2$ system, Geochim. Cosmochim. Acta **60**, 75–86.

Wilke M., Parzsch G. M., Bernhardt R. and Lattard D. (2004) Determination of the iron oxidation state in basaltic glasses using XANES at the K-edge Chemical Geology **213**, 71-87.

Wilke M., Farges F., Partzsch G. M., Schmidt C. and Behrens H. (2007) Speciation of Fe in silicate glasses and melts by in-situ XANES spectroscopy. American Mineralogist **92**, 44-56

Xue X., Stebbins J. F., Kanzaki M., McMillan P. F. and Poe, B. (1991) Pressure-induced silicon coordination and tetrahedral structural changes in alkali oxide-silica melts up to 12 GPA. NMR, Raman, and infrared spectroscopy. Am. Mineral. **76**, 8-26.

# CHAPTER III

## The Density and Compressibility of Model Basalt (An-Di-Hd) Liquids at One Bar: Evidence for Abundant 6-coordinated $Fe^{2+}$


## Abstract

The density and compressibility of three FeO-bearing model basalts in the An-Di-Hd ternary were measured in this study ($An_{50}Hd_{50}$, $Di_{50}Hd_{50}$, $An_{33}Di_{33}Hd_{33}$). Double-bob density measurements were made between 1585 and 1838 K using molybdenum bobs in a reducing atmosphere, and low-temperature liquid density data were additionally obtained at the respective limiting fictive temperature (943-990 K) for each sample. In addition, relaxed sound speed measurements were obtained on the three liquids from 1665 to 1876 K at 1 bar with a frequency sweep acoustic interferometer. An ideal mixing model recovers the new data in this study for molar volume, thermal expansivity, and isothermal compressibility. At 1723 K, the fitted values for $\overline{V}_{FeO}$ (12.86 ± 0.16 $cm^3$/mol), $\partial\overline{V}_{FeO}/\partial T$ (3.69 ± 0.58 $10^{-3}$ $cm^3$/mol-K) and $\overline{\beta}_{T,FeO}$ (4.72 ± 0.23 $10^{-2}$ $GPa^{-1}$) are presumed to reflect $Fe^{2+}$ in an average coordination of 5.7 ± 0.1, using the relationship between $\overline{V}_{FeO}$ and $Fe^{2+}$ coordination developed by Guo et al. (2013). Application of these results to predict the pressure dependence of the Fe-Mg exchange reaction between orthopyroxene and basaltic liquid indicates a slight decrease in $^{Fe\text{-}Mg}K_D$ with pressure,

whereas published phase-equilibrium results from partial melting experiments of peridotite indicate a slight increase in $^{Fe\text{-}Mg}K_D$ with pressure, consistent with an average $Fe^{2+}$ coordination between 5 and 5.5. It is postulated that this difference may reflect the role of alkalis in reducing the average coordination number of $Fe^{2+}$ toward five compared to the alkali-free model basalt compositions in this study. The results of this study may be most appropriately applied to lunar basalts, which are impoverished in alkalis.

## Introduction

Ferrous iron is an important component in magmatic liquids, with FeO concentrations in terrestrial and lunar basalts commonly ranging from 10-20 wt% (e.g. Dadd, 2011). Recent spectroscopic evidence shows that $Fe^{2+}$ can occur in four-, five- and six-fold coordination in a wide variety of multi-component silicate glasses and liquids at one bar, with an average coordination number that varies with composition (e.g., Jackson et al., 1991, 1993, 2005; Dunlap, 1998; Rossano et al., 1999, 2000; Farges et al., 2004; Wilke et al., 2004, 2007). Among the melt properties strongly affected by changes in $Fe^{2+}$ coordination are density and compressibility.

Although the systematics of one-bar silicate melt density with composition are well established for melts in air (e.g., Stein et al., 1986; Lange and Carmichael, 1987; Dingwell et al., 1988; Lange, 1997; Liu and Lange, 2001, 2006), there are few high-quality double-bob density measurements on iron-bearing liquids under reducing conditions, and none on basalt compositions. Currently, the only available data are restricted to FeO-$SiO_2$ liquids (Shirashi et al., 1978; Mo et al., 1982; Thomas et al., 2012) and CaO-FeO-$SiO_2$ (CFS) liquids (Guo et al., 2013). The results of those density

measurements provide clear evidence that the partial molar volume of FeO ($\overline{V}_{FeO}$) varies systematically with composition, reflecting changes in the coordination of $Fe^{2+}$. On the basis of sound speed measurements, Guo et al. (2013) further show that the partial molar compressibility of FeO ($\overline{\beta}_{T,FeO}$) also varies systematically with composition and $Fe^{2+}$ coordination. These results raise the question of what values for $\overline{V}_{FeO}$ and $\overline{\beta}_{T,FeO}$ should be applied to basalts.

Current models to calculate the density and compressibility of magmatic liquids (e.g., Lange and Carmichael, 1987; Kress and Carmichael, 1991) have fitted partial molar values for the FeO component that are strongly influenced by measurements on binary FeO-$SiO_2$ liquids close to fayalite composition (60-65 mol% FeO; Mo et al., 1982; Rivers and Carmichael, 1987). High-temperature X-ray absorption spectroscopy indicates an average $Fe^{2+}$ coordination between four and five for fayalite liquid (Jackson et al., 1993). However, spectroscopic evidence shows that $Fe^{2+}$ coordination varies in multicomponent liquids according to the field strength of coexisting cations (e.g., Jackson et al., 2005). Liquids with bulk compositions similar to mid-ocean ridge basalts and lunar basalts, namely those that are Mg- and Ca-rich and alkali-poor, are predicted to have $Fe^{2+}$ in a relatively high coordination environment, closer to six than to four. It is therefore unclear if density and compressibility data on FeO-$SiO_2$ binary liquids can be used to calibrate models applicable to common terrestrial and lunar basalts.

To determine what are the most appropriate values for $\overline{V}_{FeO}$ and $\overline{\beta}_{T,FeO}$ to apply to basalts, and to explore whether ideal mixing of volume and compressibility at one bar extends beyond the anorthite-diopside join (Ai and Lange, 2008; Asimow and Ahrens, 2010), a series of melt density and compressibility measurements were made in this study

on three model basalt liquids in the anorthite-diopside-hedenbergite (An-Di-Hd) ternary system. In addition, low-temperature volume measurements at the limiting fictive temperature were made on each sample, which provides liquid volume data for each sample over a wide temperature interval of ~1000 degrees and improves constraints on derived $\partial \overline{V}_{FeO} / \partial T$ values. Various applications of these new volumetric data include an evaluation of how the iron-magnesium exchange reaction between basaltic melts and mantle minerals vary with pressure.

## Experimental Methods

### Sample synthesis and composition analysis

Three model basalt samples ($An_{50}Hd_{50}$, $Di_{50}Hd_{50}$, $An_{33}Di_{33}Hd_{33}$) were synthesized by mixing appropriate proportions of reagent grade MgO, $Al_2O_3$, $CaCO_3$, $Fe_2O_3$ and $SiO_2$. Each powder was slowly dried, de-carbonated, and then fused at 1673-1873 K in air. The samples were then quenched to glass, ground into powder and then re-fused. Each sample was re-fused twice in total to ensure homogeneity. The glass compositions were analyzed with a Cameca SX-100 electron microprobe at the University of Michigan, using an accelerating voltage of 15kV with a beam current of 4 nA. The standards include two glass samples ($CaAlSi_2O_8$ and $CaMgSi_2O_6$) that were analyzed by wet-chemical method and reported in Rivers and Carmichael (1987) and Lange and Carmichael (1987), respectively. The uncertainty of a single oxide concentration is smaller than 3%. The analyzed compositions are listed in Table 3.1 and plotted in Figure 3.1. For each composition, the gram formula weight ( g.f.w.=$X_iM_i$) is tabulated in Table 3.1 as well,

where $X_i$ and $M_i$ are the mole fraction and molecular weight of each oxide component, respectively.

**Low-temperature measurement of liquid volume at $T_f'$**

The technique to measure the molar volumes of the sample liquids at their respective limiting fictive temperatures ($T_f'$) is described in detail in Lange (1996, 1997) and Tangeman et al. (2001). The $T_f'$ of any glass quenched from a liquid is uniquely defined on a volume vs. temperature curve as the extrapolated intersection of the glass and liquid volume within the glass transition interval (Moynihan et al., 1976; Scherer, 1992; Debenedetti, 1996). Because the volume of the glass is equal to that of the liquid at $T_f'$, the following equation applies to both the glass and the liquid:

$$V^{liq}(T_f^{'}) = V^{glass}(T_f^{'}) = V_{298K}^{glass} \exp[\alpha^{glass}(T_f^{'} - 298)] \quad (1)$$

where $V_{298K}^{glass}$ is the molar volume of the glass at 298 K and $\alpha^{glass}$ is the temperature-independent coefficient of thermal expansion for the glass between 298 K and $T_f'$. The molar volume of the liquid at $T_f'$ can thus be obtained from three measurements: (1) the glass volume (density) at 298 K; (2) the glass thermal expansion coefficient between 298 K and the beginning of the glass transition interval; and (3) the value of $T_f'$.

The room temperature (298 K) density of each glass sample was measured using the Archimedean method with a microbalance. For each density measurement, the glass was weighed several times in air and also weighed several times below the balance while immersed in liquid toluene.

The linear thermal expansion coefficient, $(1/L)/(\partial L/\partial T)$, of each glass sample was measured with a Perkin-Elmer Diamond TMA vertical dilatometer with a scan rate

of 10 K/min from 298 K to temperatures in the glass transition interval (Fig. 3.2). The volume thermal expansion coefficient is obtained by multiplying the linear expansion coefficient by three. Glass samples of 1.4 to 7.6 mm height were used and care taken to ensure that the bottom and top surfaces were flat and parallel. Replicate measurements indicate a reproducibility that is better than 4%, whereas the accuracy is within 3% based on our measurement of the thermal expansion of NIST Standard-731 (Fig. 3.3).

An approximation of $T_f'$ for each glass sample was obtained by choosing the temperature corresponding to the onset of the rapid rise in the $\partial L/L$ vs. T in the dilatometry curve within the glass transition interval (Fig. 3.2). Tangeman and Lange (2001) showed that estimates of $T_f'$ obtained in this manner closely match quantitative determinations of $T_f'$ calculated from Cp heating curves. For the sixteen samples studied by Tangeman and Lange (2001), the deviation is 8 degrees on average, with a maximum discrepancy of 17 degrees. On this basis, we assume a maximum uncertainty of < 20 degrees in the derived values of $T_f'$.

**High-temperature measurements of liquid volume**

Thirty-six liquid density measurements were made on the three model basalt liquids at high temperatures using the double-bob Archimedean method. The procedure is similar to that described in Chapter II, where molybdenum crucibles and bobs were used in a reducing atmosphere.

For each sample, the total amount of the sample powder (~75 g) was loaded into a Mo crucible (8.0 cm long x 4.0 cm O.D.) by four batches. Each batch was melted in a Deltech vertical tube furnace under a stream of 1%CO-99%Ar gas for an hour and added step-wise. This way promises to converte most of the ferric iron to ferrous iron. The

density measurements were performed after all ~75 g samples are in the Mo crucible. Such reducing condition makes the experimental melts to be saturated with molybdenum metal and oxygen fugacity conditions below the Mo-$MoO_2$ buffer (Chase, 1998). However, the oxygen fugacity of the experimental liquids at each temperature of measurement is constrained to be between the Mo-$MoO_2$ and Fe-FeO buffers because the activity of $MoO_2$ in the melt is less than one, and the melts are not saturated with metallic iron. At this redox condition, 4 ± 1% of the total iron as $Fe^{3+}$ is predicted from the model of Kress and Carmichael (1991), which was calibrated on a wide variety of natural liquids. In addition, Mössbauer spectroscopy confirmed that $Fe^{3+}$ concentrations are low (< 5% of the total iron) in the fayalite liquid with the same density measurement procedure (Thomas et al., 2012).

As described in Chapter II, to make a density measurement, each sample was held in a Mo crucible inside a vertical tube Deltech furnace. The furnace was moved up and down with the action of a hydraulic jack. An electronic balance with a precision of ± 0.0001 g was mounted on an aluminum shelf atop the furnace to measure the mass of the Mo bob before and after immersion into each experimental liquid. The effect of surface tension is eliminated by using at least two Mo bobs of different mass (~19.5 and ~6.5 g) with identical stem diameters. The density of the liquid is calculated from the following equation:

$$\rho(T) = \frac{B_L(T) - B_S(T)}{V_L(T) - V_S(T)} \quad (2)$$

where $B_L(T)$ and $B_S(T)$ are the buoyancy of the large and small bobs, respectively. $V_L(T)$ and $V_S(T)$ are the immersed volume of the large and small bob, respectively. The

density 10.22 g/cm$^3$ at 298 K, and thermal expansion from Gray (1972) were used to calculate the immersed volume of the Mo bobs as a function of temperature. In this study, the buoyancy of four bobs (two different large bobs and two different small bobs) was used at each temperature for each liquid, allowing four density measurements to be made.

Measurements were made at three different temperatures for each sample, spanning an interval that ranged from 185 to 228 degrees. The accuracy of using Mo bobs in a reducing atmosphere was tested by measuring the density of NaCl liquid at 1203 and 1216 K (Table 3.2, Fig. 3.4). Our measurements are consistent with those measured in air with Pt bobs (Stein et al., 1986; Liu and Lange, 2001, 2006; Lange and Carmichael, 1987), as well as those measured in a reducing atmosphere with Mo bobs in Chapter II.

**Surface tension measurements**

During immersion of each bob in the melt, the liquid surface tension on the stem affects the apparent buoyancy measurement. By using two bobs of different mass with the same stem diameters, the surface tension effect can be eliminated. However, the double-bob Archimedean method also permits the surface tension of the sample liquids against molybdenum to be derived. If a single bob is used to measure melt density, the effect of this surface tension effect must be included in the calculation of melt density:

$$\rho(T) = \frac{B(T) + S(T)}{V(T)} \quad (3)$$

where $B(T)$ is the buoyancy of the single bob, $S(T)$ is the effect of surface tension on the bob stem on the buoyancy measurement, and $V(T)$ is the immersed volume of the single

bob. Equation (2) can be rearranged to allow $S(T)$ to be calculated, from which the surface tension, $\gamma$ (N/m), can be derived with the following equation (Janz and Lorenz, 1960):

$$\gamma(T) = \frac{S(T)}{\pi d} g \tag{4}$$

where *g* is the gravitational acceleration, and *d* is the diameter of the stem.

**Sound speed measurements**

The sound speeds of the three basaltic liquids were measured by frequency sweep ultrasonic interferometer in a 1%CO-99%Ar reducing gas environment. The details of the procedure are thoroughly described in Ai and Lange (2004a, b). A 2cm-deep molybdenum crucible is held inside an alumina support rod. The depth of the liquid in the crucible is set between 3 and 4 mm by adding the appropriate mass of sample. A moveable upper buffer rod, which can be immersed into the liquid, is positioned above the crucible. A transducer, which sits on top of the upper buffer rod, is used to transmit and receive signals. A micrometer is mounted on the transducer to measure the position of the upper rod precisely (resolution 0.001mm).

During an experiment, an acoustic pulse is programmed for the desired frequency, amplitude and duration in an arbitrary wave generator. A short pulse (1s) spanning about 2 MHz and centered at 4.5 or 5.5 MHz travels down to the molybdenum upper buffer rod and reaches the rod-melt interface. Part of the signal is transmitted through the liquid and reflects off the bottom of the crucible. Two mirror reflections from the bottom of crucible return up the upper rod and are delivered to a preamplifier for amplification and then to the data acquisition system. A Fourier transform is performed on the return echo

to analyze the frequency response. The periodic function of frequency ($\Delta f$) follows this relation: $\Delta f$ =c/2S. The sound speed (c) can be calculated if $\Delta f$ and S (melt thickness) is known. However, the absolute value of melt thickness is difficult to measure precisely. Therefore, measurements at each temperature are made at two or three different rod positions, as accurate measurement of relative thickness ($\Delta S=S_1-S_2$) are readily made with the micrometer gauge. Because sound speed is independent of melt thickness, sound speed can be calculated from the relation:

$$c = \left| \frac{2\Delta S}{\Delta f_2^{-1} - \Delta f_1^{-1}} \right| \tag{5}$$

## Results

### Low-temperature density and volume of the liquids at $T_f'$

The room-temperature densities of the three glasses were measured before and after each thermal expansion experiment to evaluate the effect of any structure relaxation that may have occurred. After the first thermal expansion experiment, there was little density variation (0.03-0.15%) in the glass sample before and after subsequent TMA runs. Therefore, the last glass density measurement after the last TMA experiment is reported in Table 3.3. The volume of each glass at 298 K was calculated from the following equation:

$$V_{298K}^{glass} = g.f.w./\rho_{298K}^{glass}. \tag{6}$$

Two to three replicate thermal expansion runs (dL/L vs. T) were made for each glass sample. The volume coefficient of thermal expansion ($\alpha = \frac{1}{V}\frac{dV}{dT}$) of each glass was calculated by multiplying the linear coefficient of thermal expansion by three. The difference for $\alpha^{glass}$ between the two TMA runs ranges from 1.7% to 4.1%. The $T_f'$ values were approximated using the onset of the rapid rise in the dL/L vs. T curve (Figure 3.2), following Tangeman and Lange (2001). The difference in derived values for $T_f'$ between multiple TMA runs was always ≤ 7 degrees. By combining $V_{298K}^{glass}$, $\alpha^{glass}$ and $T_f'$ in Equation 1, the volume of each sample liquid at $T_f'$ can be calculated and is listed in Table 3.3, with an experimental uncertainty < 1% in all cases.

**Liquid volumes as a function of temperature**

The high temperature density data for the three liquids are presented in Table 3.4, along with surface tension results. The standard deviations of replicate density measurements at each temperature range from 0.03% to 0.47%.These density data were converted to molar volume using Equation (6). In Figure 3.5, the high-temperature data are combined with the low-temperature measurement at $T_f'$, providing volume data for each sample that spans a wide temperature interval of~1000 degrees.

Modeling molar volume with temperature and composition

The liquid volume data for the three model basalts in Table 3.4 were combined with molar volume data from the literature on $K_2O$-$Na_2O$-CaO-MgO-$Al_2O_3$-$SiO_2$ liquids (Bockris et al., 1956; Stein et al., 1986; Lange and Carmichael, 1987; Lange, 1996, 1997) to calibrate the following linear volume equation:

$$V^{liq}(X,T) = \sum X_i \left[ V_{i,T_{ref}} + \frac{\partial \overline{V}_i}{\partial T}(T - T_{ref}) \right] \quad (7)$$

where $X_i$ is the mole fraction of each oxide component, $\overline{V}_{i,T_{ref}}$ is the partial molar volume of each oxide component at a reference temperature ($T_{ref}$= 1723 K), and $\partial \overline{V}_i / \partial T$ is the partial molar thermal expansivity of each oxide component. The results of this regression are presented in Table 3.5a and recover measured volumes within experimental error (Fig. 3.6a). The fitted values for $\overline{V}_{FeO}$ and $\partial \overline{V}_{FeO} / \partial T$ are 12.82 ± 0.16 $cm^3$/mol and 3.69 ± 0.58 x $10^{-3}$ $cm^3$/mol-K, respectively. The thermal expansivity term for the FeO component is broadly similar to that for MgO and CaO (3.15 and 3.77 x $10^{-3}$ $cm^3$/mol-K, respectively). In comparison, the values for $\overline{V}_{FeO}$ and $\partial \overline{V}_{FeO} / \partial T$ reported in Lange and Carmichael (1987) are 13.83 ± 0.15 $cm^3$/mole and 2.92 ± 1.62 x $10^{-3}$ $cm^3$/mol-K, respectively; the larger error on $\partial \overline{V}_{FeO} / \partial T$ is due to the absence of liquid volume data at low temperatures at $T_f'$, and the significantly larger $\overline{V}_{FeO}$ value is controlled by density measurements reported in Mo et al. (1982) on a single FeO-$SiO_2$ liquid performed under reducing conditions.

Note that the effect of treating 4% of the total iron as $Fe^{3+}$, and assuming that the partial molar volume of the $Fe_2O_3$ component is 41.5 $cm^3$/mol (Liu and Lange, 2006), leads to a fitted value for $\overline{V}_{FeO}$ of 12.65 (vs. 12.86) $cm^3$/mol. Because the difference in $\overline{V}_{FeO}$ is relatively small, all iron is treated as $Fe^{2+}$ for simplicity.

When the molar volume data for pure hedenbergite ($CaFeSi_2O_6$) liquid from Guo et al. (2013) was included in the regression, it led to a large residual for this composition, well outside experimental error. This is because the fitted value for $\overline{V}_{FeO}$ in hedenbergite

liquid is 15.47 ± 0.20 $cm^3$/mole (Guo et al., 2013), substantially different from the value of 12.82 ± 0.16 $cm^3$/mole derived for the three model basalt compositions (Table 3.5a). Therefore ideal mixing does not extend to all compositions within the An-Di-Hd ternary, but does extend to a subset of compositions within the lower quadrilateral of that ternary (Fig. 3.1).

**Relaxed sound speed of the liquids**

Twenty-two relaxed sound speed measurements are reported in Table 3.6 for the three ternary samples. Each sample was measured at four different temperatures ranging between 1655 and 1876K. For each temperature, the measurements were taken at two centered frequencies (4.5 and 5.5 MHz). The sound speeds of the three basaltic liquids are independent of frequency, indicating that the liquids were relaxed. In all cases, the sound speeds decrease with increasing temperature (Fig. 3.7).

Modeling sound speed

Even though sound speed is not an extensive thermodynamic property, the following empirical model allows it to be modeled as a linear function of composition and temperature:

$$c^{liq}(X,T) = \sum X_i \left( c_{i,1723K} + \frac{\partial c_i}{\partial T}(T - 1723K) \right) \quad (8)$$

where $X_i$ is mole fraction of each oxide component, $c_i$ is the "partial molar" sound speed for each oxide component at a reference temperature (1723K), and $\partial c_i / \partial T$ is its temperature dependence. The sound speed data obtained for the three model basalt liquids in this study were combined with sound speed data in the literature for CaO-MgO-

$Al_2O_3$-$SiO_2$ liquids (Rivers and Carmichael, 1987; Secco et al., 1991; Webb and Courtial, 1996; Ai and Lange, 2008) in a regression of Equation (8), which recovers all measurements within experimental error. The results are presented in Table 3.7a and lead to a fitted $c_{FeO}$ value of 2042 (± 47) m/s at 1773 K, which differs by 17% from the value of 2389 m/s reported in Ghiorso and Kress (2004) that is largely influenced by sound speed measurements on FeO-$SiO_2$ liquids measured by Rivers and Carmichael (1987).

Modeling isothermal compressibility ($\beta_T$)

The sound speed and density data compiled in Table 3.6 were used to calculate the adiabatic compressibility from the relation, $\beta_S = 1/\rho c^2$. The adiabatic compressibility is converted to isothermal compressibility from the relation:

$$\beta_T = \beta_S + \frac{TV_T\alpha^2}{Cp} \tag{9}$$

where $T$ is temperature (K), $V_T$ is the molar volume at temperature T, $\alpha$ is the coefficient of thermal expansion and $Cp$ is the molar heat capacity. The $V_T$ and $\alpha$ terms were calculated from the results of this study (Table 3.5a). $Cp$ is calculated from the model of Lange and Navtrotsky (1992) for silicate liquids. The difference between $\beta_S$ and $\beta_T$ ranges from 2.6% to 6.5% of the value for $\beta_S$ in the model basalt liquids. The propagated uncertainty in $\beta_T$ is smaller than 3%.

For an ideal solution, $\beta_T$ varies as a linear function of the volume fraction of each oxide component (Rivers and Carmichael, 1987) and the following model includes a linear dependence on temperature:

$$\beta_T(X) = \sum X_i \frac{\overline{V}_{i,T}}{V_T}\left(\overline{\beta}_{i,T} + \frac{\partial\overline{\beta}_i}{\partial T}(T - 1723K)\right) \tag{10}$$

The data from this study (Table 3.6) and from the literature (Rivers and Carmichael, 1987; Secco et al., 1991; Webb and Courtial, 1996; Ai and Lange, 2008) were used in a regression of Equation (10), which recovers all measurements within experimental error (Fig. 3.8a).The results are presented in Table 3.8a and lead to a fitted $\overline{\beta}_{T,FeO}$ value of 4.75 ± 0.23 x $10^{-2}$ $GPa^{-1}$ at 1723 K, with no resolvable temperature dependence.

When the isothermal compressibility data for pure hedenbergite ($CaFeSi_2O_6$) liquid from Guo et al. (2013) was included in the regression of Equation (10), it led to large residuals for this composition, outside experimental error. The fitted value for $\overline{\beta}_{T,FeO}$ in hedenbergite liquid at 1723 K is 5.85 ± 0.14 $10^{-2}$ $GPa^{-1}$ (Guo et al., 2013), which differs from the value of 4.75 ± 0.23 $10^{-2}$ $GPa^{-1}$ derived for the three model basalt compositions (Table 3.8a). Therefore ideal mixing of melt compressibility does not extend to all compositions within the An-Di-Hd ternary, but does extend to a subset of compositions within the lower quadrilateral of that ternary (Fig. 3.1).

Modeling $(\partial V/\partial P)_T$

A final regression equation is presented for $\left(\partial V/\partial P\right)_T$, the derivative of volume with pressure at constant T, which is defined as $\left(\partial V/\partial P\right)_T = -V_T\beta_T$. It can be calculated for each experimental liquid from the density (molar volume) and isothermal compressibility values tabulated in Table 3.6.

For an ideal solution, $(\partial V/\partial P)_T$ varies as a linear function of composition, and the following model includes a linear dependence on temperature:

$$\left(\frac{\partial V}{\partial P}\right)_T (X,T) = \sum X_i \left(\frac{\partial \overline{V}_{i,1723}}{\partial P} + \frac{\partial^2 \overline{V}_i}{\partial P \partial T}(T - 1723K)\right) \qquad (11)$$

Again, the data from this study (Table 3.6) and from the literature (Rivers and Carmichael, 1987; Secco et al., 1991; Webb and Courtial, 1996; Ai and Lange, 2008) were used in a regression of Equation (11), which recovers all measurements within experimental error. The results are presented in Table 3.9a and lead to a fitted $\partial \overline{V}_{FeO} / \partial P$ value of -0.61 ± 0.03 $cm^3$ $mol^{-1}$ $GPa^{-1}$ at 1723 K, which differs by 27% from the fitted value of -0.46 ± 0.06 $cm^3$ $mol^{-1}$ $GPa^{-1}$ from Kress and Carmichael (1991) that is largely influenced by sound speed measurements on FeO-$SiO_2$ liquids by Rivers and Carmichael (1987).

Once again, when the $(\partial V / \partial P)_T$ data for pure hedenbergite ($CaFeSi_2O_6$) liquid from Guo et al. (2013) was included in the regression of Equation (11), it led to large residuals for this composition, well outside experimental error. The fitted value for $\partial \overline{V}_{FeO} / \partial P$ in hedenbergite liquid at 1723 K is -0.91 ± 0.03 $mol^{-1}$ $GPa^{-1}$(Guo et al., 2013), which differs from the value of -0.61 ± 0.03 $cm^3$ $mol^{-1}$ $GPa^{-1}$derived for the three model basalt compositions (Table 3.9a).

## Discussion

### Limits of ideal mixing in the An-Di-Hd ternary; variable $Fe^{2+}$ coordination

The modeling results for molar volume and compressibility, shown in Tables 3.5a, 3.8a and 3.9a, indicate that ideal mixing describes the new data presented in this study for the three liquids in the An-Di-Hd system, but does not extend to pure hedenbergite liquid.

The most likely cause of this behavior is that the three An-Di-Hd liquids from this study all share a similar average $Fe^{2+}$ coordination number, which is different from that in hedenbergite liquid.

In a recent study by Guo et al. (2013) on the density and compressibility of liquids in the CaO-FeO-$SiO_2$ system (where all liquids except hedenbergite were re-cast in the $CaFeO_2$-FeO-$SiO_2$ ternary system by assigning all available CaO to FeO to make the $CaFeO_2$ component), a case was made that fitted values for $\overline{V}_{FeO}$ and $\overline{V}_{CaFeO_2}$, derived from an ideal mixing model, represent $Fe^{2+}$ in 6-fold and 4-fold coordination, respectively, on the basis of comparisons to mineral molar volumes. For example, the fitted value for $\overline{V}_{FeO}$ of 12.11 $cm^3$/mole at 1723 K from Guo et al. (2013) is close to the volume of crystalline FeO (wüstite) at 298 K (12.06 $cm^3$/mole; Smyth and McCormick, 1995), where $Fe^{2+}$ is 6-fold coordinated. Similarly, the fitted liquid value for $\overline{V}_{CaFeO_2}$ of 33.82 $cm^3$/mole at 1723 K (Guo et al., 2013) is close to the molar volume of its crystalline equivalent at 298 K (30.64 $cm^3$/mole; Tassel et al., 2009), where $Fe^{2+}$ is 4-fold coordinated. In contrast, the derived $\overline{V}_{FeO}$ value of 17.1 $cm^3$/mole from the liquid $CaFeO_2$ component (derived by subtracting $\overline{V}_{CaO}$ from $\overline{V}_{CaFeO_2}$; Guo et al., 2013) is ~42% larger than the volume of crystalline FeO (wüstite). This large contrast in volume is of the same magnitude as that between liquid $\overline{V}_{Al_2O_3}$ (37.4 $cm^3$/mole; Table 3.4), where $Al^{3+}$ is in tetrahedral coordination, and corundum at 298 K (25.58 $cm^3$/mole; Smyth and McCormick, 1995), where $Al^{3+}$ is in octahedral coordination.

Under the assumption that the liquid $\overline{V}_{FeO}$ values of 12.1 and 17.1 $cm^3$/mole at 1723 K are closely representative of 6- and 4-coordinated $Fe^{2+}$, respectively, and that

$\overline{V}_{FeO}$ varies linearly with the average $Fe^{2+}$ coordination number in a silicate melt, Guo et al. (2013) used these two end-member $\overline{V}_{FeO}$ values to develop a linear equation to estimate the coordination number of $Fe^{2+}$:

$$CN = 10.85 - 0.401(\overline{V}_{FeO,1723K}). \quad (12)$$

From the derived value for $\overline{V}_{FeO}$ in hedenbergite liquid of 15.47 $cm^3$/mole from Guo et al. (2013), Equation 12 predicts an average $Fe^{2+}$ coordination number of 4.7, which is similar to the value of 4.5 derived from an EXAFS study on hedenbergite glass (Rossano et al., 2000). All the CFS liquids studied by Guo et al. (2013) have fitted $\overline{V}_{FeO}$ values (when added singly to a regression of Equation 7) that lead to calculated $Fe^{2+}$ coordination numbers that range from 5.2 to 4.6. In contrast, the fitted $\overline{V}_{FeO}$ value of 12.82 (± 0.32 at 2σ level)$cm^3$/mole obtained in this study for the three ternary An-Di-Hd liquids leads to an average $Fe^{2+}$ coordination number of 5.7 (± 0.1), which suggests a relatively high abundance of 6-coordinated $Fe^{2+}$ in these model basalt liquids.

**Systematic variation in $\overline{\beta}_{T,FeO}$ with $\overline{V}_{FeO}$ (and $Fe^{2+}$ coordination)?**

Given that not just the molar volumes but also the isothermal compressibilities of the three An-Di-Hd liquids mix ideally, it is of interest to evaluate how the fitted $\overline{\beta}_{T,FeO}$ value for the three model basalt liquids (4.75 x $10^{-2}$ $GPa^{-1}$) compares to the fitted $\overline{\beta}_{T,FeO}$ values for the CFS liquids studied by Guo et al. (2013). In that study, it was found that there was a strong linear and positive correlation between individually fitted $\overline{\beta}_{T,FeO}$ values and individually fitted $\overline{V}_{FeO}$ values (Fig. 3.9a), indirectly demonstrating a systematic variation between $\overline{\beta}_{T,FeO}$ and $Fe^{2+}$ coordination. Not surprisingly, the FeO

component with the largest molar volume displays the highest compressibility (Fig. 3.9). In Figure 3.9a, the fitted $\overline{\beta}_{T,FeO}$ and $\overline{V}_{FeO}$ values for the model basalts are plotted alongside the results for the CFS liquids from Guo et al. (2013). Also shown are the fitted end-member values for $\overline{\beta}_{T,FeO}$ and $\overline{V}_{FeO}$ for the FeO and $CaFeO_2$ components from that study ($Fe^{2+}$ close to 6- and 4-fold coordination, respectively). It can be seen that the results for the model basalt liquids fall off the trend line displayed by the CFS liquids, with the fitted $\overline{\beta}_{T,FeO}$ value ($4.75 \times 10^{-2}$ $GPa^{-1}$) higher than expected for its fitted $\overline{V}_{FeO}$ value (12.83 $cm^3$/mol). However, within the two-sigma error bars of the two fitted values, the displacement from the trend line is not large. Moreover, given that the concentrations of FeO in the model basalts are relatively low (8-13 mol%) compared to those in the CFS liquids (25-40 mol%), it is possible that the three An-Di-Hd liquids can be adequately modeled (within experimental error) in an ideal mixing model that includes the CFS liquids, which would then place the fitted $\overline{\beta}_{T,FeO}$ and $\overline{V}_{FeO}$ values for the model basalts on a common trend line with those from the CFS liquids in Figure 3.9b.

**A test of ideal mixing between An-Di-Hd and $CaFeO_2$-FeO-$SiO_2$ liquids**

In this section, it is evaluated whether the three An-Di-Hd liquids from this study can be combined with the $CaFeO_2$-FeO-$SiO_2$ liquids from the study of Guo et al. (2013) in regressions of the ideal model equations for molar volume (Equation 7), isothermal compressibility (Equation 10), and $\left(\partial V/\partial P\right)_T$ (Equation 11). By using the oxide components in Table 3.1 (and not assigning any FeO to be combined with CaO to create the $CaFeO_2$ component), the FeO component in the three An-Di-Hd liquids is assumed to

have the same $\overline{V}_i$, $c_i$, $\overline{\beta}_{T,i}$, and $\partial\overline{V}_i/\partial P$ (or the same average $Fe^{2+}$ coordination) as those for the FeO component in the $CaFeO_2$-FeO-$SiO_2$ liquids studied by Guo et al. (2013), which in turn is assumed to reflect an average $Fe^{2+}$ coordination close to 6-fold.

The results of those four regressions are shown in Tables 3.5b, 3.7b, 3.8b and 3.9b, and the residuals for molar volume and isothermal compressibility are shown in Figures 3.6b and 3.8b, respectively. The residuals indicate that the volumetric properties of the FeO component in the model basalt liquids can be viewed as similar to those for the FeO component in the $CaFeO_2$-FeO-$SiO_2$ liquids of Guo et al. (2103), within experimental error. The fitted $\overline{V}_{FeO}$ value at 1723 K of 12.48 ± 0.13 $cm^3$/mol (Table 3.5b) is still close to the molar volume of crystalline wüstite (12.06 $cm^3$/mol), with $Fe^{2+}$ in six-fold coordination, and substantially smaller than the derived $\overline{V}_{FeO}$ value of 16.80 $cm^3$/mol in the $CaFeO_2$ component (obtained by subtracting $\overline{V}_{CaO}$ from $\overline{V}_{CaFeO_2}$ in Table 3.5b). If a revised linear equation to estimate average $Fe^{2+}$ coordination number from these two end-member $\overline{V}_{FeO}$ values (12.48 and 16.80 $cm^3$/mol) is made, once again assuming they respectively reflect $Fe^{2+}$ in 6- and 4-fold coordination, the result leads to only slightly modified estimates of the average $Fe^{2+}$ coordination in the CFS liquids. For example, the calculated $Fe^{2+}$ coordination in hedenbergite liquid is 4.6 (vs. 4.7), once again close to the value of 4.5 obtained by EXAFS on hedenbergite glass (Rossano et al., 2000).

The fitted $\overline{\beta}_{T,FeO}$ value for the FeO component in the combined model basalts and $CaFeO_2$-FeO-$SiO_2$ liquids is 3.86 x $10^{-2}$ $GPa^{-1}$ (Table 3.8b), which is less compressible than the value of 4.75 x $10^{-2}$ $GPa^{-1}$ when the model basalts are considered without the CFS liquids, but considerably more compressible than $\overline{\beta}_{T,MgO}$ (0.47 x $10^{-2}$ $GPa^{-1}$),

presumed to reflect 6-coordinated $Mg^{2+}$, based on a comparison of $\overline{V}_{MgO}$ (11.76 $cm^3$/mol; Table 3.5), with the crystalline volume of periclase (11.72 $cm^3$/mol; Smyth and McCormick, 1995).

The results of this exercise of combining the model basalts with the CFS liquids in the same ideal mixing models for molar volume and isothermal compressibility should not be taken as evidence that $Fe^{2+}$ is fully 6-fold coordinated in the model basalts. The best estimate of the average $Fe^{2+}$ coordination in the An-Di-Hd liquids, based on the results of this study, is 5.7 ± 0.1, which can be tested further by examining the pressure dependence to the Fe-Mg exchange reaction ($^{Fe\text{-}Mg}K_D$) between orthopyroxene and basaltic melt in partial melting experiments of peridotite (e.g., Walter, 1998). Given the large variation in $\overline{V}_{FeO}$ as a function of $Fe^{2+}$ coordination number, it is expected that the pressure dependence of $^{Fe\text{-}Mg}K_D$ (opx-liq) is highly sensitive to the average $Fe^{2+}$ coordination number in basaltic liquids.

**An examination of the pressure dependence of $^{Fe\text{-}Mg}K_D$ (opx-liq)**

The Fe-Mg exchange reaction between orthopyroxene and basaltic melt can be expressed by the following equation:

$$Mg_2Si_2O_6\ (opx) + Fe_2Si_2O_6\ (liq) = Mg_2Si_2O_6\ (liq) + Fe_2Si_2O_6\ (opx) \qquad (13)$$

The pressure dependence of Equation (13) is determined by the change in volume of this exchange reaction:

$$\ln K(P) = \ln K(1\ bar) - \frac{1}{RT}\int_1^P \Delta V_T(P)\ dP\,. \qquad (14)$$

In Equation 14, the volume of the exchange reaction is the difference between the volume of fusion of enstatite and the volume of fusion of ferrosilite:

$$\Delta V_T(P) = \Delta V^{En}_{fusion}(P) - \Delta V^{Fs}_{fusion}(P) \quad (15)$$

where

$$\Delta V^{En}_{fusion}(P) = V^{liquid}_{T,Mg_2Si_2O_6}(P) - V^{crystal}_{T,Mg_2Si_2O_6}(P) \quad (16)$$

and

$$\Delta V^{Fs}_{fusion}(P) = V^{liquid}_{T,Fe_2Si_2O_6}(P) - V^{crystal}_{T,Fe_2Si_2O_6}(P). \quad (17)$$

In Figure 3.10, the molar volumes of liquid $Mg_2Si_2O_6$ and $Fe_2Si_2O_6$ and their crystalline equivalents are plotted as a function of pressure at 1723 K, using the data presented in this study (Tables 3.5b and 3.8b), as well as the X-ray diffraction data from Angel and Hugh-Jones (1994), Hugh-Jones (1997) and Hugh-Jones et al. (1997). In Figure 3.10b, the liquid volume of $Fe_2Si_2O_6$ is shown for three cases, where $Fe^{2+}$ is in 6-fold, 5-fold, and 4-fold coordination, using the linear relation in Figure 3.9b to calculate appropriate values for $\overline{V}_{FeO}$ and $\overline{\beta}_{T,FeO}$ in each case. Because it is well established that melt compressibility decreases with pressure, most strongly at low pressures (0-5 GPa), a 3rd-order Birch-Murnaghan equation of state with a $K'_0$ value of 5 was assumed for every liquid in Figure 3.10. The third-order form is:

$$P = \frac{3}{2}K_{T,0}\left(R^{7/3} - R^{5/3}\right)\left[1 - \frac{3}{4}\left(4 - K'_0\right)\left(R^{2/3} - 1\right)\right] \quad (18)$$

where $R = V_{T,0}/V_{T,P}$, $K_{T,0}$ is the bulk modulus at one bar ($=1/\beta_{T,0}$), and $K_0$' is the pressure dependence of the bulk modulus at one bar. The Birch-Murnaghan equation of state is a truncated series expansion derived from finite-strain theory (Birch, 1978) and has been successfully applied to numerous silicate liquids to several tens of GPa (e.g., Rigden et al., 1989; Stixrude and Bukowinski, 1990; Chen et al., 2002; Stixrude and Karki, 2005; Tenner et al., 2007; Lange, 2007). At pressures $\leq$ 5 GPa, the choice of $K'_0$ does not

significantly change calculated liquid volumes, and therefore the $K'_0$value of 5 applied in pMELTS by Ghiorso et al. (2002) is also used here. Direct high-pressure density measurements on liquids with variable $Fe^{2+}$ coordination are needed to specifically determine appropriate $K'_0$ values to use in Figure 3.10.

Integration of the volume term in Equation 14, using the data plotted in Figure 3.10, leads to distinctly different predictions of how the value of $^{Fe\text{-}Mg}K_D$ (opx-liq) varies with pressure (Fig. 3.11). Observations of the one-bar value between basaltic liquid and orthopyroxene range from 0.26 to 0.34 (e.g., Shi and Libourel, 1991; Grove and Juster, 1989; Juster et al., 1989; Gaetani and Grove, 1998), leading to a best estimate of 0.30 ± 0.04. Assuming a one-bar value of 0.30 ± 0.04, the value of $^{Fe\text{-}Mg}K_D$(opx-liq) is predicted to increase strongly to > 1 by 5 GPa if $Fe^{2+}$ is 4-fold coordinated, which is clearly not supported by the high-pressure phase equilibrium results of Walter (1998). Instead, the evidence in Figure 3.11 is consistent with an average $Fe^{2+}$ coordination between 5 and 6, and perhaps between 5.5 and 5 based on the absence of any evidence that $^{Fe\text{-}Mg}K_D$(opx-liq) decreases with pressure.

**The role of alkalis on $Fe^{2+}$ coordination in basaltic liquids**

One critical difference between the composition of the liquids in the experiments of Walter (1998) and the An-Di-Hd liquids from this study is in the concentration of alkalis. Partial melts of garnet peridotite in the experiments of Walter (1998) contain up to 2 wt% $Na_2O + K_2O$, whereas the liquids from this study are alkali-free. In the multi-spectroscopic study of Jackson et al. (2005) on a wide variety of $Fe^{2+}$-bearing multi-component silicate glasses, it is shown that increasing the Na/Ca ratio leads to progressively lower $Fe^{2+}$ coordination numbers. Therefore, an average $Fe^{2+}$ coordination

number of 5.7 ± 0.1, derived from this study for the An-Di-Hd liquids, may be too high for natural basalts that contain alkalis. Density and compressibility data on alkali-bearing basaltic liquids are needed to test the role of alkalis on controlling $Fe^{2+}$ coordination and therefore the most appropriate values of $\overline{V}_{FeO}$ and $\overline{\beta}_{T,FeO}$ to use for magmatic liquids.

## Acknowledgements

This research was supported by the National Science Foundation through award EAR-0855774.

**Table 3.1**
Composition of samples

| sample | Di-An-Hd | Di-Hd | An-Hd |
|---|---|---|---|
| wt% | | | |
| $SiO_2$ | 47.11 | 50.80 | 44.05 |
| $Al_2O_3$ | 13.50 | - | 18.47 |
| MgO | 5.28 | 8.62 | - |
| CaO | 23.04 | 24.23 | 21.51 |
| $Fe_2O_3^T$ | 10.20 | 15.65 | 15.31 |
| Total | 99.13 | 99.30 | 99.34 |
| mol% | | | |
| $SiO_2$ | 49.44 | 50.10 | 49.23 |
| $Al_2O_3$ | 8.35 | - | 12.16 |
| MgO | 8.26 | 12.67 | - |
| CaO | 25.90 | 25.61 | 25.76 |
| $FeO_T$ | 8.05 | 11.62 | 12.87 |
| g.f.w. | 61.86 | 57.92 | 65.66 |

**Table 3.2**

Density of molten NaCl using Mo crucibles and bobs

| Temperature (K) | density ($g/cm^3$) | Mean ($g/cm^3$) |
|---|---|---|
| 1203 | 1.482 | |
| 1203 | 1.485 | |
| 1203 | 1.484 | |
| 1203 | 1.487 | |
| | | 1.485±0.002 |
| 1216 | 1.474 | |

**Table 3.3**

Density and volume of glasses at 298 K and $T_f'$

| Sample | ρ(298 K) ($g/cm^3$) | Vol (298K) ($cm^3$/g.f.w) | $\alpha^{glass}$ ($10^{-5}$/K) | ρ($T_f'$) ($g/cm^3$) | Vol ($T_f'$) ($cm^3$/g.f.w.) | $T_f'$ (K) |
|---|---|---|---|---|---|---|
| Di-An-Hd | 2.923 | 21.16 | 2.235 | 2.879 | 21.49 | 990 |
| Di-Hd | 3.048 | 19.00 | 2.694 | 2.995 | 19.34 | 943 |
| An-Hd | 2.941 | 22.33 | 2.598 | 2.891 | 22.71 | 954 |

**Table 3.4**
Density, surface tension and volume of experimental liquids at high temperature

| Sample | T (K) | Density ($g/cm^3$) | γ(T) N/m | Vmeas ($cm^3$/g.f.w) | Vcalc ($cm^3$/g.f.w) | %Residual 100×(meas-calc)/meas |
|---|---|---|---|---|---|---|
| Di-An-Hd | 1585 | 2.732 | 0.36 | 22.64 | 22.53 | 0.48 |
| Di-An-Hd | 1585 | 2.728 | 0.35 | 22.67 | 22.53 | 0.63 |
| Di-An-Hd | 1585 | 2.736 | 0.37 | 22.61 | 22.53 | 0.34 |
| Di-An-Hd | 1585 | 2.733 | 0.35 | 22.63 | 22.53 | 0.45 |
| Di-An-Hd | 1721 | 2.713 | 0.35 | 22.80 | 22.74 | 0.26 |
| Di-An-Hd | 1721 | 2.717 | 0.37 | 22.77 | 22.74 | 0.11 |
| Di-An-Hd | 1721 | 2.712 | 0.35 | 22.81 | 22.74 | 0.29 |
| Di-An-Hd | 1721 | 2.717 | 0.37 | 22.77 | 22.74 | 0.11 |
| Di-An-Hd | 1813 | 2.706 | 0.39 | 22.86 | 22.88 | -0.10 |
| Di-An-Hd | 1813 | 2.706 | 0.39 | 22.86 | 22.88 | -0.10 |
| Di-An-Hd | 1813 | 2.706 | 0.39 | 22.86 | 22.88 | -0.10 |
| Di-An-Hd | 1813 | 2.706 | 0.39 | 22.86 | 22.88 | -0.10 |
| Di-Hd | 1653 | 2.821 | 0.34 | 20.53 | 20.58 | -0.26 |
| Di-Hd | 1653 | 2.828 | 0.38 | 20.48 | 20.58 | -0.50 |
| Di-Hd | 1653 | 2.819 | 0.33 | 20.55 | 20.58 | -0.18 |
| Di-Hd | 1653 | 2.826 | 0.38 | 20.49 | 20.58 | -0.43 |
| Di-Hd | 1723 | 2.814 | 0.36 | 20.58 | 20.71 | -0.61 |
| Di-Hd | 1723 | 2.810 | 0.35 | 20.61 | 20.71 | -0.47 |
| Di-Hd | 1723 | 2.817 | 0.38 | 20.56 | 20.71 | -0.72 |
| Di-Hd | 1723 | 2.814 | 0.37 | 20.58 | 20.71 | -0.61 |
| Di-Hd | 1838 | 2.787 | 0.38 | 20.78 | 20.92 | -0.64 |
| Di-Hd | 1838 | 2.784 | 0.36 | 20.80 | 20.92 | -0.54 |
| Di-Hd | 1838 | 2.785 | 0.37 | 20.80 | 20.92 | -0.57 |
| Di-Hd | 1838 | 2.782 | 0.35 | 20.82 | 20.92 | -0.46 |
| An-Hd | 1653 | 2.774 | 0.34 | 23.67 | 23.64 | 0.11 |
| An-Hd | 1653 | 2.782 | 0.39 | 23.60 | 23.64 | -0.17 |
| An-Hd | 1653 | 2.771 | 0.33 | 23.70 | 23.64 | 0.22 |
| An-Hd | 1653 | 2.778 | 0.38 | 23.64 | 23.64 | -0.03 |
| An-Hd | 1723 | 2.762 | 0.36 | 23.77 | 23.74 | 0.12 |
| An-Hd | 1723 | 2.761 | 0.35 | 23.78 | 23.74 | 0.16 |
| An-Hd | 1723 | 2.761 | 0.36 | 23.78 | 23.74 | 0.16 |
| An-Hd | 1723 | 2.760 | 0.35 | 23.79 | 23.74 | 0.19 |
| An-Hd | 1838 | 2.732 | 0.32 | 24.03 | 23.91 | 0.52 |
| An-Hd | 1838 | 2.729 | 0.31 | 24.06 | 23.91 | 0.63 |
| An-Hd | 1838 | 2.727 | 0.31 | 24.08 | 23.91 | 0.70 |
| An-Hd | 1838 | 2.724 | 0.30 | 24.10 | 23.91 | 0.81 |

**Table 3.5a**
Linear regression of partial molar volume of each oxide for ternary basalt liquids

| Oxide component | $\overline{V_i}(1723K) \pm 1\sigma$ ($cm^3$/mol) | $\partial\overline{V_i}/\partial T \pm 1\sigma$ ($10^{-3}cm^3$/mol-K) |
|---|---|---|
| $SiO_2$ | 26.86 ± 0.04 | -- |
| $Al_2O_3$ | 37.60 ± 0.09 | -- |
| CaO | 16.70 ± 0.06 | 3.77 ± 0.13 |
| MgO | 11.75 ± 0.08 | 3.18 ± 0.18 |
| $Na_2O$ | 29.25 ± 0.07 | 7.68 ± 0.11 |
| $K_2O$ | 46.68 ± 0.11 | 12.08 ± 0.22 |
| FeO | 12.82 ± 0.16 | 3.69 ± 0.58 |

[a]Total of 174 observations; $R^2$=0.9999, the average error is 0.25%

**Table 3.5b**
Linear regression of partial molar volume of each oxide for ternary basalts and CaO-FeO-$SiO_2$ liquids

| Oxide component | $\overline{V_i}(1723K) \pm 1\sigma$ ($cm^3$/mol) | $\partial\overline{V_i}/\partial T \pm 1\sigma$ ($10^{-3}cm^3$/mol-K) |
|---|---|---|
| $SiO_2$ | 26.84 ± 0.04 | -- |
| $Al_2O_3$ | 37.61 ± 0.09 | -- |
| CaO | 16.77 ± 0.06 | 3.84 ± 0.14 |
| MgO | 11.76 ± 0.09 | 3.17 ± 0.20 |
| $Na_2O$ | 29.26 ± 0.08 | 7.68 ± 0.12 |
| $K_2O$ | 46.70 ± 0.12 | 12.07 ± 0.24 |
| FeO | 12.48 ± 0.13 | 3.33 ± 0.63 |
| $CaFeO_2$ | 33.57 ± 0.11 | 3.89 ± 0.98 |

[a]Total of 198 observations; $R^2$=0.9999, the average error is 0.27%

**Table 3.6**
Sound speed and compressibility data for experimental liquids

| Sample | $f$ (MHz) | T (K) | $c$ (m/s) | $\beta_S$ ($10^{-2}$ GPa$^{-1}$) | $\beta_T$ ($10^{-2}$ GPa$^{-1}$) | d$V$/d$P$ ($10^{-4}$cm$^3$/bar) |
|---|---|---|---|---|---|---|
| Di-An-Hd | 4.5 | 1655 | 2831 | 4.567 | 4.754 | -1.076 |
| Di-An-Hd | 5.5 | 1655 | 2861 | 4.623 | 4.824 | -1.103 |
| Di-An-Hd | 4.5 | 1727 | 2835 | 4.473 | 4.659 | -1.055 |
| Di-An-Hd | 5.5 | 1727 | 2851 | 4.592 | 4.792 | -1.096 |
| Di-An-Hd | 4.5 | 1798 | 2827 | 4.575 | 4.769 | -1.085 |
| Di-An-Hd | 5.5 | 1798 | 2837 | 4.640 | 4.848 | -1.114 |
| Di-An-Hd | 4.5 | 1873 | 2829 | 4.524 | 4.718 | -1.073 |
| Di-An-Hd | 5.5 | 1873 | 2830 | 4.638 | 4.846 | -1.114 |
| Di-Hd | 4.5 | 1653 | 2852 | 4.440 | 4.763 | -0.992 |
| Di-Hd | 5.5 | 1653 | 2855 | 4.370 | 4.674 | -0.962 |
| Di-Hd | 4.5 | 1717 | 2846 | 4.431 | 4.754 | -0.990 |
| Di-Hd | 5.5 | 1717 | 2853 | 4.361 | 4.664 | -0.960 |
| Di-Hd | 4.5 | 1781 | 2845 | 4.489 | 4.822 | -1.009 |
| Di-Hd | 5.5 | 1781 | 2853 | 4.411 | 4.725 | -0.978 |
| Di-Hd | 4.5 | 1847 | 2838 | 4.472 | 4.805 | -1.006 |
| Di-Hd | 5.5 | 1847 | 2848 | 4.392 | 4.706 | -0.974 |
| An-Hd | 4.5 | 1663 | 2774 | 4.683 | 4.838 | -1.145 |
| An-Hd | 5.5 | 1663 | 2782 | 4.785 | 4.952 | -1.182 |
| An-Hd | 4.5 | 1733 | 2758 | 4.655 | 4.811 | -1.138 |
| An-Hd | 5.5 | 1733 | 2756 | 4.834 | 5.007 | -1.200 |
| An-Hd | 4.5 | 1803 | 2756 | 4.757 | 4.918 | -1.168 |
| An-Hd | 4.5 | 1876 | 2748 | 4.765 | 4.926 | -1.170 |

**Table 3.7a**
Regression results for $c_i$ at 1723K by Equation (8) using ternary basalt data from this study and literature[a]

| Oxide component | $c_i \pm 1\sigma$ (m/s) | $\partial c_i/\partial T \pm 1\sigma$ ($ms^{-1}$ $K^{-1}$) |
|---|---|---|
| $SiO_2$ | 2183 ± 16 | - |
| $Al_2O_3$ | 2657 ± 19 | - |
| CaO | 4205 ± 20 | -0.49 ± 0.07 |
| MgO | 3588 ± 23 | - |
| FeO | 2042 ± 47 | - |

[a]Total of 173 observations; $R^2$ = 0.9999, and average error is 0.56%.

**Table 3.7b**
Regression results for $c_i$ at 1723K by Equation (8) using ternary basalt from this study and CaO-FeO-$SiO_2$ data from literature[a]

| Oxide component | $c_i \pm 1\sigma$ (m/s) | $\partial c_i/\partial T \pm 1\sigma$ ($ms^{-1}$ $K^{-1}$) |
|---|---|---|
| $SiO_2$ | 2201 ± 18 | - |
| $Al_2O_3$ | 2669 ± 22 | - |
| CaO | 4168 ± 22 | -0.49 ± 0.07 |
| MgO | 3560 ± 26 | - |
| FeO | 2286 ± 41 | - |
| $CaFeO_2$ | 3233 ± 32 | -1.39 ± 0.17 |

[a]Total of 199 observations; $R^2$ = 0.9999, and average error is 0.66%.

**Table 3.8a**

Regression results for $\beta_i$ at 1723K by Equation (10) using ternary basalt data from this study and literature[a]

| Oxide component | $\overline{\beta_i} \pm 1\sigma$ ($10^{-2}$ $GPa^{-1}$) | $\partial\overline{\beta_i} / \partial T \pm 1\sigma$ ($10^{-2}$ $GPa^{-1}K^{-1}$) | $K_i$ (GPa) |
|---|---|---|---|
| $SiO_2$ | 7.130 ± 0.040 | - | 14.0 |
| $Al_2O_3$ | 4.496 ± 0.033 | - | 22.2 |
| CaO | -1.455 ± 0.077 | 0.00632 ± 0.00029 | -68.7 |
| MgO | 0.395 ± 0.126 | - | 253.2 |
| FeO | 4.749 ± 0.227 | - | 21.1 |

[a]Total of 173 observations; $R^2$ = 0.9999, and average error is 0.97%.

**Table 3.8b**

Regression results for $\beta_i$ at 1723K by Equation (10) using ternary basalts from this study and CaO-FeO-$SiO_2$ data from literature[a]

| Oxide component | $\overline{\beta_i} \pm 1\sigma$ ($10^{-2}$ $GPa^{-1}$) | $\partial\overline{\beta_i} / \partial T \pm 1\sigma$ ($10^{-2}$ $GPa^{-1}K^{-1}$) | $K_i$ (GPa) |
|---|---|---|---|
| $SiO_2$ | 7.108 ± 0.043 | - | 14.1 |
| $Al_2O_3$ | 4.489 ± 0.037 | - | 22.3 |
| CaO | -1.321 ± 0.082 | 0.00632 ± 0.00029 | -75.7 |
| MgO | 0.472 ± 0.137 | - | 211.8 |
| FeO | 3.859 ± 0.218 | 0.00537 ± 0.00208 | 25.9 |
| $CaFeO_2$ | 2.767 ± 0.065 | 0.00459 ± 0.00066 | 36.1 |

[a]Total of 199 observations; $R^2$ = 0.9998, and average error is 1.05%.

**Table 3.9a**
Regression results for $\partial V_i/\partial P$ at 1723K by Equation (11) using ternary basalt data from this study and literature[a]

| Oxide component | $\partial \overline{V_i} / \partial P \pm 1\sigma$ ($10^{-4}$cm$^3$ bar$^{-1}$) | $\partial^2 \overline{V_i} / \partial P \partial T \pm 1\sigma$ ($10^{-4}$ cm$^3$ bar$^{-1}$K$^{-1}$) |
|---|---|---|
| $SiO_2$ | -1.916 ± 0.011 | - |
| $Al_2O_3$ | -1.695 ± 0.013 | - |
| CaO | 0.245 ± 0.013 | -0.00102 ± 0.00005 |
| MgO | -0.047 ± 0.015 | - |
| FeO | -0.613 ± 0.031 | - |

[a]Total of 173 observations; $R^2$ = 0.9998, and average error is 0.96%.

**Table 3.9b**
Regression results for $\partial V_i/\partial P$ at 1723K by Equation (11) using ternary basalts from this study and CaO-FeO-$SiO_2$ data from literature[a]

| Oxide component | $\partial \overline{V_i} / \partial P \pm 1\sigma$ ($10^{-4}$cm$^3$ bar$^{-1}$) | $\partial^2 \overline{V_i} / \partial P \partial T \pm 1\sigma$ ($10^{-4}$ cm$^3$ bar$^{-1}$K$^{-1}$) |
|---|---|---|
| $SiO_2$ | -1.908 ± 0.011 | - |
| $Al_2O_3$ | -1.692 ± 0.014 | - |
| CaO | 0.223 ± 0.014 | -0.00102 ± 0.00005 |
| MgO | -0.057 ± 0.017 | - |
| FeO | -0.468 ± 0.028 | -0.00097 ± 0.00027 |
| $CaFeO_2$ | -0.942 ± 0.021 | -0.00152 ± 0.00022 |

[a]Total of 199 observations; $R^2$ = 0.9998, and average error is 1.06%.

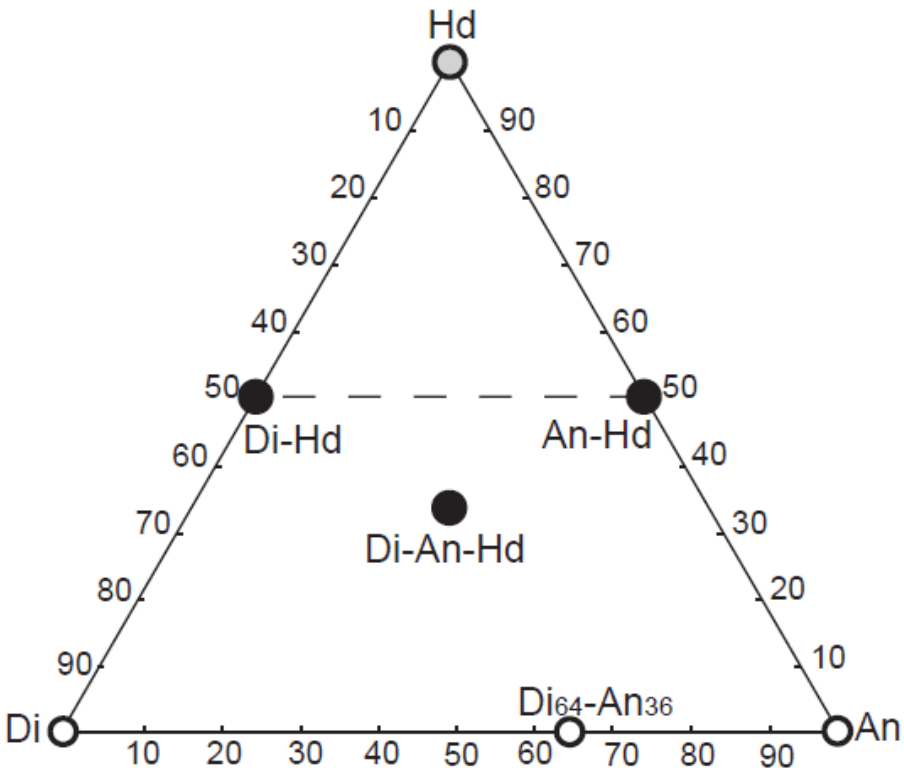


**Figure 3.1** Composition of the liquids in Di-An-Hd ternary system (mol%)

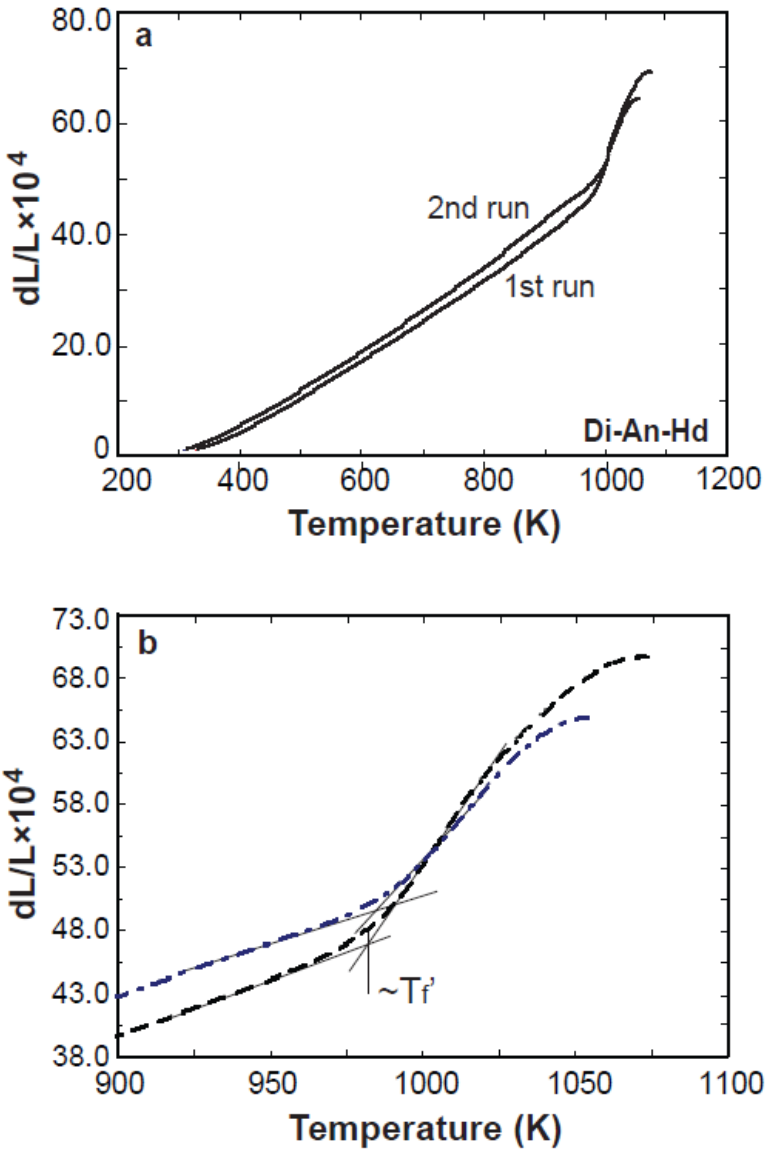


**Figure 3.2** (a) Two scans of dL/L vs. temperature for Di-An-Hd glass using a Perkin-Elmer diamond TMA at a heating rate 10K/min. (b) a blow-up of the two glass transition intervals from (a).

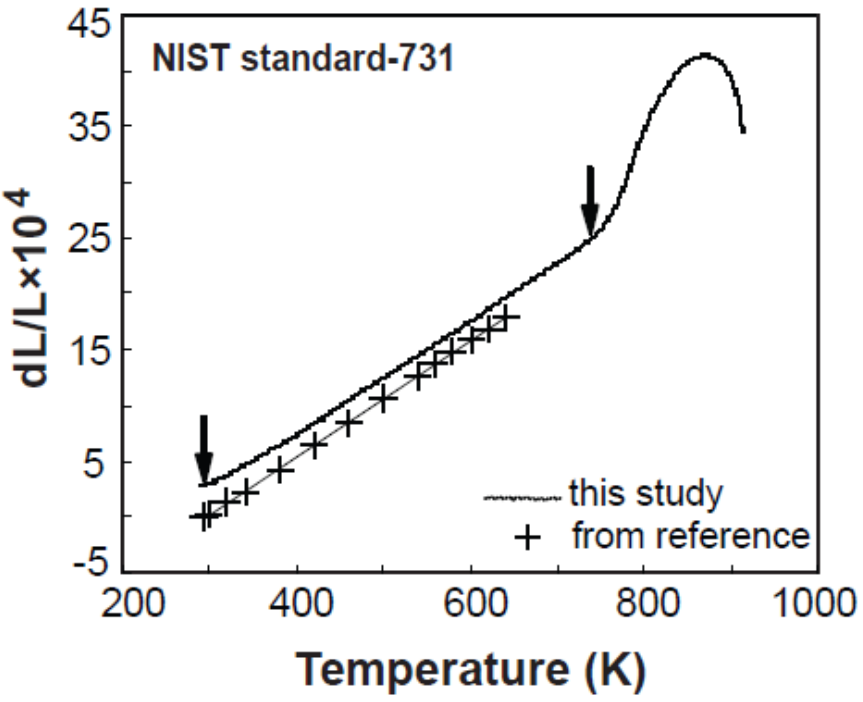


**Figure 3.3** The curve of dL/L vs. termperatue for borosilicate glass (NIST standard-731). The cross symbols are for the data from the standard reference (certificate of this material). The slope is the linear coefficient of thermal expansion. Our study takes the section between the two arrows, giving a slope as 0.0519; the slope from the reference is 0.0518

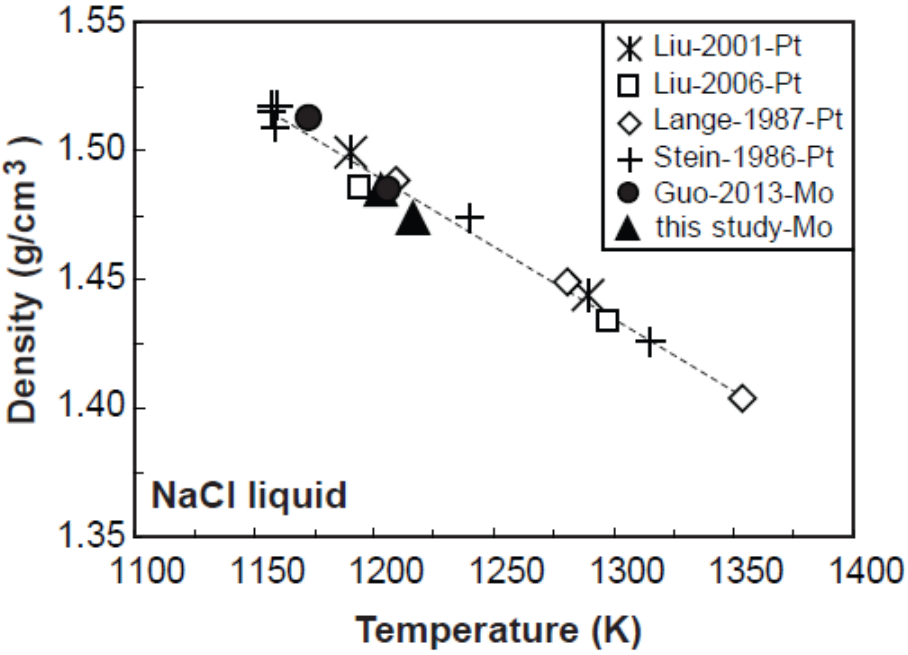


**Figure 3.4** The density of molten NaCl vs. temperature. The data from this study are shown in solid dots. The dashed line ($\rho = 2.166\text{-}5.622\times10^{-4}$ T(K)) is from early studies including Lange and Carmichael (1987), Stein et al. (1986), Liu and Lange (2001) and Liu and Lange (2006), as well as this study.

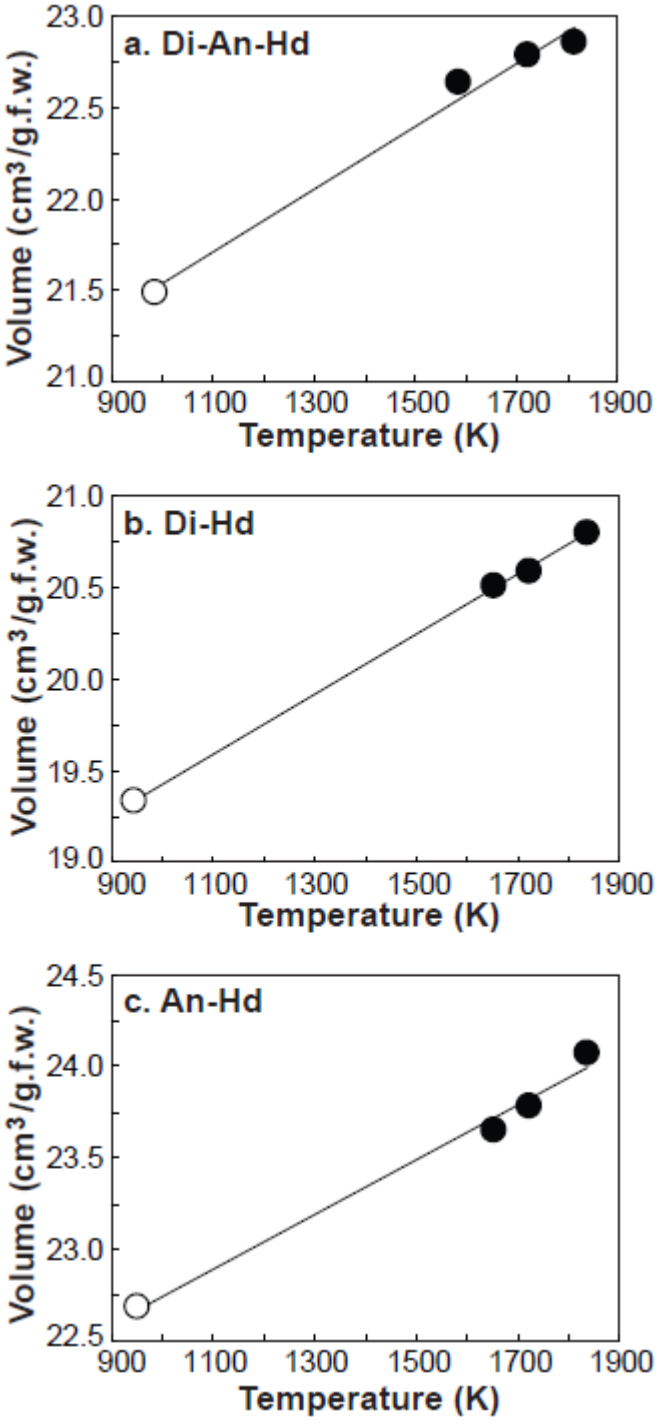


**Figure 3.5** Plots of liquid volume vs. Temperature. The solid dots are for high temperature volume data. The open dots are for low-temperature volumes at $T_f'$. The error bars are smaller than the symbols. The solid line is a linear fit to all the volume data.

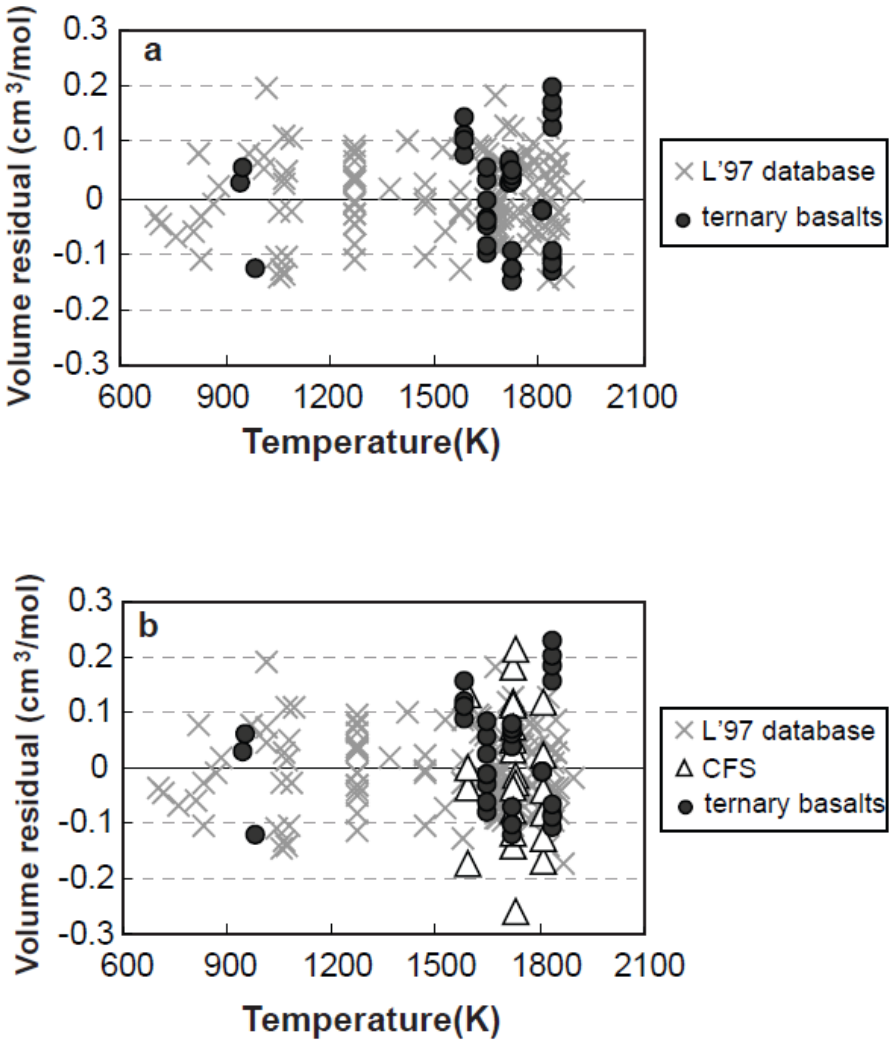


**Figure 3.6** (a) Plot of volume residual vs. temperature for ternary model basalts. The solid dots are for ternary model basalts, the cross symbols are for database from Lange (1997). (b) Plot of volume residual vs. temperature for fit with ternary model basalts and CFS liquids. The solid dots are for ternary model basalts, the open triangles are for CFS liquids with $CaFeO_2$ component from Guo et al. (2013). The database from Lange (1997) are shown by cross symbols.

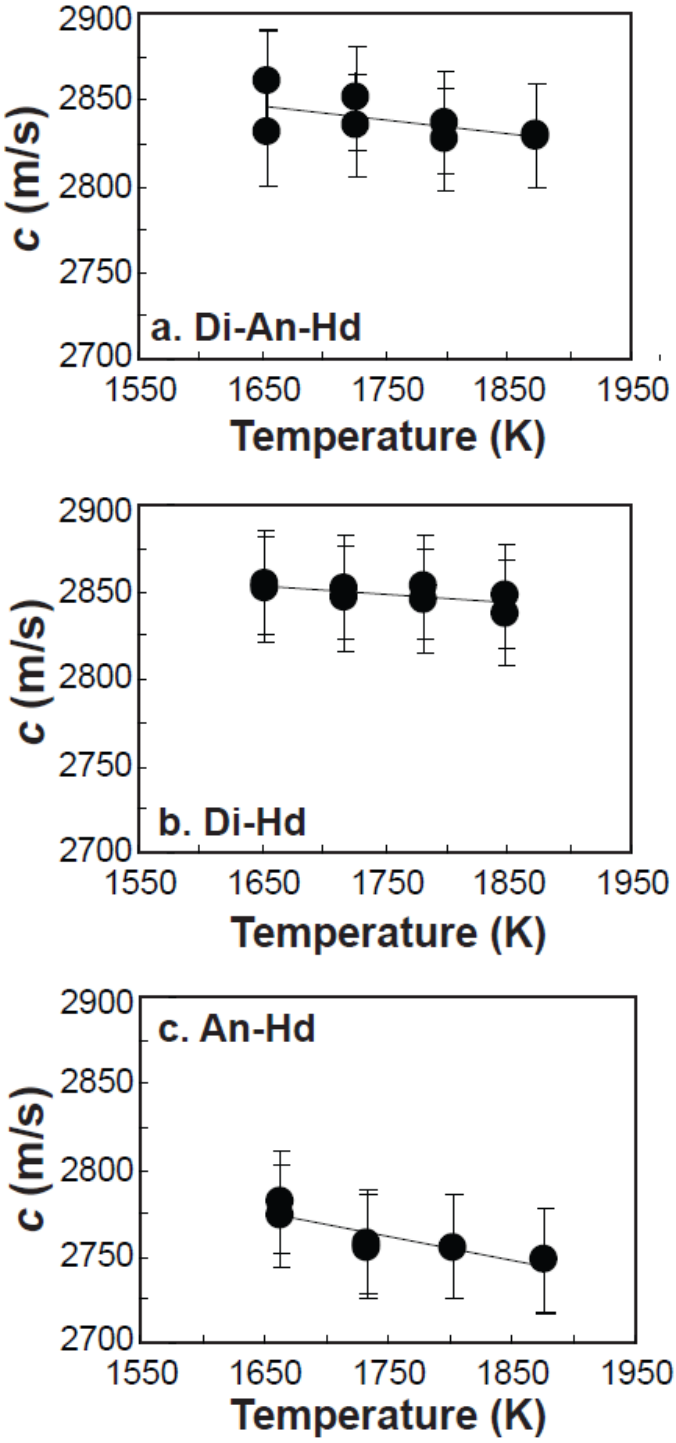


**Figure 3.7** Plots of sound speed vs. Temperature for experimental liquids. The solid line is the linear fit to the data. The errors in sound speed are ±30m/s.

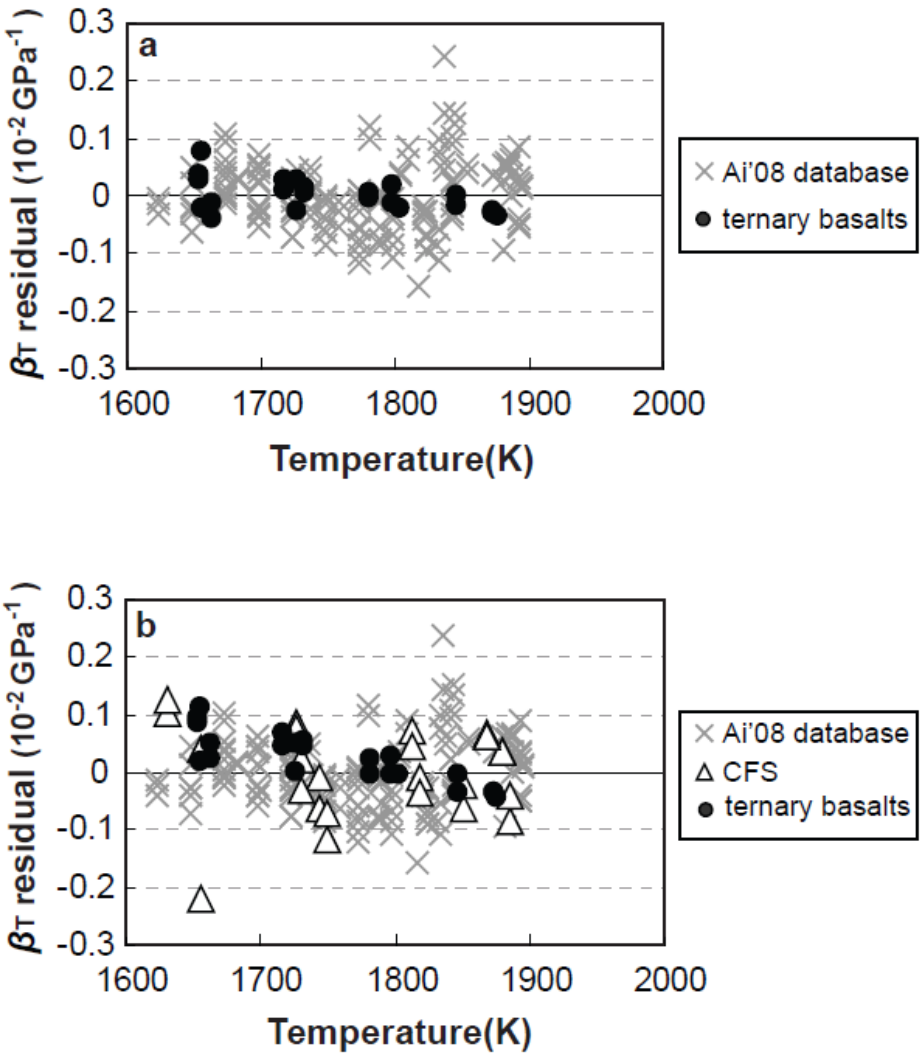


**Figure 3.8** (a) Plot of isothermal compressibility residual vs. temperature for ternary model basalts. The solid dots are for ternary model basalts, the cross symbols are for database from Ai and Lange (2008). (b) Plot of isothermal compressibility residual vs. temperature for fit with ternary model basalts and CFS liquids. The solid dots are for ternary model basalts, the open triangles are for CFS liquids with $CaFeO_2$ component from Guo et al. (2013). The database from Ai and Lange (2008) are shown by cross symbols.

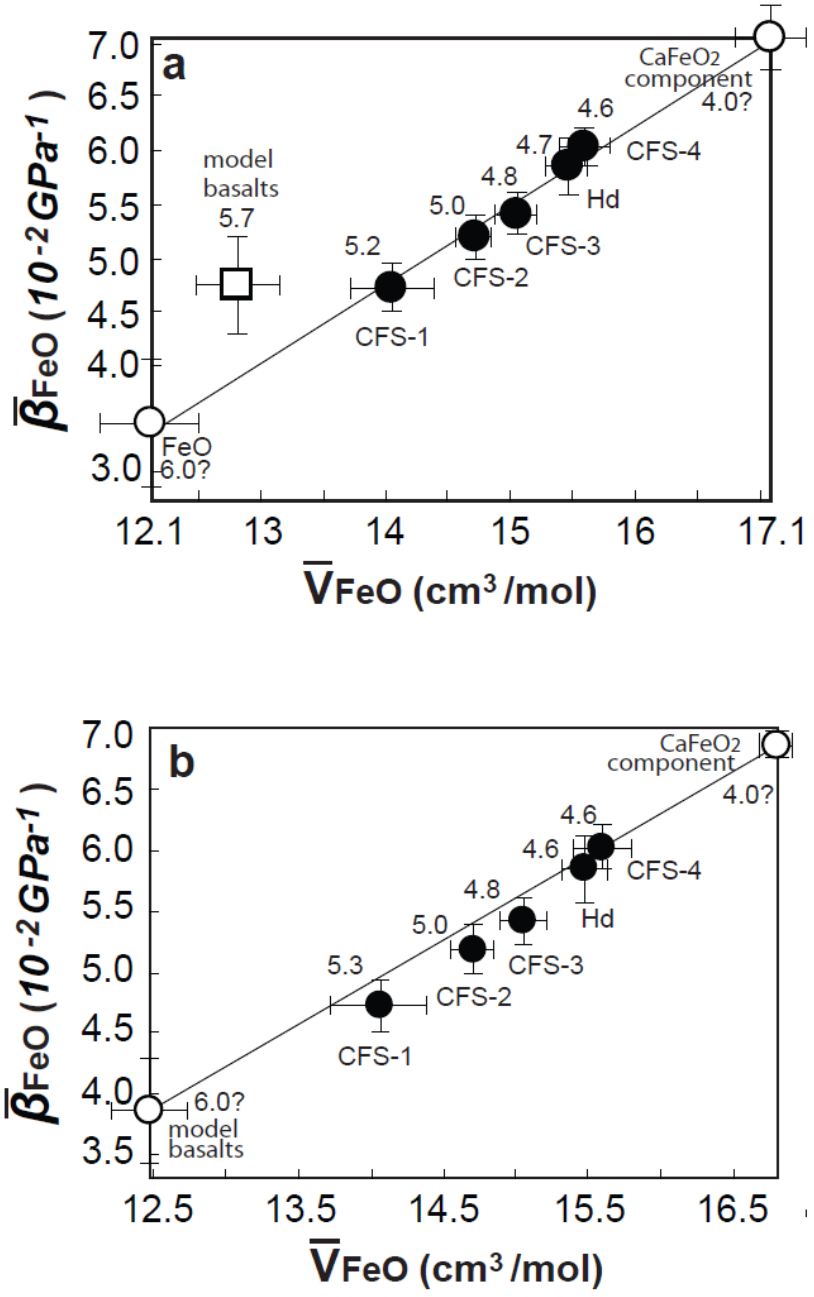


**Figure 3.9** (a) Plot of $\overline{\beta}_{FeO}$ vs. $\overline{V}_{FeO}$ for ternary model basalts and CFS liquids from Guo et al. (2013). (b) Plot of $\overline{\beta}_{FeO}$ vs. $\overline{V}_{FeO}$ for ternary model basalts combined with CFS liquids from Guo et al. (2013) as an ideal mixing. The solid line is a linear fit for 4- and 6-coordinated values. The error are 2σ.

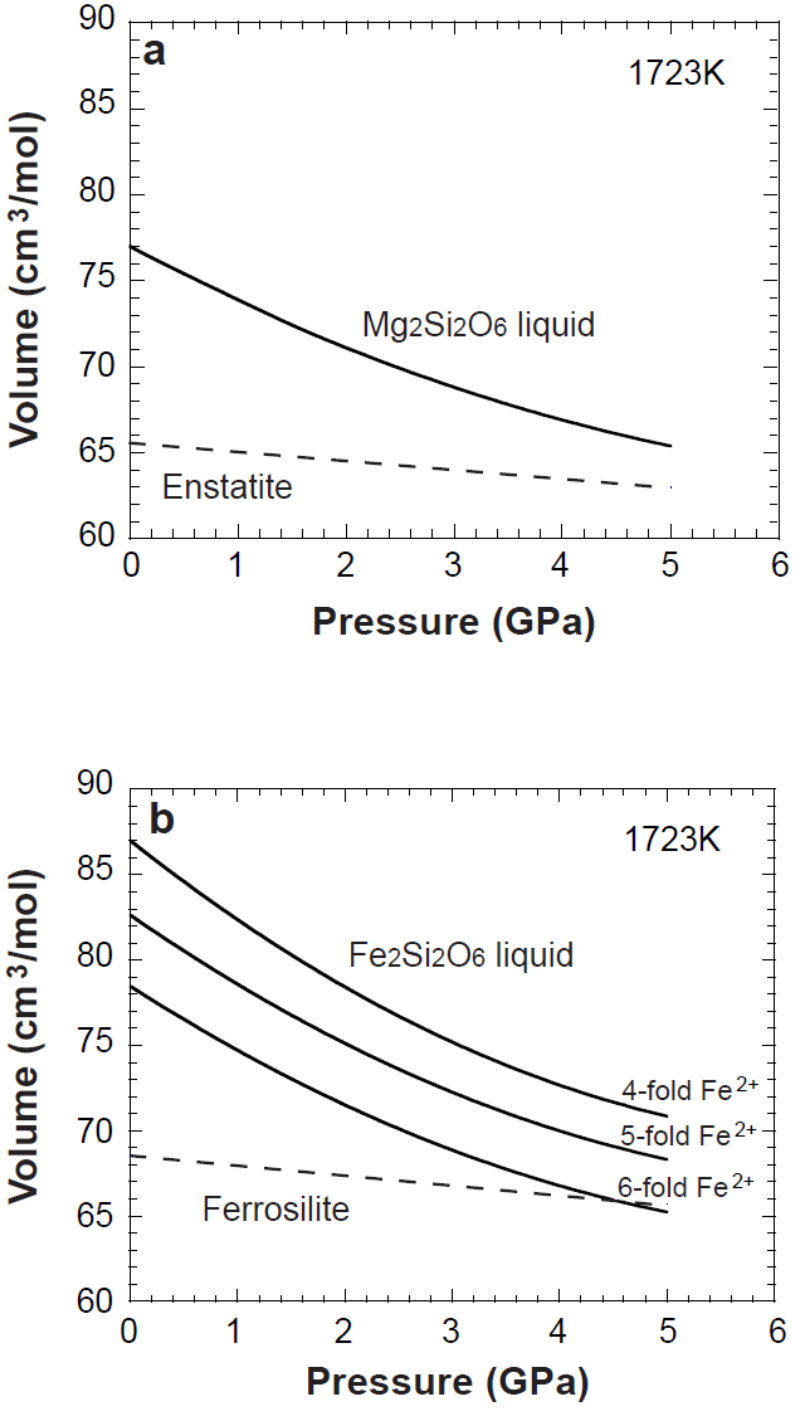


**Figure 3.10** (a) Plot of liquid and crystalline molar volume for Enstatite ($Mg_2Si_2O_6$) as a function of pressure; (b) Plot of liquid and crystalline molar volume for Ferrosilite ($Fe_2Si_2O_6$) as a function of pressure.

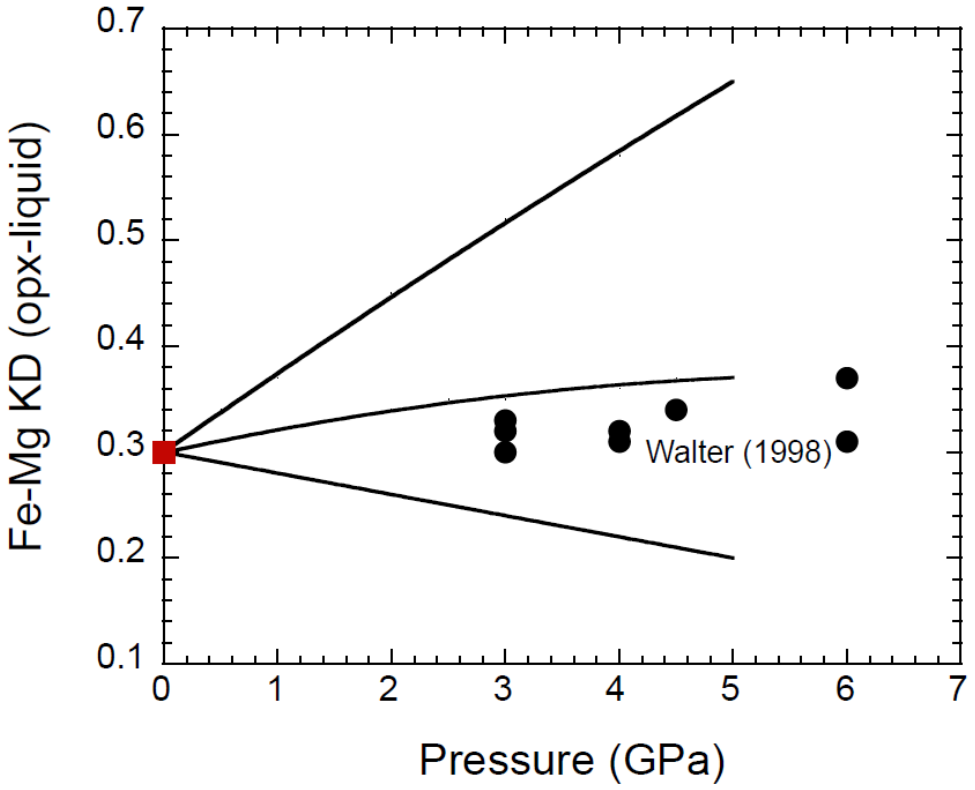


**Figure 3.11** Plot of $^{Fe\text{-}Mg}K_D$ (opx-liquid) as a function of pressure

# References


Ai, Y., Lange R., 2004a. An ultrasonic frequency sweep interferometer for liquids at high temperature: 1. Acoustic model. J. Geophys. Res. 109, B12203. doi:10.1029/2003JB00284.

Ai, Y., Lange R., 2004b. An ultrasonic frequency sweep interferometer for liquids at high temperature: 2. Mechanicalassembly, signal processing, and application. J. Geophys. Res. 109, B12204. doi:10.1029/2004JB00306.

Ai, Y., Lange, R.A., 2008. New acoustic velocity measurements on CaO-MgO-$Al_2O_3$-$SiO_2$ liquids: Reevaluation of the volume and compressibility of $CaMgSi_2O_6$-$CaAl_2Si_2O_8$ liquids to 25 GPa. Journal of Geophysical Research 113, B04203, doi:10.1029/2007JB005010.

Angel, R.J., Hugh-Jones D.A., 1994. Equations of state and thermodymic properties of enstatite pyroxenes. Journal of Geophysical Research 99, 777-783.

Asimow, P.D., Ahrens T.J., 2010. Shock compression of liquid silicates to 125 Gpa: the anorthite-diopside join. Journal of Geophysical Research 115, B10209.

Birch, F., 1978. Finite strain isotherm and velocities for single-crystal and polycrystalline NaCl at high pressures and 300K. Journal of Geophysical Research 95, 1257-1268

Bockris, J.O'M., Tomlinson, J.W., White, J.L., 1956. The structure of the liquid silicates: partial molar volumes and expansivities. Trans Faraday Soc. 52, 299-310.

Chase, M.W., 1998. MIST-JANAF thermochemical tables, fourth edition. Journal of Physical Chemistry Reference Data, Monograph Springer: Heidelberg 9.

Chen, G.Q., Ahrens, T.J., Stolper E. M., 2002. Shock-wave equation of state of molten and solid fayalite. Physics of the Earth and Planetary Interiors 134, 35-52.

Dadd, K.A., 2011. Extension-related volcanism in the Middle to Late Devonian of the Lachlan Orogen: geochemistry of mafic rocks in the Comerong Volcanics. Australian Journal of Earth Sciences 58, 209-222.

Debenedetti, P.G., 1996. Metastable liquids: Concepts and principals. Princeton University Press.

Dingwell, D.B., Brearley, M., Dickinson J. E., 1988. Melt densities in the $Na_2O$-FeO-$Fe_2O_3$-$SiO_2$ system and the partial molar volume of tetrahedrally-coordinated ferric iron in silicate melts. Geochimica et Cosmochimica Acta 52, 2467-2475

Dunlap, R.A., Edelman, D.A., Mackay, G.R., 1998. A Mossbauer effect investigation of correlated hyperfine parameters in natural glasses (tektites). J. Non-Crystal. Solids 223, 141-146.

Farges, F., Lefrere, Y., Rossano, S., Berthereau, A., Calas, G., Brown, G.E.Jr., 2004. The effect of redox state on the local structural environment of iron in silicate glasses: A molecular dynamics, combined XAFS spectroscopy, and bond valence study. Journal of Non-Crystalline Solids 344, 176-188

Gaetani, G.A., Grove, T.L., 1998. The influence of water on melting of mantle peridotite. Contrib. Mineral Petrol. 131, 323-346.

Ghiorso, M.S., Hirschmann, M.M., Reiners, P.W., Kress V.C., 2002. The pMELTS: A revision of MELTS for improved calculation of phase relations and major element partitioning related to partial melting of the mantle to 3 GPa, Geochemistry Geophysics Geosystems 3(5), 10.1029/2001GC000217

Ghiorso, M.S., Kress, V.C., 2004. An equation of state for silicate melts. II. Calibration of volumetric properties at 10(5) Pa. American Journal of Science 304, 679-751.

Gray, D. E. 1972. American Institute of Physics Handbook, 3rd ed. 4-127.

Grove, T.L., Juster, T.C, 1989. Experimental investigations of low-Ca pyroxene stability and olivine-pyroxene-liquid equilibria at 1-atm in natural basaltic and andesitic liquids. Contrib. Mineral Petrol. 103, 287-305.

Guo, X., Lange, R.A., Ai, Y., 2013. The density and compressibility of CaO-FeO-$SiO_2$ liquids: evidence for four-coordinated $Fe^{2+}$ in the $CaFeO_2$ component. submitted to Geochimica et Cosmochimica Acta.

Hugh-Jones, D., 1997. Thermal expansion of $MgSiO_3$ and $FeSiO_3$ ortho- and clinopyroxenes. American Mineralogist 82, 689-696.

Hugh-Jones, D., Chopelas, A., Augel R., 1997. Tetrahedral compression in (Mg,Fe)$SiO_3$ orthopyroxenes. Phys. Chem. Minerals 24, 301-310.

Jackson, W.E., 1991. Spectroscopic studies of ferrous iron in silicate liquids, glasses and crystals. Ph.D. dissertation, Department of Geology, Standford University. 162pp.

Jackson, W.E., Waychunas, G.A., Brown, G.E., Leon, J.M., Conradson, S., Combes, J.-M., 1993. High-temperature XAS study of Fe2SiO4 liquid: Reduced coordination of ferrous iron. Science 262, 229–232.Science, 262,229.

Jackson, W.E., Farges, F., Yeager, M., Mabrouk, P.A., Rossano, S., Waychunas, G.A., Solomon, E.I., Brown $J_R$, G.E., 2005. Multi-spectroscopic study of Fe(II) in silicate glasses: Implications for the coordination environment of Fe(II) in silicate melts. Geochimica et Cosmochimica Acta 69(17), 4315-4332.

Janz, G. J. and Lorenz, M.R., 1960. Precise measurement of density and surface tension at temperatures up to 1000$^{o}$C in one apparatus. The review of scientific instruments 31(1), 18-22

Juster, T.C., Grove, T.L., Perfit, M.R., 1989. Experimental constrains on the generation of FeTi basalts, andesites, and rhyodacites at the Galapagos spreading center, 85-degrees-W and 95-degrees-W. Journal of Geophysical research-solid earth and planets 94, B7, 9251-9274, DOI: 10.1029/JB094iB07p09251

Kress, V.C., Carmichael, I.S.E., 1991. The compressibility of silicate liquids containing $Fe_2O_3$ and the effect of composition, temperature, oxygen fugacity and pressure on their redox states. Contributions to Mineralogy and Petrology 108, 82-92.

Lange, R.A., Carmichael, I.S.E., 1987. Densities of $Na_2O$-$K_2O$-CaO-MgO-FeO-$Fe_2O_3$-$Al_2O_3$-$TiO_2$-$SiO_2$ liquids: New measurements and derived partial molar properties. Geochimica et Cosmochimica Acta 51, 2931-2946

Lange, R.A., 1996. Temperature independent thermal expansivities of sodium aluminosilicate melts between 713 and 1835 K. Geochimica et Cosmochimica Acta 60, 4989–4996.

Lange, R.A., 1997. A revised model for the density and thermal expansivity of $K_2O$-$Na_2O$-CaO-MgO-$Al_2O_3$-$SiO_2$ liquids from 700 to 1900 K: Extension to crustal magmatic temperatures. Contributions to Mineralogy and Petrology, 130, 1–11.

Lange, R.A., Navtrotsky A., 1992. Heat capacities of $Fe_2O_3$-bearing silicate liquids. Contrib. Mineral Petrol. 110, 311-320.

Liu, Q., Lange, R.A., 2001. The partial molar volume and thermal expansivity of $TiO_2$ in alkali silicate melts: Systematic variation with Ti coordination. Geochimica et Cosmochimica Acta 65(14), 2379-2393

Liu, Q. and Lange, R.A., 2006. The partial molar volume of $Fe_2O_3$ in alkali silicate melts: Evidence for an average $Fe^{3+}$ coordination number near five. American Mineralogist 91, 385-393.

Mo, X., Carmichael, I.S.E., Rivers, M., Stebbins, J.F., 1982. The partial molar volume of $Fe_2O_3$ in multicomponent silicate liquids and the pressure-dependence of oxygen fugacity in magmas. Mineralogical Magazine 45, 237-245

Moynihan, C.T., Easteal, A.J., Debolt, M.A., Tucker J., 1976. Dependence of fictive temperature of glass on cooling rate. Journal of the American Ceramic Society 59, 12-16.

Rigden, S.M., Ahrens, T.J., Stolper E. M., 1989. Shock compression of molten silicate: results for a model basaltic composition. J. Geophys. Res. 94, 9508-9522.

Rivers, M.L., Carmichael, I.S.E., 1987. Ultrasonic studies of silicate melts. J. Geophys. Res. Solid Earth Planets 92, 9247–9270.

Rossano, S., Balan, E., Morin, G., Bauer, J.P., Brouder C., Calas G.,1999. $^{57}Fe$ Mossbauer spectroscopy of tektite. Phys. Chem. Mineral 26, 530-538.

Rossano, S., Ramos, A.Y., Delaye, J.-M., 2000. Environment of ferrous iron in $CaFeSi_2O_6$ glass: contributions of EXAFS and molecular dynamics. Journal of Non-Crystalline Solids 273, 48-52.

Secco, R.A., Manghnani M.H., Liu T.C., 1991. The bulk modulusattenuation-viscosity systematics of diopside-anorthite melts, Geophys. Res. Lett. 18, 93– 96.

Scherer, G.W., 1992. Relaxation in glass and composites. Krieger Publishing Company, Malabar, Florida.

Shi, P., Libourel, G., 1991. The effects of FeO on the system CMAS at low pressure and implications for basalt crystallization processes 108, 129-143.

Shiraishi, Y., Ikeda K., Tamura A., Saito T., 1978. On the viscosity and density of the molten FeO-$SiO_2$ system. Transactions of the Japan Institue of Metals 19, 264-274.

Smyth, J.R., McCormick, T.C., 1995. Crystallographic data for minerals. In T. Ahrens, Ed., Mineral Physics and Crystallography, p.1-17. AGU Reference shelf 2, Washington, D.C.

Stein, D.J., Stebbins, J.F., Carmichael, I.S.E., 1986. Density of molten sodium aluminosilicates. J. Am. Ceram. Soc. 69, 396–399.

Stixrude, L., Karki B., 2005. Structure and freezing of $MgSiO_3$ liquid in Earth's lower Mantle. Science 310, 297-299

Stixrude, L., Bukowinski, M.S.T., 1990. Fundamental thermodynamic relations and silicate melting with implications for the constitution of D". Journal of Geophysical Research-Solid Earth and Planets 95, 19311-19325

Tangeman, J.A., Lange, R.A., 2001. Determination of the limiting fictive temperature of silicate glasses from calorimetric and dilatometric methods: application to low-temperature liquid volume measurements. American Mineralogist 86, 1331-1344.

Tenner, T.J., Lange, R.A., Downs, R.T., 2007. The albite fusion curve re-examined: New experiments and the high-pressure density and compressibility of high albite and naAlSi$_3$O$_8$ liquid. American Mineralogist 92, 1573-1585.

Thomas, C.W., Liu, Q., Agee, C.B., Asimow P.D., Lange, R.A., 2012. Multi-technique equation of state for $Fe_2SiO_4$ melt and the density of Fe-bearing silicate melts from 0 to 161 GPa. Journal of Geophysical Research-Solid Earth 117, B10206, doi: 10.1029/2012JB009403.

Walter, M.J., 1998. Melting of garnet peridotite and the origin of komatitite and depleted lishosphere. J. Petrol. 39, 29-60.

Webb, S., Courtial P., 1996, Compressibility of melts in the $CaOAl_2O_3$-$SiO_2$ system, Geochim. Cosmochim. Acta 60, 75–86.

Wilke, M., Parzsch, G.M., Bernhardt, R., Lattard D., 2004. Determination of the iron oxidation state in basaltic glasses using XANES at the K-edge Chemical Geology 213, 71-87.

Wilke, M., Farges, F., Partzsch, G.M., Schmidt, C., Behrens H., 2007. Speciation of Fe in silicate glasses and melts by in-situ XANES spectroscopy. American Mineralogist 92, 44-56.

# CHAPTER IV

## Density and Acoustic Velocity Measurements on $Na_2O$-FeO-$SiO_2$ Liquids: Evidence of a Highly Compressible FeO Component Related to Five-coordinated $Fe^{2+}$


## Abstract

Double-bob density measurements using molybdenum bobs in a reducing atmosphere were made on four $Na_2O$-FeO-$SiO_2$ (NFS) liquids between 1323 and 1649 K. These data were combined with low-temperature density measurements at the limiting fictive temperature to provide liquid density data over a wide temperature interval, spanning ~800 degrees. In addition, relaxed sound speeds were measured in these liquids with an acoustic interferometer at centered frequencies of 4.5 and 5.5 MHz between 1420 and 1829 K. An ideal mixing model using the oxide components ($Na_2O$-FeO-$SiO_2$) for molar volume and isothermal compressibility cannot recover the experimental results within error. When each experimental liquid is fitted individually, the partial molar volume of the FeO component ($\overline{V}_{FeO}$) increases systematically with $Na_2O$ concentration, consistent with a composition-induced decrease in the average $Fe^{2+}$ coordination number from 5.2 to 4.5. In contrast, the isothermal compressibility ($\overline{\beta}_{T,FeO}$), which has anomalously high

values from 10.1 to 14.9 $10^{-2}$ $GPa^{-1}$, decrease with $Na_2O$ concentration (and increase with $Fe^{2+}$ coordination). The high values of $\overline{\beta}_{T,FeO}$ in sodic liquids are similar to those observed for $\overline{\beta}_{T,TiO_2}$ in sodic liquids, and it is proposed they are related to $Fe^{2+}$ and $Ti^{4+}$ in square-pyramidal coordination sites at the interface of alkali-rich and silica-rich domains in the melt, which promotes topological mechanisms of compression.

## Introduction

Iron is the only major element in natural silicate melts with more than one oxidation state ($Fe^{2+}/Fe^{3+}$). To model various magmatic processes, thermodynamic information on both the FeO and $Fe_2O_3$ components in silicate melts is therefore necessary. For example, the partial molar volume and compressibility of FeO and $Fe_2O_3$ must be known to calculate how the $Fe^{2+}/Fe^{3+}$ ratio in magmatic liquids changes with depthin the mantle (Kress and Carmichael, 1991).

It is well established that $Fe^{2+}/Fe^{3+}$ equilibrium behaves differently in calcic vs. sodic vs. natural liquids (e.g., Thornber et al., 1980; Sack et al., 1980; Kress and Carmichael, 1988, 1989; Lange and Carmichael, 1989). Some of these differences may be caused by changes in the coordination environment of $Fe^{2+}$(4-, 5-, and 6-fold) in these liquids as a function of the field strength of coexisting cations (e.g., Jackson et al., 1993, 2005; Brown et al., 1995; Wilke et al., 2007).

To date, high-quality double-bob density measurements on $Fe^{2+}$-bearing silicate liquids in a reducing environment have been restricted to alkali-free liquids, including those in the FeO-$SiO_2$ system (Shirashi et al., 1978; Mo et al., 1982; Thomas et al., 2012), the CaO-FeO-$SiO_2$ system (Guo et al., 2013a), and the CaO-MgO-FeO-$Al_2O_3$-$SiO_2$

system (Guo et al., 2013b). In this study, we present the first systematic study of the effect of variable $Na_2O$ concentration on the partial molar volume, thermal expansivity and compressibility of the FeO component in silicate melts.

The capacity of $Fe^{2+}$ to occur in variable coordination environments (4, 5 and 6) in silicate liquids at one bar is a feature it shares with $Ti^{4+}$ (e.g., Farges et al., 1996a, 1996b, 1996c; Farges, 1997). Therefore, one of the goals of this study is to explore the similarities and differences between the volumetric properties of FeO- and $TiO_2$-bearing sodium silicate liquids. For example, Liu and Lange (2001) and Liu et al. (2007) found that $\overline{V}_{TiO_2}$, $\partial\overline{V}_{TiO_2}/\partial T$ and $\overline{\beta}_{T,TiO_2}$ all vary systematically with $Na_2O$ concentration in silicate melts, which they related to composition-induced changes in $Ti^{4+}$ coordination. Moreover, Liu et al. (2007) documented an extraordinarily large compressibility for the $TiO_2$ component (nearly three times larger than the $SiO_2$ component) when $Ti^{4+}$ is five-fold coordinated. In this study we test whether similar trends are observed in FeO-bearing sodium silicate liquids, or whether the volumetric properties of FeO in sodic liquids are similar to those in calcic liquids (Guo et al., 2013a).

## Experimental Methods

### Sample preparation

The four $Na_2O$-FeO-$SiO_2$ (NFS) samples used in this study are from Liu and Lange (2006), which were synthesized and analyzed in air. For all property measurements, the samples were first equilibrated in a reducing atmosphere (1% CO-99%Ar) in a molybdenum crucible or foil container. During this procedure, because the activity of $MoO_2$ in the samples was less than one, and because the melts were not saturated with

metallic iron, the oxygen fugacity of the sample liquids at each temperature of equilibration was constrained to be between the Mo-$MoO_2$ and Fe-FeO buffers (~4.3 log units below the Ni-NiO buffer). At this redox condition, the model of Kress and Carmichael (1991) predicts 4 ± 1% of the total iron as $Fe^{3+}$. The bulk compositions are listed in Table 4.1, Figure 4.1, with all the iron reported as FeO, for simplicity. For each composition, the gram formula weight ( g.f.w.=$X_i M_i$) is tabulated in Table 4.1 as well, where $X_i$, $M_i$ are the mole fraction and molecular weight of each oxide component respectively.

**Low-temperature measurements of liquid volume at $T_f$'**

Following the technique described in Lange (1996, 1997), the low-temperature liquid volume of each sample was obtained at its limiting fictive temperature ($T_f$'). The limiting fictive temperature ($T_f$') is defined as the temperature where an extrapolated first order property (e.g. volume) of glass and liquid intersect (Scherer, 1992; Moynihan, 1995; Debenedetti, 1996). Because the volume of the glass is equal to that of the liquid at $T_f$', the following equation applies to both the glass and the liquid:

$$V^{liq}(T_f^{'}) = V^{glass}(T_f^{'}) = V_{298K}^{glass} \exp[\alpha^{glass}(T_f^{'} - 298)] \quad (1)$$

where $V_{298K}^{glass}$ is the glass volume at 298K and $\alpha^{glass}$ is the temperature-independent coefficient of thermal expansion for glass between 298K and $T_f$'. Therefore, with knowing (1) the glass volume (density) at 298 K; (2) the glass thermal expansion coefficient between 298 K and the beginning of the glass transition interval; and (3) the value of $T_f$', the molar volume of the liquid at $T_f$' can be obtained.

The room temperature (298 K) density of each glass sample was measured using the Archimedean method with a microbalance. For each density measurement, the glass was weighed several times both in air and in liquid toluene below the balance.

The Perkin-Elmer Diamond TMA vertical dilatometer was used to measure the linear thermal expansion coefficient, $(1/L)/(\partial L/\partial T)$, of each glass sample with a scan rate of 10 K/min and a constant force 10mN (Fig. 4.2). The volume thermal expansion coefficient is three times of the linear expansion coefficient. The measured glass samples have height between 1.6 and 4.7 mm. Each glass sample was polished to ensure that the bottom and top surfaces were flat and parallel. Replicate measurements indicate a reproducibility that is better than 13%, whereas the accuracy is within 3% based on our measurement of the thermal expansion of NIST Standard-731.

The $T_f'$ for each sample was chosen as the onset of the rapid rise in the dilatometry heating curves (dL/L vs. T) at the glass transition interval in our study. The accuracy of $T_{onset}$ as an approximation of the true value of $T_f'$, with a deviation smaller than 17 degrees, was established by comparing $T_{onset}$ values derived from dilatometry heating curves to values of $T_f'$ obtained quantitatively from heat capacity measurements (Tangeman and Lange, 2001).

**High-temperature liquid density measurements**

The density measurements of the four NFS liquids at high temperatures were measured by the double-bob Archimedean method by using molybdenum crucibles and bobs were used in a reducing atmosphere. The procedure is similar to that described by Guo et al. (2013a).

For each experiment, ~75 g of sample powder was melted in a Mo crucible and reduced in a stream of 1%CO-99%Ar gas by four batches. In this way, most of the ferric iron was converted to ferrous iron. A similar procedure was followed for fayalite liquid prior to density measurements in Thomas et al. (2012), and Mössbauer spectroscopy confirmed that $Fe^{3+}$ concentrations are low (< 5% of the total iron), consistent with saturation of the experimental melts with molybdenum metal and oxygen fugacity conditions below the Mo-$MoO_2$ buffer (Chase, 1998).

Each liquid sample was held in a Mo crucible inside a vertical tube Deltech furnace. The bob was immersed into the liquid by moving the furnace up and down. An electronic balance with a precision of ± 0.0001 g was mounted on an aluminum shelf atop the furnace to measure the buoyancy of the bob. The effect of surface tension is eliminated by using two Mo bobs of different mass (~19.5 and ~6.5 g) with identical stem diameters. The details were described in Guo et al. (2013a). The density of the liquid is calculated from the following equation:

$$\rho(T) = \frac{B_L(T) - B_S(T)}{V_L(T) - V_S(T)} \quad (2)$$

where $B_L(T)$ and $B_S(T)$ are the buoyancy of the large and small bobs, respectively, and $V_L(T)$ and $V_S(T)$ are the immersed volume of the large and small bob, respectively. The density as 10.22 g/cm$^3$ at 298 K) and thermal expansion from Gray (1972) for molybdenum metal are used to calculate the immersed volume of the Mo bobs as a function of temperature. For each temperature, the buoyancy of two different large bobs and two different small bobs were measured, allowing four density measurements to be made.

**Surface tension measurements**

The surface tension of the sample liquids against molybdenum can be derived from the density measurements with double-bob Archimedean method. If a single bob is used to measure melt density, the effect of this surface tension effect must be included in the calculation of melt density:

$$\rho(T) = \frac{B(T) + S(T)}{V(T)} \tag{3}$$

where $B(T)$ is the buoyancy of the single bob, $S(T)$ is the effect of surface tension on the bob stem on the buoyancy measurement, and $V(T)$ is the immersed volume of the single bob. Equation (2) can be rearranged to allow $S(T)$ to be calculated, from which the surface tension, $\gamma$ (N/m), can be derived with the following equation (Janz and Lorenz, 1960):

$$\gamma(T) = \frac{S(T)}{\pi d} g \tag{4}$$

where $g$ is the gravitational acceleration, and $d$ is the diameter of the stem.

**Sound speed measurements**

Sound speeds were measured in each sample liquid at one bar with a frequency sweep ultrasonic interferometer under a stream of 1%CO-99%Ar gas. The details are described in Ai and Lange (2004a, b). For each run, a wide-band acoustic pulse spanning 1-2MHz travels down the molybdenum upper buffer rod to the rod-melt interface. Part of the acoustic pulse is transmitted through the liquid and reflects off the polished base of the crucible. Two mirror reflections are returned up the buffer rod and delivered to the data acquisition system for signal processing, where a Fourier transform is performed,

which allows the returned signal to be evaluated as a periodic function of frequency, $\Delta f$, from which the sound speed is measured from the relation: $\Delta f = c/2S$, where $S$ is melt thickness. For each temperature and centered frequency, measurements are made at two or three different rod positions to get accurate measurement of relative thickness ($\Delta S = S_1 - S_2$), which is measured by a micrometer (resolution 0.001mm) mounting on the upper buffer rod. Because sound speed is independent of melt thickness, the relation can be expressed as:

$$c = \left| \frac{2\Delta S}{\Delta f_2^{-1} - \Delta f_1^{-1}} \right|. \quad (5)$$

## Results

### Low- and high-temperature liquid density data

The results of the low-temperature glass density and thermal expansion measurements are reported in Table 4.2, along with estimates of $T_f'$, which permit the volume of the supercooled liquid at $T_f'$ for each sample to be obtained. NFS-11 is not included in Table 4.2 because a sufficiently large glass sample for the 298 K density measurement could not be obtained (the sample tended to shatter during quench).

The high temperature density data for the four NFS liquids are presented in Table 4.3. Each sample was measured at three different temperatures. The standard deviations of the density range from 0.02% to 0.27%. These density data are converted to molar volume by using the following equation,

$$V(T) = g.f.w./\rho(T) \quad (6)$$

where *g.f.w.* is the gram formula weight, $\rho(T)$ is the liquid density at temperature T. Figure 4.3 shows that the molar volume for each sample increases linearly with temperature over an interval that spans> 900 degrees.

**Modeling molar volume as a function of temperature and composition**

The liquid volume data for the four $Na_2O$-FeO-$SiO_2$ liquids in Table 4.3 were combined with density data from the literature on $K_2O$-$Na_2O$-CaO-MgO-$Al_2O_3$-$SiO_2$ liquids (Bockris et al., 1956; Stein et al., 1986; Lange and Carmichael, 1987; Lange, 1996, 1997) to calibrate the following linear volume equation:

$$V^{liq}(X,T) = \sum X_i \left[ V_{i,T_{ref}} + \frac{\partial \overline{V}_i}{\partial T}(T - T_{ref}) \right] \qquad (7)$$

where $X_i$ is the mole fraction of each oxide component, $\overline{V}_{i,T_{ref}}$ is the partial molar volume of each oxide component at a reference temperature ($T_{ref}$ = 1723 K), and $\partial \overline{V}_i / \partial T$ is the partial molar thermal expansivity of each oxide component. The results of this regression led to a poor fit to the data (Fig. 4.4a), outside experimental error, in contrast to a regression of the same data set minus the $Na_2O$-FeO-$SiO_2$ liquids (Lange, 1997).

To test whether the poor fit to Eqn. 7 reflects a systematic variation in $\overline{V}_{FeO}$ with melt composition, the molar volumes of each individual liquid were added singly to the FeO-free data set in a series of regressions of Eqn. 7. The results are presented in Table 4.4 and Fig. 4.4b, and the fitted $\overline{V}_{FeO}$ and $\partial \overline{V}_{FeO} / \partial T$ values for each sample display a strong linear correlation with $X_{Na2O}$ (Fig. 4.5a, b). Values of $\overline{V}_{FeO}$ at 1723 K range from 14.07 (±0.10) to 15.86 (±0.13) $cm^3$/mol (Table 4.4), which are considerably larger than the $\overline{V}_{FeO}$ value of 12.82 ± 0.16 $cm^3$/mol derived from model basalt liquids in the

anorthite-diopside-hedenbergite ternary (Guo et al., 2013b), but overlap the $\overline{V}_{FeO}$ value of 15.47 ± 0.20 $cm^3$/mol in hedenbergite liquid (Guo et al., 2013a). Fitted $\partial\overline{V}_{FeO}/\partial T$ values range from 1.86 to 5.96 $10^{-3}$ $cm^3$/mol-K and are inversely correlated with $\overline{V}_{FeO}$. Unlike the case for the CaO-FeO-$SiO_2$ samples studies by Guo et al. (2013a), attempts to recast the liquids in terms of the $Na_2FeO_2$-FeO-$SiO_2$components failed to lead to a successful ideal mixing model for all four NFS liquids.

**Relaxed sound speed of the liquids**

Thirty-eight relaxed sound speed measurements are reported in Table 4.5 for the four NFS liquid samples. Each sample was measured at four to five different temperatures ranging between 1420 and 1829 K. For each temperature, the measurements were taken at two centered frequencies (4.5 and 5.5 MHz). The sound speeds of the NFS liquids are independent of frequency, indicating that the liquids were relaxed. In all cases, the sound speeds decrease linearly with increasing temperature (Fig. 4.6).

**Modeling sound speed**

Even though sound speed is not an extensive thermodynamic property, the following empirical model allows it to be modeled as a linear function of composition and temperature:

$$c^{liq}(X,T) = \sum X_i \left( c_{i,1723K} + \frac{\partial c_i}{\partial T}(T - 1723K) \right) \quad (8)$$

where $X_i$ is mole fraction of each oxide component, $c_i$ is the "partial molar" sound speed for each oxide component at a reference temperature (1723K), and $\partial c_i/\partial T$ is its temperature dependence. The sound speed data of the four NFS liquids were fitted into

the linear regression by combining with $Na_2O$-$Al_2O_3$-$SiO_2$ database from the literature (Rivers and Carmichael, 1987; Kress et al., 1988). The inclusion of all four NFS liquids to the regression gives a poor fit to the data, in contrast to the same dataset without FeO-bearing liquids. To test whether this reflects a systematic variation in $c_{FeO}$ with composition, the sound speeds of each individual liquid were added singly to the FeO-free data set in a series of regressions of Eqn. 8. The results are presented in Table 4.6 and the fitted $c_{FeO}$ values at 1723 K for each sample display a systematic variation with $X_{Na2O}$, similar to that seen for $\overline{V}_{FeO}$. In all cases, the fitted $c_{FeO}$ values (1215 to 1535 m/s) are significantly lower than the value of 2389 m/s reported in Ghiorso and Kress (2004), which is based largely on sound speed measurements on FeO-$SiO_2$ liquids from Rivers and Carmichael (1987).

**Modeling isothermal compressibility ($\beta_T$)**

The sound speed and density data compiled in Table 4.5 were used to calculate the adiabatic compressibility from the relation, $\beta_S = 1/\rho c^2$. The adiabatic compressibility is converted to isothermal compressibility from the relation:

$$\beta_T = \beta_S + \frac{TV_T\alpha^2}{Cp} \qquad (9)$$

where $T$ is temperature (K), $V_T$ is the molar volume at temperature T, $\alpha$ is the coefficient of thermal expansion and $Cp$ is the molar heat capacity. The $V_T$ and $\alpha$ terms were calculated from the results of this study (Table 4.4). $Cp$ is calculated from the model of Lange and Navtrotsky (1992) for silicate liquids. The difference between $\beta_S$ and $\beta_T$

ranges from 8.5% to 10.4% of the value for $\beta_S$ in the model basalt liquids. The propagated uncertainty in $\beta_T$ is smaller than 3%.

For an ideal solution, $\beta_T$ varies as a linear function of the *volume fraction* of each oxide component (Rivers and Carmichael, 1987) and the following model includes a linear dependence on temperature:

$$\beta_T(X) = \sum X_i \frac{\overline{V}_{i,T}}{V_T}\left(\overline{\beta}_{i,T} + \frac{\partial \overline{\beta}_i}{\partial T}(T - 1723K)\right) \qquad (10)$$

The volume and compressibility data from this study (Table 4.4, 4.5), combined with the $Na_2O$-$Al_2O_3$-$SiO_2$ data set from literature (Rivers and Carmichael, 1987; Kress et al., 1988), were used in a regression of Eq. (10). The results of this overall regression lead to poor fit, with residuals that range up to 5.7% (Fig. 4.7a) in excess of experimental errors.

When the NFS liquids are added singly in a series of regressions to Eqn. 10, the fitted values for $\overline{\beta}_{FeO}$ at 1723 K vary systematically with $X_{Na2O}$ (Fig. 4.5c), following the same pattern as that displayed for $\overline{V}_{FeO}$ and $\partial\overline{V}_{FeO}/\partial T$ in Figures 4.5a and 4.5b. The results from these individual regressions are tabulated in Table 4.7 and the residuals are shown in Figure 4.7b. In all cases, the fitted $\overline{\beta}_{T,FeO}$ values are remarkably large (10.08 to 14.91 $10^{-2}$ $GPa^{-1}$), all higher than the fitted $\overline{\beta}_{T,Na_2O}$ value of 9.10 (± 0.10) $10^{-2}$ $GPa^{-1}$. Unlike the case for the CaO-FeO-$SiO_2$ samples studies by Guo et al. (2013a), attempts to recast the liquids in terms of the $Na_2FeO_2$-FeO-$SiO_2$ components failed to lead to a successful ideal mixing model for the compressibility of the four NFS liquids.

**Modeling $(\partial V/\partial P)_T$**

A final regression equation is presented for $\left(\partial V/\partial P\right)_T$, the derivative of volume with pressure at constant T, which is defined as $\left(\partial V/\partial P\right)_T = -V_T\beta_T$. It can be calculated for each experimental liquid from the density (molar volume) and isothermal compressibility values tabulated in Table 4.5.

For an ideal solution, $(\partial V/\partial P)_T$ varies as a linear function of composition, and the following model includes a linear dependence on temperature:

$$\left(\frac{\partial V}{\partial P}\right)_T (X,T) = \sum X_i \left(\frac{\partial \overline{V}_{i,1723}}{\partial P} + \frac{\partial^2 \overline{V}_i}{\partial P \partial T}(T - 1723K)\right) \qquad (11)$$

Again, the data from this study (Table 4.5) and from the literature (Rivers and Carmichael, 1987; Kress et al., 1988) were used in a regression of Equation (11). The results lead to a poor fit to the data, with residuals in excess of experimental errors. To examine how $\partial \overline{V}_{FeO}/\partial P$ varies between the individual samples, each NFS liquid was added singly to the FeO-free data set in a series of regressions of Eqn. 11. The results are presented in Table 4.8 and show that fitted values for $\partial \overline{V}_{FeO}/\partial P$ vary systematically with $X_{Na2O}$, as seen for $\overline{V}_{FeO}$, $\partial \overline{V}_{FeO}/\partial T$ and $\overline{\beta}_{T,FeO}$. Fitted $\partial \overline{V}_{FeO}/\partial P$ values range from -1.59 to $-2.11\times10^{-4}$ $cm^3$/mol-bar and are 4-5 times larger than the value of -0.46 $10^{-4}$ $cm^3$/mol-bar reported in Kress and Carmichael (1991). Unlike the case for the CaO-FeO-$SiO_2$ samples studies by Guo et al. (2013a), attempts to recast the liquids in terms of the $Na_2FeO_2$-FeO-$SiO_2$ components failed to lead to a successful ideal mixing model for all four NFS liquids.

## Discussion

**Linear relation between $\overline{V}_{FeO}$ and $Fe^{2+}$ coordination?**

In Figure 4.8a, fitted $\overline{V}_{FeO}$ values for the four NFS liquids increase linearly with $Na_2O$ concentration, which is similar to the pattern observed by Liu and Lange (2001) for fitted $\overline{V}_{TiO_2}$ values in the $Na_2O$-$TiO_2$-$SiO_2$ system (Fig. 4.8b) and by Guo et al. (2013a) for fitted $\overline{V}_{FeO}$ values in the CaO-FeO-$SiO_2$ system (Fig. 4.8c). In the latter two cases, the systematic increase in $\overline{V}_{TiO_2}$ and $\overline{V}_{FeO}$ were related to composition-induced changes in the coordination of $Ti^{4+}$(5.4 to 4.6) and $Fe^{2+}$ (5.2 to 4.6) respectively. In all cases, the effect of increasing polymerization leads to higher average coordination numbers.

In the study by Guo et al. (2013a) on the density and compressibility of liquids in the CaO-FeO-$SiO_2$ system, a case was made that derived values for $\overline{V}_{FeO}$ at 1723 K of 12.1 and 17.1 $cm^3$/molrepresent $Fe^{2+}$ in 6-fold and 4-fold coordination, respectively, on the basis of comparisons to mineral molar volumes. For example, the fitted value for $\overline{V}_{FeO}$ of 12.11 $cm^3$/mol (Guo et al., 2013a) is close to the volume of crystalline FeO (wüstite) at 298 K (12.06 $cm^3$/mole; Smyth and McCormick, 1995), where $Fe^{2+}$ is 6-fold coordinated. Similarly, the fitted liquid value for $\overline{V}_{CaFeO_2}$ of 33.82 $cm^3$/mole K (Guo et al., 2013a) is close to the molar volume of its crystalline equivalent at 298 K (30.64 $cm^3$/mole; Tassel et al., 2009), where $Fe^{2+}$ is 4-fold coordinated. By subtracting $\overline{V}_{CaO}$ from $\overline{V}_{CaFeO_2}$, the resulting value for $\overline{V}_{FeO}$ is 17.1 $cm^3$/mol. Guo et al. (2013a) used the two end-member $\overline{V}_{FeO}$ values to develop a linear equation to estimate the coordination number of $Fe^{2+}$:

$$CN = 10.85 - 0.401(\overline{V}_{FeO,1723K}). \quad (12)$$

When Equation 12 is applied to the fitted $\overline{V}_{FeO}$ values from this study, the estimated average $Fe^{2+}$ coordination in the four NFS liquid ranges from 5.2 to 4.5. This result is consistent with numerous spectroscopic studies on multicomponent silicate glasses that show that $Fe^{2+}$ primarily occurs in 5- and 4-fold coordination in sodium silicate glasses (e.g., Galoisy et al., 2001; Jackson et al., 2005; Wilke et al., 2007).

**Systematic variation in $\overline{\beta}_{T,FeO}$ and $\partial\overline{V}_{FeO}/\partial T$ with $\overline{V}_{FeO}$ (and $Fe^{2+}$ coordination)**

One of the most intriguing results of this study is the linear inverse correlation between individually fitted $\overline{\beta}_{T,FeO}$ values (Table 4.7) and individually fitted $\overline{V}_{FeO}$ values (Table 4.4) for the four NFS liquids, which is illustrated in Figure 4.9. This is opposite the relationship seen in the CaO-FeO-$SiO_2$ system, where $\overline{\beta}_{T,FeO}$ and $\overline{V}_{FeO}$ show a linear positive correlation (Fig. 4.9). What is most striking is the remarkably large compressibility of the $\overline{\beta}_{T,FeO}$ component in sodium-silicate liquids, which extends up to $14.9\times10^{-2}$ $GPa^{-1}$ and is twice the value of $\overline{\beta}_{T,FeO}$ when $Fe^{2+}$ is in 4-fold coordination ($7.1\times10^{-2}$ $GPa^{-1}$). The latter value is remarkably similar to the fitted values for both $\overline{\beta}_{T,SiO_2}$ ($6.9\times10^{-2}$ $GPa^{-1}$; Table 4.7) and $\overline{\beta}_{T,TiO_2}$ ($6.6\times10^{-2}$ $GPa^{-1}$; Liu et al., 2007), where $Si^{4+}$ and $Ti^{4+}$ are both in 4-fold coordination.

It is not just $\overline{\beta}_{T,FeO}$ that increases linearly with $Fe^{2+}$ coordination (Fig. 4.10a), but also $\partial\overline{V}_{FeO}/\partial T$ (Fig. 4.11a). Values of $\partial\overline{V}_{FeO}/\partial T$ reach a peak value of 5.9 x $10^{-3}$ $cm^3$/mol-K when $\overline{\beta}_{T,FeO}$ reaches a peak of $14.9\times10^{-2}$ $GPa^{-1}$ (Fig. 4.12a), which is similar to the behavior seen for the $TiO_2$ component (Fig. 4.10b, 4.11b, 4.12b). Extrapolation to

4-coordinated $Fe^{2+}$ shows that $\partial\overline{V}_{FeO}/\partial T$ follows the same behavior as $\partial\overline{V}_{SiO_2}/\partial T$ and $\partial\overline{V}_{TiO_2}/\partial T$, which is to have a value of zero when in 4-fold coordination (Lange, 1997; Liu and Lange, 2001). The emerging view is that the FeO component in sodium silicate liquids is most thermally expansive when it is also most compressible, which appears to be the case when there is abundance of 5- and/or 6-coordinated $Fe^{2+}$.

**Topological mechanisms of FeO compressibility and thermal expansivity**

The enhanced thermal expansion and compressibility of the FeO component as a function of increasing $Fe^{2+}$ coordination in $Na_2O$-$SiO_2$ liquids is closely mirrored by the behavior of $\overline{\beta}_{T,TiO_2}$ and $\partial\overline{V}_{TiO_2}/\partial T$ as a function of increasing $Ti^{4+}$ coordination(Fig. 4.10 and 4.11), as documented in Liu and Lange (2001) and Liu et al. (2007). In those two studies, it was suggested that the enhanced thermal expansion of the $TiO_2$ component might be related to the abundance of five-coordinated $Ti^{4+}$, but not to a change in $Ti^{4+}$ coordination with temperature, on the basis of spectroscopic evidence. For example, Farges et al. (1996b) performed XAFS spectroscopy on several sodium titanosilicate samples from 293 to 1650 K and found no evidence for any change in Ti coordination with temperature. Similarly, Cormier et al. (2001) conducted neutron diffraction experiments on a potassium titanosilicate glass from room temperature up to the liquid state (1360 K) and found no significant change in the Ti coordination number. Although the two studies found no change in Ti coordination with temperature, they both report significant structural changes in the network (i.e., topology) of the melts. Moreover, in all of the samples studied, the most abundant Ti coordination site was a square pyramidal geometry with unique properties.

For example, several spectroscopic studies (e.g., Yarker et al., 1986; Farges et al., 1996b; Cromier et al., 1998) have shown that 5-coordinated $Ti^{4+}$ in a square pyramidal site occurs in alkali silicate liquids with one non-bridging oxygen atom doubly bonded to Ti (and four alkali atoms) and four bridging oxygen atoms bonded to Si or Ti (and two other alkali atoms). As a consequence of this geometry, 5-coordinated $Ti^{4+}$ occurs at the interface of two domains, one that is relatively rich in alkalis (percolation domains) and the other that is rich in silica (network formers). This unique geometry for $Ti^{4+}$ in alkali silicate liquids leads to a potentially large number of different topological configurations of network connectivity, which may each lead to a substantially different liquid density as a function of either temperature or pressure.

Given the remarkable similarity between the enhanced compressibility and thermal expansivity of the FeO and $TiO_2$ components in sodium silicate liquids, which increase with increasing $Fe^{2+}$ and $Ti^{4+}$ coordination, it is tempting to postulate a common underlying mechanism. However, two issues remain unclear. First, it is uncertain if $\overline{\beta}_{T,FeO}$ and $\overline{\beta}_{T,TiO_2}$ continue to increase in sodium silicate liquids as $Fe^{2+}$ and $Ti^{4+}$ coordination numbers increase beyond an average coordination number of ~5.2 (± 0.2) to 6. To test this trend, density and sound speed measurements on melt compositions with relatively low $Na_2O$ concentrations (<10 mol%) are required, which is difficult because such melts are so viscous. If $\overline{\beta}_{T,FeO}$ and $\overline{\beta}_{T,TiO_2}$ do not peak when 5-coordinated $Fe^{2+}$ and $Ti^{4+}$ are maximized, this undermines the postulate that the enhanced topological mechanisms of compressibility and thermal expansion are related to the unique geometry of square pyramidal 5-coordinated sites. Second, it is unknown if five-coordinated $Fe^{2+}$ occurs in square pyramidal sites, at the interface of alkali-rich and silica-rich domains,

similar to $Ti^{4+}$. What is clear is that the volumetric properties of the FeO component, which vary with $Fe^{2+}$ coordination, are completely different in $Na_2O$-$SiO_2$ vs. CaO-$SiO_2$ liquids. This raises the question of what the most appropriate values for $\overline{V}_{FeO}$, $\overline{\beta}_{T,FeO}$ and $\partial\overline{V}_{FeO}/\partial T$ to apply to naturally occurring basaltic liquids, which often contain some alkalis.

In a previous study by Guo et al. (2013b) on the density and compressibility of FeO-bearing model basalts in the anorthite-diopside-hedenbergite ternary, there were no alkalis in any of the liquid samples. Given the notably large values of $\overline{\beta}_{T,FeO}$ and $\partial\overline{V}_{FeO}/\partial T$ in the sodium-silicate liquids from this study, in marked contrast to the results on CaO-MgO-FeO-$Al_2O_3$-$SiO_2$ liquids (Guo et al., 2013a,b), future density and compressibility studies should focus on FeO-bearing basalt liquids that contain both $Na_2O$ and $K_2O$. This is particularly necessary in order to determine what volumetric properties for FeO to apply to basalts in intraplate settings, such as continental rifts and oceanic islands, where the magmatism is often alkaline.

## Acknowledgements

This research was supported by the National Science Foundation through award EAR-0855774.

**TABLE 4.1.** Composition of samples from Liu and Lange (2001) (mol%)

| Sample | $SiO_2$ | $Na_2O$ | FeO | g.f.w |
|---|---|---|---|---|
| NFS-9 | 49.56 | 21.42 | 29.03 | 63.91 |
| NFS-10 | 56.14 | 15.45 | 28.42 | 63.72 |
| NFS-11 | 45.18 | 25.86 | 28.96 | 63.98 |
| NFS-12 | 41.29 | 29.95 | 28.77 | 64.04 |

**TABLE 4.2.** Density and volume of glasses at 298 K and $T_f'$

| Sample | ρ(298 K) ($g/cm^3$) | Vol (298K) ($cm^3$/g.f.w) | $\alpha^{glass}$ ($10^{-5}$/K) | Vol (Tf') ($cm^3$/g.f.w.) | $T_f'$ (K) |
|---|---|---|---|---|---|
| NFS-9 | 3.131 | 20.41 | 4.212 | 20.74 | 709 |
| NFS-10 | 3.121 | 20.42 | 3.378 | 20.72 | 737 |
| NFS-12 | 3.029 | 21.14 | 4.755 | 21.49 | 647 |

**TABLE 4.3.** Density, surface tension and volume of NFS liquids at high temperature

| Sample | T (K) | Density ($g/cm^3$) | γ(T) N/m | Vmeas ($cm^3$/g.f.w) | Vcalc ($cm^3$/g.f.w) | %Residual 100×(meas-calc)/meas |
|---|---|---|---|---|---|---|
| NFS-9 | 1448 | 2.835 | 0.31 | 22.54 | 22.59 | -0.22 |
| NFS-9 | 1448 | 2.831 | 0.28 | 22.57 | 22.59 | -0.09 |
| NFS-9 | 1448 | 2.833 | 0.30 | 22.56 | 22.59 | -0.13 |
| NFS-9 | 1448 | 2.829 | 0.27 | 22.59 | 22.59 | 0.00 |
| NFS-9 | 1323 | 2.774 | 0.32 | 23.04 | 22.96 | 0.35 |
| NFS-9 | 1323 | 2.773 | 0.32 | 23.05 | 22.96 | 0.39 |
| NFS-9 | 1323 | 2.773 | 0.31 | 23.05 | 22.96 | 0.39 |
| NFS-9 | 1323 | 2.773 | 0.31 | 23.05 | 22.96 | 0.39 |
| NFS-9 | 1573 | 2.744 | 0.27 | 23.29 | 23.33 | -0.17 |
| NFS-9 | 1573 | 2.749 | 0.30 | 23.25 | 23.33 | -0.34 |
| NFS-9 | 1573 | 2.742 | 0.27 | 23.31 | 23.33 | -0.09 |
| NFS-9 | 1573 | 2.747 | 0.30 | 23.26 | 23.33 | -0.30 |
| NFS-10 | 1486 | 2.774 | 0.28 | 22.97 | 22.92 | 0.22 |
| NFS-10 | 1486 | 2.774 | 0.28 | 22.97 | 22.92 | 0.22 |
| NFS-10 | 1486 | 2.780 | 0.29 | 22.92 | 22.92 | 0.00 |
| NFS-10 | 1486 | 2.780 | 0.29 | 22.92 | 22.92 | 0.00 |
| NFS-10 | 1588 | 2.742 | 0.24 | 23.24 | 23.21 | 0.13 |
| NFS-10 | 1588 | 2.746 | 0.26 | 23.20 | 23.21 | -0.04 |
| NFS-10 | 1588 | 2.739 | 0.24 | 23.26 | 23.21 | 0.21 |
| NFS-10 | 1588 | 2.742 | 0.25 | 23.24 | 23.21 | 0.13 |
| NFS-10 | 1649 | 2.730 | 0.26 | 23.34 | 23.38 | -0.17 |
| NFS-10 | 1649 | 2.727 | 0.24 | 23.37 | 23.38 | -0.04 |
| NFS-10 | 1649 | 2.734 | 0.27 | 23.31 | 23.38 | -0.30 |
| NFS-10 | 1649 | 2.731 | 0.25 | 23.33 | 23.38 | -0.21 |
| NFS-11 | 1323 | 2.779 | 0.23 | 23.02 | 23.05 | -0.13 |
| NFS-11 | 1323 | 2.781 | 0.24 | 23.01 | 23.05 | -0.17 |
| NFS-11 | 1323 | 2.779 | 0.23 | 23.02 | 23.05 | -0.13 |
| NFS-11 | 1323 | 2.781 | 0.24 | 23.01 | 23.05 | -0.17 |
| NFS-11 | 1448 | 2.750 | 0.26 | 23.27 | 23.29 | -0.09 |
| NFS-11 | 1448 | 2.754 | 0.29 | 23.23 | 23.29 | -0.26 |
| NFS-11 | 1448 | 2.749 | 0.26 | 23.27 | 23.29 | -0.09 |
| NFS-11 | 1448 | 2.753 | 0.29 | 23.24 | 23.29 | -0.22 |
| NFS-11 | 1573 | 2.712 | 0.29 | 23.59 | 23.54 | 0.21 |
| NFS-11 | 1573 | 2.708 | 0.26 | 23.63 | 23.54 | 0.38 |
| NFS-11 | 1573 | 2.714 | 0.29 | 23.57 | 23.54 | 0.13 |
| NFS-11 | 1573 | 2.710 | 0.27 | 23.61 | 23.54 | 0.30 |
| NFS-12 | 1323 | 2.744 | 0.24 | 23.34 | 23.29 | 0.21 |
| NFS-12 | 1323 | 2.744 | 0.24 | 23.34 | 23.29 | 0.21 |
| NFS-12 | 1323 | 2.747 | 0.24 | 23.31 | 23.29 | 0.09 |
| NFS-12 | 1323 | 2.747 | 0.24 | 23.31 | 23.29 | 0.09 |
| NFS-12 | 1448 | 2.711 | 0.18 | 23.62 | 23.64 | -0.08 |
| NFS-12 | 1448 | 2.722 | 0.25 | 23.52 | 23.64 | -0.51 |
| NFS-12 | 1448 | 2.717 | 0.19 | 23.57 | 23.64 | -0.30 |
| NFS-12 | 1448 | 2.728 | 0.26 | 23.47 | 23.64 | -0.72 |
| NFS-12 | 1573 | 2.661 | 0.16 | 24.06 | 23.99 | 0.29 |
| NFS-12 | 1573 | 2.664 | 0.18 | 24.04 | 23.99 | 0.21 |
| NFS-12 | 1573 | 2.663 | 0.17 | 24.05 | 23.99 | 0.25 |
| NFS-12 | 1573 | 2.666 | 0.19 | 24.02 | 23.99 | 0.12 |

**TABLE 4.4.** Individually fitted partial molar volume of FeO at 1723K for NFS liquids

| Oxide | $\overline{V}_{FeO} \pm 1\sigma$ ($cm^3$/mol) | $\partial\overline{V}_i / \partial T \pm 1\sigma$ ($10^{-3}cm^3$/mol-K) | C.N. of $Fe^{2+}$ |
|---|---|---|---|
| $SiO_2$ | 26.86 ± 0.03 | - | - |
| $Al_2O_3$ | 37.42 ± 0.08 | - | - |
| MgO | 11.86 ± 0.07 | 3.27 ± 0.16 | - |
| CaO | 16.72 ± 0.05 | 3.74 ± 0.11 | - |
| $Na_2O$ | 29.26 ± 0.06 | 7.68 ± 0.09 | - |
| $K_2O$ | 46.67 ± 0.10 | 12.08 ± 0.19 | - |
| FeO(NFS-9) | 14.48 ± 0.13 | 4.63 ± 0.31 | 5.0 |
| FeO(NFS-10) | 14.07 ± 0.10 | 5.94 ± 0.29 | 5.2 |
| FeO(NFS-11) | 15.20 ± 0.07 | 3.61 ± 0.67 | 4.8 |
| FeO(NFS-12) | 15.86 ± 0.13 | 1.81 ± 0.32 | 4.5 |

[a]Total of 148 observations; $R^2$ = 0.9999, and average error is 0.21%.

C.N. of $Fe^{2+}$ =10.854-0.401$\overline{V}_{FeO}$ (Guo et al., 2013)

**TABLE 4.5.** Sound speed and compressibility data for NFS liquids

| Sample | $f$ (MHz) | T (K) | $c$ (m/s) | density (g/cm$^3$) | $\beta_S$ ($10^{-2}$ GPa$^{-1}$) | $\beta_T$ ($10^{-2}$ GPa$^{-1}$) | d$V$/d$P$ ($10^{-4}$cm$^3$/bar) |
|---|---|---|---|---|---|---|---|
| NFS-9 | 4.5 | 1420 | 2340 | 2.794 | 6.537 | 7.192 | -1.645 |
| NFS-9 | 5.5 | 1420 | 2337 | 2.794 | 6.554 | 7.209 | -1.649 |
| NFS-9 | 4.5 | 1501 | 2287 | 2.764 | 6.916 | 7.601 | -1.757 |
| NFS-9 | 5.5 | 1501 | 2284 | 2.764 | 6.934 | 7.619 | -1.762 |
| NFS-9 | 4.5 | 1588 | 2237 | 2.734 | 7.310 | 8.027 | -1.877 |
| NFS-9 | 5.5 | 1588 | 2227 | 2.734 | 7.376 | 8.092 | -1.892 |
| NFS-9 | 4.5 | 1668 | 2206 | 2.706 | 7.594 | 8.339 | -1.970 |
| NFS-9 | 5.5 | 1668 | 2202 | 2.706 | 7.622 | 8.366 | -1.976 |
| NFS-9 | 4.5 | 1749 | 2180 | 2.678 | 7.856 | 8.629 | -2.059 |
| NFS-9 | 5.5 | 1749 | 2174 | 2.794 | 7.899 | 8.672 | -2.069 |
| NFS-10 | 4.5 | 1529 | 2198 | 2.766 | 7.484 | 8.138 | -1.875 |
| NFS-10 | 5.5 | 1529 | 2208 | 2.766 | 7.416 | 8.070 | -1.859 |
| NFS-10 | 4.5 | 1612 | 2178 | 2.737 | 7.701 | 8.383 | -1.952 |
| NFS-10 | 5.5 | 1612 | 2180 | 2.737 | 7.687 | 8.369 | -1.948 |
| NFS-10 | 4.5 | 1697 | 2157 | 2.709 | 7.934 | 8.645 | -2.034 |
| NFS-10 | 5.5 | 1697 | 2168 | 2.709 | 7.854 | 8.565 | -2.015 |
| NFS-10 | 4.5 | 1780 | 2136 | 2.682 | 8.173 | 8.911 | -2.118 |
| NFS-10 | 5.5 | 1780 | 2150 | 2.682 | 8.067 | 8.805 | -2.092 |
| NFS-10 | 4.5 | 1829 | 2125 | 2.666 | 8.307 | 9.061 | -2.166 |
| NFS-10 | 5.5 | 1829 | 2144 | 2.666 | 8.160 | 8.914 | -2.131 |
| NFS-11 | 4.5 | 1424 | 2382 | 2.758 | 6.390 | 7.051 | -1.636 |
| NFS-11 | 5.5 | 1424 | 2388 | 2.758 | 6.357 | 7.018 | -1.628 |
| NFS-11 | 4.5 | 1504 | 2336 | 2.730 | 6.713 | 7.403 | -1.735 |
| NFS-11 | 5.5 | 1504 | 2334 | 2.730 | 6.722 | 7.413 | -1.738 |
| NFS-11 | 4.5 | 1586 | 2288 | 2.701 | 7.071 | 7.792 | -1.846 |
| NFS-11 | 5.5 | 1586 | 2288 | 2.701 | 7.073 | 7.793 | -1.846 |
| NFS-11 | 4.5 | 1671 | 2226 | 2.672 | 7.553 | 8.304 | -1.989 |
| NFS-11 | 5.5 | 1671 | 2224 | 2.672 | 7.565 | 8.316 | -1.991 |
| NFS-12 | 4.5 | 1430 | 2392 | 2.715 | 6.439 | 7.000 | -1.651 |
| NFS-12 | 5.5 | 1430 | 2398 | 2.715 | 6.405 | 6.966 | -1.643 |
| NFS-12 | 4.5 | 1510 | 2368 | 2.689 | 6.629 | 7.216 | -1.719 |
| NFS-12 | 5.5 | 1510 | 2364 | 2.689 | 6.653 | 7.240 | -1.724 |
| NFS-12 | 4.5 | 1591 | 2317 | 2.663 | 6.996 | 7.608 | -1.829 |
| NFS-12 | 5.5 | 1591 | 2322 | 2.663 | 6.961 | 7.573 | -1.821 |
| NFS-12 | 4.5 | 1671 | 2252 | 2.639 | 7.475 | 8.112 | -1.969 |
| NFS-12 | 5.5 | 1671 | 2264 | 2.639 | 7.394 | 8.031 | -1.949 |
| NFS-12 | 4.5 | 1752 | 2218 | 2.614 | 7.779 | 8.441 | -2.068 |
| NFS-12 | 5.5 | 1752 | 2215 | 2.614 | 7.796 | 8.457 | -2.072 |

**TABLE 4.6.** Individual regression results for $c_i$ at 1723K by Equation (8) using data from this study and literature[a]

| Oxide | $c_i \pm 1\sigma$(m/s) | $\partial c_i/\partial T \pm 1\sigma$(ms$^{-1}$ K$^{-1}$) |
|---|---|---|
| $SiO_2$ | 2514 ± 11 | - |
| $Al_2O_3$ | 4478 ± 36 | -2.289 ± 0.220 |
| $Na_2O$ | 2523 ± 22 | -1.956 ± 0.076 |
| FeO(NFS-9) | 1393 ± 17 | - |
| FeO(NFS-10) | 1214 ± 20 | - |
| FeO(NFS-11) | 1455 ± 19 | - |
| FeO(NFS-12) | 1535 ± 18 | - |

[a]Total of observations varies from 74 to 76; $R^2$ = 0.9999, and average error is 0.44%.

**TABLE 4.7.** Individual regression results for $\beta_i$ at 1723K by Equation (10) using data from this study and literature[a]

| Oxide | $\overline{\beta_i} \pm 1\sigma$ ($10^{-2}$ GPa$^{-1)}$) | $\partial\overline{\beta_i}/\partial T \pm 1\sigma$ ($10^{-2}$ GPa$^{-1}$K$^{-1}$) |
|---|---|---|
| $SiO_2$ | 6.901 ± 0.053 | - |
| $Al_2O_3$ | -2.355 ± 0.128 | -0.0077 ± 0.0008 |
| $Na_2O$ | 9.108 ± 0.099 | 0.0103 ± 0.0004 |
| FeO(NFS-9) | 13.146 ± 0.208 | 0.0090 ± 0.0012 |
| FeO(NFS-10) | 14.910 ± 0.176 | 0.0031 ± 0.0012 |
| FeO(NFS-11) | 12.175 ± 0.294 | 0.0105 ± 0.0015 |
| FeO(NFS-12) | 10.078 ± 0.205 | 0.0055 ± 0.0012 |

[a]Total of observations varies from 74 to 76; $R^2$ = 0.9999, and average error is 0.76%.

**TABLE 4.8.** Individually fit results for $\partial V_i/\partial P$ at 1723K by Equation (11) using data from this study and literature[a]

| Oxide | $\partial\overline{V_i}/\partial P \pm 1\sigma$ ($10^{-4}$cm$^3$ bar$^{-1}$) | $\partial^2\overline{V_i}/\partial P\partial T \pm 1\sigma$ ($10^{-4}$ cm$^3$ bar$^{-1}$K$^{-1}$) |
|---|---|---|
| $SiO_2$ | -1.849 ± 0.014 | - |
| $Al_2O_3$ | 0.861 ± 0.047 | -0.0025 ± 0.0003 |
| $Na_2O$ | -2.647 ± 0.029 | -0.0036 ± 0.0001 |
| FeO(NFS-9) | -1.900 ± 0.034 | -0.0017 ± 0.0002 |
| FeO(NFS-10) | -2.109 ± 0.027 | -0.0014 ± 0.0002 |
| FeO(NFS-11) | -1.826 ± 0.036 | -0.0018 ± 0.0003 |
| FeO(NFS-12) | -1.593 ± 0.036 | -0.0010 ± 0.0002 |

[a]Total of observations varies from 74 to 76; $R^2$ = 0.9999, and average error is 0.76%.

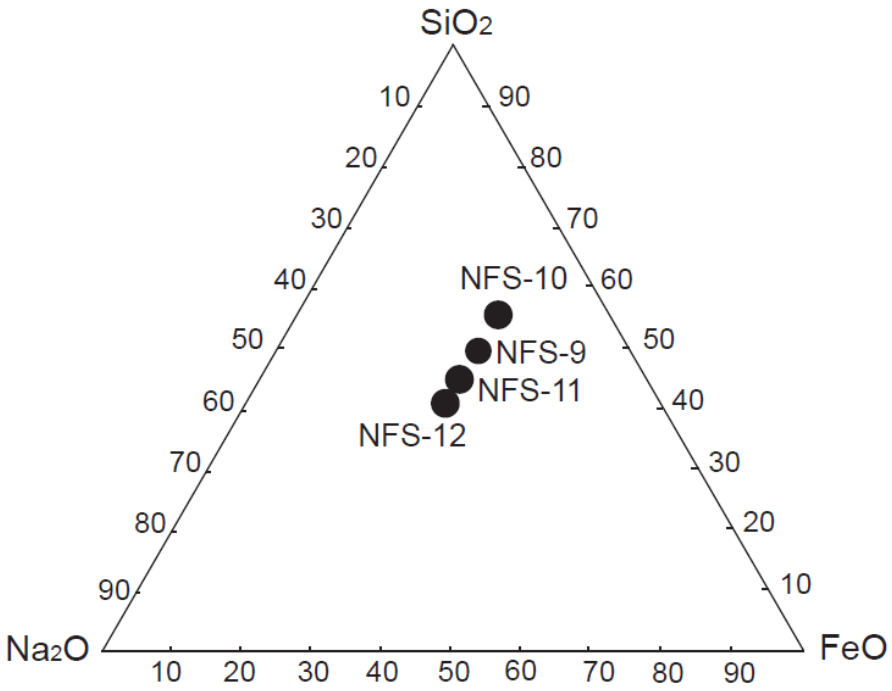


**FIGURE 4.1.** Composition of the liquids in $Na_2O$-FeO-$SiO_2$ ternary system (mol%)

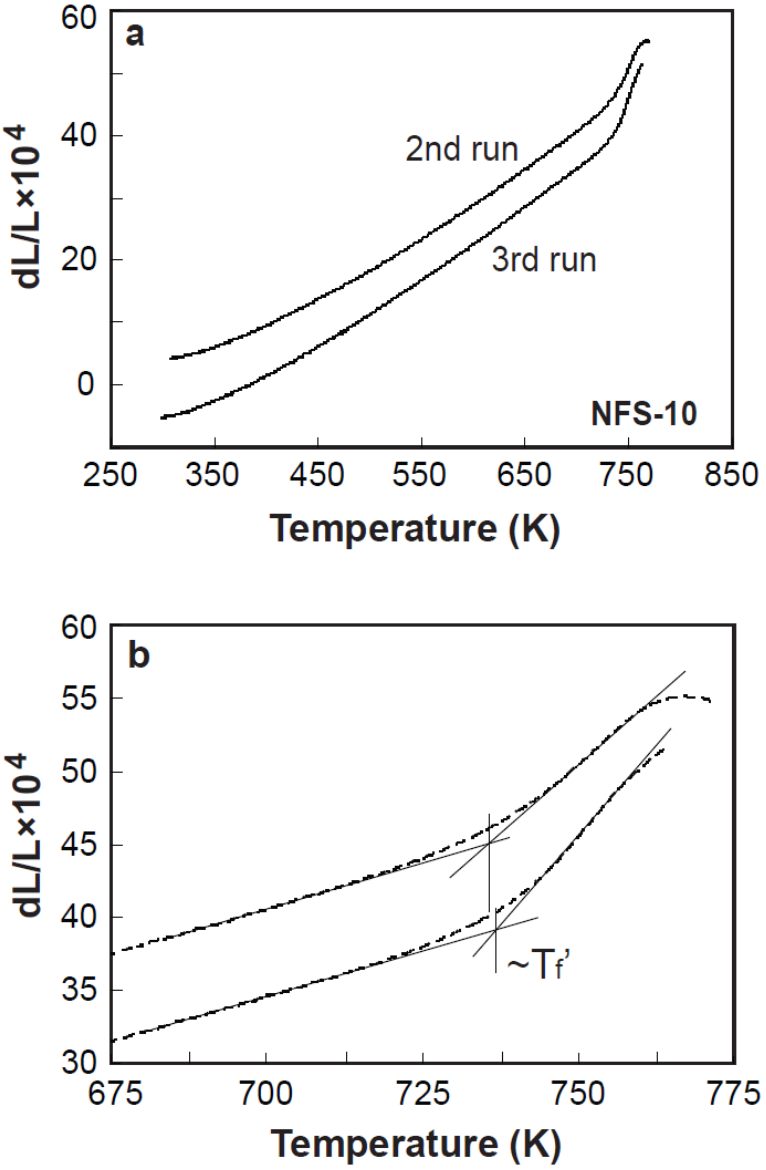


**FIGURE 4.2.** (a) Two scans of dL/L vs. temperature for NFS-10 glass using a Perkin-Elmer diamond TMA at a heating rate 10K/min. (b) a blow-up of the two glass transition intervals from (a).

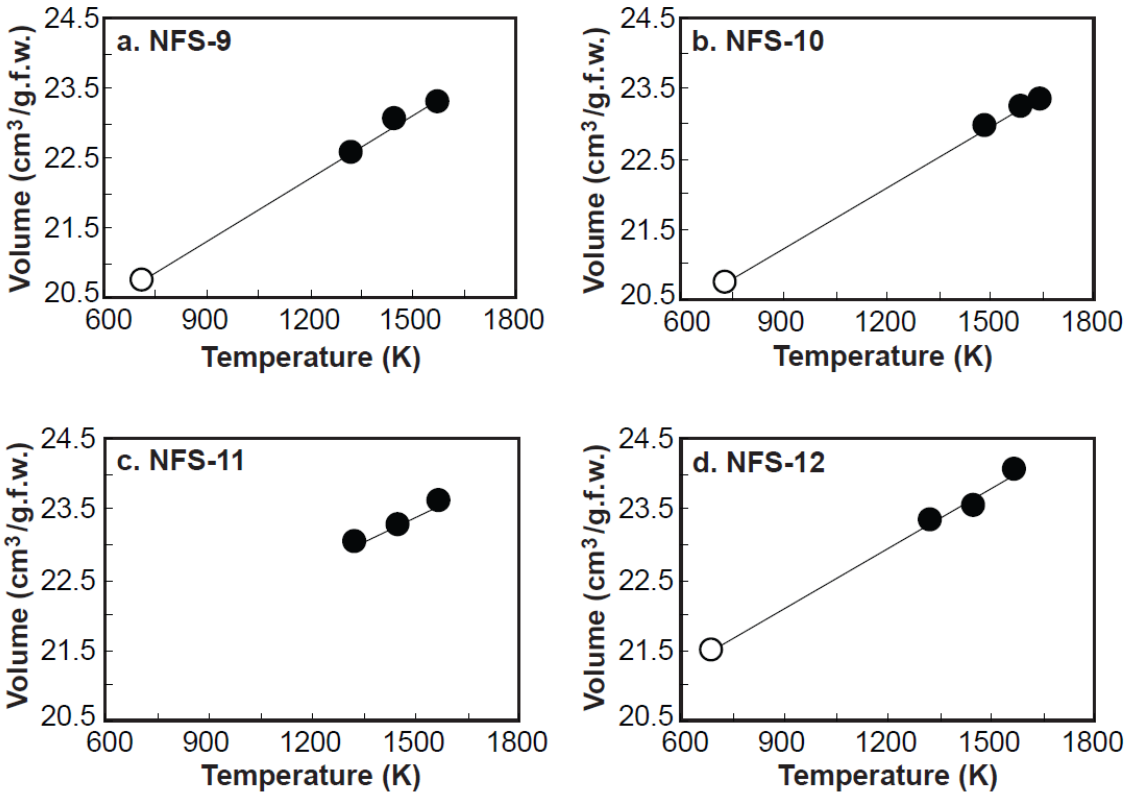


**FIGURE 4.3.** Plots of liquid volume vs. Temperature. The solid dots are for high temperature volume data. The open dots are for low-temperature volumes at $T_f'$. There is no low-temperature volume for NFS-11 because a sufficiently large glass sample for the 298 K density measurement could not be obtained. The error bars are smaller than the symbols. The solid line is a linear fit to all the volume data.

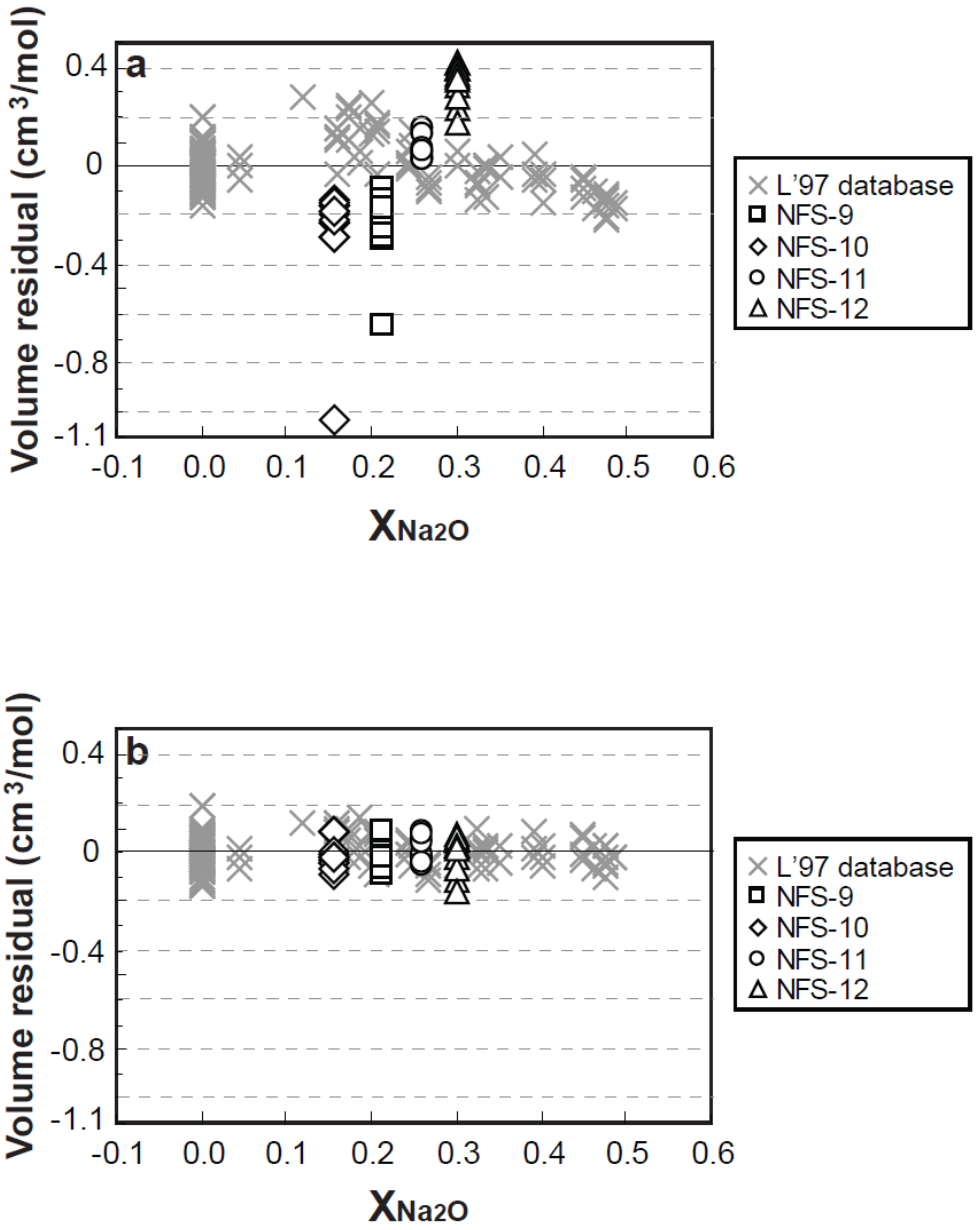


**FIGURE 4.4.** (a) Plot of volume residuals vs. $X_{Na2O}$ for overall fit. (b) Plot of volume residuals vs. $X_{Na2O}$ for individual fit. The database is from Lange (1997).

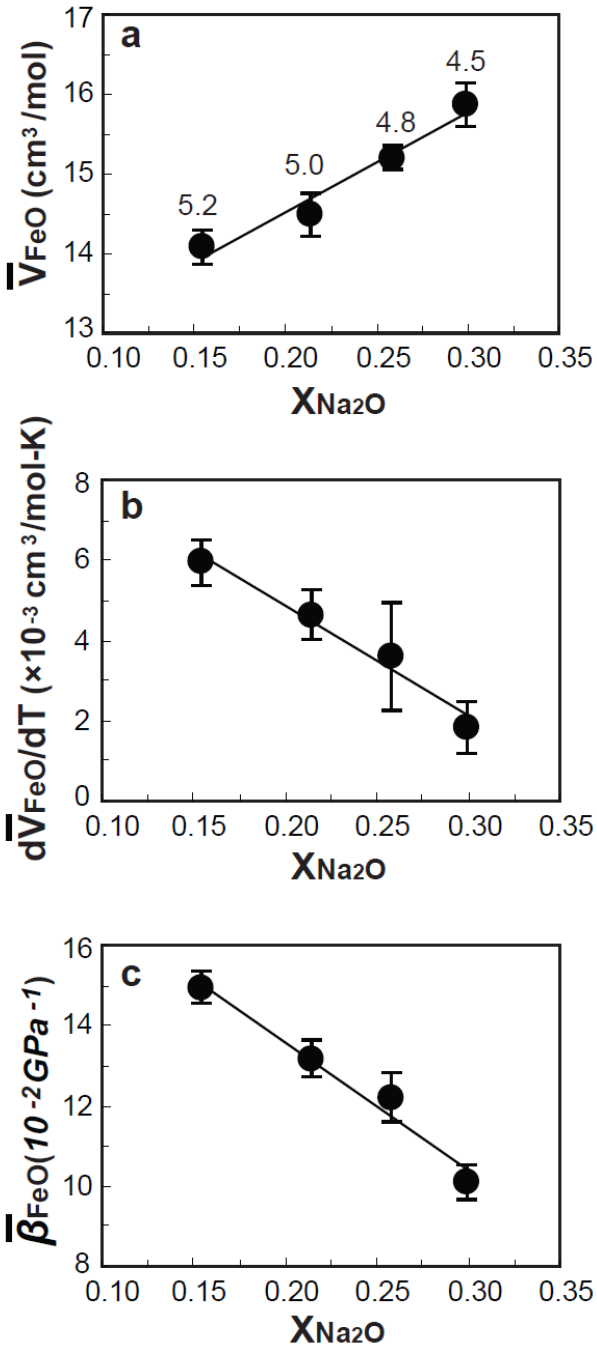


**FIGURE 4.5.** (a) Plot of $\bar{V}_{FeO}$ vs. $X_{Na2O}$ for NFS liquids. (b) Plot of $d\bar{V}_{FeO}/dT$ vs. $X_{Na2O}$. (c) Plot of $\bar{\beta}_{FeO}$ vs. $X_{Na2O}$. The solid line is the linear fit to all the data. The errors are 2σ.

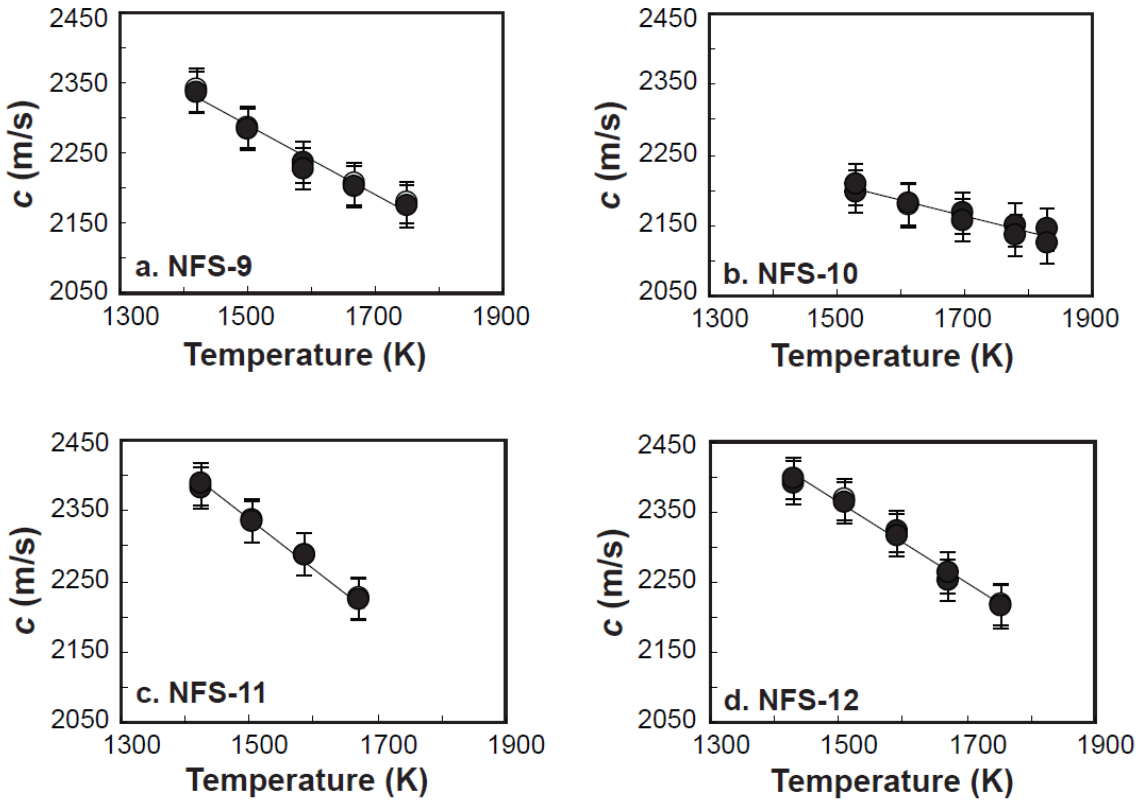


**FIGURE 4.6.** Plots of sound speed vs. Temperature for experimental liquids. The solid line is the linear fit to the data. The errors in sound speed are ±30m/s.

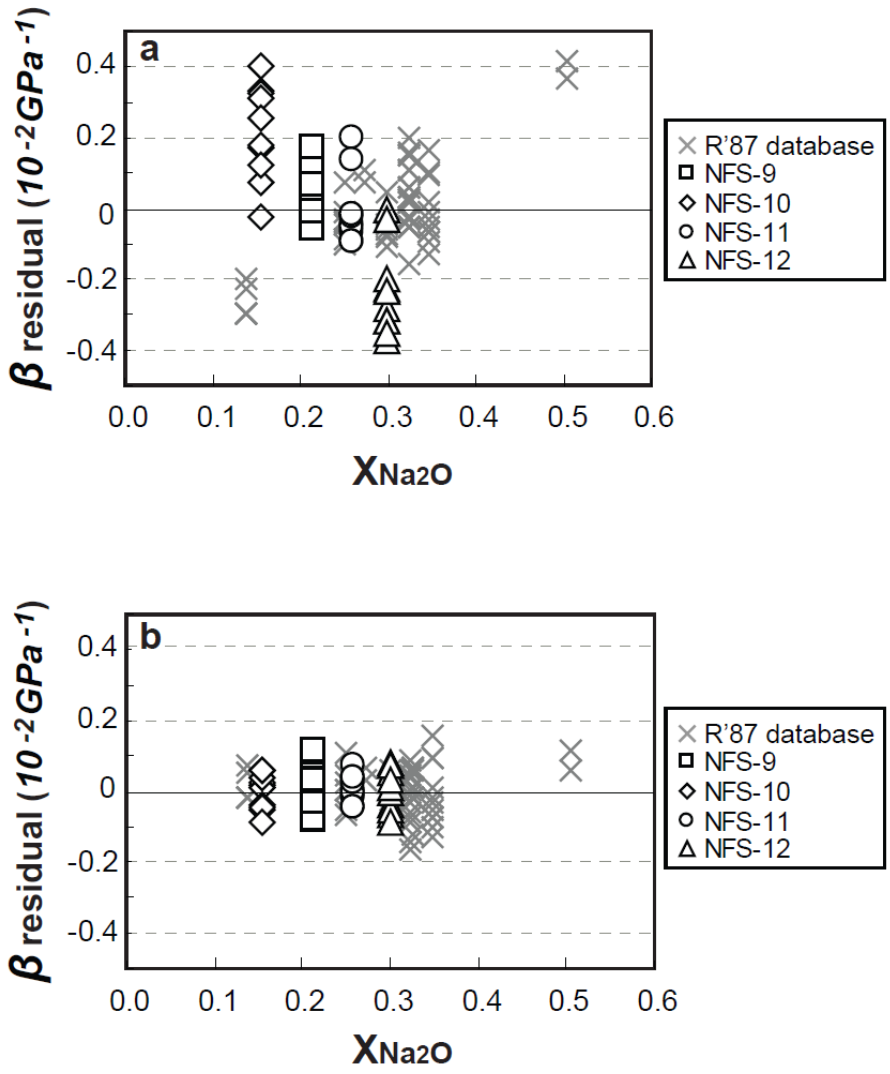


**FIGURE 4.7.** (a) Plot of isothermal compressibility residuals vs. $X_{Na2O}$ for overall fit. (b) Plot of isothermal compressibility residuals vs. $X_{Na2O}$ for individually fit. The database are from Rivers and Carmichael (1987) and Kress et al. (1988).

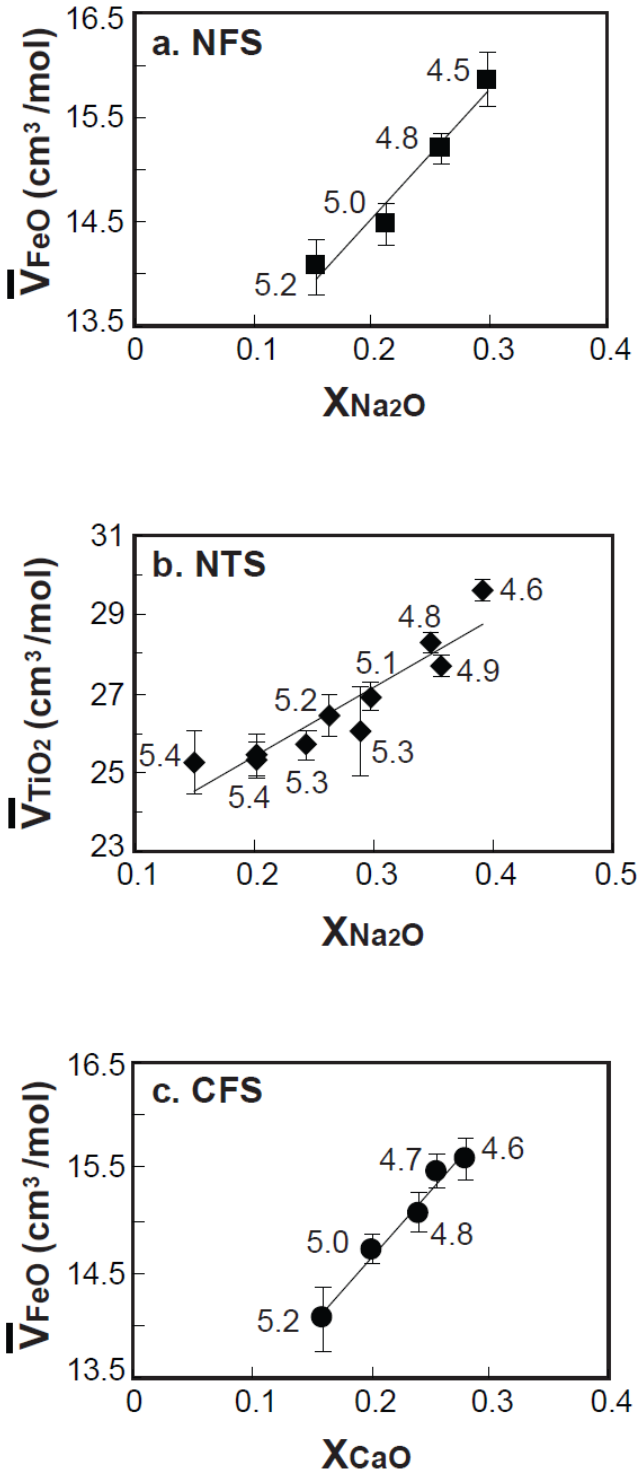


**FIGURE 4.8.** (a) Plot of $\overline{V}_{FeO}$ vs. $X_{Na2O}$ for NFS liquids, the coordination number of $Fe^{2+}$ for each liquid is shown. (b) Plot of $\overline{V}_{TiO_2}$ vs. $X_{Na2O}$ for NTS liquids from Liu and Lange (2001). (c) Plot of $\overline{V}_{FeO}$ vs. $X_{CaO}$ for CFS liquids from Guo et al. (2013)

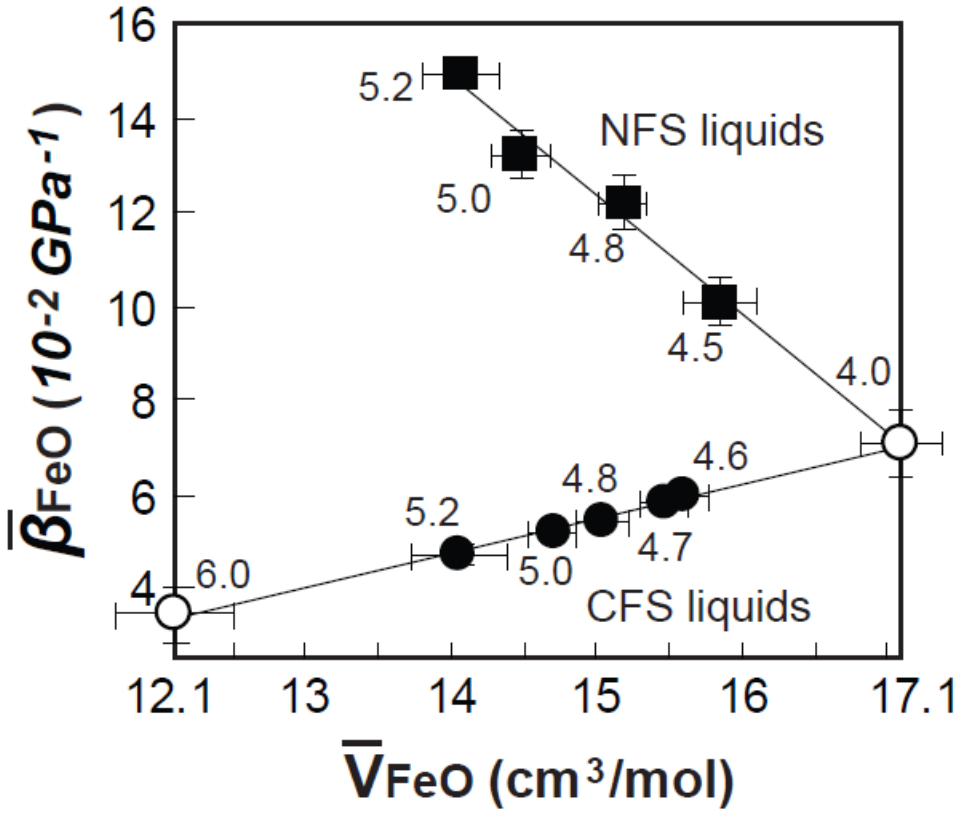


**FIGURE 4.9.** Plot of $\overline{\beta}_{FeO}$ vs. $\overline{V}_{FeO}$ for NFS liquids. The $\overline{\beta}_{FeO}$ and $\overline{V}_{FeO}$ of CFS liquids from Guo et al. (2013) are shown for comparison. The solid squares are for NFS liquids, the solid circles are for CFS liquids, the open circles are for the values when $Fe^{2+}$ is 4- and 6-fold coordinated.

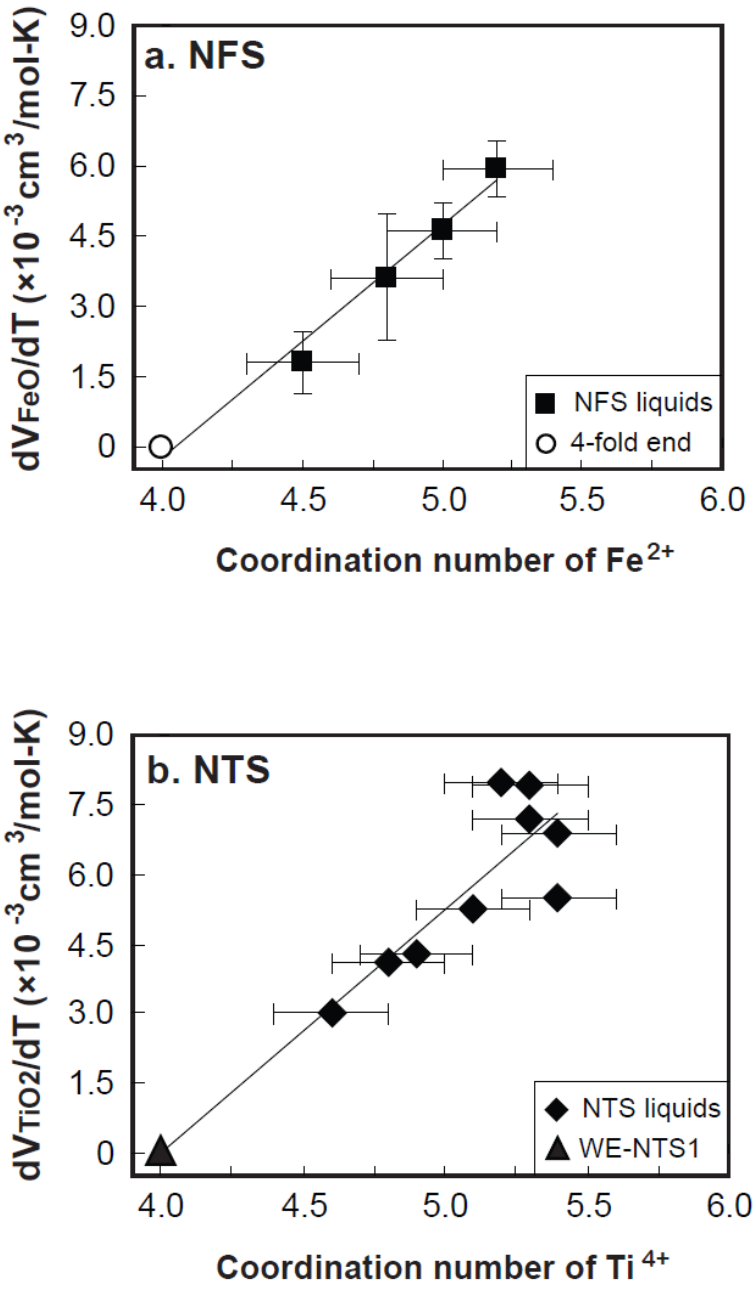


**FIGURE 4.10.** (a) Plot of $d\overline{V}_{FeO}/dT$ vs. coordination number of $Fe^{2+}$. The open circle is for the value of $d\overline{V}_{FeO}/dT$ when $Fe^{2+}$ is 4-fold coordinated from Guo et al. (2013). (b) Plot of $d\overline{V}_{TiO_2}/dT$ vs. coordination number of $Ti^{4+}$ from Liu and Lange (2001).

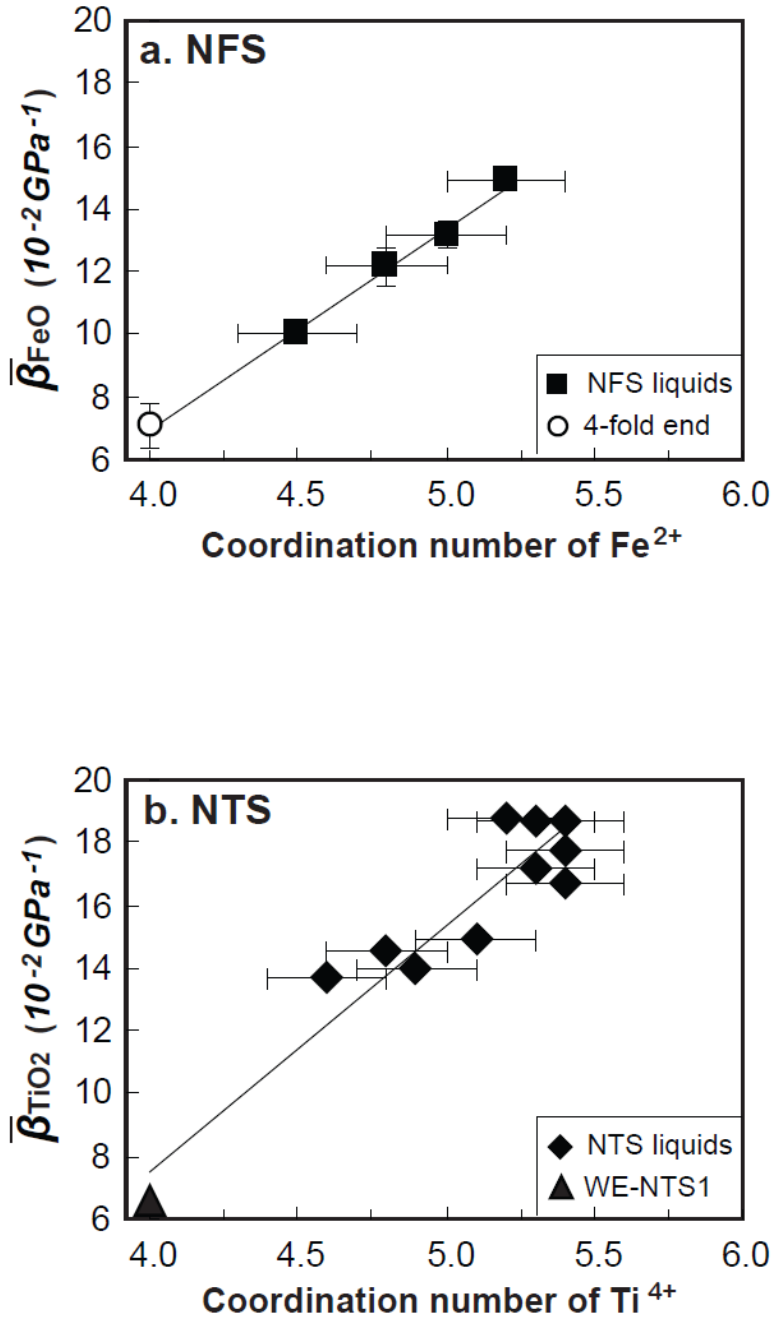


**FIGURE 4.11.** (a) Plot of $\overline{\beta}_{FeO}$ vs. coordination number of $Fe^{2+}$. The open circle is for the value of $\overline{\beta}_{FeO}$ when $Fe^{2+}$ is 4-fold coordinated from Guo et al. (2013). (b) Plot of $\overline{\beta}_{TiO_2}$ vs. coordination number of $Ti^{4+}$ from Liu and Lange (2001).

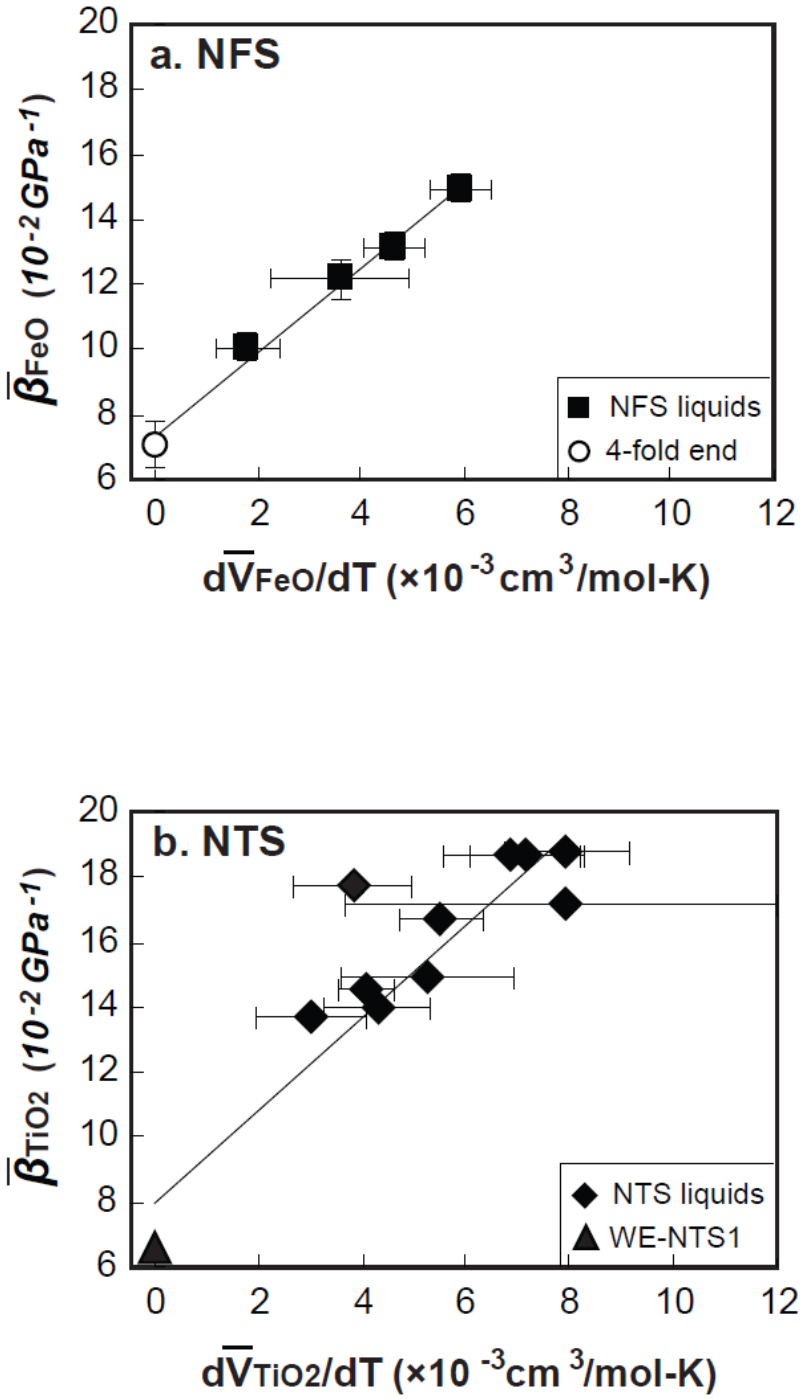


**FIGURE 4.12.** (a) Plot of $\overline{\beta}_{FeO}$ vs. $d\overline{V}_{FeO}/dT$ . The open circle is for the values of $\overline{\beta}_{FeO}$ and $d\overline{V}_{FeO}/dT$ when $Fe^{2+}$ is 4-fold coordinated from Guo et al. (2013). (b) Plot of $\overline{\beta}_{TiO_2}$ vs. $d\overline{V}_{TiO_2}/dT$ from Liu and Lange (2001).

# References


Ai, Y., Lange, R.A. (2004a) An ultrasonic frequency sweep interferometer for liquids at high temperature: 1. Acoustic model. J.Geophys. Res., 109, B12203, doi:10.1029/2003JB002842.

Ai, Y., Lange, R.A. (2004b) An ultrasonic frequency sweep interferometer for liquids at high temperature: 2. Mechanical assembly, signal processing, and application. J. Geophys. Res., 109, B12204, doi:10.1029/2004JB003062

Bockris, J.O'M., Tomlinson, J.W., and White, J.L. (1956) The structure of the liquid silicates: partial molar volumes and expansivities. Trans Faraday Soc., 52, 299-310.

Brown, G.E.Jr., Farges, F., Calas, G. (1995) X-ray scattering and x-ray spectroscopy studies of silicate melts. In Structure, Dynamics and Properties of Silicate Melts (eds. J. F. Stebbins, P. F. McMillan, and D. B. Dingwell), Reviews in Mineralogy, Vol. 32, 317-410, Mineralogical Society of America, Washington, DC.

Chase, M.W. (1998) MIST-JANAF thermochemical tables, fourth edition. Journal of Physical Chemistry Reference Data, Monograph Springer: Heidelberg 9.

Debenedetti, P.G. (1996) Metastable liquids: Concepts and principals. Princeton University Press.

Farges, F., Brown, G.E., and Rehr, J.R. (1996a) Coordination chemistry of Ti(IV) in silicate glasses and melts: I. XAFS study of the titanium coordination in oxide model compounds. Geochimca et Cosmochimica Acta, 60, 3023-3038.

Farges, F., Brown, G.E., Navrotsky, A., Gan, H., and Rehr, J.R. (1996b) Coordination chemistry of Ti(IV) in silicate glasses and melts: II Glasses at ambient temperature and pressure. Geochimca et Cosmochimica Acta, 60, 3039-3053.

Farges, F., Brown, G.E., Navrotsky, A., Gan, H., and Rehr, J.R. (1996c) Coordination chemistry of Ti(IV) in silicate glasses and melts: III. Glasses and melts from ambient to high temperature. Geochimca et Cosmochimica Acta, 60, 3055-3065

Farges, F. and Brown, G.E. (1997) Coordination chemistry of Ti(IV) in silicate glasses and melts: IV. XANES studies of synthetic and natural volcanic glasses and tektites at ambient temperature and pressure. Geochimca et Cosmochimica Acta, 61, 1863-1870.

Galoisy, L., Calas, G., and Arrio, M.-A. (2001) High-resolution XANES spectra of iron in minerals and glasses: Structural information from the pre-edge. Chem. Geol., 174, 307-319.

Ghiorso, M.S. and Kress, V.C. (2004) An equation of state for silicate melts. II. Calibration of volumetric properties at 10(5) Pa. American Journal of Science 304, 679-751.

Gray, D.E. (1972) American Institute of Physics Handbook, 3rd ed. 4-127.

Guo, X., Lange, R.A. and Ai, Y. (2013a) The density and compressibility of CaO-FeO-$SiO_2$ liquids: evidence for four-coordinated $Fe^{2+}$ in the $CaFeO_2$ component. submitted to Geochimica et Cosmochimica Acta.

Guo, X., Lange, R.A. and Ai, Y. (2013b) The density and compressibility of model basalt (An-Di-Hd) liquids at one bar: Evidence for abundant 6-coordinated $Fe^{2+}$. submitted to Earth and Planetary Science Letters.

Jackson, W.E., Waychunas, G.A., Brown, G.E., Leon, J.M., Conradson, S. and Combes, J.-M. (1993) High-temperature XAS study of Fe2SiO4 liquid: Reduced coordination of ferrous iron. Science 262, 229–232

Jackson, W.E., Farges, F., Yeager, M., Mabrouk, P.A., Rossano, S., Waychunas, G.A., Solomon, E.I. and Brown, G.E. (2005) Multi-spectroscopic study of Fe(II) in silicate glasses: Implications for the coordination environment of Fe(II) in silicate melts. Geochimica et Cosmochimica Acta, 69(17), 4315-4332.

Janz, G.J. and Lorenz, M.R. (1960) Precise measurement of density and surface tension at temperatures up to 1000$^{o}$C in one apparatus. The review of scientific instruments 31(1), 18-22.

Kress, V.C., Williams Q. and Carmichael I.S.E. (1988) Ultrasonic investigation of melts in the system $Na_2O$-$Al_2O_3$-$SiO_2$. Geochimica et Cosmochimica Acta, 52, 283-293.

Kress, V.C. and Carmichael, I.S.E. (1988) Stoichiometry of the iron oxidation reaction in silicate melts. Am. Mineral., 73, 1267-1274.

Kress, V.C. and Carmichael, I.S.E. (1989) The lime-iron-silicate melt system: Redox and volume systematics. Geochimica et Cosmochimica Acta, 53, 2883-2892.

Kress, V.C. and Carmichael, I.S.E. (1991) The compressibility of silicate liquids containing $Fe_2O_3$ and the effect of composition, temperature, oxygen fugacity and

pressure on their redox states. Contributions to Mineralogy and Petrology, 108, 82-92.

Lange, R.A. and Carmichael, I.S.E. (1987) Densities of $Na_2O$-$K_2O$-CaO-MgO-FeO-$Fe_2O_3$-$Al_2O_3$-$TiO_2$-$SiO_2$ liquids: New measurements and derived partial molar properties. Geochimica et Cosmochimica Acta, 51, 2931-2946.

Lange, R.A. and Carmichael, I.S.E. (1989) Ferric-ferrous equilibria in $Na_2O$-FeO-$Fe_2O_3$-$SiO_2$ melts: Effects of analytical techniques on derived partial molar volume. Geochimica et Cosmochimica Acta, 53, 2195-2204.

Lange, R.A. (1996) Temperature independent thermal expansivities of sodium aluminosilicate melts between 713 and 1835 K. Geochimica et Cosmochimica Acta, 60, 4989–4996.

Lange, R.A. (1997) A revised model for the density and thermal expansivity of $K_2O$-$Na_2O$-CaO-MgO-$Al_2O_3$-$SiO_2$ liquids from 700 to 1900 K: Extension to crustal magmatic temperatures. Contributions to Mineralogy and Petrology, 130, 1–11.

Lange, R.A. and Navtrotsky, A. (1992) Heat capacities of $Fe_2O_3$-bearing silicate liquids. Contrib. Mineral Petrol, 110, 311-320.

Liu, Q., Lange, R.A. (2001) The partial molar volume and thermal expansivity of $TiO_2$ in alkali silicate melts: Systematic variation with Ti coordination. Geochimica et Cosmochimica Acta, 65(14), 2379-2393.

Liu, Q. and Lange, R.A. (2006) The partial molar volume of $Fe_2O_3$ in alkali silicate melts: Evidence for an average Fe3+ coordination number near five. American Mineralogist, 91, 385-393.

Liu, Q., Lange, R.A. and Ai, Y. (2007) Acoustic velocity measurements on $Na_2O$-$TiO_2$-$SiO_2$ liquids: Evidence for a highly compressible $TiO_2$ component related to five-coordinated Ti. Geochimica et Cosmochimica Acta, 71, 4314-4326

Mo X., Carmichael I.S.E., Rivers M. and Stebbins J.F. (1982) The partial molar volume of $Fe_2O_3$ in multicomponent silicate liquids and the pressure-dependence of oxygen fugacity in magma. Mineralogical Magzine, 45, 237-245.

Moynihan, C.T. (1995). Structural relaxation and the glass transition. In: Stebbins JF et al. (eds) Structure, dynamics and properties of silicate melts (Reviews in Mineralogy vol. 32). Mineralogical Society of America, Washington DC, pp 1-19

Rivers, M. L. and Carmichael, I.S.E. (1987) Ultrasonic studies of silicate melts. J. Geophys. Res. Solid Earth Planets, 92, 9247–9270.

Sack, R.O., Carmichael, I.S.E., Rivers, M., and Ghiorso, M.S. (1980) Ferric-ferrous equilibria in natural silicate liquids at 1 bar. Contrib. Mineral. Petrol., 75, 369-376

Scherer, G.W. (1992) Relaxation in glass and composites. Krieger Publishing Company, Malabar, Florida.

Smyth, J.R. and McCormick T.C. (1995) Crystallographic data for minerals. In T. Ahrens, Ed., Mineral Physics and Crystallography, p.1-17. AGU Reference shelf 2, Washington, D.C.

Shiraishi, Y., Ikeda K., Tamura A. and Saito T. (1978) On the viscosity and density of the molten $FeO$-$SiO_2$ system. Transactions of the Japan Institue of Metals, 19, 264-274.

Stein, D.J., Stebbins, J.F. and Carmichael, I.S.E. (1986) Density of molten sodium aluminosilicates. J. Am. Ceram. Soc., 69, 396–399.

Tangeman, J.A. and Lange, R.A. (2001) Determination of the limiting fictive temperature of silicate glasses from calorimetric and dilatometric methods: application to low-temperature liquid volume measurements. American Mineralogist, 86, 1331-1344.

Thomas, C.W., Liu, Q., Agee, C.B., Asimow, P.D. and Lange R. A. (2012) Multi-technique equation of state for $Fe_2SiO_4$ melt and the density of Fe-bearing silicate melts from 0 to 161 GPa. Journal of Geophysical Research-Solid Earth, 117, B10206, doi: 10.1029/2012JB009403.

Thornber, C.R., Roeder, P.L., and Foster, J.R. (1980) The effect of composition on the ferric-ferrous ratio in basaltic liquids at atmospheric pressure. Geochimca et Cosmochimica Acta, 44, 525-532.

Wilke, M., Farges, F., Partzsch, G.M., Schmidt, C., Behrens, H. (2007) Speciation of Fe in silicate glasses and melts by in-situ XANES spectroscopy. American Mineralogist, 92, 44-56

Yarker, C.A., Johnson, P.A.V., Wright, A.C., Wong, J., Greegor, R.B., Lytle, F.W., Sinclair, R.N. (1986) Neutron diffraction and EXAFS evidence for $TiO_5$ units in vitreous $K_2O$-$TiO_2$-$2SiO_2$. J.Non-Cryst. Solids, 79, 117-136

# CHAPTER V

## The density and compressibility of alkali-bearing basalt liquids under reducing conditions: evidence for 5-coordinated $Fe^{2+}$ and ideal mixing using the components $KAlO_2$-$K_2O$-$NaAlO_2$-$Na_2O$-CaO-MgO-FeO-$Al_2O_3$-$SiO_2$


## Abstract

Three FeO-bearing alkali-bearing model basalts and four Fe-free alkali-bearing silicate liquids are employed in this study. The densities of the three Fe-bearing alkali basalts were measured between 1535 and 1767 K in a reducing atmosphere by the molybdenum double-bob Archimedean method. In addition, low-temperature density data were obtained at the limiting fictive temperature, providing density data for these $Fe^{2+}$-bearing liquids over a wide temperature interval of 800 degrees. By fitting the molar volumes into a linear model, the derived partial molar volume ($\pm 1\sigma$) of FeO is 14.76 (± 0.15) $cm^3$/mol, with a thermal expansivity of 1.03 (± 0.61) $\times 10^{-3} cm^3$/mol-K. In addition, relaxed sound speed measurements were performed on all seven alkali-bearing liquids from 1501 to 1869 K at 1 bar with the frequency sweep acoustic interferometer. Because the alkali-bearing basalt liquids contain both alkalis and alkaline-earth components, and because the compressibility of the $Al_2O_3$ component differs in alkali vs. alkaline-earth

silicate melts, calibration of model equations for sound speed and compressibility were calibrated on liquids from this study and the literature with components recast as $KAlO_2$-$K_2O$-$NaAlO_2$-$Na_2O$-CaO-MgO-FeO-$Al_2O_3$-$SiO_2$. The following rules were followed to calculate the $KAlO_2$ and $NaAlO_2$ components: (1) all $K_2O$ is assigned to available $Al_2O_3$ to form the $KAlO_2$ component; (2) if $Al_2O_3$ is left over, then 45% of $Na_2O$ is assigned to $Al_2O_3$ to form the $NaAlO_2$ component. The results of an ideal mixing model for isothermal compressibility leads to a partial molar compressibility of FeO of 5.22 (±0.47) ($\times 10^{-2}$ $GPa^{-1}$).

## Introduction

In three previous studies of the density and compressibility of $Fe^{2+}$-bearing silicate liquids (Guo et al., 2013a, b, c), it was found that the partial molar volume, thermal expansivity and compressibility of FeO all vary strongly with melt composition, raising the question of what are the most appropriate values to apply to magmatic liquids. In the study of Guo et al. (2013a) on a series of CaO-FeO-$SiO_2$ liquids, it was found that fitted values of $\overline{V}_{FeO}$ and $\overline{\beta}_{T,FeO}$ vary with $Fe^{2+}$ coordination, and they display a positive linear correlation with one another. In a second study of model basalt liquids in the anorthite-diopside-hedenbergite system (Guo et al., 2013b), it was found that fitted values for $\overline{V}_{FeO}$ and $\overline{\beta}_{T,FeO}$ are consistent with an average $Fe^{2+}$ coordination of 5.7. However, because spectroscopic evidence (e.g., Jackson et al., 2005; Wilke et al., 2007) shows that the effect of alkalis is to drive $Fe^{2+}$ coordination to lower values closer to 5-fold, it is essential to test what is the effect of alkalis on derived values of $\overline{V}_{FeO}$ and $\overline{\beta}_{T,FeO}$ on basalt liquids. The evidence presented in Guo et al. (2013c) is that the compressibility of

$\overline{\beta}_{T,FeO}$ can be exceptionally large in sodium silicate liquids and does not follow the same correlation with $\overline{V}_{FeO}$ as observed in calcium silicate liquids. Thus is it essential to perform a set of new sound speed measurements on alkali-bearing basalt liquids. Modeling these results are complicated by the variable compressibility of the $Al_2O_3$ component in alkali- vs. alkaline-earth bearing silicate liquids (Kress et al., 1988. 1991; Ai and Lange, 2008; Ghiorso and Kress, 2004). Therefore, new sound speed measurements on four alkali-bearing Fe-free silicate liquids were additionally performed to further constrain the compressibility of the $Al_2O_3$ component, particularly in potassic liquids.

## Experimental Methods

### Sample synthesis and compositional analysis

Five alkali-bearing silicate samples, of which three are Fe-bearing (alkali model basalts), were synthesized by mixing appropriate proportions of reagent grade MgO, $Al_2O_3$, $CaCO_3$, $Na_2CO_3$, $K_2CO_3$, $Fe_2O_3$ and $SiO_2$. Each powder was slowly dried, de-carbonated, and then fused at 1573 to 1673 K in air. The samples were then quenched to glass, ground into powder and then re-fused. Each sample was melted twice in total to ensure homogeneity. Two additional samples for this study (LC-18 and LC-19) were synthesized and analyzed by Lange and Carmichael (1987).

The compositions of the five samples synthesized in this study were analyzed with a Cameca SX-100 electron microprobe at the University of Michigan. An accelerating voltage of 15kV with a beam current of 4.0nA was used in all analysis. The standards include anorthite and diopside glass, which were analyzed by wet-chemical

methods and reported in Rivers and Carmichael (1987) and Lange and Carmichael (1987), respectively. The two additional samples used in this study (C-18 and LC-19) were synthesized and analyzed by wet-chemical methods by Lange and Carmichael (1987). All analyses are listed in Table 5.1a. For each composition, the gram formula weight ( g.f.w.=$X_iM_i$) is tabulated, where $X_i$, $M_i$ are the mole fraction and molecular weight of each oxide component respectively.

**Low-temperature measurements of liquid volume at $T_f'$**

Low-temperature measurements of the liquid volume of two of the three alkali-bearing model basalts at their respective limiting fictive temperatures ($T_f'$) were obtained using the method described in Lange (1997). The $T_f'$ of any glass quenched from a liquid is uniquely defined on a volume vs. temperature curve as the extrapolated intersection of the glass and liquid volume within the glass transition interval (Moynihan et al., 1976; Scherer, 1992; Debenedetti, 1996). Because the volume of the glass is equal to that of the liquid at $T_f'$, the following equation applies to both the glass and the liquid:

$$V^{liq}(T_f') = V^{glass}(T_f') = V_{298K}^{glass} \exp[\alpha^{glass}(T_f' - 298)] \quad (1)$$

where $V_{298K}^{glass}$ is the molar volume of the glass at 298 K and $\alpha^{glass}$ is the temperature-independent coefficient of thermal expansion for the glass between 298 K and $T_f'$. The molar volume of the liquid at $T_f'$ can thus be obtained from three measurements: (1) the glass volume (density) at 298 K; (2) the glass thermal expansion coefficient between 298 K and the beginning of the glass transition interval; and (3) the value of $T_f'$.

The K-basalt glass sample had abundant bubbles and tended to shatter upon quench and so suitable glass samples for room-temperature density and thermal

expansion measurements were only obtained for the Na-basalt and K-Na basalt samples. The room temperature (298 K) density of each sample was measured using the Archemidean method, by weighing the sample several times in air and several times below the balance while immersed in liquid toluene.

The glass samples have height between 2.1 and 6.9 mm with flat and bottom and top surfaces. The linear thermal expansion coefficient, $(1/L)/(\partial L/\partial T)$, of each glass sample was measured with a Perkin-Elmer Diamond TMA vertical dilatometer with a scan rate of 10 K/min and a constant force of 10 mN (Fig. 5.1). The volume thermal expansion coefficient is equal to three times of the linear expansion coefficient. The onset of the rapid rise in the $\partial L/L$ as a function of temperature at the beginning of the glass transition interval was taken as an approximation of $T_f'$ for each glass sample (Fig. 5.1). Tangeman and Lange (2001) showed that estimates of $T_f'$ obtained in this manner match quantitative determinations of $T_f'$ calculated from Cp heating curves within 8 degrees on average. The accuracy of the measurement in this study is estimated to be within 3% based on the thermal expansion of NIST Standard-731 (Guo et al., 2013b).

**High-temperature liquid density measurements**

Thirty-two liquid density measurements were made on the three alkali-bearing model basalt liquids at high temperatures using the double-bob Archimedean method. The procedure is similar to that described by Guo et al. (2013a), where molybdenum crucibles and bobs were used in a reducing environment by 1%CO-99%Ar. The oxygen fugacity of such environment was bracketed by Mo-$MoO_2$ buffer (Chase, 1998) and Fe-FeO buffer because of the saturation of Mo but unsaturated metallic iron in the liquid. At this redox condition, the model of Kress and Carmichael (1991), calibrated on a wide

variety of natural liquids, predicts 4 ± 1% of the total iron as $Fe^{3+}$. This is consistent with Mössbauer spectroscopy on faylite liquid with the same density measurement (Thomas et al., 2012), which indicates that $Fe^{3+}$ concentrations are < 5% of the total iron.

Each sample powder was melted and reduced by four batches which were added stepwise. The density measurement was performed when the entire sample was in the Mo crucible. The buoyancy of the bob was recorded by the electronic balance with a precision of ± 0.0001 g that was mounted on an aluminum shelf atop the furnace. By using at least two Mo bobs of different mass with identical stem diameters, the effect of surface tension is eliminated. The density of the liquid is calculated from the following equation:

$$\rho(T) = \frac{B_L(T) - B_S(T)}{V_L(T) - V_S(T)} \quad (2)$$

where $B_L(T)$ and $B_S(T)$ are the buoyancy of the large and small bobs, respectively, and $V_L(T)$ and $V_S(T)$ are the immersed volume of the large and small bob, respectively. In this study, the buoyancy of four bobs (two different large bobs and two different small bobs) was used at each temperature for each liquid, allowing four density measurements to be made. The standard deviations of these measured densities range from 0.05 to 0.25%. The immersed volume of the Mo bobs as a function of temperature is calculated from the density (10.22 g/cm$^3$ at 298 K) and thermal expansion (Gray, 1972) of molybdenum metal.

**Sound speed measurements**

The sound speeds of the three alkali-bearing model basalt liquids, along with the other four alkali-bearing samples (Table 5.1a), were measured by frequency sweep

ultrasonic interferometer in a 1%CO-99%Ar reducing gas environment. The details of the procedure are thoroughly described in Ai and Lange (2004a, b). A 2 cm-deep molybdenum crucible is held inside an alumina support rod with the depth of the liquid between 3 and 4 mm. A short pulse (1s) spanning about 2 MHz and centered at 4.5 or 5.5 MHz travels down to the molybdenum upper buffer rod and reaches the rod-melt interface. Part of the signal is transmitted through the liquid and reflects off the bottom of the crucible. Two mirror reflections from the bottom of crucible return up the upper rod and are delivered to the data acquisition system. A Fourier transform is performed on the return echo to analyze the frequency response. The periodic function of frequency ($\Delta f$) follows this relation: $\Delta f$ =c/2S. Two or three different rod positions are made with the micrometer gauge to give an accurate measurement of relative thickness ($\Delta S=S_1-S_2$). Because sound speed is independent of melt thickness, sound speed can be calculated from the relation:

$$c = \left| \frac{2\Delta S}{\Delta f_2^{-1} - \Delta f_1^{-1}} \right| \tag{3}$$

## Results

### Low-temperature density and volume of the liquids at $T_f'$

The room-temperature densities of the two glasses were measured before and after each thermal expansion experiment to evaluate the effect of any structure relaxation that may have occurred. After the first thermal expansion experiment, there was little density variation ($\leq 0.1\%$) in the glass sample before and after subsequent TMA runs. Therefore, the last glass density measurements after the last TMA experiment is reported

in Table 5.2. The volume of each glass at 298 K was calculated from the following equation:

$$V_T = g.f.w./\rho_T . \quad (4)$$

Two to three replicate thermal expansion runs (dL/L vs. T) were made for each glass sample. The volume coefficient of thermal expansion ($\alpha = \frac{1}{V}\frac{dV}{dT}$) of each glass was calculated by multiplying the linear coefficient of thermal expansion by three. The difference for $\alpha^{glass}$ between the two TMA runs ranges ≤ 11%, which contributes < 0.2% error to V($T_f$'). The $T_f$' values were approximated using the onset of the rapid rise in the dL/L vs. T curve, following Tangeman and Lange (2001). The difference in derived values for $T_f$' between multiple TMA runs was always ≤ 7 degrees. By combining $V_{298K}^{glass}$, $\alpha^{glass}$ and $T_f$' in Equation 1, the volume of each sample liquid at $T_f$' can be calculated and is listed in Table 5.2, with an experimental uncertainty < 1% in all cases.

**Liquid volumes as a function of temperature**

The high temperature density data for the three alkali-bearing model basalt liquids are presented in Table 5.3. The standard deviations of replicate density measurements at each temperature range from 0.05% to 0.25%. These density data were converted to molar volume using Equation 4. In Figure 5.2, the high-temperature data are combined with the low-temperature measurement at $T_f$', providing volume data for the two Na-bearing samples that spans a wide temperature interval of 800-860 degrees.

*Modeling molar volume with temperature and composition*

The liquid volume data for the three model basalts in Table 5.3 were combined with molar volume data from the literature on $K_2O$-$Na_2O$-CaO-MgO-$Al_2O_3$-$SiO_2$ liquids (Bockris et al., 1956; Stein et al., 1986; Lange and Carmichael, 1987; Lange, 1996, 1997) to calibrate the following linear volume equation:

$$V^{liq}(X,T) = \sum X_i \left[ \overline{V}_{i,T_{ref}} + \frac{\partial \overline{V}_i}{\partial T}(T - T_{ref}) \right] \quad (5)$$

where $X_i$ is the mole fraction of each oxide component, $\overline{V}_{i,T_{ref}}$ is the partial molar volume of each oxide component at a reference temperature ($T_{ref}$ = 1723 K), and $\partial \overline{V}_i / \partial T$ is the partial molar thermal expansivity of each oxide component. The results of this regression are presented in Table 5.4a and recover measured volumes within experimental error (Fig. 5.3a). The fitted values for $\overline{V}_{FeO}$ (14.76 $cm^3$/mol) and $\partial \overline{V}_{FeO} / \partial T$ (1.03 x$10^{-3}$ $cm^3$/mol-K) are significantly larger and smaller, respectively, than those obtained for alkali-free liquids in the An-Di-Hd ternary (12.82 $cm^3$/mol and 3.69 x $10^{-3}$ $cm^3$/mol-K; Guo et al., 2013b). A second regression of Equation 5 was performed that includes the volume data on the An-Di-Hd liquids from Guo et al. (2013b). The results of this regression are presented in Table 5.4b and the residuals in Fig. 5.3b show a systematic difference between the alkali-bearing and alkali-free liquids, suggesting that the value of $\overline{V}_{FeO}$ is distinctly different between the two sets of liquids.

Note that the effect of treating 4% of the total iron as $Fe^{3+}$, and assuming that the partial molar volume of the $Fe_2O_3$ component is 41.5 $cm^3$/mol (Liu and Lange, 2006), leads to a fitted value for $\overline{V}_{FeO}$ of 14.56 (vs. 14.76) $cm^3$/mol. Because the difference in $\overline{V}_{FeO}$ is relatively small, all iron is treated as $Fe^{2+}$ for simplicity.

**Relaxed sound speed of the liquids**

Forty-four relaxed sound speed measurements are reported in Table 5.5 for the seven alkali-bearing samples at temperatures ranging between 1501 and 1876 K. For each temperature, most measurements were taken at two centered frequencies (4.5 and 5.5 MHz). The sound speeds of all liquids are independent of frequency, indicating that the liquids were relaxed. In all cases, the sound speeds decrease with increasing temperature (Fig. 5.4).

**Modeling the sound speed and compressibility data of Fe-free liquids**

Before the sound speed and compressibility data of the alkali- and Fe-bearing model basalt liquids can be incorporated into regression equations, it is first necessary to adequately model the variable compressibility of the $Al_2O_3$ component when it coexists with $K_2O$, $Na_2O$, CaO and MgO. It has long been known that the partial molar compressibility of the $Al_2O_3$ component is different in sodic liquids than in alkaline-earth aluminosilicate liquids (Kress et al., 1988; Kress and Carmichael, 1991; Ai and Lange, 2008), which led Kress and Carmichael (1991) and Ghiorso and Kress (2004) to invoke the use of a Na-Al interaction parameter in their models of liquid dV/dP and sound speed, respectively. In this study, an alternative approach is to recast the $Na_2O$-$Al_2O_3$-$SiO_2$ liquids of Kress et al. (1988) into the components $NaAlO_2$-$Na_2O$-$SiO_2$. For the new data for LC-19 in this study, the components were cast as $KAlO_2$-$K_2O$-$SiO_2$. Because the compressibility of $Al_2O_3$ does not vary between CaO- and MgO-bearing silicate melts (Ai and Lange, 2008), it is not necessary to create $Ca_{0.5}AlO_2$ or $Mg_{0.5}AlO_2$ components for modeling purposes. Instead, the fitted values for the $Al_2O_3$ component in the models presented below are for CaO- and MgO-bearing silicate melts.

*Fe-free $KAlO_2$-$NaAlO_2$-CaO-MgO-$Al_2O_3$-$SiO_2$ liquid sound speeds*

The following empirical equation models sound speed as a linear function of composition and temperature:

$$c^{liq}(X,T) = \sum X_i \left( c_{i,1723K} + \frac{\partial c_i}{\partial T}(T - 1723K) \right) \quad (6)$$

where $X_i$ is mole fraction of each oxide component, $c_i$ is the "partial molar" sound speed for each oxide component at a reference temperature (1723 K), and $\partial c_i / \partial T$ is its temperature dependence. The sound speed data obtained for the four Fe-free alkaline silicate liquids from this study in Table 5.5 were combined with sound speed data in the literature for $Na_2O$-$Al_2O_3$-$SiO_2$ liquids (Rivers and Carmichael, 1987; Kress et al., 1988) and CaO-MgO-$Al_2O_3$-$SiO_2$ liquids (Secco et al., 1991; Webb and Courtial, 1996; Ai and Lange, 2008) and recast in terms of the $KAlO_2$-$K_2O$-$NaAlO_2$-$Na_2O$-CaO-MgO-$Al_2O_3$-$SiO_2$ components a regression of Equation (6). The results are presented in Table 5.6a. By subtracting the value of $c_{K_2O}$ and $c_{Na_2O}$ from $2c_{KAlO_2}$ and $2c_{NaAlO_2}$, respectively, the resulting values of $c_{Al_2O_3}$ are different from one another and different from the fitted $c_{Al_2O_3}$ value in Table 5.6a . The results confirm that the "partial molar" sound speed of the $Al_2O_3$ component is different in potassic (5036 m/s) vs. sodic (4717 m/s) vs. alkaline-earth liquids (2589 m/s) and that it is necessary to create the $NaAlO_2$ and $KAlO_2$ components, in addition to $Al_2O_3$, in model equations of sound speed for mixed alkali and alkaline-earth aluminosilicate melts.

*Fe-free $KAlO_2$-$NaAlO_2$-CaO-MgO-$Al_2O_3$-$SiO_2$ liquid $\beta_T$ model*

The sound speed and density data compiled in Table 5.5 were used to calculate the adiabatic compressibility from the relation, $\beta_S = 1/\rho c^2$. The adiabatic compressibility is converted to isothermal compressibility from the relation:

$$\beta_T = \beta_S + \frac{TV_T\alpha^2}{Cp} \quad (7)$$

where $T$ is temperature (K), $V_T$ is the molar volume at temperature T, $\alpha$ is the coefficient of thermal expansion and $Cp$ is the molar heat capacity. The $V_T$ and $\alpha$ terms were calculated from Lange (1997). $Cp$ is calculated from the model of Lange and Navtrotsky (1992) for silicate liquids. The propagated uncertainty in $\beta_T$ is smaller than 3%.

For an ideal solution, $\beta_T$ varies as a linear function of the volume fraction of each oxide component (Rivers and Carmichael, 1987) and the following model includes a linear dependence on temperature:

$$\beta_T(X) = \sum X_i \frac{\overline{V}_{i,T}}{V_T}\left(\overline{\beta}_{i,T} + \frac{\partial\overline{\beta}_i}{\partial T}(T - 1723K)\right) \quad (8)$$

The isothermal compressibility data obtained for the four Fe-free alkaline silicate liquids from this study in Table 5.5 were combined with compressibility data in the literature for $Na_2O$-$Al_2O_3$-$SiO_2$ liquids (Rivers and Carmichael, 1987; Kress et al., 1988) and CaO-MgO-$Al_2O_3$-$SiO_2$ liquids (Secco et al., 1991; Webb and Courtial, 1996; Ai and Lange, 2008), and recast in terms of the $KAlO_2$-$K_2O$-$NaAlO_2$-$Na_2O$-CaO-MgO-$Al_2O_3$-$SiO_2$ components, in a regression of Equation (8), which recovers most of the measurements within error (Fig. 5.5a). The results are presented in Table 5.6b and lead to a fitted $\overline{\beta}_{Al_2O_3}$ value of 4.53 ± 0.05 $10^{-2}$ $GPa^{-1}$, similar to that derived in Ai and Lange (2008) for CaO-MgO-$Al_2O_3$-$SiO_2$ liquids (4.51 ± 0.04 $10^{-2}$ $GPa^{-1}$). By subtracting the volume fraction of

$\overline{\beta}_{T,K_2O}$ and $\overline{\beta}_{T,Na_2O}$ from $2\overline{\beta}_{KAlO_2}$ and $2\overline{\beta}_{NaAlO_2}$, respectively, the resulting values of $\overline{\beta}_{T,Al_2O_3}$ are different from one another (-2.36 and -3.54 $10^{-2}$ $GPa^{-1}$, respectively) and different from the fitted value in Table 5.6b. The negative values for the $Al_2O_3$ components in the alkali-bearing liquids are consistent with the results of Kress et al. (1988) on $Na_2O$-$Al_2O_3$-$SiO_2$, where they derive a value for $\overline{\beta}_{T,Al_2O_3}$ of -4.78 $10^{-2}$ $GPa^{-1}$. Their empirical model equation, however, is based on mole fractions and not volume fractions, and so their derived value of $\overline{\beta}_{T,Al_2O_3}$ cannot be directly compared to that from this study. Nonetheless, the clear result is that the $Al_2O_3$ component is less compressible when $Al^{3+}$ is charged balance with K vs. Na vs. Ca and Mg.

*Fe-free $KAlO_2$-$NaAlO_2$-CaO-MgO-$Al_2O_3$-$SiO_2$ liquid $(\partial V/\partial P)_T$ model*

A final regression equation is presented for $(\partial V/\partial P)_T (=-V_T\beta_T)$. For an ideal solution, $(\partial V/\partial P)_T$ varies as a linear function of composition, and the following model includes a linear dependence on temperature:

$$\left(\frac{\partial V}{\partial P}\right)_T (X,T) = \sum X_i \left(\frac{\partial \overline{V}_{i,1723}}{\partial P} + \frac{\partial^2 \overline{V}_i}{\partial P \partial T}(T - 1723K)\right) \qquad (9)$$

Again, the Fe-free data from this study (Table 5.5) and from the literature (Rivers and Carmichael, 1987; Kress et al., 1988; Secco et al., 1991; Webb and Courtial, 1996; Ai and Lange, 2008), and recast in terms of the $KAlO_2$-$K_2O$-$NaAlO_2$-$Na_2O$-CaO-MgO-$Al_2O_3$-$SiO_2$ components, were used in a regression of Equation (9). The model results are presented in Table 5.6c and lead to a fitted $\partial\overline{V}_{Al_2O_3}/\partial P$ value of -1.71 ± 0.02 $10^{-4}$ $cm^3$/mol-bar. By subtracting the fitted value of $\partial\overline{V}_{K_2O}/\partial P$ and $\partial\overline{V}_{Na_2O}/\partial P$ from

$2\partial\overline{V}_{KAlO_2}/\partial P$ and $2\partial\overline{V}_{NaAlO_2}/\partial P$, respectively, the resulting values of $\partial\overline{V}_{Al_2O_3}/\partial P$ are different from one another (+1.25 and +0.90 $10^{-4}$ $cm^3$/mol-bar, respectively) and different from the fitted value in Table 5.6c. Again, the $Al_2O_3$ component is less compressible when $Al^{3+}$ is charged balance with K vs. Na vs. Ca and Mg.

**Modeling the sound speed and compressibility data of the FeO- and alkali-bearing model basalt liquids**

Before the sound speed and compressibility data for the model alkali basalt liquids from this study, which contain both alkali and alkaline earth components along with $Al_2O_3$, it must first be established how to apportion the $Al_2O_3$ component between the $K_2O$, $Na_2O$, CaO and MgO components. None of the liquids in the previous regressions have concentrations of $K_2O$ and $Na_2O$ as well as $Al_2O_3$, which is the case for the K-Na-basalt sample (Table 5.1). Nor do any of the liquids have mixed alkali and alkaline earth components. To establish the rules of how to apportion $Al_2O_3$ between $Na_2O$ and CaO, data for two liquid samples from the sound speed study of Rivers and Carmichael (1987) can be employed (RC-17 and RC-19), which contain all three components (Table 5.1). When the sound speed and compressibility data for both samples are included in the three regressions of sound speed and compressibility (Equations 6, 8 and 9), residuals are minimized when 45% of the total concentration of $Na_2O$ is apportioned to $Al_2O_3$ to form the $NaAlO_2$ component, and the remaining 55% is left as the $Na_2O$ component. The $Al_2O_3$ that is left over is indirectly apportioned to CaO and MgO. This result was applied to the Na-basalt and Na-K basalt samples (Table 5.1b), where 45% of the $Na_2O$ concentration was apportioned to $Al_2O_3$ to form the $NaAlO_2$ component in both samples. For the K-basalt and Na-K basalt samples, it was found that

internally consistent results were obtained when 100% of the total concentration of $K_2O$ was apportioned to $Al_2O_3$ to form the $KAlO_2$ component in both cases.

To summarize, the following set of rules were followed to apportion the $Al_2O_3$ between $K_2O$, $Na_2O$, CaO and MgO. First, all $K_2O$ is assigned to $Al_2O_3$ to form the $KAlO_2$ component. Second, if $Al_2O_3$ is left over, then 45% of the $Na_2O$ component is assigned to $Al_2O_3$ to form the $NaAlO_2$ component. The remaining $Al_2O_3$ is indirectly assigned to CaO and MgO. These rules are broadly consistent with free energy calculations using the JANF thermochemical tables (Chase, 1998). In Table 5.7, the free energies of four reactions between oxide solids with corundum to form alumina complexes are tabulated. The results show the clear preference of $Al^{3+}$ to form complexes with various cations in the order K > Na > Ca > Mg.

When the components for the three alkali basalt samples were recast in terms of $KAlO_2$-$K_2O$-$NaAlO_2$-$Na_2O$-CaO-MgO-FeO-$Al_2O_3$-$SiO_2$, following the rules outlined above, and included in the regressions of Equation 6, 8 and 9, the results recover all measurements well within experimental error (Fig. 5.5b). The results of these three regressions are presented in Tables 5.8, 5.9 and 5.10. The fitted values for $c_{FeO}$ (1632 m/s), $\overline{\beta}_{T,FeO}$ (5.22 $10^{-2}$ $GPa^{-1}$), and $\partial\overline{V}_{FeO}/\partial P$ (-0.734 $10^{-4}$ $cm^3$/mol-bar), differ from those obtained for the alkali-free liquids in the An-Di-Hd system studied by Guo et al. (2013b) (2042 m/s, 4.75 $10^{-2}$ $GPa^{-1}$, and -0.613 $10^{-4}$ $cm^3$/mol, respectively), and reflect a more compressible FeO component in the alkali-bearing liquids.

## Discussion

**The coordination number of $Fe^{2+}$ in alkali-bearing basalts**

It is well known that $Fe^{2+}$ occupies 6-coordinated sites in commonly minerals (e.g., olivine, pyroxenes, micas, amphiboles). However, the coordination number of $Fe^{2+}$ in multi-component silicate liquids is far more variable. Many earlier studies on FeO-bearing silicate glasses and melts using Mossbauer and optical absorption methods (e.g. Boon & Fyfe, 1972; Goldman & Berg, 1980; Fox et al., 1982) suggested that $Fe^{2+}$ is dominantly 6-coordinated. In contrast, more recent studies using Mossbauer, micro-Roman spectra and XAFS spectroscopy methods show that $Fe^{2+}$ occurs in 4- and 5- and 6-fold coordination in various silicate glasses (e.g., Jackson et al., 1993; Brown et al., 1995; Rossano et al., 2000). The most common coordination site for $Fe^{2+}$ is 5-fold coordination, and the effect of increasing alkalis vs. alkaline earth components is to drive $Fe^{2+}$ coordination to lower values (e.g., Jackson et al., 1993; Wilke et al., 2007).

In the study by Guo et al. (2013a) on the density and compressibility of liquids in the CaO-FeO-$SiO_2$ system, a case was made that derived values for $\overline{V}_{FeO}$ at 1723 K of 12.1 and 17.1 $cm^3$/mol represent $Fe^{2+}$ in 6-fold and 4-fold coordination, respectively, on the basis of comparisons to mineral molar volumes. From this result, they derived a linear equation to estimate the coordination number of $Fe^{2+}$:

$$CN = 10.85 - 0.401(\overline{V}_{FeO,1723K}). \quad (10)$$

When Equation 10 is applied to the fitted $\overline{V}_{FeO}$ value from this study at 1723 K (14.76 ± 0.15 $cm^3$/mol) for the alkali basalt liquids (Table 5.4a), the estimated average $Fe^{2+}$ coordination is 4.9. This value contrasts with the $Fe^{2+}$ coordination number of 5.7 calculated for alkali-free model basalts in the An-Di-Hd system, on the basis of the value for $\overline{V}_{FeO}$ derived for those liquids (12.82 ± 0.16 $cm^3$/mol; Guo et al., 2013b). This result

confirms spectroscopic evidence from the literature that the effect of increasing alkalis is to decrease the average coordination number for $Fe^{2+}$ in multicomponent silicate liquids.

**Systematic variation in $\overline{\beta}_{T,FeO}$ with $\overline{V}_{FeO}$ (and $Fe^{2+}$ coordination)?**

Given the evidence that the effect of increasing alkali concentrations in model basalt liquids changes the value of $\overline{V}_{FeO}$ compared to that in alkali-free liquids, the next question is what affect do alkalis have on the compressibility of the FeO component. In a previous study on the density and compressibility of $Na_2O$-FeO-$SiO_2$ silicate liquids, Guo et al. (2013c) showed that fitted $\overline{\beta}_{T,FeO}$ values in sodic liquids have remarkably large values ($\leq 14.9\times10^{-2}$ $GPa^{-1}$), more than the values for $\overline{\beta}_{T,Na_2O}$ and $\overline{\beta}_{T,SiO_2}$ ($9.1$ and $6.1\times10^{-2}$ $GPa^{-1}$, respectively). Moreover, these fitted $\overline{\beta}_{T,FeO}$ values in the NFS liquids vary systematically and *inversely* with fitted $\overline{V}_{FeO}$ values, which is opposite the behavior observed by Guo et al. (2013a) for CaO-FeO-$SiO_2$ liquids, where fitted values of $\overline{\beta}_{T,FeO}$ and $\overline{V}_{FeO}$ are positively correlated with one another (Fig. 5.6). Therefore, an outstanding question to be addressed in this study is what affect does the addition of alkalis have on $\overline{\beta}_{T,FeO}$ in model basalt liquids.

The results in Fig. 6 show that the alkali-bearing model basalt liquids follow the trend-line of the CFS liquids and not the NFS liquids. This indicates that even though it appears that $Fe^{2+}$ is largely in 5-fold coordination in the alkali-bearing model basalts, it does not contribute to an anomalously large compressibility as seen in the NFS liquids. This may be due to the interaction of $Al^{3+}$ with $Na^{+}$ and $K^{+}$ in the model basalt liquids, in contrast to the Al-free NFAS liquids.

**Recommended values of $\overline{V}_{FeO}$, $\partial\overline{V}_{FeO}/\partial T$ and $\overline{\beta}_{T,FeO}$ in basaltic liquids**

The most important objective of this study was to determine the most appropriate values for $\overline{V}_{FeO}$, $\partial\overline{V}_{FeO}/\partial T$ and $\overline{\beta}_{T,FeO}$ to apply to naturally occurring basalt liquids.

Based on the evidence that the abundance of alkalis affects fitted values of $\overline{V}_{FeO}$ at 1723 K, the following equation is recommended for use in Equation 5:

$$\overline{V}_{FeO,1723K} = 12.82 + 0.175(K_2O + Na_2O\ mol\%) \quad (11)$$

For the $\partial\overline{V}_{FeO}/\partial T$ term, the fitted values of 3.69 and 1.03 x $10^{-3}$ $cm^3$/mol-K for the alkali-free and alkali-bearing model basalts, respectively, are combined with a value of zero for the case when $Fe^{2+}$ is in 4-fold coordination (corresponding to $\overline{V}_{FeO}$ = 17.1 $cm^3$/mol; Guo et al., 2013a) to derive the following equation, recommended for use in Equation 5:

$$\partial\overline{V}_{FeO}/\partial T = 13.9 - 0.829(\overline{V}_{FeO})\ 10^{-3}\ cm^3/mol-K \quad (12)$$

Finally, for the $\overline{\beta}_{T,FeO}$ term, the trend-line for CFS liquids in Figure 5.6 is used to derive the following equation, recommended for use in Equation 8:

$$\overline{\beta}_{T,FeO} = -5.35 + 0.728(\overline{V}_{FeO})\ 10^{-2}\ GPa^{-1} \quad (13)$$

## Acknowledgements

This research was supported by the National Science Foundation through award EAR-0855774.

Table 5.1a Composition of experimental liquids

| sample | Na basalt | K basalt | KNa basalt | LC 19 | LC 18 | KCaSi | NaCaSi | RC17 | RC19 |
|---|---|---|---|---|---|---|---|---|---|
| wt% | | | | | | | | | |
| $SiO_2$ | 46.73 | 44.94 | 45.83 | 61.22 | 54.63 | 44.27 | 49.72 | | |
| $Al_2O_3$ | 16.44 | 15.51 | 16.07 | | 7.88 | - | - | | |
| MgO | 6.19 | 5.79 | 6.00 | | | - | - | | |
| CaO | 9.03 | 8.77 | 8.78 | | | 21.20 | 24.10 | | |
| $\mathbf{Fe_2O_3^T}$ | 11.54 | 10.89 | 11.04 | | | - | - | | |
| $Na_2O$ | 9.80 | - | 4.76 | 15.00 | 37.15 | - | 26.78 | | |
| $K_2O$ | - | 14.58 | 7.40 | 23.17 | | 34.98 | - | | |
| Total | 99.73 | 100.48 | 99.88 | 99.69 | 99.66 | 100.45 | 100.60 | | |
| mol% | | | | | | | | | |
| $SiO_2$ | 49.46 | 49.62 | 49.69 | 64.47 | 69.97 | 49.58 | 48.98 | 62.70 | 58.60 |
| $Al_2O_3$ | 10.25 | 10.09 | 10.27 | - | 7.20 | - | - | 6.29 | 12.40 |
| MgO | 9.77 | 9.54 | 9.70 | - | - | - | - | 11.90 | 7.83 |
| CaO | 10.23 | 10.37 | 10.20 | - | - | 25.44 | 25.58 | 13.00 | 17.10 |
| $FeO_T$ | 10.21 | 10.06 | 10.01 | - | - | - | - | - | - |
| $Na_2O$ | 10.06 | - | 5.00 | 16.03 | - | - | 25.44 | 5.90 | 4.07 |
| $K_2O$ | - | 10.27 | 5.12 | 16.50 | 22.83 | 24.98 | - | - | - |
| g.f.w. | 63.42 | 66.69 | 65.07 | 66.02 | 70.89 | 67.59 | 59.54 | 59.83 | 63.12 |

All samples analyzed by electron microprobe (see text) except LC-19, LC-18, RC-17 and RC-19, which were analyzed by wet chemistry.

Table 5.1b Composition of experimental liquids with re-adjustment for the components(mol%)

| sample | Na basalt | K basalt | KNa basalt | LC19 | LC18 | KCaSi | NaCaSi | RC17 | RC19 |
|---|---|---|---|---|---|---|---|---|---|
| $SiO_2$ | 49.46 | 49.62 | 49.69 | 64.47 | 69.97 | 49.58 | 48.98 | 62.70 | 58.60 |
| $Al_2O_3$ | 5.72 | - | 2.90 | - | - | - | - | 3.64 | 10.57 |
| MgO | 9.77 | 9.54 | 9.70 | - | - | - | - | 11.90 | 7.83 |
| CaO | 10.23 | 10.37 | 10.20 | - | - | 25.44 | 25.58 | 13.00 | 17.10 |
| $FeO_T$ | 10.21 | 10.06 | 10.01 | - | - | - | - | - | - |
| $Na_2O$ | 5.53 | - | 2.75 | 16.03 | - | - | 25.44 | 3.25 | 2.24 |
| $K_2O$ | - | 0.17 | - | 16.50 | 15.63 | 24.98 | - | - | - |
| $NaAlO_2$ | 9.05 | - | 4.50 | - | - | - | - | 5.31 | 3.66 |
| $KAlO_2$ | - | 20.20 | 10.24 | - | 14.40 | - | - | - | |
| g.f.w. | 63.42 | 66.69 | 65.07 | 66.02 | 70.89 | 67.59 | 59.54 | 59.83 | 63.12 |

Table 5.2 Density and volume of glasses at 298 K and $T_f'$

| Sample | ρ(298 K) ($g/cm^3$) | Vol (298K) ($cm^3$/g.f.w) | $\alpha^{glass}$ ($10^{-5}$/K) | ρ($T_f'$) ($g/cm^3$) | Vol ($T_f'$) ($cm^3$/g.f.w.) | $T_f'$ (K) |
|---|---|---|---|---|---|---|
| Na-basalt | 2.785 | 22.77 | 2.802 | 2.740 | 23.15 | 890 |
| KNa-basalt | 2.784 | 23.38 | 3.144 | 2.729 | 23.85 | 930 |

Table 5.3 Density, surface tension and volume of experimental liquids at high temperature

| Sample | T (K) | Density ($g/cm^3$) | $\gamma(T)$ N/m | Vmeas ($cm^3$/g.f.w) | Vcalc ($cm^3$/g.f.w) | %Residual 100×(meas-calc)/meas |
|---|---|---|---|---|---|---|
| Na-basalt | 1535 | 2.626 | 0.26 | 24.15 | 24.15 | 0.03 |
| Na-basalt | 1535 | 2.623 | 0.24 | 24.18 | 24.15 | 0.14 |
| Na-basalt | 1535 | 2.619 | 0.25 | 24.22 | 24.15 | 0.30 |
| Na-basalt | 1535 | 2.617 | 0.23 | 24.24 | 24.15 | 0.37 |
| Na-basalt | 1628 | 2.605 | 0.24 | 24.35 | 24.29 | 0.23 |
| Na-basalt | 1628 | 2.604 | 0.23 | 24.36 | 24.29 | 0.26 |
| Na-basalt | 1628 | 2.607 | 0.24 | 24.33 | 24.29 | 0.15 |
| Na-basalt | 1628 | 2.606 | 0.24 | 24.34 | 24.29 | 0.19 |
| Na-basalt | 1749 | 2.597 | 0.29 | 24.42 | 24.48 | -0.25 |
| Na-basalt | 1749 | 2.595 | 0.28 | 24.44 | 24.48 | -0.17 |
| Na-basalt | 1749 | 2.588 | 0.27 | 24.51 | 24.48 | 0.10 |
| Na-basalt | 1749 | 2.587 | 0.26 | 24.52 | 24.48 | 0.13 |
| K-basalt | 1651 | 2.549 | 0.20 | 26.17 | 26.11 | 0.21 |
| K-basalt | 1651 | 2.552 | 0.20 | 26.14 | 26.11 | 0.10 |
| K-basalt | 1651 | 2.558 | 0.25 | 26.07 | 26.11 | -0.14 |
| K-basalt | 1651 | 2.561 | 0.26 | 26.04 | 26.11 | -0.26 |
| K-basalt | 1767 | 2.541 | 0.21 | 26.25 | 26.35 | -0.37 |
| K-basalt | 1767 | 2.533 | 0.19 | 26.33 | 26.35 | -0.06 |
| K-basalt | 1767 | 2.537 | 0.19 | 26.29 | 26.35 | -0.22 |
| K-basalt | 1767 | 2.529 | 0.17 | 26.37 | 26.35 | 0.10 |
| KNa-basalt | 1535 | 2.602 | 0.23 | 25.01 | 25.04 | -0.10 |
| KNa-basalt | 1535 | 2.597 | 0.20 | 25.06 | 25.04 | 0.09 |
| KNa-basalt | 1535 | 2.599 | 0.23 | 25.04 | 25.04 | 0.01 |
| KNa-basalt | 1535 | 2.594 | 0.20 | 25.09 | 25.04 | 0.20 |
| KNa-basalt | 1628 | 2.587 | 0.26 | 25.15 | 25.20 | -0.19 |
| KNa-basalt | 1628 | 2.578 | 0.21 | 25.24 | 25.20 | 0.16 |
| KNa-basalt | 1628 | 2.594 | 0.28 | 25.09 | 25.20 | -0.46 |
| KNa-basalt | 1628 | 2.586 | 0.23 | 25.16 | 25.20 | -0.15 |
| KNa-basalt | 1749 | 2.557 | 0.19 | 25.45 | 25.42 | 0.11 |
| KNa-basalt | 1749 | 2.561 | 0.22 | 25.41 | 25.42 | -0.05 |
| KNa-basalt | 1749 | 2.559 | 0.19 | 25.43 | 25.42 | 0.03 |
| KNa-basalt | 1749 | 2.563 | 0.22 | 25.39 | 25.42 | -0.12 |

Table 5.4a Linear regression of partial molar volume of each oxide for alkali-bearing basalts

| Oxide component | $\overline{V_i}(1723K) \pm 1\sigma$ (cm$^3$/mol) | $\partial\overline{V_i} / \partial T \pm 1\sigma$ (10$^{-3}$cm$^3$/mol-K) |
|---|---|---|
| $SiO_2$ | 26.86 ± 0.03 | -- |
| $Al_2O_3$ | 37.41 ± 0.08 | -- |
| CaO | 16.70 ± 0.05 | 3.74 ± 0.11 |
| MgO | 11.86 ± 0.07 | 3.27 ± 0.16 |
| $Na_2O$ | 29.27 ± 0.06 | 7.68 ± 0.11 |
| $K_2O$ | 46.65 ± 0.09 | 12.06 ± 0.19 |
| FeO | 14.76 ± 0.15 | 1.03 ± 0.61 |

[a]Total of 169 observations; $R^2$=0.9999, the average error is 0.21%

Table 5.4b Linear regression of partial molar volume of each oxide for alkali-bearing basalts and ternary model basalt liquids from Guo et al.(2013)

| Oxide component | $\overline{V_i}(1723K) \pm 1\sigma$ (cm$^3$/mol) | $\partial\overline{V_i} / \partial T \pm 1\sigma$ (10$^{-3}$cm$^3$/mol-K) |
|---|---|---|
| $SiO_2$ | 26.78 ± 0.05 | -- |
| $Al_2O_3$ | 37.89 ± 0.11 | -- |
| CaO | 16.58 ± 0.07 | 3.77 ± 0.16 |
| MgO | 11.94 ± 0.09 | 3.18 ± 0.22 |
| $Na_2O$ | 29.38 ± 0.09 | 7.72 ± 0.14 |
| $K_2O$ | 46.92 ± 0.13 | 12.19 ± 0.27 |
| FeO | 13.76 ± 0.15 | 2.15 ± 0.58 |

[a]Total of 208 observations; $R^2$=0.9999, the average error is 0.32%

Table 5.5 Sound speed and compressibility data for experimental liquids

| Sample | *f* | T (K) | *c* (m/s) | ρ ($cm^3$/mol) | $\beta_S$ ($10^{-2}$ $GPa^{-1}$) | $\beta_T$ ($10^{-2}$ $GPa^{-1}$) | d*V*/d*P* ($10^{-4}$$cm^3$/bar) |
|---|---|---|---|---|---|---|---|
| LC-19 | 4.5 | 1709 | 2321 | 2.167 | 8.567 | 9.232 | -2.813 |
| LC-19 | 5.5 | 1709 | 2326 | 2.167 | 8.530 | 9.195 | -2.801 |
| LC-19 | 4.5 | 1876 | 2230 | 2.129 | 9.444 | 10.161 | -3.150 |
| LC-19 | 5.5 | 1876 | 2220 | 2.129 | 9.529 | 10.247 | -3.177 |
| LC-18 | 4.5 | 1867 | 2317 | 2.179 | 8.549 | 9.019 | -2.934 |
| LC-18 | 4.5 | 1792 | 2341 | 2.193 | 8.322 | 8.776 | -2.837 |
| KCaSi | 4.5 | 1501 | 2637 | 2.384 | 6.031 | 6.972 | -1.976 |
| KCaSi | 4.5 | 1583 | 2581 | 2.357 | 6.368 | 7.349 | -2.107 |
| KCaSi | 4.5 | 1649 | 2523 | 2.336 | 6.725 | 7.738 | -2.239 |
| KCaSi | 4.5 | 1671 | 2501 | 2.329 | 6.864 | 7.888 | -2.289 |
| KCaSi | 5.5 | 1501 | 2651 | 2.384 | 5.967 | 6.909 | -1.958 |
| KCaSi | 5.5 | 1583 | 2585 | 2.357 | 6.348 | 7.329 | -2.101 |
| KCaSi | 5.5 | 1649 | 2535 | 2.336 | 6.661 | 7.674 | -2.220 |
| KCaSi | 5.5 | 1671 | 2522 | 2.329 | 6.750 | 7.774 | -2.256 |
| NaCaSi | 4.5 | 1600 | 2886 | 2.428 | 4.945 | 5.572 | -1.366 |
| NaCaSi | 5.5 | 1600 | 2897 | 2.428 | 4.907 | 5.534 | -1.357 |
| NaCaSi | 4.5 | 1671 | 2858 | 2.408 | 5.084 | 5.734 | -1.418 |
| NaCaSi | 4.5 | 1709 | 2830 | 2.397 | 5.209 | 5.870 | -1.458 |
| NaCaSi | 5.5 | 1709 | 2840 | 2.397 | 5.172 | 5.834 | -1.449 |
| NaCaSi | 4.5 | 1753 | 2797 | 2.385 | 5.360 | 6.035 | -1.507 |
| NaCaSi | 5.5 | 1753 | 2804 | 2.385 | 5.333 | 6.008 | -1.500 |
| K-basalt | 4.5 | 1707 | 2722 | 2.543 | 5.307 | 5.594 | -1.467 |
| K-basalt | 5.5 | 1707 | 2719 | 2.543 | 5.318 | 5.606 | -1.470 |
| K-basalt | 4.5 | 1762 | 2694 | 2.532 | 5.441 | 5.736 | -1.511 |
| K-basalt | 5.5 | 1762 | 2698 | 2.532 | 5.425 | 5.720 | -1.506 |
| K-basalt | 4.5 | 1817 | 2676 | 2.522 | 5.538 | 5.841 | -1.545 |
| K-basalt | 5.5 | 1817 | 2686 | 2.522 | 5.497 | 5.800 | -1.534 |
| K-basalt | 4.5 | 1869 | 2665 | 2.512 | 5.606 | 5.916 | -1.571 |
| K-basalt | 5.5 | 1869 | 2677 | 2.512 | 5.556 | 5.866 | -1.558 |
| Na-basalt | 4.5 | 1637 | 2736 | 2.609 | 5.120 | 5.298 | -1.288 |
| Na-basalt | 5.5 | 1637 | 2742 | 2.609 | 5.097 | 5.275 | -1.282 |
| Na-basalt | 4.5 | 1709 | 2713 | 2.597 | 5.231 | 5.416 | -1.323 |
| Na-basalt | 5.5 | 1709 | 2712 | 2.597 | 5.235 | 5.420 | -1.324 |
| Na-basalt | 4.5 | 1781 | 2697 | 2.585 | 5.318 | 5.510 | -1.352 |
| Na-basalt | 5.5 | 1781 | 2704 | 2.585 | 5.291 | 5.483 | -1.345 |
| Na-basalt | 4.5 | 1863 | 2681 | 2.572 | 5.410 | 5.610 | -1.384 |
| NaK-basalt | 4.5 | 1651 | 2743 | 2.578 | 5.156 | 5.381 | -1.359 |
| NaK-basalt | 5.5 | 1651 | 2750 | 2.578 | 5.130 | 5.355 | -1.352 |
| NaK-basalt | 4.5 | 1706 | 2722 | 2.568 | 5.257 | 5.488 | -1.391 |
| NaK-basalt | 5.5 | 1706 | 2715 | 2.568 | 5.284 | 5.515 | -1.398 |
| NaK-basalt | 4.5 | 1788 | 2684 | 2.553 | 5.438 | 5.679 | -1.448 |
| NaK-basalt | 5.5 | 1788 | 2686 | 2.553 | 5.430 | 5.671 | -1.446 |
| NaK-basalt | 4.5 | 1869 | 2664 | 2.538 | 5.552 | 5.802 | -1.488 |
| NaK-basalt | 5.5 | 1869 | 2681 | 2.538 | 5.482 | 5.732 | -1.470 |

Table 5.6a Regression results for $c_i$ at 1723K by Equation (6) using data of FeO-free alkali-bearing liquids from this study and literature[a]

| Oxide component | $c_i \pm 1\sigma$ (m/s) | $\partial c_i/\partial T \pm 1\sigma$ ($ms^{-1}$ $K^{-1}$) |
|---|---|---|
| $SiO_2$ | 2384 ± 16 | - |
| $Al_2O_3$ | 2589 ± 27 | - |
| CaO | 3968 ± 22 | - |
| MgO | 3367 ± 33 | - |
| $Na_2O$ | 2723 ± 35 | -1.99 ± 0.15 |
| $K_2O$ | 1388 ± 62 | -1.13 ± 0.43 |
| $NaAlO_2$ | 3720 ± 37 | - |
| $KAlO_2$ | 3212 ± 190 | - |

[a]Total of 240 observations; $R^2$ = 0.9999, and average error is 0.87%.

Table 5.6b Regression results for $\beta_i$ at 1723K by Equation (8) using data of FeO-free alkali-bearing silicate liquids from this study and literature[a]

| Oxide component | $\overline{\beta_i} \pm 1\sigma$ ($10^{-2}$ $GPa^{-1}$) | $\partial\overline{\beta_i}/\partial T \pm 1\sigma$ ($10^{-2}$ $GPa^{-1}K^{-1}$) |
|---|---|---|
| $SiO_2$ | 7.154 ± 0.042 | - |
| $Al_2O_3$ | 4.525 ± 0.047 | - |
| MgO | 0.454 ± 0.146 | - |
| CaO | -1.592 ± 0.084 | 0.0067 ± 0.0004 |
| $Na_2O$ | 8.661 ± 0.084 | 0.0105 ± 0.0004 |
| $K_2O$ | 13.732 ± 0.104 | 0.0176 ± 0.0007 |
| $NaAlO_2$ | 2.478 ± 0.082 | - |
| $KAlO_2$ | 6.046 ± 0.379 | - |

[a]Total of 240 observations; $R^2$ = 0.9998, and average error is 1.05%.

Table 5.6c Regression results for $\partial V_i/\partial P$ at 1723K by Equation (9) using data of FeO-free alkali-bearing silicate liquids from this study and literature[a]

| Oxide component | $\partial\overline{V_i}/\partial P \pm 1\sigma$ ($10^{-4}cm^3\,bar^{-1}$) | $\partial^2\overline{V_i}/\partial P\partial T \pm 1\sigma$ ($10^{-4}\,cm^3\,bar^{-1}K^{-1}$) |
|---|---|---|
| $SiO_2$ | -1.921 ± 0.012 | - |
| $Al_2O_3$ | -1.708 ± 0.021 | - |
| CaO | 0.274 ± 0.016 | -0.0011 ± 0.0001 |
| MgO | -0.058 ± 0.025 | - |
| $Na_2O$ | -2.557 ± 0.026 | -0.0037 ± 0.0001 |
| $K_2O$ | -6.442 ± 0.048 | -0.0097 ± 0.0003 |
| $NaAlO_2$ | -0.831 ± 0.028 | - |
| $KAlO_2$ | -2.596 ± 0.145 | - |

[a]Total of 240 observations; $R^2$ = 0.9998, and average error is 1.17%.

Table 5.7 Free energy of reactions

| Reaction | $\Delta G(298\ K)$ |
|---|---|
| $1/2K_2O + 1/2Al_2O_3 = KAlO_2$ | -157.8 |
| $1/2Na_2O + 1/2Al_2O_3 = 1/2NaAlO_2$ | -97.8 |
| $1/2CaO + 1/2Al_2O_3 = 1/2CaAl_2O_4$ | -63.8 |
| $1/2MgO + 1/2Al_2O_3 = 1/2MgAl_2O_4$ | -21.9 |

From JANAF tables (Chase, 1998)

Table 5.8 Regression results for $c_i$ at 1723K by Equation (6) using data of alkali-bearing basalts from this study and literature[a]

| Oxide component | $c_i \pm 1\sigma$ (m/s) | $\partial c_i/\partial T \pm 1\sigma$ ($ms^{-1}$ $K^{-1}$) |
|---|---|---|
| $SiO_2$ | 2381 ± 15 | - |
| $Al_2O_3$ | 2588 ± 26 | - |
| CaO | 3977 ± 20 | -0.24 ± 0.11 |
| MgO | 3336 ± 26 | - |
| $Na_2O$ | 2727 ± 33 | -1.99 ± 0.14 |
| $K_2O$ | 1403 ± 56 | -0.95 ± 0.38 |
| FeO | 1632 ± 102 | -2.22 ± 0.86 |
| $NaAlO_2$ | 3726 ± 35 | - |
| $KAlO_2$ | 3126 ± 79 | - |

[a]Total of 265 observations; $R^2$ = 0.9999, and average error is 0.82%.

Table 5.9 Regression results for $\beta_i$ at 1723K by Equation (8) using data of alkali-bearing basalts from this study and literature[a]

| Oxide component | $\overline{\beta_i} \pm 1\sigma$ ($10^{-2}$ GPa$^{-1}$) | $\partial\overline{\beta_i} / \partial T \pm 1\sigma$ ($10^{-2}$ GPa$^{-1}$K$^{-1}$) | $K_i$ (GPa) |
|---|---|---|---|
| $SiO_2$ | 7.157 ± 0.041 | - | 14.0 |
| $Al_2O_3$ | 4.524 ± 0.046 | - | 22.1 |
| CaO | -1.598 ± 0.082 | 0.0068 ± 0.0004 | -62.6 |
| MgO | 0.447 ± 0.142 | - | 223.8 |
| $Na_2O$ | 8.645 ± 0.081 | 0.0104 ± 0.0004 | 11.6 |
| $K_2O$ | 13.790 ± 0.093 | 0.0180 ± 0.0006 | 7.3 |
| FeO | 5.223 ± 0.468 | 0.0162 ± 0.0040 | 19.1 |
| $NaAlO_2$ | 2.485 ± 0.079 | - | 40.2 |
| $KAlO_2$ | 5.556 ± 0.132 | - | 18.0 |

[a]Total of 265 observations; $R^2$ = 0.9998, and average error is 1.13%.

Table 5.10 Regression results for $\partial V_i/\partial P$ at 1723K by Equation (9) using data alkali-bearing basalts from this study and literature[a]

| Oxide component | $\partial\overline{V_i}/\partial P \pm 1\sigma$ ($10^{-4}$cm$^3$ bar$^{-1}$) | $\partial^2\overline{V_i}/\partial P\partial T \pm 1\sigma$ ($10^{-4}$ cm$^3$ bar$^{-1}$K$^{-1}$) |
|---|---|---|
| $SiO_2$ | -1.922 ± 0.012 | - |
| $Al_2O_3$ | -1.708 ± 0.020 | - |
| CaO | 0.275 ± 0.016 | -0.0011 ± 0.0001 |
| MgO | -0.056 ± 0.024 | - |
| $Na_2O$ | -2.550 ± 0.025 | -0.0037 ± 0.0001 |
| $K_2O$ | -6.473 ± 0.043 | -0.0099 ± 0.0003 |
| FeO | -0.734 ± 0.079 | -0.0029 ± 0.0007 |
| $NaAlO_2$ | -0.833 ± 0.027 | - |
| $KAlO_2$ | -2.373 ± 0.061 | - |

[a]Total of 265 observations; $R^2$ = 0.9998, and average error is 1.14%.

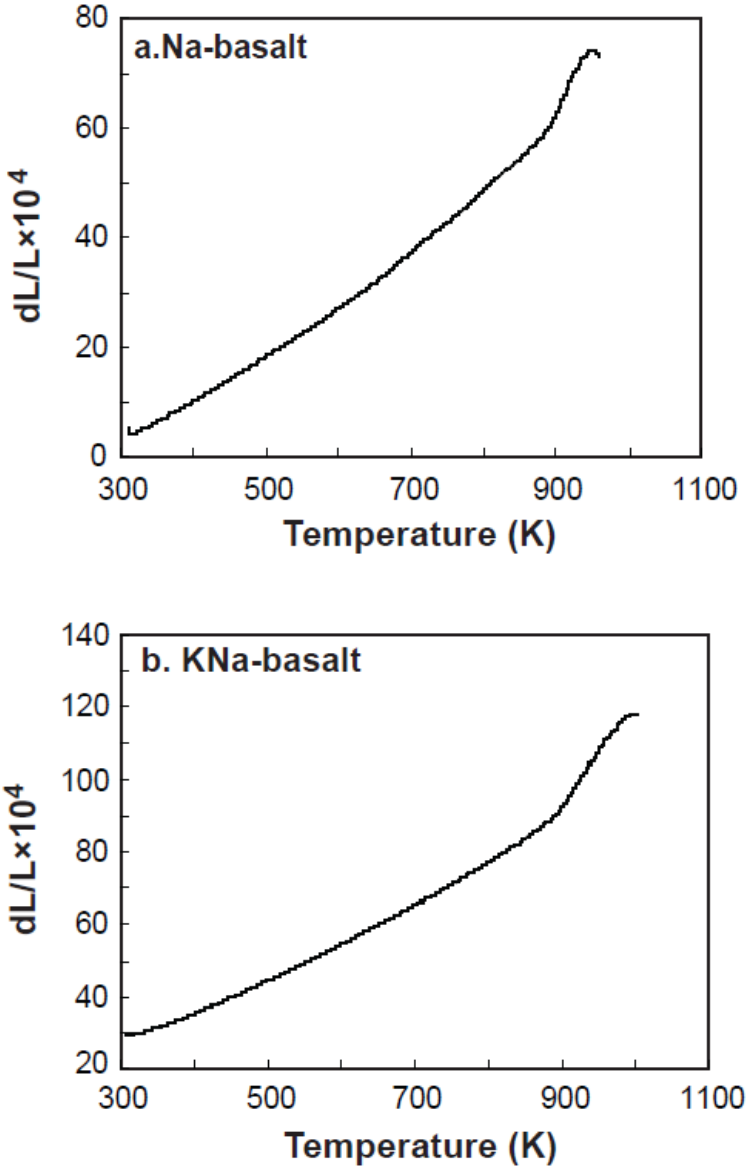


Figure 5.1 (a) Scan of dL/L vs. Temperature for Na-basalt. (b) Scan of dL/L vs. temperature for KNa-basalt. Heating rate is 10K/min.

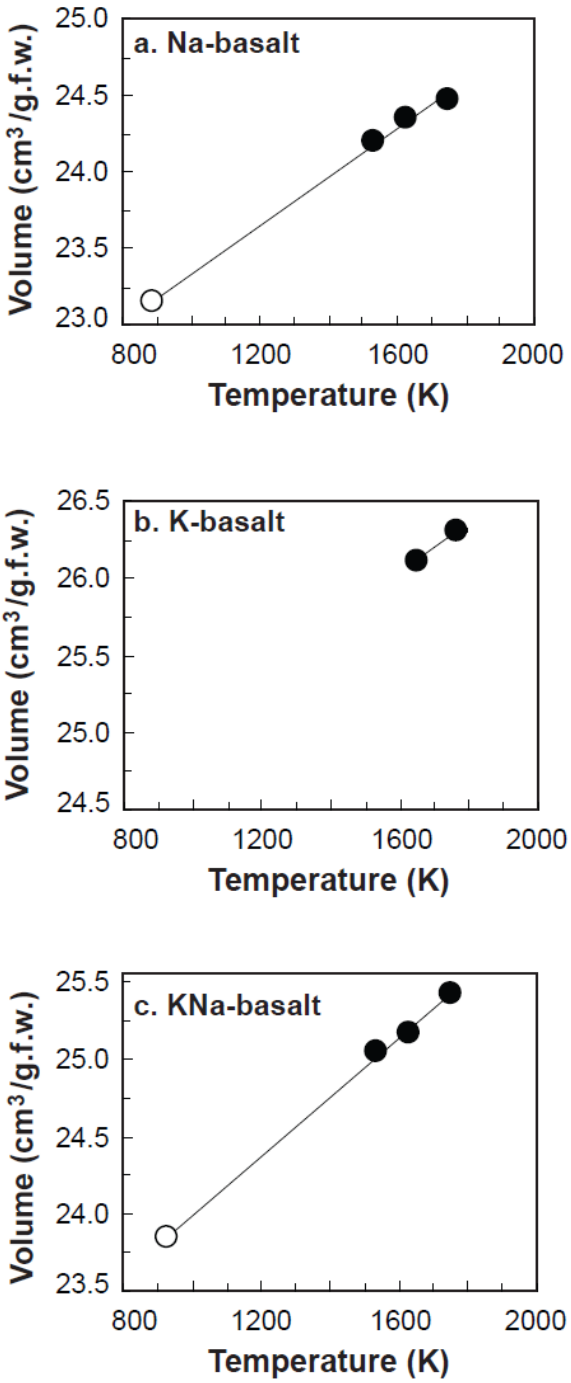


Figure 5.2 Plots of liquid volume vs. Temperature. The solid dots are for high temperature volume data. The open dots are for low-temperature volumes at $T_f'$. There is no low-temperature volume for K-basalt because a sufficiently large glass sample for the 298 K density measurement could not be obtained. The error bars are smaller than the symbols. The solid line is a linear fit to all the volume data.

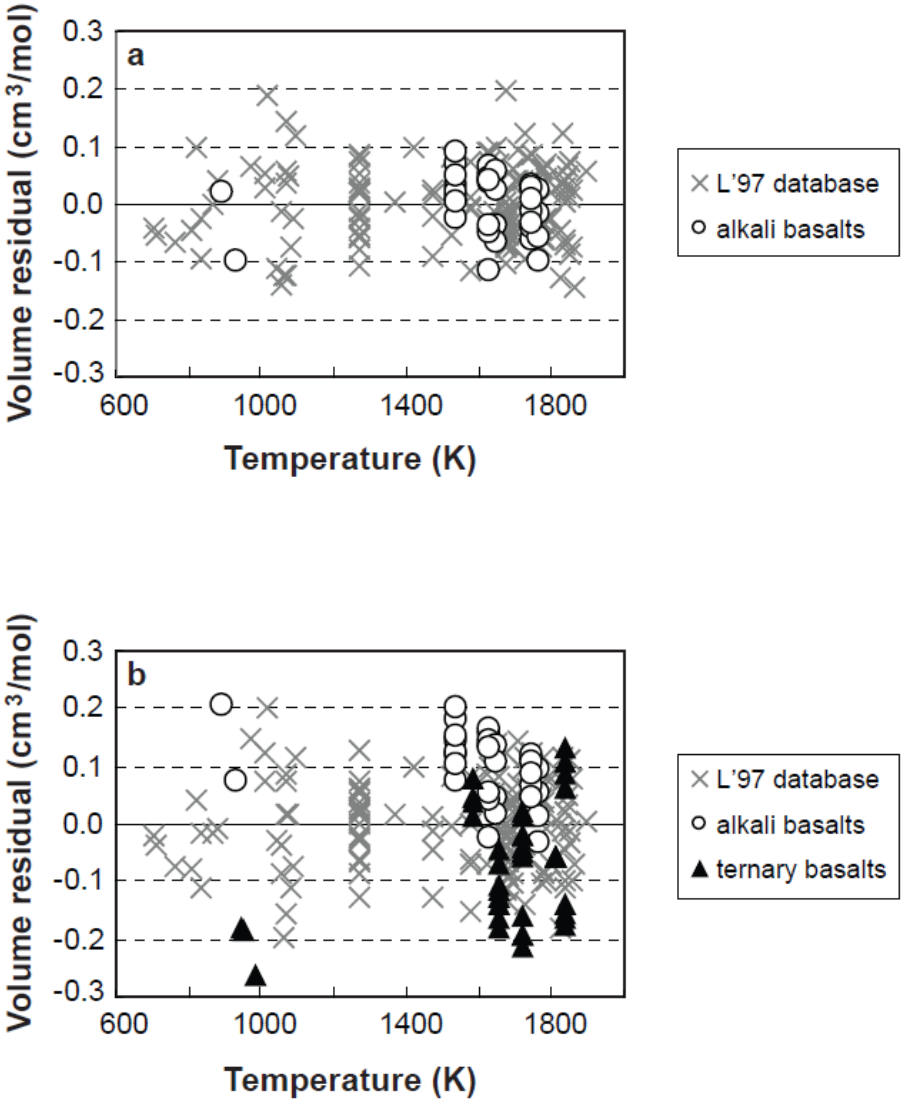


Figure 5.3 (a) Plot of volume residuals vs. Temperature for alkali basalts. (b) Plot of volume residuals vs. Temperature for alkali basalts, and ternary model basalts from Guo et al. (2013). The database is from Lange (1997).

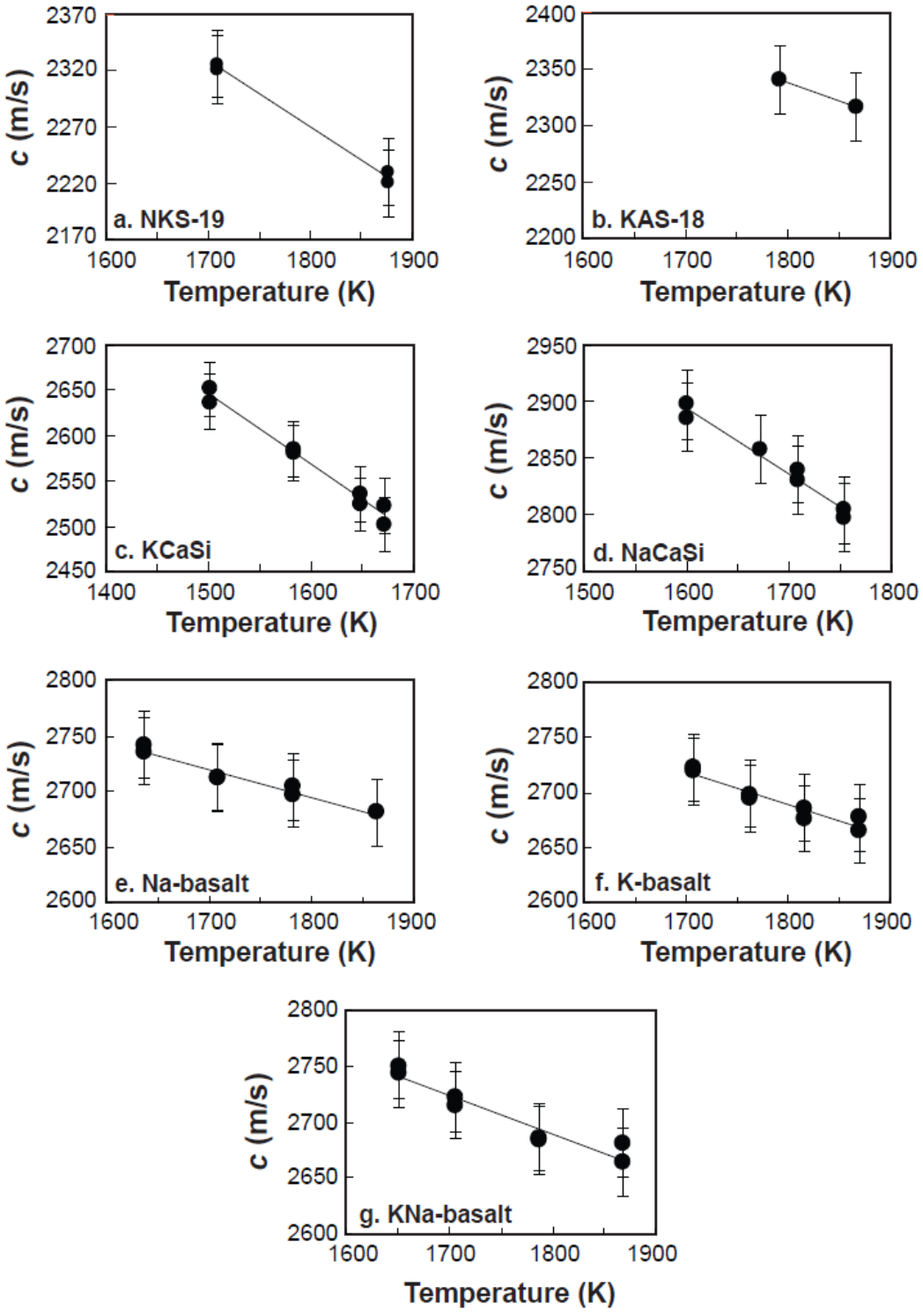


Figure 5.4 Plots of sound speed vs. Temperature for alkali-bearing liquids. The solid line is the linear fit to the data. The errors in sound speed are ±30m/s.

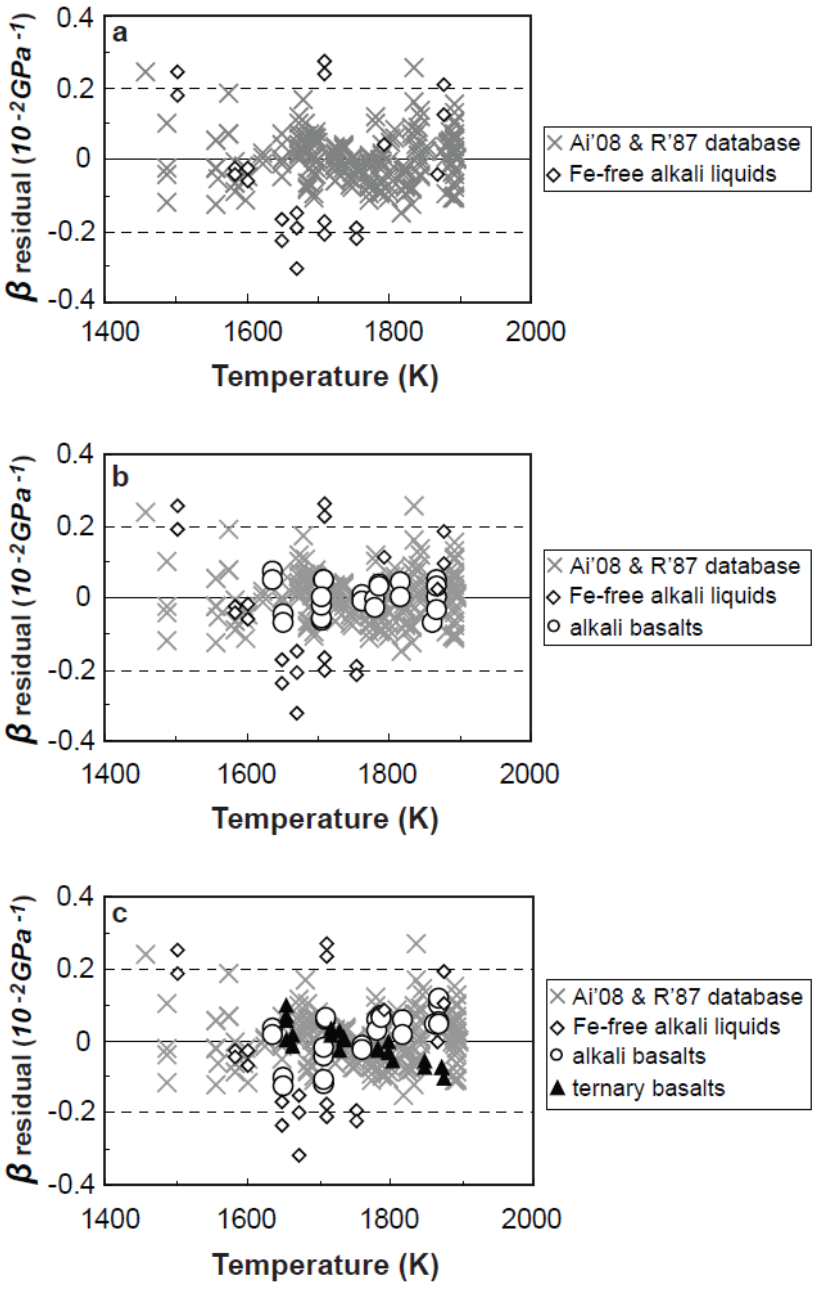


Figure 5.5 (a) Plot of isothermal compressibility residuals vs. Temperature for FeO-free alkali liquids. (b) Plot of isothermal compressibility residuals vs. Temperature for alkali basalts. (c) Plot of isothermal compressibility residuals vs. Temperature for alkali basalts, and ternary model basalts from Guo et al. (2013). The database is from Ai and Lang (2008), Rivers and Carmichael (1987) and Kress et al. (1988).

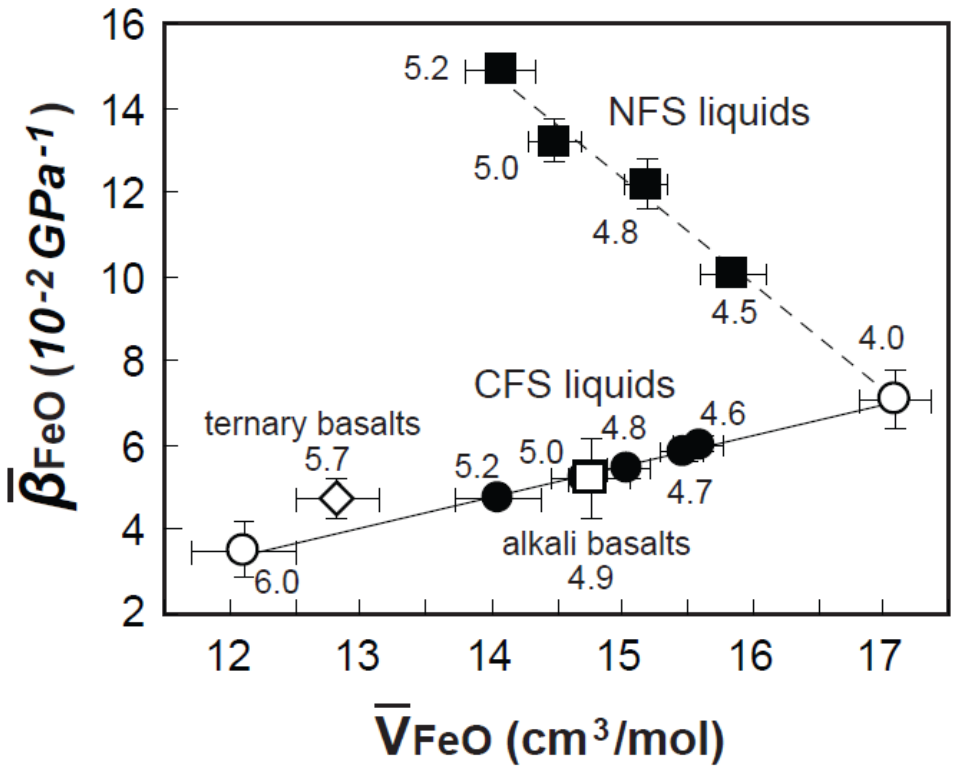


Figure 5.6 Plot of $\overline{\beta}_{FeO}$ vs. $\overline{V}_{FeO}$ for alkali basalts (open square), ternary model basalts (open diamond) from Guo et al. (2013b), CFS liquids (solid circles) from Guo et al. (2013a), and NFS liquids (solid squares) from Guo et al. (2013c). The open circles are for the values of $\overline{\beta}_{FeO}$ and $\overline{V}_{FeO}$ when $Fe^{2+}$ is 4- and 6-coordinated. The coordination number of $Fe^{2+}$ in each liquid is listed in the figure. The error bars are for 2σ, which sometimes is smaller than the symbol. The solid line is a linear fit for all the CFS liquids; the dash line is a linear fit for all the NFS liquids.

## References


Ai Y, Lange RA (2004a) An ultrasonic frequency sweep interferometer for liquids at high temperature: 1. Acoustic model. J.Geophys. Res. 109: B12203, doi:10.1029/2003JB002842

Ai Y, Lange RA (2004b) An ultrasonic frequency sweep interferometer for liquids at high temperature: 2. Mechanical assembly, signal processing, and application. J. Geophys. Res. 109, B12204, doi:10.1029/2004JB003062

Ai Y, Lange RA, (2008) New acoustic velocity measurements on $CaO$-$MgO$-$Al_2O_3$-$SiO_2$ liquids: Reevaluation of the volume and compressibility of $CaMgSi_2O_6$-$CaAl_2Si_2O_8$ liquids to 25 GPa. Journal of Geophysical Research 113: B04203, doi:10.1029/2007JB005010

Bockris JO'M, Tomlinson JW, White JL (1956) The structure of the liquid silicates: partial molar volumes and expansivities. Trans Faraday Soc. 52: 299-310

Boon JA, Fyfe WS (1972) The coordination number of ferrous ions in silicate glasses. Chem. Geol. 10:287–298

Brown GEJr., Farges F, Calas G (1995) X-ray scattering and x-ray spectroscopy studies of silicate melts. In Structure, Dynamics and Properties of Silicate Melts (eds. J. F. Stebbins, P. F. McMillan, and D. B. Dingwell), Reviews in Mineralogy, Vol. 32, 317-410, Mineralogical Society of America, Washington, DC

Chase MW (1998) MIST-JANAF thermochemical tables, fourth edition. Journal of Physical Chemistry Reference Data, Monograph Springer: Heidelberg 9

Debenedetti PG (1996) Metastable liquids: Concepts and principals. Princeton University Press

Fox KE, Furukawa T, White WB (1982) Transition metal ions in silicate melts. Part2. Iron in sodium silicate glasses. Phys. Chem. Glasses 23: 169–178

Ghiorso MS, Kress VC (2004) An equation of state for silicate melts. II. Calibration of volumetric properties at 10(5) Pa. American Journal of Science 304: 679-751

Goldman DS, Berg J (1980) Spectral study of ferrous iron in Ca-Al borosilicate glass at room and melt temperatures. J. Non-Crystal. Solids 38/39: 183–188

Gray DE (1972) American Institute of Physics Handbook, 3rd ed. 4-127

Guo X, Lange RA, Ai Y (2013a) The density and compressibility of $CaO$-$FeO$-$SiO_2$ liquids: evidence for four-coordinated $Fe^{2+}$ in the $CaFeO_2$ component. submitted to Geochimica et Cosmochimica Acta

Guo X, Lange RA, Ai Y (2013b) The density and compressibility of model basalt (An-Di-Hd) liquids at one bar: evidence for abundant 6-coordinated $Fe^{2+}$. submitted to Earth and Planetary Science Letters

Guo X, Lange RA, Ai Y (2013c) Density and acoustic velocity measurements on $Na_2O$-$FeO$-$SiO_2$ liquids: evidence of a highly compressible FeO component related to five-coordinated $Fe^{2+}$. Submitted to American Mineralogist

Jackson WE, Waychunas GA, Brown GE, Leon JM, Conradson S, Combes J-M (1993) High-temperature XAS study of Fe2SiO4 liquid: Reduced coordination of ferrous iron. Science 262: 229–232

Jackson WE, Farges F, Yeager M, Mabrouk PA, Rossano S, Waychunas GA, Solomon EI, Brown GE (2005) Multi-spectroscopic study of Fe(II) in silicate glasses: Implications for the coordination environment of Fe(II) in silicate melts. Geochimica et Cosmochimica Acta 69(17): 4315-4332

Kress VC, Williams Q, Carmichael ISE (1988) Ultrasonic investigation of melts in the system $Na_2O$-$Al_2O_3$-$SiO_2$. Geochimica et Cosmochimica Acta 52: 283-293

Kress VC, Carmichael ISE (1991) The compressibility of silicate liquids containing $Fe_2O_3$ and the effect of composition, temperature, oxygen fugacity and pressure on their redox states. Contributions to Mineralogy and Petrology 108: 82-92

Lange RA, Carmichael ISE (1987) Densities of $Na_2O$-$K_2O$-$CaO$-$MgO$-$FeO$-$Fe_2O_3$-$Al_2O_3$-$TiO_2$-$SiO_2$ liquids: New measurements and derived partial molar properties. Geochimica et Cosmochimica Acta 51: 2931-2946

Lange RA (1996) Temperature independent thermal expansivities of sodium aluminosilicate melts between 713 and 1835 K. Geochimica et Cosmochimica Acta 60: 4989–4996

Lange RA (1997) A revised model for the density and thermal expansivity of $K_2O$-$Na_2O$-$CaO$-$MgO$-$Al_2O_3$-$SiO_2$ liquids from 700 to 1900 K: Extension to crustal magmatic temperatures. Contributions to Mineralogy and Petrology 130: 1–11

Lange RA, Navtrotsky A (1992) Heat capacities of $Fe_2O_3$-bearing silicate liquids. Contrib. Mineral Petrol. 110: 311-320

Liu Q, Lange RA (2006) The partial molar volume of $Fe_2O_3$ in alkali silicate melts: Evidence for an average Fe3+ coordination number near five. American Mineralogist 91: 385-393

Moynihan CT, Easteal AJ, Debolt MA, Tucker J (1976) Dependence of fictive temperature of glass on cooling rate. Journal of the American Ceramic Society 59: 12-16

Rivers ML, Carmichael ISE (1987) Ultrasonic studies of silicate melts. J. Geophys. Res. Solid Earth Planets 92: 9247–9270

Rossano S, Ramos AY, Delaye J-M (2000) Environment of ferrous iron in $CaFeSi_2O_6$ glass: contributions of EXAFS and molecular dynamics. Journal of Non-Crystalline Solids 273: 48-52

Secco RA, Manghnani MH, Liu TC (1991) The bulk modulusattenuation-viscosity systematics of diopside-anorthite melts, Geophys. Res. Lett. 18: 93– 96

Scherer GW (1992) Relaxation in glass and composites. Krieger Publishing Company, Malabar, Florida

Stein DJ, Stebbins JF, Carmichael ISE (1986) Density of molten sodium aluminosilicates. J. Am. Ceram. Soc. 69: 396–399

Tangeman JA, Lange RA (2001) Determination of the limiting fictive temperature of silicate glasses from calorimetric and dilatometric methods: application to low-temperature liquid volume measurements. American Mineralogist 86: 1331-1344

Thomas CW, Liu Q, Agee CB, Asimow PD, Lange R.A (2012) Multi-technique equation of state for $Fe_2SiO_4$ melt and the density of Fe-bearing silicate melts from 0 to 161 GPa. Journal of Geophysical Research-Solid Earth 117: B10206, doi: 10.1029/2012JB009403

Webb S, Courtial P (1996) Compressibility of melts in the $CaOAl_2O_3$-$SiO_2$ system, Geochim. Cosmochim. Acta 60: 75–86

Wilke M, Farges F, Partzsch GM, Schmidt C, Behrens H (2007) Speciation of Fe in silicate glasses and melts by in-situ XANES spectroscopy. American Mineralogist 92: 44-56

# Chapter VI

# Conclusions

This dissertation is the first to systematically investigate the high temperature density and compressibility of FeO-bearing silicate melts as a function of composition, using the double-bob Archimedean method and frequency-sweep acoustic interferometery. This study shows that the partial molar volume and compressibility of FeO varies systematically with changes in the average coordination number of $Fe^{2+}$. The experimental liquids include CaO-FeO-$SiO_2$ liquids (Chapter II), ternary model basalts (Di-An-Hd system, Chapter III), $Na_2O$-FeO-$SiO_2$ liquids (Chapter IV), and alkali-bearing model basalts (Chapter V).

The work on CaO-FeO-$SiO_2$ (CFS) liquids reveals that the partial molar volume and compressibility of FeO change systematically with the concentration of CaO, consistent with a composition-induced decrease in the average $Fe^{2+}$ coordination number. This is different from earlier studies (e.g., Lange and Carmichael, 1987; Rivers and Carmichael, 1987), which assumed that the partial molar volumetric properties of FeO did not change with composition. When the CFS liquids are recast in terms of the $CaFeO_2$-FeO-$SiO_2$ components, an ideal mixing model for both volume and compressibility recovers the data within experimental error. The $CaFeO_2$ component corresponds to a crystalline structure that contains $Fe^{2+}$ in 4-fold coordination (Tassel et

al., 2009). At 1723 K, the derived $\overline{V}_{FeO}$ and $\overline{\beta}_{T,FeO}$ values are 12.1 ± 0.2 $cm^3$/mol and 3.5 ± 0.3 x $10^{-2}$ $GPa^{-1}$ for 6-fold coordination of $Fe^{2+}$, as well as 17.1 ± 0.2 $cm^3$/mol and 7.1 ± 0.2 x $10^{-2}$ $GPa^{-1}$ for 4-fold coordination of $Fe^{2+}$. These two end-member values for $\overline{V}_{FeO}$ are used to develop a linear equation to calculate $Fe^{2+}$ coordination as a function of $\overline{V}_{FeO}$, which leads to average $Fe^{2+}$ coordination numbers in the CFS liquids that range from 5.2 to 4.6, including a value of 4.7 for hedenbergite ($CaFe_2Si_2O_6$) liquid.

In Di-An-Hd ($CaMgSi_2O_6$-$CaAl_2Si_2O_8$-$CaFeSi_2O_6$) ternary model basalts, $\overline{V}_{FeO}$ is 12.86 ± 0.16 $cm^3$/mol, which corresponds to a calculated coordination number of $Fe^{2+}$ of ~5.7 (± 0.2). Within the Di-($Di_{0.5}Hd_{0.5}$)-($Hd_{0.5}$-$An_{0.5}$)-An quadrilateral area, the liquid molar volumes and isothermal compressibility mix ideally because they share the same coordination number of $Fe^{2+}$. The derived $\partial\overline{V}_{FeO}/\partial T$ is 3.69 ± 0.58 $10^{-3}$ $cm^3$/mol-K) and $\overline{\beta}_{FeO}$ is 4.72 ± 0.23 $10^{-2}$ $GPa^{-1}$). The results of this study may be most appropriately applied to lunar basalts, which contain few alkalis.

Similar to what was found for the CFS liquids, $\overline{V}_{FeO}$ in the $Na_2O$-FeO-$SiO_2$ liquids (NFS) increase with $X_{Na2O}$, related to a composition-induced decrease in the coordination of $Fe^{2+}$ (5.2 to 4.6). In contrast, the enhanced $\overline{\beta}_{FeO}$ and $\partial\overline{V}_{FeO}/\partial T$ in NFS liquids increase linearly with $Fe^{2+}$ coordination. This is opposite the behavior seen for these two properties in the CFS liquids and similar to the behavior seen $\overline{\beta}_{TiO_2}$ and $\partial\overline{V}_{TiO_2}/\partial T$ in $Na_2O$-$TiO_2$-$SiO_2$. This similarity suggests that there are interactions between $Fe^{2+}$ and sodium (and $Ti^{4+}$ and sodium) that permit significant changes in the network topology with pressure and temperature. In the literature, this has been

attributed to five-coordinated $Ti^{4+}$ in a square-pyramidal site, which might also apply to $Fe^{2+}$ as well.

In the alkali-bearing basalts, the derived $\overline{V}_{FeO}$ is higher (14.76 $cm^3$/mole) than that in Di-Hd-An model basalts, implying an effect of alkalis on $\overline{V}_{FeO}$ (and thus $Fe^{2+}$ coordination). Using the relation derived in chapter 2, the calculated average $Fe^{2+}$ coordination number is ~4.9 ± 0.2. Deriving the compressibility of the FeO component in these alkali-bearing basalts is complicated by the variable compressibility of the $Al_2O_3$ component in alkali vs. alkaline-earth silicate melts, and additional work is needed in this area. The results of this study may be most appropriately applied to basalts in intraplate settings such as continental rifts and oceanic islands, where the magmatism is often alkaline.

One application of the data in this study is to improve equation-of-state (P-V-T) models for magmatic liquids. For example, by combining the one-bar density and compressibility data from this study with high-pressure density data obtained from sink/float and/or shockwave experiments, the compositional dependence to the pressure dependence of melt compressibility can be obtained (e.g., Ai and Lange, 2008; Asimow and Ahrens, 2010). Other applications include the calculation of how the oxygen fugacity in basalt liquid changes with pressure, as well as how the Fe-Mg exchange between pyroxene and liquid changes with pressure, both of which depend on the volumetric properties of the FeO component, obtained in this thesis.

Another important application of this study is an understanding of the differences and similarities between the $MgO$-$SiO_2$ and $FeO$-$SiO_2$ binary phase diagrams. It is commonly known that fayalite ($Fe_2SiO_4$) has a much lower melting temperature (1205°C)

than forsterite ($Mg_2SiO_4$) (1890 $^oC$, Bowen and Schairer, 1935). However, at higher $SiO_2$ contents along the binary, the minerals ferrosilite ($FeSiO_3$) and enstatite ($MgSiO_3$) have similar melting temperatures of 1558 and 1550°C (Jung et al., 2004). In the FeO-$SiO_2$ system, the effect of increasing $SiO_2$ is to increase the melting temperature, whereas along the MgO-$SiO_2$ system, the effect of increasing $SiO_2$ is to decrease the melting temperature. Another way to view the two binaries is to note that the liquidus temperatures across them are very similar between the $SiO_2$-$MgSiO_3$ and $SiO_2$-$FeSiO_3$ segments (Fig. 6.1). However, the liquidus temperatures along $MgSiO_3$-MgO segment are far higher than those along $FeSiO_3$-FeO segment (see Fig. 6.2). The probable cause for the strong decrease in melting temperature from $FeSiO_3$ to FeO is the increase in the liquid volume that occurs as the average coordination of $Fe^{2+}$ decreases from 6-fold in $FeSiO_3$ liquid to a value between 4 and 5 in $Fe_2SiO_4$ liquid, according to spectroscopic results (Jackson et al., 1993). A larger molar volume in the liquid phase promotes melting at a lower temperature, which is predicted by the Clausius-Clapeyron equation ($dT/dP = \Delta V/\Delta S$). The melting temperature of a compound will decrease more vs. less strongly with decreasing pressure more strongly in the case of a larger vs. smaller volume of fusion. Recent spectroscopic studies indicate that $Fe^{2+}$ in fayalite has a coordination number between 4 and 5 (Jackson et al., 1993). Our studies suggest that decreasing $X_{SiO2}$ can induce an increase in the partial molar volume of FeO, corresponding to a decrease in the coordination number of $Fe^{2+}$ from 6 toward 4. Thus the decrease in melting temperature from $FeSiO_3$ to $Fe_2SiO_4$ is due to the decrease in $Fe^{2+}$ coordination, which causes an increase in the molar volume of the liquid and promotes a lower melting temperature. In contrast, although $Mg^{2+}$ also has a lower coordination number than 6-

fold along the binary (Wilding et al., 2004), it is proposed that its average coordination number is greater than that for $Fe^{2+}$ at a similar position along the binary, and thus the volume increase with $Mg^{2+}$ coordination change is smaller.

In a combined spectroscopic and theoretical study (Trcera et al., 2009), it was found that the average $Mg^{2+}$ coordination in various alkali-bearing silicate liquids decreases as the field strength of the alkali decreases, similar to the behavior observed for $Ti^{4+}$ (Farges et al., 1996; Liu and Lange., 2001). For liquids containing K and Na, respectively, it is predicted that $Mg^{2+}$ coordination may be 4- and 5-fold, respectively. It is notable that existing density measurements on MgO-bearing silicate liquids are restricted to the CaO-MgO-$Al_2O_3$-$SiO_2$ quaternary and do not include MgO-$Na_2O$-$K_2O$-$SiO_2$ melts. Therefore, in order to know how alkalis affect the partial molar volume and compressibility of MgO, it is necessary to perform new density and sound speed measurements on the relevant compositions in the future.

The sound speed database employed in Chapter V only has three $K_2O$-bearing liquids that are available until now. More sound speed data are need in the future on K-bearing liquids to make better constrain the database. In addition, natural magma contains $Fe_2O_3$ and $TiO_2$ components as well, the partial molar volume and compressibility of which are compositionally dependent. In order to build up a model that can be applied to natural magma with versatile composition, all the components including FeO, $Fe_2O_3$ and $TiO_2$ have to be considered. Therefore, to build a comprehensive model for future use, it is critical to include all the oxide components. Last but not least, to validate the interpretation of our volumetric data, direct measurement of $Fe^{2+}$ coordination number of $Fe^{2+}$ by spectroscopic methods of our sample liquids is required.

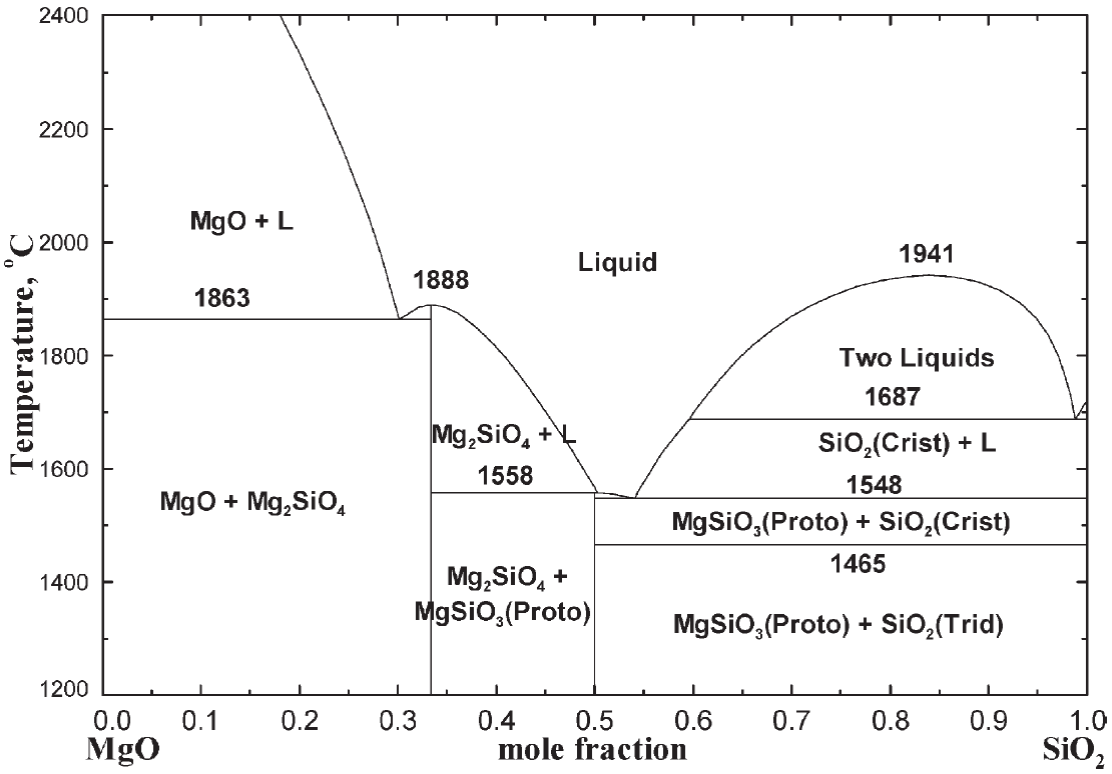


Figure 6.1. MgO-$SiO_2$ phase diagram from Jung et al. (2004)

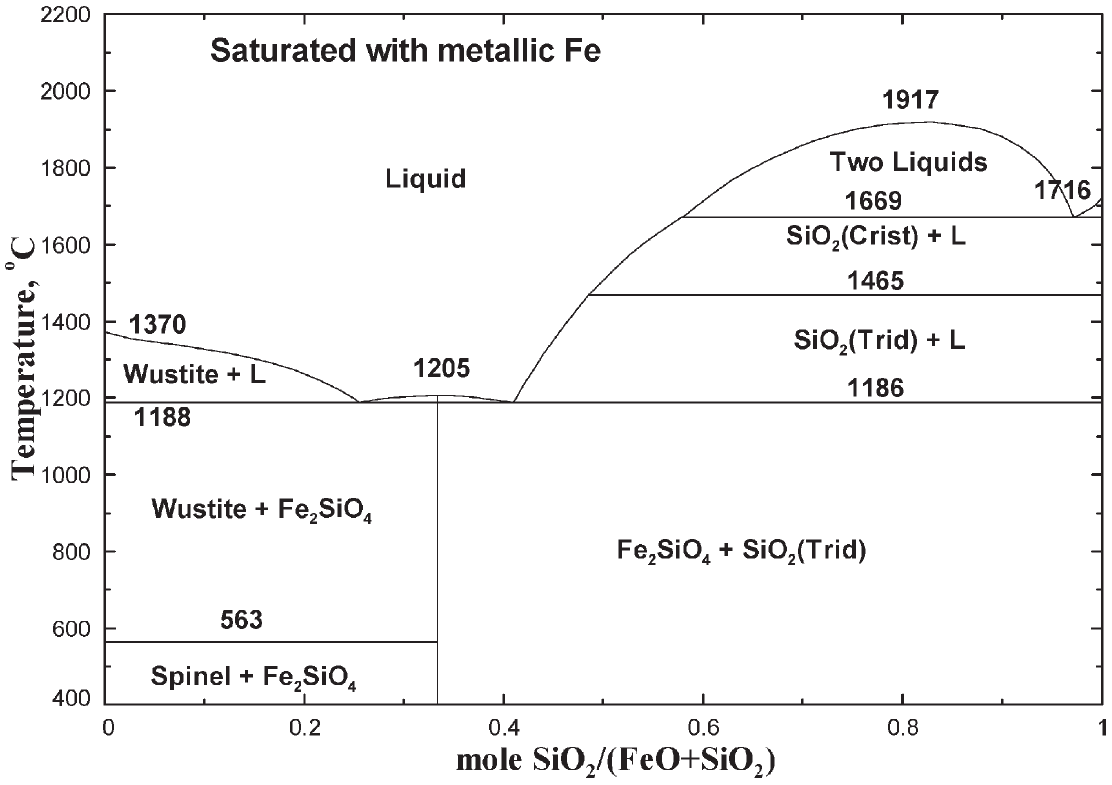


Figure 6.2. FeO-$SiO_2$ phase diagram from Jung et al. (2004)

# References


Ai Y. and Lange R. A., 2008. New acoustic velocity measurements on CaO-MgO-$Al_2O_3$-$SiO_2$ liquids: Reevaluation of the volume and compressibility of $CaMgSi_2O_6$-$CaAl_2Si_2O_8$ liquids to 25 GPa. Journal of Geophysical Research **113**, B04203, doi:10.1029/2007JB005010.

Asimow, P.D., Ahrens T.J., 2010. Shock compression of liquid silicates to 125 Gpa: the anorthite-diopside join. Journal of Geophysical Research 115, B10209.

Bowen, N.L. and Schairer, J.F., 1935. The system, MgO-FeO-$SiO_2$. American Journal Science. 29(170), 151-217.

Farges, F., Brown, G.E., Navrotsky, A., Gan, H., and Rehr, J.R., 1996. Coordination chemistry of Ti(IV) in silicate glasses and melts: III. Glasses and melts from ambient to high temperature. Geochimca et Cosmochimica Acta, 60, 3055-3065

Jackson, W.E., Waychunas, G.A., Brown, G.E., Leon, J.M., Conradson, S. and Combes, J.-M., 1993. High-temperature XAS study of Fe2SiO4 liquid: Reduced coordination of ferrous iron. Science 262, 229–232.Science, 262,229.

Jung I., Decterov S.A., and Pelton A.D., 2004. Critical thermodynamic evalution and optimization of the FeO-$Fe_2O_3$-MgO-$SiO_2$ system. Metallurgical and Materials Transactions B, 35B, 877-889.

Lange, R.A., Carmichael, I.S.E., 1987. Densities of $Na_2O$-$K_2O$-CaO-MgO-FeO-$Fe_2O_3$-$Al_2O_3$-$TiO_2$-$SiO_2$ liquids: New measurements and derived partial molar properties. Geochimica et Cosmochimica Acta, 51, 2931-2946

Liu, Q. and Lange, R.A., 2001. The partial molar volume and thermal expansivity of $TiO_2$ in alkali silicate melts: Systematic variation with Ti coordination. Geochimica et Cosmochimica Acta, 65(14), 2379-2393.

Liu, Q., Lange, R.A. and Ai, Y., 2007. Acoustic velocity measurements on $Na_2O$-$TiO_2$-$SiO_2$ liquids: Evidence for a highly compressible $TiO_2$ component related to five-coordinated Ti. Geochimica et Cosmochimica Acta, 71, 4314-4326

Rivers, M.L., Carmichael, I.S.E., 1987. Ultrasonic studies of silicate melts. J. Geophys. Res. Solid Earth Planets 92, 9247–9270.

Tassel C., Pruneda J.M., Hayashi N., Watanabe T., Kitada A., Tsujimoto Y., Kageyama H., Yoshimura K., Takano M., Nishi M., Ohayama K., Mizumaki M., Kawamura N., Iniguez J. and Canadell E., 2009. $CaFeO_2$: A new type of layered structure with iron in a distorted square planar coordination. Journal of the American chemical society **131**: 221-229.

Trcera N., Cabaret D., Rossano S., Farges F., Flank A. and Lagarde P., 2009. Experimental and theoretical study of the structural environment of magnesium in

minerals and silicate glasses using X-ray absorption near-edge structure. Phys. Chem. Minerals. 36, 241-257.

Wilding M.C., Benmore C.J., Tangeman J.A., Sampath S., 2004. Coordination changes in magnesium silicate glasses. Europhys Lett 67(2):212-218.